ANALYSIS OF THE THERMAL HYDRAULICS OF A MULTIPHASE OXYGEN PRODUCTION REACTOR IN THE Cu-Cl CYCLE

by

MOHAMMED W. ABDULRAHMAN

A Thesis Submitted in Partial Fulfillment
of the Requirements for the Degree of
Doctor of Philosophy

in

The Faculty of Engineering and Applied Science
Mechanical Engineering

University of Ontario Institute of Technology

June 2016

ABSTRACT

In the thermochemical water splitting process by Cu-Cl cycle, oxygen gas is produced by an endothermic thermolysis process in a three-phase reactor. In this thesis, the required heat for the thermolysis process is provided by adopting the idea of heating some of the stoichiometric oxygen gas by using a nuclear reactor heat source. Then, the gas is re-injected into the reactor from the bottom, to transfer heat directly to the slurry bed of molten salt and solid reactant. In this thesis, the thermal hydraulics of the oxygen slurry bubble column reactor (SBCR) is investigated experimentally and numerically. In the experiments, lower temperature alternative materials, such as helium gas at 90^{o}C and water at 22^{o}C, are used to mimic the actual materials of the oxygen gas at 600^{o}C and molten CuCl at 530^{o}C. From the experimental studies, new forms of empirical equations are formulated for the overall gas holdup and the volumetric heat transfer coefficient in terms of the design and input parameters of the SBCR, such as; the superficial gas velocity, reactor height, and solid particles concentration. The empirical equations are obtained for both bubbly and churn-turbulent flow regimes. It is also determined experimentally the flow regime transition point between bubbly and churn-turbulent flow regimes. Furthermore, it is found experimentally that the solid particle diameter has insignificant effect on the overall gas holdup.

To better understand the thermal hydraulics of the oxygen SBCR, a computational fluid dynamics (CFD) models are developed by using the ANSYS FLUENT software. All CFD simulation results are validated by the experimental results of the alternative materials system with good agreements. From the CFD simulations, it is also found that the gas temperature decreases dramatically near the bottom of the reactor, and the effects of the superficial gas velocity, reactor height, and solid concentration on the gas temperature are negligible. Finally, a simple correlation is obtained to calculate the number of oxygen reactors in terms of the superficial gas velocity of the oxygen gas and the oxygen production rate.

Keywords: Cu-Cl cycle; oxygen gas; multiphase; thermolysis; slurry bubble column; direct contact heat transfer.

ACKNOWLEDGEMENT

In the name of Allah, Most Gracious, Most Merciful

All praise and glory to Almighty Allah for all his grants, strengths and blessing that he bestowed on me to complete this thesis. I would like to express my grateful words of thanks and deep gratitude to my parents (Allah bless their souls) for their great role in my life and their numerous sacrifices for me. I also would particularly like to thank my wife Basma for her continuous support, encouragement and quiet patience.

I truly acknowledge the valuable time and support of my supervisory team. Their insightful comments, remarks and feedback in addition to their encouragement and support, made enormous contributions to this Ph.D. thesis. I would also like to thank Dr. Bekir Yilbaş and Dr. David Naylor and acknowledge with much appreciation their crucial roles in this thesis. Advices and comments given by them have been a great help to my thesis works. Moreover, I would like to thank Dr. Ibrahim Dincer and Dr. Kamiel Gabriel for their supports and advices during the completion of the thesis work.

Finally, my thanks go to the people and organizations that support this research by providing critical financial resources, especially Dr. Martin Agelin-Chaab and Dr. Zhaolin Wang. Support from the Natural Sciences and Engineering Research Council of Canada (NSERC), the Ontario Research Fund, Atomic Energy of Canada Limited, Phoenix Canada Oil Company Limited, Marnoch Thermal Power Inc. and the Faculty of Engineering and Applied Science at UOIT are gratefully acknowledged.

TABLE OF CONTENTS

LIST OF TABLES

LIST OF FIGURES

LIST OF APPENDICES

NOMENCLATURE

A_i	Interfacial area (m^2)
Bo	Bond number
C_D	Drag coefficient
C_p	Specific heat at constant pressure (J/kg.K)
C_{p,Al_2O_3}	Specific heat at constant pressure of alumina
C_{p,Cu_2OCl_2}	Specific heat at constant pressure of Cu_2OCl_2
$C_{p,g}$	Specific heat at constant pressure of gas (J/kg.K)
C_{p,H_2O}	Specific heat at constant pressure of water (J/kg.K)
$C_{p,l}$	Specific heat at constant pressure of liquid (J/kg.K)
$C_{p,s}$	Specific heat at constant pressure of solid (J/kg.K)
$C_{p,sl}$	Specific heat at constant pressure of slurry (J/kg.K)
C_s	Volumetric solid concentration
d_b	Bubble diameter (m)
d_m	Mean diameter of solid particles (m)
d_o	Orifice diameter (m)
d_P	Particle diameter (m)
D_R	Diameter of reactor (m)
f	Drag function
Fr	Froude number
g	Gravitational acceleration (m^2/s)
$\boldsymbol{g}$	Gravitational acceleration vector (m^2/s)
Ga	Gallilei number
h	Heat transfer coefficient ($W/m^2.K$) / Height distance (m)
h_g	Specific enthalpy of gas phase (J/kg.K)
h_{sl}	Specific enthalpy of slurry phase (J/kg.K)
H	Height of static liquid (m)
H_R	Height of reactor (m)
I.D.	Inner diameter (m)

j_E	Experimental drift flux (m/s)
j_T	Theoretical drift flux (m/s)
k	Thermal conductivity (W/m.^{o}C) / Turbulent kinetic energy (J)
k_g	Thermal conductivity of gas (W/m.^{o}C)
k_l	Thermal conductivity of liquid (W/m.^{o}C)
k_s	Thermal conductivity of solid (W/m.^{o}C)
k_{sl}	Thermal conductivity of slurry (W/m.^{o}C) / Turbulent kinetic energy of slurry (J)
$\dot{m}$	Mass flow rate (kg/s)
$\dot{m}_g$	Mass flow rate of the gas (kg/s)
$\dot{m}_{H_2}$	Mass flow rate of hydrogen gas (kg/s)
$\dot{m}_{O_2}$	Mass flow rate of oxygen gas (kg/s)
M_D	Drag force (N/m^3)
M_i	Total interfacial force acting between phases (N/m^3)
M_L	Lift force (N/m^3)
M_{VM}	Virtual mass force (N/m^3)
N	Number of reactors
Nu	Nusselt number
P	Pressure (Pa)
Pr	Prandtle number
Q	Phase flow rate (m^3/s) / Heat transfer flux (W/m^2)
$Q_{g,sl}$	Intensity of heat exchange between gas and slurry phases (W/m^3)
$\dot{Q}$	Heat flow rate (W)
R	Gas constant (J/mol.K)
Re	Reynolds number
S_g	Source term of gas phase (W/m^3)
S_{sl}	Source term of slurry phase (W/m^3)
Stk	Stokes number
T	Temperature (^{o}C)
T_g	Temperature of gas (^{o}C)

$T_{g,in}$	Inlet gas temperature (°C)
$T_{g,out}$	Outlet gas temperature (°C)
T_{sl}	Temperature of slurry (°C)
$\bar{T}_g$	Average gas temperature (°C)
$\bar{T}_{sl}$	Average slurry temperature (°C)
u	Slip speed of bubble (m/s)
u_o	Terminal velocity of bubble (m/s)
U_{gs}	Superficial velocity of gas (m/s)
$U_{g-trans}$	Transition superficial velocity of gas (m/s)
U_l	Velocity of liquid (m/s)
U_{ls}	Superficial velocity of liquid (m/s)
U_V	Volumetric heat transfer coefficient (W/m^3.K)
$v_{x,g}$	Velocity component in x-direction of gas phase (m/s)
$v_{x,sl}$	Velocity component in x-direction of slurry phase (m/s)
$v_{y,g}$	Velocity component in y-direction of gas phase (m/s)
$v_{y,sl}$	Velocity component in y-direction of slurry phase (m/s)
V_g	Volume of gas phase (m^3)
V_l	Volume of liquid phase (m^3)
V_R	Internal volume of the reactor (m^3)
V_s	Volume of solid phase (m^3)
V_{sl}	Volume of slurry (m^3)
$\boldsymbol{V_g}$	Velocity field of gas phase (m/s)
$\boldsymbol{V_{sl}}$	Velocity field of slurry phase (m/s)
We	Weber number
W_l	Weight fraction of liquid
W_s	Weight fraction of solid

Greek Letters

α_g	Gas holdup
$\alpha_{g-trans}$	Transition gas holdup
α_l	Liquid holdup
α_s	Solid holdup
α_{sl}	Slurry holdup
β	Thermal expansion coefficient (1/K)
ΔH	Height difference between transducers (m)
ΔP	Static pressure drop (Pa)
ΔT	Temperature difference (^oC)
ΔT_{lm}	Logarithmic mean temperature difference (^oC)
ε	Dissipation rate (m^2/s^3)
μ_b	Dynamic viscosity at bulk temperature (Pa.s)
μ_{eff}	Effective dynamic viscosity (Pa.s)
μ_g	Dynamic viscosity of gas phase (Pa.s)
μ_l	Dynamic viscosity of liquid phase (Pa.s)
μ_r	Relative dynamic viscosity (dimensionless)
μ_{sl}	Dynamic viscosity of slurry phase (Pa.s)
ρ	Density (kg/m^3)
$\rho_{Cu_2OCl_2}$	Density of Cu_2OCl_2 (kg/m^3)
ρ_F	Density of the three-phase system (kg/m^3)
ρ_g	Density of gas (kg/m^3)
ρ_l	Density of liquid (kg/m^3)
ρ_s	Density of solid (kg/m^3)
ρ_{sl}	Density of slurry (kg/m^3)
$\hat{\rho}_g$	Effective density of gas phase (kg/m^3)
$\hat{\rho}_{sl}$	Effective density of slurry phase (kg/m^3)
σ	Surface tension (N/m)
σ_{H_2O}	Water surface tension (N/m)
τ_b	Particulate relaxation time (s)

$\bar{\bar{\tau}}_g$	Viscous stress tensor of gas phase (N/m^2)
$\bar{\bar{\tau}}_{sl}$	Viscous stress tensor of slurry phase (N/m^2)

Acronyms

ANL	Argonne National Laboratories
BC	Bubble Column
CANDU	Canada Deuterium Uranium
CARPT	Computer-Automated Radioactive Particle Tracking
CFD	Computational Fluid Dynamic
CFSTR	Continuous Flow Stirred Tank Reactor
CSTR	Continuous Stirred-Tank Reactor
DGD	Dynamic Gas Disengagement
GIF	Generation-IV International Forum
HTGR	High Temperature Gas Reactor
LDV	Laser Doppler Velocimetry
PIV	Particle Image Velocimetry
RANS	Reynolds-Averaged Navier-Stokes
R&D	Research and Development
SBC	Slurry Bubble Column
SBCR	Slurry Bubble Column Reactor
SCWR	Super Critical Water Reactor
STR	Stirred Tank Reactor

CHAPTER 1
INTRODUCTION

There is a common belief that in the future, hydrogen will be an effective factor to the supply of sustainable energy (Forsberg, 2007), because hydrogen usage would decrease the atmospheric pollution by decreasing the emissions of greenhouse gas. Greenhouse gases are generated in large quantities from conventional gasoline and diesel vehicles, and in much less quantities from the production of hydrogen gas from various fuel gases (Nguyen et al., 2013).

Hydrogen is used in large quantities by many industries. Therefore, the demand of hydrogen is anticipated to be higher in the future. Currently, most of the hydrogen production methods use processes that emit large amounts of carbon dioxide, such as steam-methane reforming or partial oxidation of heavy hydrocarbons. With the fast growing need of hydrogen, the major economical challenge of the hydrogen production is the sustainable production of hydrogen in large quantities and lower costs compared with the existing technologies (Naterer et al., 2008a).

The alternative methods that can be used for hydrogen production, are the thermochemical cycles. One of the most important advantages of the thermochemical cycles is that they require heat at lower temperatures to split water into hydrogen and oxygen than that required for direct water splitting through heating. Therefore, the range of heat sources that can be applied to the thermochemical cycles increases (Forsberg, 2003). For large scale production of hydrogen, thermochemical cycles can be linked to nuclear plants. In this way, the efficiencies of the thermochemical cycles will increase and the costs of hydrogen production as well as the generation of greenhouse gases will decrease in comparison with the other conventional technologies (Naterer et al., 2008a).

Copper-chlorine (Cu-Cl) cycle was identified as one of the promising lower temperature cycles (Lewis et al., 2003; Serban et al., 2004). The Cu–Cl cycle includes three chemical reactions to decompose water into hydrogen and oxygen. Two of the chemical reactions are thermal and one is an electrochemical reaction

(Marin, 2012). The primary advantage of the Cu-Cl cycle is the low operating temperature (530^{o}C) compared to other thermochemical cycles. At this operating temperature, the Cu–Cl cycle can be linked to Canada's Generation IV nuclear reactor, which is the CANDU Super-Critical Water Reactor (CANDU-SCWR). Other advantages of the Cu-Cl cycle are lower construction materials, minimal handling of solids, and all chemicals are recycled. In spite of the above advantages, there are few challenges encountered in the Cu-Cl cycle, such as; solids handling between processes and the corrosive materials used in the reactions (Naterer et al., 2011a).

The three reaction steps of the Cu-Cl cycle (Fig. 1.1) are (Marin, 2012);

$$2CuCl\ (a) + 2HCl\ (g) \rightarrow 2CuCl_2\ (a) + H_2\ (g) \qquad 100°C \qquad step\ (1) \qquad (1.1)$$

$$2CuCl_2\ (s) + H_2O\ (g) \leftrightarrow Cu_2OCl_2\ (s) + 2HCl\ (g) \qquad 375\ °C \qquad step\ (2) \qquad (1.2)$$

$$Cu_2OCl_2\ (s) \rightarrow 2CuCl\ (l) + ½\ O_2\ (g) \qquad 530\ °C \qquad step\ (3) \qquad (1.3)$$

where a, s, l and g denote to aqueous, solid, liquid and gas respectively.

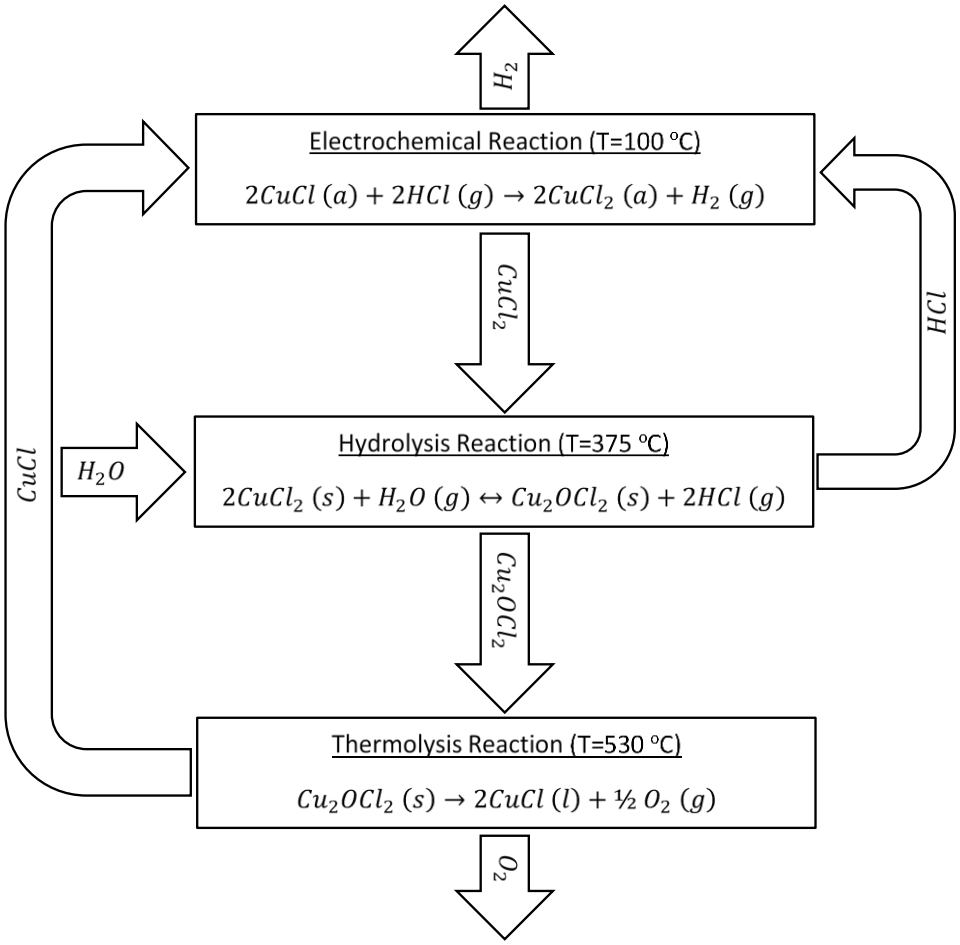

Fig. 1.1 Three reaction steps of the Cu-Cl cycle.

In the oxygen production step of the Cu-Cl cycle (Step 3), a solid copper oxychloride (Cu_2OCl_2), is decomposed thermally into oxygen gas (O_2) and molten cuprous chloride (CuCl). The solid Cu_2OCl_2 is fed to the oxygen production reactor from the $CuCl_2$ hydrolysis reaction (Step 2) that operates at a temperature range of 350–450°C. The materials leaving the oxygen reactor are oxygen gas (which is evolved over a temperature range of 450 to 530°C) and molten CuCl. In the oxygen reactor, the decomposition of Cu_2OCl_2 to oxygen and molten CuCl is an endothermic reaction requiring a reaction heat of 129.2 kJ/mol and a temperature of 530°C, which is the highest temperature in the Cu-Cl cycle. Thus, heat must be added to increase the temperature of the bulk inside the reactor. The total amount of heat required is the sum of reaction heat and the heat required to raise the

reactant temperature from 375^{o}C (average temperature of solid particles from the hydrolysis reaction) to 530^{o}C (Naterer et al., 2008b).

1.1. Background

1.1.1. Types of Multiphase Reactors

The oxygen reactor contains three phases; copper oxychloride solid particles, liquid molten salt and oxygen gas. Multiphase reactions are widely used in chemical processes. There are several types of multiphase reactors available in the industry which could be classified into two main groups: fixed beds and slurry phase reactors. The fixed beds or the packed beds are reactors in which the solid phase is stationary. Since the feeding process of the solid phase in the oxygen reactor is continuous, it can't be considered as a fixed bed reactor.

The slurry phase reactors, which can be continuous reactors, are mainly stirred tank reactors (STR) and slurry bubble column reactors (SBCRs). The continuous stirred tank reactor (CSTR), is a mechanically agitated reactor, where there are continuous feeding and withdrawing into the reactor for the streams of reactants and products respectively. Generally, a continuous flow stirred tank reactor (CFSTR) assumes that the fluid is perfectly well mixed. Therefore, the system properties such as; concentration, density and temperature, are uniform throughout the reactor. In the SBCR, the upward flow of gaseous bubbles will suspend the solid particles in the liquid phase.

Type of the oxygen reactor

Oxygen reactor can be considered as either CFSTR or a SBCR. The choice between these types of reactors depends on the efficiency of heat transfer rate, efficiency of agitation, scale up and other design criteria. The thermal design of the oxygen reactor requires enough agitation inside the reactor and sufficiently high heat transfer rate to the solid particles. Agitation can be provided either by using a mechanical agitator such as in the CFSTR or by using gaseous bubbles such as in the SBCR. The rate of agitation by mechanical agitator is higher than that by bubbles but the mechanical agitator is undesirable in a highly corrosive medium

like the oxygen reactor, because of the many internals that are required inside the reactor, such as the propeller, the shaft, baffles and other accessories that support the mixing system.

Heating can be achieved by two different mechanisms which can involve indirect and direct contact heating. The two most common indirect contact mechanisms involve the use of a jacket surrounding the vessel or an internal coil. Direct contact heating mechanism can be achieved by using gaseous bubbles, and is more efficient than the indirect contact heating mechanism but is more complex in scale-up. In the oxygen reactor, oxygen gas that leaves the reactor at a temperature of about 530^{o}C, can be heated to a higher temperature (such as 600^{o}C) and then re-injected into the oxygen reactor from the bottom through a sparger. In this case, direct contact heat transfer can occur between the hot oxygen gas and the slurry inside the oxygen reactor.

From the above comparison, it can be concluded that SBCR is more efficient in heat transfer than CFSTR but is more complex in scale up. In SBCR, however, thermal energy can be transferred to the reactor by using direct contact heating from gas bubbles which can also be used to provide enough agitation for the contents of the reactor. Therefore, SBCR is used in this thesis.

1.1.2. Oxygen Reactor System Description

1.1.2.1. Introduction

Like any chemical reactor, the oxygen reactor requires accurate control of heat transfer to obtain optimum productivity. This section examines the sources of heat for the oxygen reactor and the suitable methods of heat transfer configuration that can be used to provide this heat. Moreover, the factors that influence the size of the oxygen reactor are also explained in detail.

1.1.2.2. Heat Source

The oxygen reaction is a high temperature process, which needs a high temperature heat source. This heat can be provided from the generation IV nuclear reactor concepts, such as the sodium-cooled reactor, the Canada Deuterium

Uranium super critical water reactor (CANDU-SCWR), and the high temperature gas reactor (HTGR). Although the first two reactors are lower temperature reactors (T=510^{o}C - 625^{o}C), they are still well suited for matching a low temperature Cu-Cl thermochemical cycle. However, matching low temperature cycles with the HTGR (T=1000^{o}C) may provide a greater opportunity for cogeneration, which may result in significantly higher hydrogen production efficiencies (Tsoulfanidis, 2012). In this work, CANDU-SCWR is considered as a heat source for heat transfer modelling.

CANDU Super Critical Water-cooled Reactor (CANDU-SCWR) is one of the reactors considered by the Generation-IV International Forum (GIF) for international collaborative research and development (R&D) (Chow and Khartabil, 2007). The coolant of this reactor is light water at a pressure of 25MPa, and inlet and outlet temperatures of 350°C and up to 625°C respectively. The thermodynamic efficiency of the supercritical water working as a coolant can be increased to over 40% compared to that of CANDU's reactor which is 33% (Yetisir, 2012).

1.1.2.3. Method of Heating the Oxygen Reactor

A suitable method of heating the oxygen reactor is needed to provide enough heat that is necessary for solid decomposition. Heating the Cu_2OCl_2(s) particles only is undesirable, because of relatively slow rate of heat transfer. A better option is to heat the molten salt inside the oxygen reactor to in turn transfer the heat within the reactor from the liquid (molten CuCl) to the solid Cu_2OCl_2 (reactant) particles. The molten salt bath can be sustained by the reaction product itself. This approach is the most applicable and the recommended one (Naterer et al., 2008b).

There are two main heating methods for reactor: electrical heating and fluid heating. The main disadvantage of electrical heating is the limited efficiency of electricity generation from nuclear heat (currently less than 35%) (Beaty & Fink, 2013). A more suitable method is to heat the molten salt by using a heating fluid without using electricity.

Two main configurations of molten salt heating by a fluid can be used: direct and indirect contact heating. In direct contact heating, the heating fluid will be in

direct contact with the heated medium. The advantage of direct contact heating is that, it is approximately 100% efficient, which will help in accelerating the heat and removing the thermal lag. In direct contact heating, there are no heat losses that are due to the intermediate heat transfer medium. Direct contact heating can be applied by using a Slurry Bubble Column Reactor (SBCR), where the heating gas can be introduced to the reactor from a gas sparger at the bottom of the reactor.

Indirect contact heating uses a heat transfer medium to transfer the heat to the reactor vessel. Different kinds of indirect contact heat transfer surfaces can be used in an industrial oxygen reactor such as jackets, helical tubes immersed directly inside the reactor and vertical tube baffles (Oldshue, 1983). In this thesis, direct contact heat transfer configuration is investigated because of its high efficiency in heat transfer.

1.1.2.4. Factors Affecting the Oxygen Reactor Size

- **Terminal Settling Velocity of Particles**

The required time for solid particles to settle in a reactor of a finite size is an important parameter to design the reactor correctly (Felice & Kehlenbeck, 2000). The speed of particles descent has a significant effect on reactor height. It is recommended for the descent speed of particles to be small to provide enough time to complete the decomposition process before reaching the bottom of the reactor. In this case a large reactor height is not required.

Since the density of the solid particle of Cu_2OCl_2 is greater than that of molten CuCl, the falling velocity of the single particle under gravity will be higher than that of the molten CuCl. The acceleration of the particle will continue for a very short time and then the falling velocity will remain constant, where the effective weight of the particle and the drag force will be equal. Hence, the period of constant-velocity fall (terminal settling velocity) is the most important one. The terminal velocity of the solid particles is affected by many parameters including solid particle size, the particle shape (roundness), solid concentration and density of the solid, as well as the viscosity and density of the liquid (Nguyen & Schulze, 2003).

a- *Particle size*

In industry, solids particles usually do not have the same sizes, but have distribution of sizes. It is well known that larger particles have higher settling velocity than smaller ones. Baldi et al. (1978) have suggested that for a distribution of particle sizes, it is suitable to use the mass-mean diameter to express the particle diameter when calculating the settling velocity.

b- *Particle shape*

The shape of solid particles is generally assumed spherical in the theoretical calculations. For non-spherical particles, the size can be expressed as a sphere with an equivalent volume. The falling velocity of a spherical particle is higher than that of a non-spherical one that has the same volume and density (Nguyen & Schulze, 2003).

c- *Particles concentration:*

When a cloud of solid particles is falling in a quiescent liquid, additional hindering effects influence its falling velocity. These are the increased drag caused by the particles closeness within the cloud and the liquid up flow when it is displaced by the descending particles. The hindering effects depend significantly on the volumetric concentration of solids in the cloud (C_s). The hindered falling velocity is usually a fraction of the free falling velocity. For example, for a solid concentration of 30% and a solid particle diameter range of 0.074-2 mm, the hindered velocity of the sand is approximately 20-40% of the value for the single particle terminal velocity (Richardson and Zaki, 1954).

In the design of oxygen reactor size, it is important to specify whether the settling velocity of the solid particles will give enough residence time for the complete decomposition of these particles before they settle at the bottom of the reactor. It is well known that the highest settling velocity is for a single spherical particle falling in an infinitely deep fluid. Other effects like the particle shape, reactor wall and hindering effects are reducing the settling velocity of the particles. In the oxygen reactor, the descent speed of particles is also reduced by the up flow motion of the oxygen bubbles.

- **Oxygen Bubbles**

Oxygen bubbles are created at the surface of the solid particles, and will leave the particle surface soon after they are formed, because of the large density difference between oxygen gas and solid particle. The bubbles then move to the liquid (molten salt) surface and the moment that they reach the liquid surface, they are removed from the reactor immediately, because of the large density difference between gas bubbles and the molten salt (Naterer et al., 2008b). During the ascending of bubbles to the liquid level, the size of some bubbles grows and occupies a portion of the reactor volume.

- **Reactor Heating Rate**

As mentioned earlier, in the oxygen reactor, the decomposition of Cu_2OCl_2 to oxygen and molten CuCl is an endothermic reaction and requires a reaction heat of 129.2 KJ/mol (Naterer et al., 2008b). To provide this amount of heat, high heat transfer rate is needed inside the reactor. Since the velocities of the reactor contents are not enough to provide this amount of heat transfer rate, a large size reactor is needed in this case to provide enough area for heat transfer.

- **Fouling**

Oxygen reactor contains corrosive materials such as oxygen gas and molten CuCl. Because of low velocities of oxygen reactor contents, the tendency for fouling increases. To overcome the fouling problem, more heat transfer area as well as a larger reactor volume is needed.

An option to minimize the above problems is to use agitation, which can be achieved by using a mechanical propeller or gas bubbles. Agitation will increase the residence time of Cu_2OCl_2 particles in the molten salt and help decrease the reactor height (Naterer et al., 2008b). Also, agitation mixes the involved substances well and helps break the aggregation of Cu_2OCl_2 particles, thus increasing the contact area between Cu_2OCl_2 particles and molten CuCl as well as increasing the local rates of heat transfer. Moreover, increasing the speed of

reactor mixture reduces the tendency for fouling inside the reactor. The overall effect results in a reduction of the reactor size.

1.1.3. Slurry Bubble Column Reactors (SBCRs)

Slurry bubble columns are systems that contain three-phases; gas, liquid, and solid, in which gaseous bubbles are dispersed through a liquid-solid slurry in a vertical column (Fig. 1.2) (Shaikh, 2007). The flow of the slurry phase with respect to the gas flow, can be either co-current, counter-current, or in batch mode (Shaikh, 2007). In the oxygen reactor, molten CuCl and O_2 gas are produced from the decomposition process of the solid Cu_2OCl_2. The molten CuCl produced overflows outside the oxygen reactor. If the overflow speed of the molten CuCl is taken into consideration, then the reactor is in co-current mode.

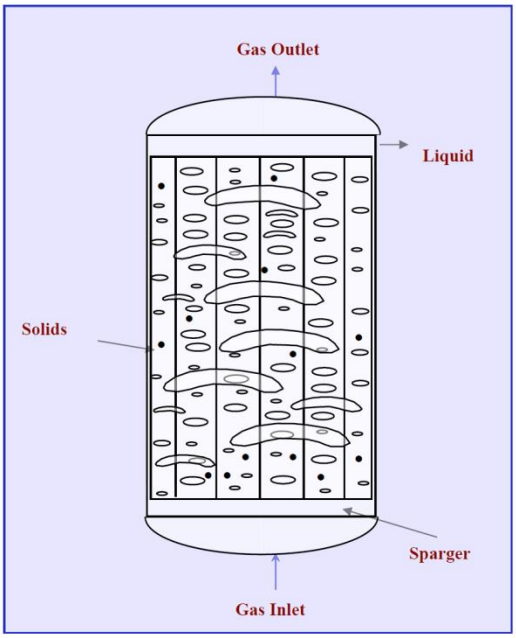

Fig. 1.2 Schematic diagram of a slurry bubble column (Shaikh, 2007).

Slurry bubble column reactors are used in different industrial applications because of their advantages. Since the heat capacity of the liquid is relatively high, the existence of the liquid in the SBCRs is beneficial because it provides a better control to the temperature of the system (Nigam and Schumpe, 1996).

1.1.3.1. Hydrodynamics of SBCRs

The hydrodynamics of the oxygen SBCR have a significant effect on its scale up analysis. In SBCRs, gas phase that is moving upward transfers momentum to the slurry phase that is either stagnant or moving slower than the gas. Therefore, the hydrodynamics of SBCRs are controlled mainly by the gas flow (Shaikh, 2007). It has been reported that the operating conditions and design as well as the geometry of the column strongly affect the hydrodynamics of the SBCRs (Deckwer et al., 1980; Guy et al., 1986; Saxena and Chen, 1994). The hydrodynamic characteristics of the SBCRs are;

a) Flow Regimes

The hydrodynamics of SBCRs have strong dependence on the type of the flow regime in the column (Guy et al., 1986). The flow regimes in bubble columns can be classified into three types (Wallis, 1969);

1- Homogeneous regime (bubbly flow): This flow regime can be obtained when the superficial gas velocities are low. The sizes and rise velocities of the bubbles in this regime are relatively uniform. In this case, the liquid motion will not be affected by gas bubbles. The bubble distribution in this regime is uniform along the entire cross-sectional area of the column and the mixing rate is small (Hyndman et al., 1997).

2- Heterogeneous regime (churn-turbulent flow): This flow regime is obtained when the gas velocity is increased. In this case, gas bubbles will be more interacted and bubbles coalescence and break up are observed which will lead to a broad distribution of bubble size. Consequently, bubbles in this regime can be arbitrary classified into “small”, and “large”.

3- Slug flow regime: This flow regime is obtained in small diameter columns. In this case, when the gas velocity increases, the bubbles of the gas will coalesce to form slugs with large diameters. Fig. 1.3 shows the differences between the discussed flow regimes.

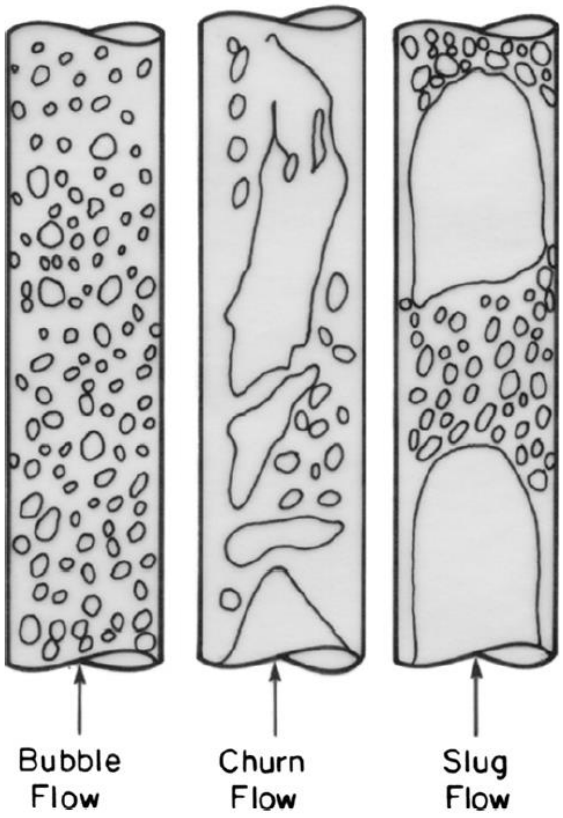

Fig. 1.3 Schematic of possible flow regimes in a bubble column (Ashfaq and Muthanna, 2013).

It is very important to detect the regime transition points, because there are significant changes in the hydrodynamic behaviour of the system when the transition takes place (Nigar et al., 2005). Different flow maps for regime transition were proposed. Fig. 1.4 shows a typical flow map for a bubble column that was initially proposed by Deckwer et al. (Deckwer et al., 1980; Shah et al., 1982) for air/water system based on the column diameter as a function of gas velocity. This map can be used for slurry bubble columns with a stagnant low viscous liquid phase (Nigar et al., 2005). Since the flow regime transition depends on different parameters, the boundaries between the regimes in Fig. 1.4 are not exact. Thus, in this study, the regime transition flow map will be specified for viscous slurry ($CuCl+Cu_2OCl_2$) and oxygen gas.

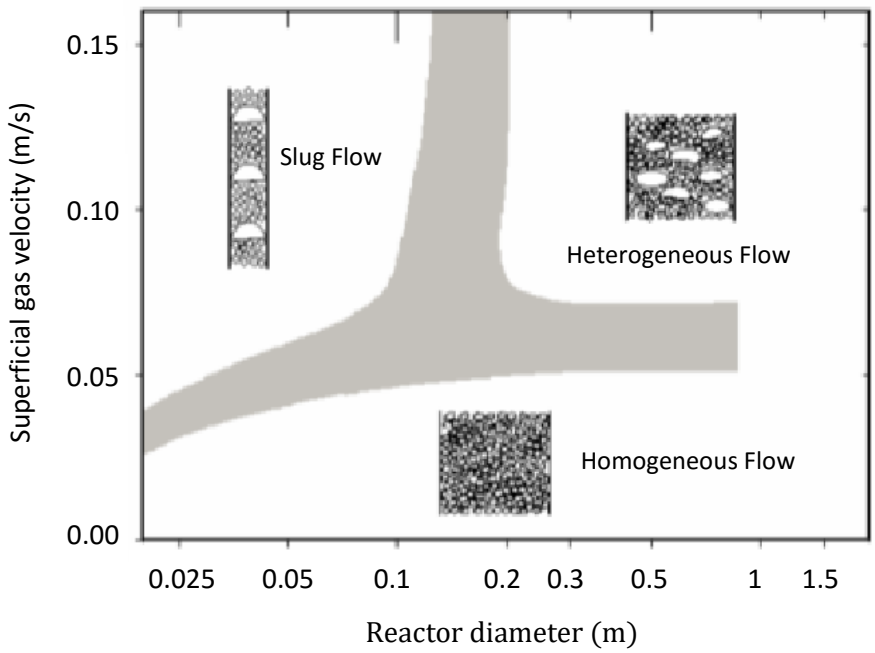

Fig. 1.4 Flow-regime map for the bubble column reactor (Deckwer et al., 1980; Nigam and Schumpe, 1996).

b) Gas Holdup (α_g)

Gas holdup is an important parameter that can be used for the performance description of the slurry bubble column reactors (Fan et al., 1999). In the SBCRs, the total volume (V_t) of the three-phase system is given by the following expression (Behkish, 2004);

$$V_t = V_g + V_l + V_s\,, \tag{1.4}$$

where V_g, V_l, and V_s are the volumes of gas, liquid and solid phases respectively. The holdup of any phase (i), is defined as the ratio of the volume occupied by this phase to the total volume in the reactor (Behkish, 2004);

$$\alpha_i = \frac{V_i}{V_g + V_l + V_s}, \tag{1.5}$$

and accordingly,

$$\alpha_g + \alpha_l + \alpha_s = 1\,, \tag{1.6}$$

where α_g, α_l, and α_s are the holdups of gas, liquid and solid phases respectively (Behkish, 2004). There are many different factors that affect the behavior of the gas holdup, such as; physical properties of the different phases, reactor size, gas sparger design, and the operating variables. (Kim et al., 2014).

Effect of the superficial gas velocity on α_g

The superficial gas velocity can be calculated from the division of the volumetric flow rate of the gas to the column cross-sectional area. Superficial gas velocity is a very important parameter in the calculation of gas holdup (Shah et al., 1982). Gas holdup can be related to the superficial gas velocity as (Deckwer, 1992);

$$\alpha_g \propto U_{gs}^{n}\,, \qquad (1.7)$$

where n depends on the flow regime, and its range suggests that the effect of the superficial gas velocity on the gas holdup in both the homogeneous and heterogeneous flow regimes is strongly dependent on the physical properties of the system, operating conditions, as well as the design parameters of the column.

Effect of the physical properties of the liquid on α_g

The properties of the liquid phase affect bubble formation and/or coalescing tendencies. Therefore, liquid phase properties are important factors influencing gas holdup. When liquid dynamic viscosity increases, large bubbles are produced, where their rising velocities are higher, and this will lead to a lower gas holdup. The influence of the liquid properties can have a major impact on the gas holdup, especially if the liquid has high dynamic viscosity such as CuCl molten salt. The effect of the surface tension on α_g is also significant. Increasing the surface tension will help the formation of more gas bubbles within the liquid.

Changing the temperature can also alter the physical properties of the liquid. In the oxygen reactor, the decomposition process takes place at a temperature of about 530^{o}C, and under such high temperature, the molten salt dynamic viscosity and surface tension are decreased. Thus, the hydrodynamic of the reactor

changes significantly and the data obtained at ambient condition should not depict the actual performance of the oxygen reactor.

Effect of liquid velocity on α_g

In principle, gas holdup will decrease for co-current upward flow, while for a counter-current liquid flow, gas holdup will increase (Otake et al., 1981). In the oxygen reactor, molten salt is moving upward with a relatively low velocity due to the overflow. There are different methods to correlate gas holdup with the liquid velocity (Hills, 1976). In general, if the liquid velocity remains below 30 cm/s, its influence on α_g can be neglected (Hills, 1976). In this thesis, the influence of the overflow velocity on α_g is neglected.

Effect of solid concentration and size on α_g

In SBCRs, the volumetric solid concentration greatly affects the hydrodynamics. Solid particles concentration in the liquid phase changes the slurry physical properties namely increase the density, and the dynamic viscosity. Because of the increase in the dynamic viscosity of the slurry phase, the gas holdup will decrease with solid concentration. This will enhance the creation of large gas bubbles which will increase the bubble rise velocity and will reduce the residence time of the bubbles in the reactor.

Effect of reactor size on α_g

The hydrodynamics of SBCRs depend significantly on the column geometry (Deckwer, 1992). It has been found that the aspect ratio (ratio of height of the reactor to its diameter (H_R/D_R)) has a significant effect on gas holdup (Kastanek et al., 1984; Pino et al., 1992; Wilkinson et al., 1992). In this thesis, the effect of the aspect ratio on gas holdup for highly viscous slurry is studied by considering different heights of the reactor column with the same diameter.

Effect of gas distributor on α_g

Gas distributors have significant effects on the scale-up of SBCRs (Behkish, 2004). The type of the gas sparger can affect the values of the gas holdup. There are many types of gas spargers with different sizes and numbers of orifices, such as; perforated plate, porous plate, membrane, ring type distributors and arm spargers (Behkish, 2004). Figure 1.5 illustrates some of gas distributors. In this thesis, a spider type sparger with six arms is used.

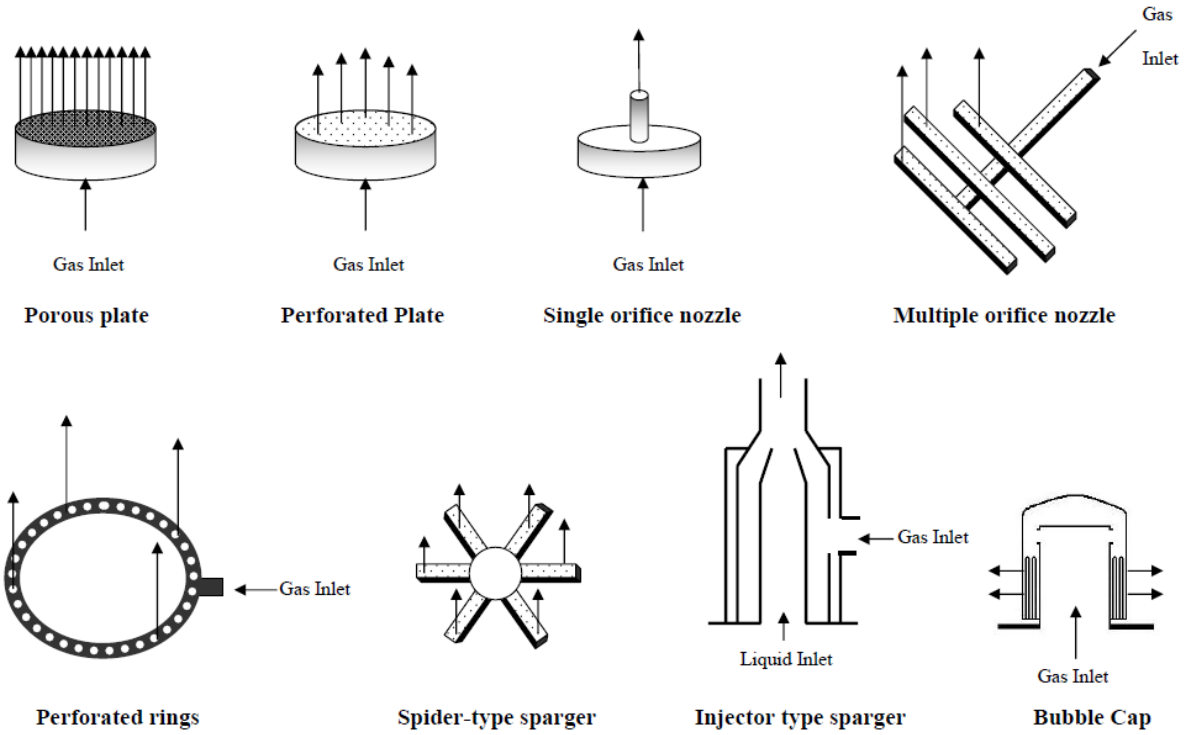

Fig. 1.5 Different types of gas distributors employed in bubble and slurry bubble column reactors (Behkish, 2004).

1.1.3.2. Heat Transfer in SBCRs

Thermal control in the oxygen reactor is important, since the decomposition reaction is an endothermic reaction. Because of the high heat transfer rates of the bubble columns, they have been widely used in different industrial applications (Deckwer, 1992). Direct contact heat transfer can occur whenever two substances at different temperatures come into physical contact. In this way, where there is no

intervening wall, the thermal resistances are small and the rate of energy transport between the two substances will be high. Also, the physical interaction between the two substances can lead to a mass transfer between them, which in some cases, is not a desirable phenomenon (Bejan & Kraus, 2003). This thesis investigates the heat transfer between the hot gaseous bubbles and the slurry directly without any heating object.

The local instantaneous heat transfer coefficient h (W/m^2.^{o}C) for a gaseous bubble to bed system, can be calculated from the following relation (Nigar et al., 2005);

$$h = \frac{Q}{\Delta T} \qquad (1.8)$$

where ΔT is the temperature difference between the bubble surface and the bulk, and Q is the corresponding heat transfer flux. The basic parameters that can influence the heat transfer rate are; the superficial gas velocity, solid particle size and concentration, liquid viscosity, solid particle density and column dimensions (Nigar et al., 2005).

1.2. Motivation

In spite of the fact that SBCRs are simple in construction, accurate scale-up of such reactors requires a comprehensive knowledge of the hydrodynamic and heat transfer characteristics at the same conditions of the targeted process (Shaikh, 2007). This scale-up generally depends on the evaluation of heat transfer and mixing characteristics, as well as chemical kinetics of the reacting system (Nigar et al., 2005). In the oxygen SBCR, the hydrodynamics affect the mixing rate and gas-slurry interfacial area, which also affect the volumetric heat transfer coefficient, which is the heat transfer coefficient based on the volume of the reactor, and hence affect the decomposition process rate. Scale up analysis in the oxygen SBCR is complex, because it depends on the fluid dynamic phenomena and heat transfer properties. Various design parameters (e.g., reactor dimensions, sparger design, etc.) and operating parameters (e.g., system pressure and temperature, gas and slurry flow rates, solid particles size and concentration, etc.)

along with phase properties and kinetics, affect the reactor hydrodynamics and heat transfer rates in the oxygen SBCR (Shaikh, 2007). Because of that, the hydrodynamics of the SBCRs have still not recognized very well.

The thermal decomposition process inside the oxygen reactor needs to be carried out for a moderate viscous molten salt slurry at high temperature, high solid particles loading, and in reactors with large diameters. The studies of the literature that are performed on the hydrodynamics of molten salts are limited to some of these conditions, such as molten salts at high temperatures but in small diameter reactors and no solid particles loading (Cho et al., 2002). Also, the reported heat transfer studies in SBCR have been limited to the heat transfer between the slurry and the surface of either the reactor wall or an internal object (Nigar et al., 2005). In the literature, there is no reported work related to the studies of hydrodynamics and direct contact heat transfer studies of SBCR at the conditions of the oxygen reactor. Therefore, the lack of such studies motivates the present work, which looks to fill this lack by investigating the oxygen SBCR using water liquid and helium gas phases at lower temperatures to mimic the high temperature molten CuCl liquid and oxygen gas.

In general, there are many advantages of using slurry bubble column reactors for oxygen production that motivates doing more detailed studies with this type of reactors. These advantages are; higher decomposition rate per unit volume; better temperature control; lower pressure drop; and high volumetric heat transfer rates. Additional advantages include; higher values of effective interfacial areas; relatively cheap to construct and operate, require less floor space (Shah et al., 1982); and no challenges of material selection for heating jacket or insertions because of the highly corrosive contents.

In summary, this work aims to investigate the hydrodynamics and direct contact heat transfer between gas bubbles and the slurry under the operating conditions of the oxygen reactor in the Cu-Cl cycle. These investigations include both experimental and numerical studies. The experimental results are used to evaluate and validate the computational fluid dynamics (CFD) models that are developed for the scale up of the oxygen reactor. The case studies that are

investigated in this thesis can be divided into two main sections which are; hydrodynamics and heat transfer.

1.3. Objectives

The design and scale-up of the oxygen reactor must be studied from different perspectives, such as; kinetics, hydrodynamics, mass and heat transfer. In this thesis, the overall objective is to study the scale up analyses of the oxygen reactor from the perspectives of hydrodynamics and heat transfer in a steady state condition. In order to achieve this objective, experimental and numerical works will be conducted in a pilot-scale slurry bubble column reactor. The experimental works will be performed with alternative materials that are safe to be used in the lab and simulate the industrial conditions of the oxygen reactor from the perspectives of hydrodynamics and heat transfer. The experimental works of this thesis, aim to achieve the following objectives;

- To determine the optimal heat transfer configuration by using the direct contact heat transfer from the pre-heated stoichiometric oxygen gas to the slurry of the molten CuCl and the solid Cu_2OCl_2. The stoichiometric oxygen gas produced at 530^{o}C, can be heated to a higher temperature by using a nuclear reactor heat source. Then, the heated oxygen gas can be re-injected into the oxygen reactor from the bottom, to directly transfer the heat required for the decomposition process to the slurry of the oxygen reactor.
- To specify the type of the flow regime that will exist in the oxygen reactor by determining the transition velocity of the gas. Furthermore, the effects of the static liquid height and the solid particles concentration on the transition velocity, will be investigated.
- To investigate the most important parameters of the hydrodynamics and heat transfer in the oxygen SBCR, such as; the overall gas holdup and the volumetric heat transfer coefficient. Moreover, the effects of the superficial gas velocity, static liquid height and the solid particles concentration on these parameters will be examined.

- To formulate new forms of empirical equations for the overall gas holdup and the volumetric heat transfer coefficient for different flow regimes. The empirical equations will be formulated in terms of the design and input parameters only.

The purpose of the numerical works is to develop and validate new predictive CFD models by using the well-known software packages (ANSYS FLUENT). The CFD models will be developed by using two dimensional simulations to predict the values of the gas hold-up and the volumetric heat transfer coefficient at different superficial gas velocities, static liquid heights and solid concentrations.

1.4. Summary

Large scale production of hydrogen can be achieved by integrating the nuclear reactors with the low temperature thermochemical Cu-Cl cycle. The highest temperature step in the Cu-Cl cycle is the oxygen production step in which the endothermic decomposition reaction of the Cu_2OCl_2 solid particles requires a large amount of heat and a sufficiently high transfer rate for the heat.

In the oxygen reactor, the total amount of heat required to achieve this reaction is the reaction heat (129.2 KJ/mol) plus the heat required to raise the reactant temperature from 375^{o}C to 530^{o}C. This heat can be provided from nuclear reactors such as SCWR and HTGR. Direct and indirect contact heating are two possible methods of heating the reaction system. Each heating method has some advantages and disadvantages.

The most efficient way to meet the heat transfer requirements is to use a direct contact heat transfer where the heat is transferred directly from oxygen gas bubbles to the Cu_2OCl_2 solid particles through the CuCl molten salt. The motion of the oxygen bubbles help also in agitating the slurry bed inside the oxygen reactor, which enhances the heat transfer rate. The thermal design of the oxygen reactor is affected by some factors which are; terminal settling velocity of particles, oxygen bubbles, reactor heating rate and fouling. This thesis investigates the thermal hydraulics of the slurry bubble column oxygen reactor by examining the heat transfer rate and the hydrodynamics of this system experimentally and numerically.

1.5. Thesis Organization

The remaining chapters of the thesis are organized as follows. Chapter 2 reviews the literature that is relevant to this work. Material simulation, experimental setup and procedure of the SBCR are presented in Chapter 3. Chapter 4 examines the CFD simulations of both hydrodynamic and heat transfer in the slurry bubble column oxygen reactor. The experimental and numerical results and discussion of the results are presented in Chapters 5 and 6. Finally, Chapter 7 contains the conclusions and future works.

CHAPTER 2
LITERATURE SURVEY

2.1. Oxygen Reactor in the Thermochemical Cu-Cl Cycle

There are many studies in the literature about hydrogen production copper-chlorine (Cu-Cl) cycle. Orhan (2011) has studied the simulations of Aspen Plus of the copper oxychloride (Cu_2OCl_2) thermal decomposition in the Cu-Cl cycle (Naterer et al., 2011b). Ikeda and Kaye (2008) have investigated the thermochemical properties of Cu_2OCl_2 by developing a method that uses a stoichiometric amounts of CuO and $CuCl_2$ instead of Cu_2OCl_2 because of its commercial unavailability (Naterer et al., 2011b). Trevani et al. (2011) have also examined the thermochemical properties of Cu_2OCl_2 by using an easy scalable method to produce pure samples of copper oxychloride with larger amounts (Naterer et al., 2011b). Zamfirescu et al. (2010) have investigated the thermo physical properties of copper compounds in the Cu-Cl cycle such as; Cu_2OCl_2, CuO, $CuCl_2$ and CuCl. Since there is no previous available data related to the thermal conductivity and dynamic viscosity of molten CuCl, they have used estimations to evaluate these properties.

Serban et al. (2004) have examined another method to produce oxygen, by decomposing an equimolar mixture of CuO and $CuCl_2$ at 500^{o}C (Marin et al. 2011). Lewis et al. (2003, 2005) have studied the oxygen production reaction experimentally by using a stoichiometric mixture of CuO and $CuCl_2$. They have found that the yield of oxygen was 85% when the mixture of CuO and $CuCl_2$ was heated to 500^{o}C (Marin et al. 2011).

Marin (2012) has studied experimentally and theoretically the scale-up of the CuO*$CuCl_2$ decomposition reactor. He has determined the endothermic reaction rate of the decomposition process, and solved numerically, the conservation and chemical reaction equations for a suddenly immersed particle in a viscous medium. Naterer et al. (2008b) have studied the thermal design of the oxygen reactor in the Cu-Cl cycle and discussed the main challenges and the possible solutions for them. Also, they have discussed in details the mixing process by bubbles in the

molten salt. They have concluded that bubbles may increase the contact area between solid particles and molten CuCl, which will lead to an increase in the heat transfer rates (Marin et al. 2011).

Abdulrahman et al. (2013), have studied the scale up of the oxygen reactor in the Cu-Cl cycle from the perspective of material balance for different hydrogen production rates and different residence times. They have investigated in details the factors that influence the size of the oxygen reactor, such as; solid particles characteristics (size, shape and concentration), oxygen bubbles, reactor heating rate and fouling.

Abdulrahman (2016a; 2016b), has investigated the thermal scale up analyses of the oxygen continuous stirred tank reactor (CSTR), by using indirect heat transfer methods, such as; a half pipe jacket (Abdulrahman, 2016a), and an internal helical tube (Abdulrahman, 2016b). He has examined the size of the oxygen CSTR for different hydrogen production rates, and different heat sources of nuclear reactors. He has reported that the size of the oxygen CSTR that is heated indirectly, is dominated by the heat balance rather than the material balance. Also, he has found that the dominant contribution to the total thermal resistance of the oxygen CSTR system is from the reactor wall when using a half pipe jacket (Abdulrahman, 2016a), and is from the helical tube wall and the service side when using an internal helical tube (Abdulrahman, 2016b). Furthermore, he has concluded that using a nuclear reactor of the type High Temperature Gas Reactor (HTGR) reduces the size of the oxygen CSTR by 3 to 4 times than that when using the CANDU Super Critical Water Reactor (CANDU-SCWR).

2.2. Slurry Bubble Column Reactor

In the literature, there are many studies related to SBCRs, such as hydrodynamics and flow regimes, as well as design and scale up analyses. Nigar et al. (2005) have reviewed bubble column reactors (BCRs) by focusing on the reactor design, fluid dynamics and flow regime transitions of reactors. The most investigated parameter was gas holdup and for gas velocities up to 35 cm/s. They

have presented a general summary of SBCRs reviewed from previous literature as shown in Table 2.1.

Table 2.1 Summary of the slurry system properties of several past studies (Nigar et al., 2005).

Author	System	Column-gas distributor	Gas velocity (cm/s)	Parameters investigated
Deckwer et al. (1980)	Nitrogen–molten paraffin-catalyst particles (Fischer–Tropsch process), 5 mm powdered Al_2O_3 catalyst particles concentration up to 16% (w/w)	4.1 and 10 cm I.D. column, perforated plate sparger with 75 mm hole diameters	Up to 4	Gas holdup, heat transfer
Saxena et al. (1990)	Air–water and air–water–glass beads, glass beads of 50, 90, 143.3 mm diameter, up to 20% (w/w) concentration	30.5, 10.8 cm I.D. columns, perforated plate sparger	Up to 28	Gas holdup, bubble characteristics
Pino et al. (1992)	Air–kerosene-four different solid particles, with 1.5, 5, 90, 135 mm diameters, concentration between 0 and 500 kg/m^3	29 and 10 cm I.D. columns, perforated plate distributor with 3 mm hole diameters	Up to 15	Gas holdup
Li and Prakash (1997)	Air–water–glass beads of 35 mm diameter and concentration up to 40% (v/v)	0.28 m I.D. column, 6-arm distributor with 1.5 mm	5–35	Gas holdup

Table 2.1 Summary of the slurry system properties of several past studies (Nigar et al., 2005) (Continued).

Author	System	Column-gas distributor	Gas velocity (cm/s)	Parameters investigated
Krishna et al. (1997)	Air–parafinic oil–silica particles, concentration up to 36% (v/v), with size distribution: 10% < 27 mm; 50% < 38 mm; 90% < 47 mm	10–19–3 cm I.D. columns, perforated plate sparger with 50 mm hole diameters		Gas holdup, bubble characteristics
Luo et al. (1999)	Paratherm NF heat transfer fluid-nitrogen gas–alumina particles, particle diameter 100 mm with solids volume fractions up to 0.19	10.2 cm column I.D., perforated plate sparger with 1.5 mm hole diameters	Up to 45	Gas holdup, bubble characteristics (bubble sizes, rise velocity and holdup)
Li and Prakash (1999)	Air–water–glass beads, 35 mm glass beads of concentration up to 40% (v/v)	0.28 m I.D. column, 6-arm sparger with 1.5 mm hole diameters	5–35	Gas holdup, bubble characteristics, heat transfer
Li and Prakash (2000)	Air–water and Air–water–glass beads, 35 mm glass beads of concentration up to 40% (v/v)	0.28 m I.D. column, 6-arm sparger with 1.5 mm hole diameters	5–35	Gas holdup, bubble characteristics

2.2.1. Hydrodynamics

2.2.1.1. Flow Regimes

Because of the importance of flow regimes in the hydrodynamics of the slurry bubble column reactors, lots of studies can be found in the literature regarding this area. For homogeneous regime, Kawagoe et al. (1976) have shown that the gas holdup has a linear increase with the superficial gas velocity in the homogeneous flow regime. Thorat and Joshi (2004) have found that, in the heterogeneous flow, the average size of the bubble is controlled by the coalescence and break-up processes (Hibiki and Ishii, 2000; Millies and Mewes, 1999; Olmos et al., 2001; Wu et al., 2001). In the slug flow, it has been shown that bubble slugs can be formed more frequently when the diameter of the column is less than 15 cm (Nigar et al., 2005). Nevertheless, the high viscosity, or a contamination of the liquid have been found to facilitate the formation of slugs even at very low superficial gas velocity (Anderson and Quinn, 1970; Schumpe, 1981).

Different studies have been performed to investigate the boundaries of the flow regimes in bubble column reactors. For example, it has been shown that bubbly flow regime dominates when the superficial gas velocity is less than 4 cm/s (Hyndman et al., 1997; Pino et al., 1992), while, Schumpe and Grund (1986) proposed this velocity to be less than 5 cm/s. The transition superficial gas velocity ($U_{g-trans}$) and gas holdup ($\alpha_{g-trans}$) from homogeneous to heterogeneous flow regimes for the air-water system, are shown in Table 2.2 (Joshi et al., 2001; Nigar et al., 2005). From this table, it can be seen that the transition velocity of air-water system can range from 3 to 5 cm/s.

Table 2.2 Experimental values of the transition velocity and gas holdup for air–water system bubble columns (Joshi et al., 2001; Nigar et al., 2005).

Author	$U_{g-trans}$ **(m/s)**	$\alpha_{g-trans}$
Bach and Pilhofer (1978)	0.046	0.277
Oels et al. (1978)	0.039	0.178
Krishna et al. (1991)	0.033	0.198
Yamashita and Inoue (1975)	0.040	0.234
Hyndman et al. (1997)	0.037	0.137

In the literature, transitions velocity correlations are basically empirical or semi-empirical. The main disadvantage of these correlations is that they are used for specific cases according to the operating and design conditions of the experiments and they consider the effects of only specific parameters (Mena et al., 2005). Unfortunately, for water-helium system (the system that is used in this thesis), there are not many of them available at present. Two such experiments were performed by Krishna et al. (1991) and Reilly et al. (1994). Krishna et al. (1991) have performed experiments at pressures range of (0.1 -2MPa) with different gases such as; N_2, CO_2, Ar, He and SF_6 in deionized water. The dimensions of the bubble column were 0.16 m diameter and 1.2 m height. For water-helium experiments, the pressure range was from 0.1-0.7MPa and the temperature was ambient temperature. The superficial gas velocity at the regime transition point, $U_{g-trans}$, was related to the gas density (ρ_g) for all experiments in water, including the effects of both pressure and molar mass as shown in Fig. 2.1.

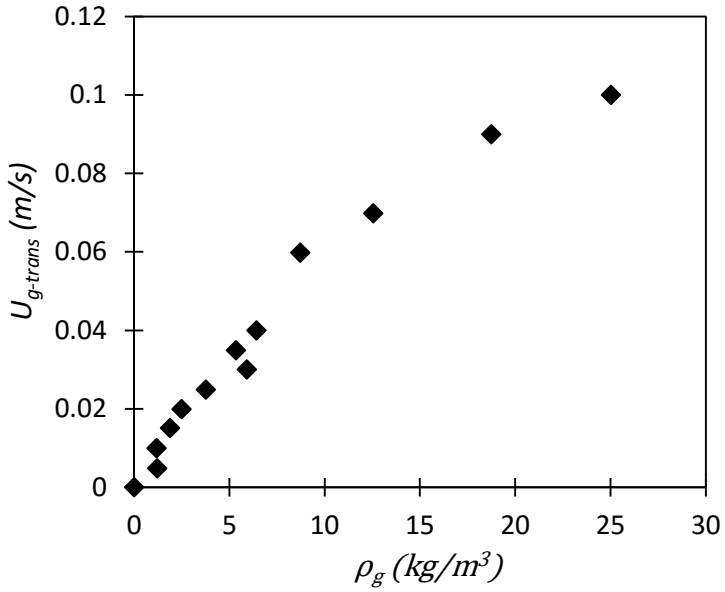

Fig. 2.1 Regime transition velocity $(U_{g-trans})$ versus gas density (ρ_g) in water (reproduced from Krishna et al. (1991).

Reilly et al. (1994) have performed experimental studies in a column with a diameter of 15 cm. They have studied the influence of gas density on the transition

of flow regime by using different gases such as; He, N_2, air, Ar and CO_2 in the water and non-aqueous liquids. They have proposed the following correlations of transition gas holdup $(\alpha_{g-trans})$ and transition superficial gas velocity $(U_{g-trans})$;

$$\alpha_{g-trans} = 0.59\ (B)^{1.5} \left[\frac{\rho_g^{0.96}\ \sigma^{0.12}}{\rho_l}\right]^{0.5}, \tag{2.1}$$

$$U_{g-trans} = \frac{1}{2.84}\ \frac{1}{\rho_g^{0.04}}\ \sigma^{0.12}\ \alpha_{g-trans}\left(1-\alpha_{g-trans}\right), \tag{2.2}$$

where $B = 3.85$, ρ_g and ρ_l are gas and liquid densities (Kg/m^3) respectively, σ is the liquid surface tension (N/m).

A comprehensive study of the published works on $U_{g-trans}$ from homogeneous to heterogeneous flow regimes has been done by Sarrafi et al. (1999), where it can be seen that $U_{g-trans}$ generally lies in the range of 0.044-0.067 m/s. Nevertheless, regime transitions in bubble columns are still under investigation and several methods such as particle image velocimetry (PIV), laser Doppler velocimetry (LDV), and computer-automated radioactive particle tracking (CARPT) are being employed to determine the flow behavior of the bubble column reactors (Lee et al., 2001; Vial et al., 2001).

Shaikh and Al-Dahhan (2007) have reviewed most hydrodynamic studies that investigated the flow regime transition in bubble columns. They have summarized the reported experimental studies, along with their operating and design conditions. Table 2.3 summarizes the effects of various operating and design conditions on flow regime transition.

Table 2.3 Generalized effect of operating and design parameters on flow regime transition (Shaikh and Al-Dahhan, 2007).

Parameter	Effect on Flow Regime Transition	Reference
Pressure	In general, an increase in pressure results in an increase in transition velocity	Krishna et al. (1991); Lin et al. (1999); Reilly et al. (1994); Shaikh and Al-Dahhan (2005); Wilkinson et al. (1992)
Temperature	An increase in temperature increases the transition velocity and delays flow regime transition	Bukur et al. (1987); Lin et al. (1999)
Viscosity	An increase in viscosity, in general, advances flow regime transition	Ruzicka et al. (2001b); Wilkinson (1991)
Surface tension	Reduction in surface tension increases transition velocity	Urseanu (2000)
Solids loading	An increase in solids loading, in general, decreases transition velocity	Krishna et al. (1999); Mena et al. (2005); Shaikh and Al-Dahhan (2006); Vandu (2005)
Sparger (hole size)	Transition velocity decreases with an increase in the hole size up to certain hole size.	Jamialahmadi et al. (2000); Sarrafi et al. (1999)
Sparger (perforation pitch)	Transition velocity increases with perforation pitch and then remains the same after certain critical value	Jamialahmadi et al. (2000); Sarrafi et al. (1999)
Liquid height	An increase in liquid height reduces the transition velocity	Ruzicka et al. (2001a); Sarrafi et al. (1999)
Column diameter	Conflicting results. An increase in column diameter increases transition velocity (Group 1) while column diameter advances flow regime transition (Group 2)	Group 1: Jamialahmadi et al. (2000); Ohki and Inoue (1970); Sarrafi et al. (1999); Urseanu (2000) Group 2: Ruzicka et al. (2001a); Zahradnik et al. (1997)
Aspect ratio	Aspect ratio decreases the transition velocity. However, it alone is not sufficient to provide reliable information on flow regime stability	Ruzicka et al. (2001a); Thorat and Joshi (2004)

Effect of Operating Pressure

Most researchers have reported that transition velocities increase with increasing pressure (Chilekar et al., 2005; Lin et al., 2001; Lin et al., 1999; Reilly et al., 1994;, Shaikh and Al-Dahhan, 2005; Wilkinson, 1991). Krishna et al. (1991) have found that the transition velocity increases by increasing the density of the gas (Nigar et al. 2005). Letzel et al. (1997), and Lin et al. (1999) have studied the effect of pressure on the flow regime transition from homogeneous to heterogeneous flow in bubble column reactors and have found that the transition was delayed with increasing system pressure. Their studies showed that both the gas velocity and gas holdup at the regime transition increase by increasing the density of the gas, i.e., system pressure.

Effect of Temperature

There are few studies that have examined the effect of temperature on flow regime transition (Bukur et al., 1987; Grover et al., 1986; Lin et al., 1999). The effect of temperature can be accounted for by the change in physical properties of fluid. Lin et al. (1999) have performed some experiments in a column with a nitrogen-Paratherm system at various temperatures (298-350 K) and operating pressures (0.1-15MPa). They have observed that, due to generation of small bubbles, flow regimes are sustained at higher velocities with an increase in temperature. An increase in pressure and temperature was found to have a favorable effect on flow regime stability and results in increasing transition velocity. They also found that transition velocity does not vary as pressure exceeds a critical value, particularly at higher temperature.

Effect of Viscosity

The liquid phase viscosity has been found to have a significant impact on the hydrodynamic characteristics of bubble columns. When the viscosity increases, this will lead to a stable bubble interface and then an increase in coalescence rate and decrease in breakup rate. This gives rise to an early occurrence of large bubble and hence should advance the flow regime transition.

Ruzicka et al. (2001b) have examined the influence of viscosity by using an air-aqueous solution of glycol in a column at ambient conditions with a diameter of 0.14 m. They have found that for dynamic viscosities between 3-22mPa-s, the homogeneous regime will be destabilized, thereby reducing transition velocity. For dynamic viscosities between 1-3mPa-s, the homogeneous regime will be stabilized, thereby increasing the transition velocity as viscosity increases in this narrow range.

Effect of Surface Active Agents

Gas holdup behavior in the presence of alcohols has been studied by various authors (Kelkar et al., 1983; Schügerl et al., 1977; Urseanu, 2000; Zahradnik et al., 1997). The only difference between water and aqueous alcohol solutions is the surface tension. The presence of alcohols in water systems reduces surface tension and hence induces non coalescing tendencies in the system.

Urseanu (2000) has examined the influence of the percentage of ethanol in water on gas holdup and transition. Using dynamic gas disengagement (DGD) in various column diameters at ambient pressure, they have observed a larger number of small bubbles in alcohol solution than in water. In alcohol solutions, the flow regime transition was found to be delayed due to suppression of the coalescing tendencies of small bubbles.

Effect of Solids Concentration

In slurry bubble columns, there are various studies that have investigated the influence of solids concentration on gas holdup (Behkish, 2005; Krishna et al., 1999; Ruthiya, 2005). When adding solids to the liquid, the ‘pseudo-viscosity’ of the liquid phase will increase and the interface will stabilize. Hence, the coalescence rate is increased and the breakup rate is reduced, resulting in an early appearance of large bubbles.

Mena et al. (2005) have investigated the influence of solids concentration on flow regime stability in a 0.14 m diameter column using air, distilled water, and calcium alginate beads. They have found that transition velocity increases with

solids loading up to 3 % vol. and then decreases at higher solids loading (> 3 % vol.). A possible explanation for such dual effect behavior is based on bubble-particle interaction. The stabilizing and then destabilizing effects with an addition of solids appear qualitatively similar to those observed by Ruzicka et al. (2001b), who have increased viscosity by an addition of glycerol.

Vandu and Krishna (2004) and Shaikh and Al-Dahhan (2006) have observed a decrease in transition velocity when increasing solids concentration, without the maximum as observed by Mena et al. (2005). However, it is worth mentioning that these authors have not studied low solids loading in the range between 0-3 % vol. where Mena et al. (2005) observed a maximum in transition velocity. In addition, the particle size used by Mena et al. (2005) was larger (2.1 mm) than the one commonly employed in slurry bubble columns and also used by these authors (50-150 μm).

Jamialahmadi and Muller-Steinhagen (1991) have shown that the change in gas holdup in the air-water system by adding solids, depends on the kind of the solids. It has been found that gas holdup will decrease by adding non-wettable solids, while gas holdup will increase when adding wettable solids. Hence, the effect of solids on transition velocity needs to be studied in terms of the nature of the solids.

Effect of the Sparger

In general, the effect of the sparger is dominant in bubbly flow and diminishes in churn turbulent flow. The bubble sizes in the bubbly flow is the direct result of the nature of distributor. Sarrafi et al. (1999) have examined the impact of sparger configurations on transition velocity using reported data on gas holdup and also their own data in the air-water system. They have reported that, for a hole diameter $< 1.5\,mm$, the transition velocity will decrease with increasing the diameter, and for a hole diameter $> 1.5\,mm$, the effect of the hole diameter on the transition velocity is negligible.

Effect of Liquid Height

In general, it has been observed that, due to gravity effect an increase in liquid height decreases overall gas holdup up to a certain height. Beyond this height, however there is an insignificant influence on overall gas holdup (Wilkinson, 1991). Sarrafi et al. (1999) have found that an increase in liquid static height decreases the transition velocity up to 4 m, and beyond this, it almost becomes independent of liquid static height. Ruzicka et al. (2001a) have performed experiments in three different diameter columns (0.14, 0.29, and 0.4 m) in an air-water system. They have found that an increase in liquid static height, in general, reduces transition velocity.

Effect of Column Diameter

In general, it is believed that, when increasing the column diameter, the overall gas holdup will decrease, up to a critical column diameter. Beyond this critical value, column diameter has an insignificant impact on overall gas holdup. Many authors have found the critical value of column diameter to be around 0.15 m (Kastanek et al., 1984; Wilkinson, 1991; Yoshida and Akita, 1965; Sarrafi et al., 1999). Forret et al. (2003) have shown that the influence of column diameter on overall gas holdup is insignificant for a range of diameters between 0.15 to 1 m (Shaikh, 2007).

Effect of Aspect Ratio

Reactor dimensions are generally expressed in terms of the dimensionless aspect ratio (H_R/D_R). An increase in aspect ratio reduces overall gas holdup. However, according to Wilkinson (1991), above $H_R/D_R = 5$, aspect ratio has little effect on overall gas holdup, and have suggested to use an aspect ratio larger than 5 for scale up purposes. Thorat and Joshi (2004) have performed experiments in an air-water system and studied the effect of aspect ratio on flow regime transition. They have found that an increase in aspect ratio decreases transition gas holdup. However, their experiments were performed using only one column diameter (0.385 m). Ruzicka et al. (2001a) have studied the effect of aspect ratio on

transition velocity in an air-water system using columns of diameter 0.14, 0.29, and 0.4 m. For any particular diameter, the transition velocity showed a decreasing trend with an increase in aspect ratio.

Summary

The following points are summarized from the literature survey of the flow regimes in SBCRs;

- The transition gas velocity depends on the system physical properties, as well as on column dimensions and sparger design.
- In general, the transition velocity ranges between 0.033 to 0.067 m/s.
- The transition velocity increases with increasing the temperature of the system.
- The transition velocity increases with increasing the pressure of the system (or gas density).
- The transition velocity decreases with increasing the surface tension of the liquid.
- The transition velocity decreases with increasing liquid dynamic viscosity for moderate viscous liquids (3-22mPa.s), and increases for low viscous liquids (1-3mPa.s).
- The transition velocity decreases with increasing solid concentration when the solid concentration is more than 3%, and increases when the solid concentration is less or equal to 3%.
- The transition velocity decreases with increasing the sparger hole diameter, up to 1.5 mm, and the effect of the diameter is negligible after that.
- The column diameter has an insignificant effect on transition velocity when it is beyond around 0.15 m
- The transition velocity decreases with increasing the height of the static liquid up to 4 m and beyond this, it almost becomes independent of liquid height.
- The aspect ratio of the reactor has a little effect on the transition velocity when it is above 5.
- The formation of the slugs happens more frequently in columns of diameters less than 0.15 m

From above literature, it can be seen that, the transition regions boundaries can be determined according to the system studied. One of the major challenges that this thesis will study, is specifying the boundaries of the flow regime transitions in the oxygen reactor. Accordingly, it is possible to know in which regime the oxygen reactor can work to specify the operating conditions of the oxygen reactor and the type of the modeling. Most of the previous studies in flow regime transition were carried out in air-water systems. In this thesis, the flow regime transition is specified for molten salt of CuCl and oxygen gas.

2.2.1.2. Gas Holdup (α_g)

Gas holdup parameter is very important in the scale up of bubble columns. In a slurry bubble column, gas holdup can be expressed as (Nigar et al., 2005);

$$\alpha_g = 1 - \frac{1}{g\,(\rho_l \alpha_l + \rho_s \alpha_s)} \frac{\Delta P}{\Delta H} \qquad (2.3)$$

where, α is the phase holdup, g is the gravitational acceleration, ρ is the density, ΔP is the static pressure drop along the bed height ΔH, which is the height difference between pressure transducers. The subscripts g, l and s represent gas, liquid and solid phases respectively. In the literature, there are many different correlations to determine α_g in slurry bubble columns. Some of the gas holdup correlations that are frequently used in the literature are shown in Table 2.4 (Nigar et al. 2005).

Behkish (2004) has used two SBCRs with different diameters to measure the gas holdup for five different gases (N_2, H_2, CO, He and CH_4) in Isopar-M liquid. He also studied the effect of solid particles on α_g by using two different solids (Al_2O_3 powder and glass beads). The data were obtained under wide ranges of pressures (1-27 bar), superficial gas velocities (0.08-0.4 m/s), temperatures (323-453K), and solid concentrations (0-36 vol. %).

Cho et al. (2002) have measured gas holdup of air in a molten salt (molten sodium carbonate salt) oxidation reactor for various gas velocities and a temperature range of 870–970^{o}C. They have used the pressure drop measurement to evaluate the gas holdup experimentally. They have found that,

when the temperature is increased, the gas holdup will increase, and when the gas velocity is increased, the rate of increase of gas holdup will decrease.

Table 2.4 Correlations of gas holdup in bubble columns (Nigar et al. 2005).

Correlation	Reference
$\alpha_g = \frac{U_{gs}}{0.3 + 2\,U_{gs}}$	(Joshi and Sharma, 1979)
$U_{gs}\left(1-\alpha_g\right) + U_{ls}\,\alpha_g = V_b\,\alpha_g\left(1-\alpha_g\right)^{2.39}\left(1+2.55\,\alpha_g^3\right)$	(Lockett and Kirkpatrick, 1975)
$\alpha_g = \frac{U_{gs}}{31+\beta\,(1-e)\sqrt{U_{gs}}}$, $\beta = 4.5 - 3.5\,exp(-0.064\,D_R^{1.3})$ $e = -\frac{0.18\,U_{gs}^{1.8}}{\beta}$	(Koide et al., 1979)
$\alpha_g = 0.32\left(1-\alpha_g\right)^4\,Bo^{0.21}\,Ga^{0.086}\,Fr\left(\rho_g/\rho_l\right)^{0.068}$	(Saxena et al., 1990)
$\alpha_g = 0.728\,U' - 0.485\,U'^2 + 0.0975\,U'^3$ $U' = U_{gs}\left[\rho_l^2/\{\sigma(\rho_l-\rho_g)g\}\right]^{1/4}$	(Saxena et al., 1990)
$\alpha_g = \left(\frac{1+a\,P_V}{b\,P_V}\right)\left(\frac{U_{gs}\,\mu_l}{\sigma}\right)^{0.76}\left(\frac{\mu_l^4\,g}{\rho_l\,\sigma^3}\right)^{-0.27}\left(\frac{\rho_g}{\rho_l}\right)^{0.09}\left(\frac{\mu_g}{\mu_l}\right)^{0.35}$ $a = 1.1\times10^{-4}\;and\;b = 5\times10^{-4}$	(Saxena et al., 1990)
$\alpha_g = 0.17283\left(\frac{\mu_l^4\,g}{\rho_l\,\sigma^3}\right)^{-0.15}\left(\frac{U_{gs}\,\mu_l}{\sigma}\right)^{0.58}\left(\frac{P+P_V}{P}\right)^{1.61}$	(Saxena et al., 1990)
$\alpha_g = \frac{1}{2+(0.35/U_{gs})(\rho_l\,\sigma/72)^{1/3}}$	(Shimizu et al., 2000)
$\alpha_g = 1.07\,Fr^{1/3}$	(Kawase and Moo-Young, 1987)
$\frac{\alpha_g}{1+\alpha_g} = 0.0625\left(\frac{U_{gs}}{\nu_l\,g}\right)^{1/4}$	(Shimizu et al., 2000)
$\frac{\alpha_g}{\left(1-\alpha_g\right)^4} = \alpha\left(\frac{D_R^2\,\rho_l\,g}{\sigma}\right)^{\frac{1}{8}}\left(\frac{g\,D_R^3\,\rho_l^2}{\mu_l^2}\right)^{\frac{1}{2}}\frac{U_{gs}}{\sqrt{g\,D_R}}$ $\alpha = 0.2$ for pure liquids and non-electrolyte solutions $\alpha = 0.25$ for salt solutions	(Deckwer and Schumpe, 1993)
$\alpha_g = 0.505\,U_{gs}^{0.47}\left(\frac{0.072}{\sigma}\right)^{2/3}\left(\frac{0.001}{\mu_l}\right)^{0.05}$	(Ozturk et al., 1987)

Table 2.4 Correlations of gas holdup in bubble columns (Nigar et al. 2005) (continued).

Correlation	Reference
$\alpha_g = 0.672\, f \left(\frac{U_{gs}\,\mu_l}{\sigma}\right)^{0.578} \left(\frac{\mu_l^4\, g}{\rho_l\, \sigma^3}\right)^{-0.131} \left(\frac{\rho_g}{\rho_l}\right)^{0.062} \left(\frac{\mu_g}{\mu_l}\right)^{0.107}$ $f = 1$ for pure liquids and non-electrolyte solutions f is a function of ionic strength for ionic solutions	(Deckwer and Schumpe, 1993)
$\alpha_g = 0.009 + 296\, U_{gs}^{0.44}\, (\rho_l \text{ or } \rho_{sl})^{-0.98}\, \sigma^{-0.16}\, \rho_g^{0.19}$	(Saxena et al., 1990)
$\alpha_g = 0.239\, U_{gs}^{0.634}\, D_R^{-0.5}$, for viscous media in slug flow regime	(Deckwer and Schumpe, 1993)
$\frac{\alpha_g}{(1-\alpha_g)^3} = 0.019\, U_\infty^{1/16}\, \nu_s^{-0.125 U_\infty^{-0.16}} U_{gs}$	(Sada et al., 1984)
$\alpha_g = 0.2 \left(\frac{D_R^2\, \rho_l\, g}{\sigma}\right)^{-0.13} \left(\frac{g\, D_R^3\, \rho_l^2}{\mu_{sl,eff}^2}\right)^{0.11} \left(\frac{U_{gs}}{\sqrt{g\, D_R}}\right)^{0.54}$ $1.4 \times 10^3 \le Bo \le 1.4 \times 10^5$ $1.2 \times 10^7 \le Ga \le 6.5 \times 10^{10}$ $3 \times 10^{-3} \le Fr \le 2.2 \times 10^{-1}$	(Deckwer and Schumpe, 1993)
$\alpha_g = \left[2.25 + \frac{0.379}{U_{gs}} \left(\frac{\rho_l \text{ or } \rho_{sl}}{72}\right)^{0.31} (\mu_l \text{ or } \mu_{sl})^{0.016}\right]^{-1}$ $\mu_{sl} = \mu_l\, exp\left[\frac{(5/3)\, \nu_s}{1-\nu_s}\right]$	(Saxena et al., 1990)
$\alpha_g = 3.88 \times 10^{-3} \left[Re_T \left(\frac{\sigma_{H_2O}}{\sigma}\right)^{1/3} (1-\nu_s)^3\right]^{0.44}$ $Re_T > 500$, $\nu_s = \frac{W_s/\rho_s}{(W_s/\rho_s) + (W_l/\rho_l)}$	(Saxena et al., 1990)
$\frac{\alpha_g}{(1-\alpha_g)^4} = \frac{k_l \left(U_{gs}\, \mu_l/\sigma\right)^{0.918}}{1 + 4.35 \nu_s^{0.748} [(\rho_s - \rho_l)/\rho_l]^{0.88}} \frac{\left(g\, \mu_l^4/(\rho_l\, \sigma_l^3)\right)^{-0.252}}{\left(D_R\, U_{gs}/\rho_l\right)^{-0.168}}$	(Koide et al., 1984)

Effect of the Superficial Gas Velocity on Gas Holdup

Most published studies have shown an increasing trend of the gas holdup with superficial gas velocity in spite of the different systems that were investigated (Bach and Pilhofer, 1978; Deckwer et al., 1980; Daly et al., 1992; Hyndman et al., 1997; Krishna et al., 1997; Li and Prakash, 2000; Pino et al., 1992; Prakash et al., 2001; Saxena et al., 1990; Schumpe and Grund, 1986). In the bubbly flow regime,

it has been found that the increase of gas holdup is proportional to the superficial gas velocity (Kara et al., 1982; Lockett and Kirkpatrick, 1975), while in the churn turbulent regime, the influence of superficial gas velocity on gas holdup increase was found to have less effect (Kare et al., 1982; Koide et al., 1984). This less effect was attributed to the increase in large bubbles holdup with the constancy of small bubbles contribution to the overall gas holdup (Hyndman et al., 1997). However, in bubbly flow, the gas holdup of small bubbles increases significantly with the superficial gas velocity (Nigar et al. 2005).

Effect of the Physical Properties of the Liquid on Gas Holdup

It has been found that α_g decreases with increasing liquid viscosity (Godbole et al., 1984; Neme et al., 1997; Yasunishi et al., 1986). Crabtree and Bridgwater (1971) have explained this behavior by suggesting that high liquid viscosity promotes bubble coalescence. It is therefore, expected that the gas holdup of a high viscous liquid will be due to larger gas bubbles.

Effect of Operating Conditions on Gas Holdup

Most literature that studied the effect of pressure on α_g have found that the gas holdup of bubbles in various slurry bubble columns increased with increasing system pressure (Nigar et al., 2005). Several authors have attributed this increase to an increase of gas density (Reilly et al., 1994; Wilkinson and Dierendonck, 1990; Nigar et al., 2005). Therefore, it can be concluded that gases with higher molecular weight will lead to higher gas holdup. Clark (1990), however, has found that at low gas velocity, the gas holdup of N_2 was significantly lower than that of H_2. Only when the gas velocity was greater than 0.05 m/s, the trend was reversed and the gas holdup of N_2 became greater than that of H_2. He proposed that in the velocity range below 0.05 m/s, the gas holdup was more influenced by the gas bubble surface tension than pressure (Nigar et al., 2005). Pohorecki et al. (1999) have also observed no apparent impact of pressure on the values of gas holdup of N_2-water system in the velocity range of 0.002-0.02 m/s (Nigar et al., 2005). Kemoun et al. (2001) have measured the radial gas holdup in a bubble column for pressures up

to 7 bar and found that the average gas holdup increased with increasing pressure, and the gas holdup was higher at the center of the column than near the walls. It is, however, widely accepted that an increase of pressure is mainly responsible for reducing gas bubbles coalescence and subsequently increases the volume fraction of the small gas bubbles (Nigar et al., 2005). Saxena et al. (1990) have studied the effect of operating temperature on gas holdup. They have examined two and three-phase bubble columns with a temperature range of 297–343 K. They have concluded that gas holdup depends on temperature only in the two phase system (Nigar et al., 2005). Some studies have been conducted to determine the gas holdup in SBCs under high temperatures and Table 2.5 summarizes some of these studies available in the literature (Behkish, 2004).

Table 2.5 Available studies on high temperature bubble and slurry bubble column reactors (Behkish, 2004).

Author	System: gas/liquid/ solid	Condition	Column ID x Height	Remarks
Grover et al. (1986)	Air / H_2O, NaCl, $CuCl_2$	P_{atm} $U_{gs} = 0.001 - 0.045\ m/s$ $T = 30 - 80°C$	$0.1 \times 1.5\ m$	α_g decreased with T for air/H_2O but increased for air/electrolyte at low U_{gs}).
Zou et al. (1988)	Air / H_2O, Alcohol, 5%, NaCl	P_{atm} $U_{gs} = 0.01 - 0.16\ m/s$ $U_{ls} = 0.007\ m/s$ $T = 25 - 96.56\ °C$	$0.1 \times 1.05\ m$	α_g increased with U_{gs} and T.
Lau et al. (2004)	N_2, Air / Paratherm NF	$P\ up\ to\ 42.4\ bar$ $U_{gs}\ up\ to\ 0.4\ m/s$ $U_{ls} = 0.08 - 0.89\ cm/s$ $T\ up\ to\ 365\ K$	2 columns of 0.0508 and 0.1016 m I.D.	α_g increased with P and T. Influence of column diameter. Influence of U_{gs} and U_{ls} on α_g.
Deckwer et al. (1980)	N_2 / Paraffin wax / Al_2O_3	$P = up\ to\ 11\ bar$ $U_{gs}\ up\ to\ 0.04\ m/s$ $T = 416\ and\ 543\ K$ $C_s\ up\ to\ 16\ wt.\%$	2 Reactors of 0.04 and 0.1 m I.D.	α_g decreased with T in small column, but independent in large column. No effect of P on α_g.

Effect of Solid Concentration and Size on Gas Holdup

There are several studies that have investigated the impact of solid concentration and size on α_g. Most of these studies have found that gas holdup decreases by increasing solids concentration (Nigar et al., 2005; Behkish, 2004). Sada et al. (1984) have found that the effect of solids concentration is insignificant when the solids loading is less than 5 vol. %. On the contrary, Kara et al. (1982) have reported a significant effect of solids concentration on gas holdup at low solids loading. Kato et al. (1973) have found that solid concentrations affect gas holdup significantly when the gas velocities are higher than 10-20 cm/s (Nigar et al. 2005). de Swart et al (1996) have studied the gas holdup of air in a paraffin oil liquid and glass beads solid particles at atmospheric conditions. Their solid concentration was varied up to 20 vol. %. They have found that the holdup of the large gas bubbles was independent on the slurry concentration. This result was confirmed by Krishna et al. (1997) who used the same three phase system with solid concentration as high as 36 vol.% while using three different column diameters.

The knowledge of the slurry viscosity is therefore important for estimating the gas holdup in SBCRs. Table 2.6 summarizes some available correlations for predicting the slurry viscosity (Behkish, 2004). Figure 2.2 shows the slurry viscosity obtained from equations in Table 2.6 as a function of solid volumetric concentration. In this figure it can be seen that most correlations are independent of the nature of the solid particles. The correlation proposed by Riquarts (1978), however, takes into account the density of the particles.

Table 2.6 Available correlations for predicting slurry viscosity (Behkish, 2004).

Author	Correlation
Saxena and Chen (1994)	$\mu_{sl} = \mu_l(1 + 4.5\ C_s)$
Thomas (1965)	$\mu_{sl} = \mu_l\left(1 + 2.5\ C_s + 10.05\ {C_s}^2 + 0.00273\ e^{16.6\ C_s}\right)$
Guth and Simba (1936)	$\mu_{sl} = \mu_l\left(1 + 2.5\ C_s + 14.1\ {C_s}^2\right)$
Barnea and Mizrahi (1973)	$\mu_{sl} = \mu_l\ exp\left(\frac{\frac{5}{3}\ C_s}{1 - C_s}\right)$
Roscoe (1952)	$\mu_{sl} = \mu_l(1 - C_s)^{-2.5}$
Riquarts (1978)	$\mu_{sl} = \mu_l\left(1 + \frac{\rho_s + \rho_l}{\rho_l} C_s\right)(1 - C_s)^{-2.59}$
Vand (1948)	$\mu_{sl} = \mu_l\ exp\left(\frac{2.5\ C_s}{1 - 0.609\ C_s}\right)$

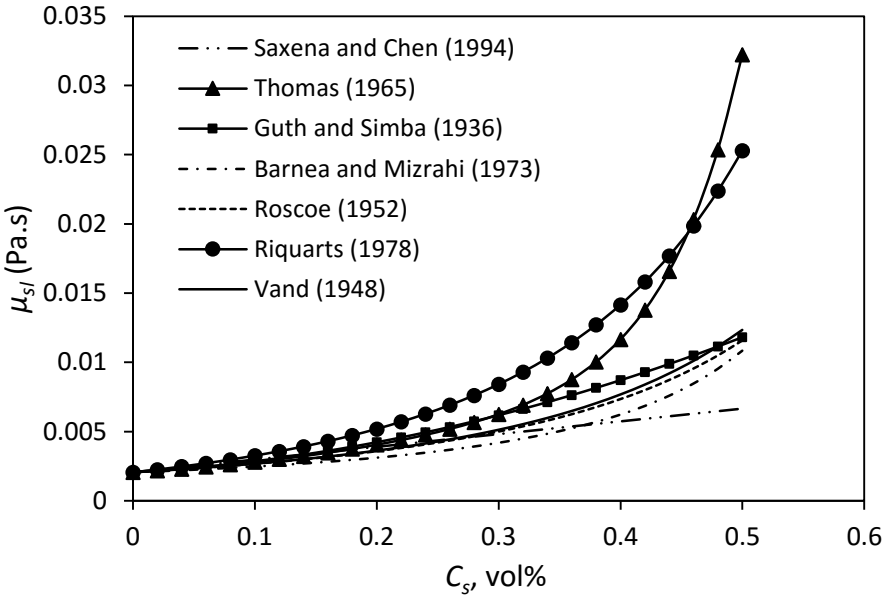

Fig. 2.2 Correlations for predicting slurry viscosity in molten salt CuCl.

Effect of Reactor Size on Gas Holdup

In the literature, the influence of column size on gas holdup is widely studied. It has been found that the influence of the column diameter on gas holdup is insignificant for a column diameter larger than 10-15 cm (Shah et al., 1982), and

the effect of the column height on gas holdup can be neglected for a height larger than 1-3 m and for an aspect ratio larger than 5 (Luo et al., 1999). Koide et al. (1984) have performed studies on gas holdup for the churn-turbulent flow regime. They have concluded that α_g values for a diameter of 0.218 and 0.3 m were equal, but less than α_g values for a diameter of 0.1 and 0.14 m (Behkish, 2004). Eickenbusch et al. (1995) have determined the effect of column diameter on the hydrodynamics by studying three columns with different diameters (0.19, 0.29 and 0.6 m) and different aspect ratios (10.2, 10.3 and 6.5), respectively. They have found that churn turbulent flow regime was dominant and the column diameter had a minor effect on gas holdup. Moustiri et al. (2001) have examined the gas holdup in the homogeneous flow regime in two columns with different diameters (0.15 and 0.2 m). They have found that gas holdup increases with decreasing column diameter when the superficial gas velocity is low. They have attributed this increase to the delay in gas bubble acceleration due to the prevailing wall effect (Behkish, 2004).

Effect of Gas Distributor on Gas Holdup

The design of the sparger can influence the initial size and distribution of the bubble created at the sparger orifice. It has been found that the initial bubble size cannot describe the size distribution of the bubbles along the total height of the bubble column, because of the gas bubbles breakup and coalescence (Behkish, 2004). Several studies have found that when the orifice diameters are larger than 1-2 mm, there is no significant influence on gas holdup by gas sparger (Behkish, 2004). Schügerl et al. (1977) have reported that the effect of the gas sparger on α_g is insignificant for a coalescing system such as water (Behkish, 2004). Pohorecki et al. (1999) have used different kinds of gas spargers. They have reported that there is no significant effect of the type of gas sparger on the gas holdup. Although Pohorecki et al. (1999) gave no further technical details of their spargers, it is believed that they used multiple orifice nozzles in their studies (Behkish, 2004).

Summary

The following summary can be considered from the literature survey of the gas holdup;

- α_g increases with increasing U_{gs}.
- α_g increases with increasing ρ_g.
- α_g decreases with increasing the dynamic viscosity of the liquid.
- α_g increases with increasing system pressure.
- α_g decreases with increasing C_s.
- The influence of D_R with α_g is insignificant for $D_R \geq 0.15\ m$.
- The effect of the H_R on α_g is negligible for $H_R \geq 4\ m$.
- The influence of the column aspect ratio on gas holdup is insignificant when it is larger than 5.
- The effect of gas sparger on α_g is negligible for orifice diameters $\geq 2\ mm$.

In this thesis, the gas holdup is investigated for different superficial gas velocities, different static liquid heights, and different solid concentrations, in the oxygen reactor system.

2.2.2. Heat Transfer Coefficient

In bubble columns, the majority of the previous heat transfer studies were related to the steady-state condition heat transfer of two cases: wall-to-bed and immersed object-to-bed heat transfer (Nigar et al., 2005). It has been found that the evaluation of instantaneous heat transfer coefficients can give more detailed description of heat transfer, while using average heat transfer coefficient can create a lack of knowledge of the instantaneous effect of bubble dynamics on heat transfer (Chen et al., 2003). There are several studies regarding the local instantaneous heat transfer coefficient such as; Kumar et al. (1992), Li and Prakash (1999, 2002) and Cho et al. (2002). Table 2.7 summarizes some of the heat transfer coefficient equations that are available in the literature for slurry bubble columns (Nigar et al., 2005).

Table 2.7 Heat transfer correlations for three phase slurry bubble columns (Nigar et al., 2005).

Author	Correlation	Reference
Zehner (1986)	$h = 0.18(1-\alpha_g)\left[\frac{k_l^2\,\rho_l^2\,C_{p,l}\,v_f^2}{d_p\left(\frac{\pi}{6\,\alpha_g}\right)^{\frac{1}{3}}\mu_l}\right]^{\frac{1}{3}}$, $v_f = \left[\frac{d_p\left(\frac{\pi}{6\,\alpha_g}\right)}{2.5}\left(\frac{\rho_l-\rho_g}{\rho_l}\right) g\, D_R\, U_{gs}\right]^{\frac{1}{3}}$ $Nu = 350.8\, Re^{0.108}\left(\frac{d_p}{d_o}\right)^{0.05}$, for $1 < \frac{d_p}{d_o} < 5$	(Saxena et al., 1990)
Kim et al., (1986)	$h = 0.0722\left(k_l\,\rho_l\,C_{P,l}\{[U_{gs}(\alpha_g\,\rho_g + \alpha_l\,\rho_l + \alpha_s\,\rho_s)]g(\alpha_l\,\mu_l)^{-1}\}^{1/2}\right)^{1/2}$	(Saxena et al., 1990)
Deckwer (1980)	$St = 0.1(Re\,Fr\,Pr^2)^{-0.25}$ where $St = \frac{h_w}{\rho_l\,C_p\,U_{gs}}$ $Re = \frac{U_{gs}\,d_p\,\rho_l}{\mu_l}$, $Fr = \frac{V_g^2}{g\,D_R}$, $Pr = \frac{C_p\,\mu_l}{k_l}$	(Deckwer, 1980)
Suh and Deckwer (1989)	$h = 0.1\left(k_l\,\rho_l\,C_{P,l}\{[U_{gs}(\alpha_s\,\rho_s + \alpha_l\,\rho_l + \alpha_g\,\rho_g)]\,g\,(\alpha_l\,\mu_b)^{-1}\}^{1/2}\right)^{1/2}$ where $\mu_b = \mu_l\,exp\left(\frac{2.5\,\nu_s}{1-0.609\,\nu_s}\right)$	(Saxena et al., 1990)

2.2.2.1. Effect of Superficial Gas Velocity on Heat Transfer Coefficient

There are several studies that examined the impact of superficial gas velocity on heat transfer coefficients in slurry bubble columns (Deckwer et al., 1980; Prakash et al., 2001; Saxena et al., 1990). In general, it has been reported that increasing superficial gas velocity will increase the heat transfer coefficients in slurry bubble columns regardless of the different types of systems. This increase was attributed to the increase of turbulence in the medium. (Nigar et al., 2005). Also, it has been found that the increasing rate of heat transfer coefficients with superficial gas velocity decreases by increasing the superficial gas velocity (Nigar et al., 2005).

2.2.2.2. Effect of Liquid Phase Properties on Heat Transfer Coefficient

The influence of liquid dynamic viscosity on heat transfer, has been investigated in different studies. It has been found that heat transfer coefficient will decrease by increasing the dynamic viscosity of the liquid in the three-phase systems (Nigar et al., 2005). This behavior is due to the decrease in turbulence for viscous liquids.

2.2.2.3. Effect of Solid Size and Concentration on Heat Transfer Coefficient

There are many studies in SBCs examined the impact of solid concentration and particle size on heat transfer coefficient (Nigar et al., 2005). Generally, it has been found that the impact of particle size on heat transfer coefficients is insignificant when the sizes of particle are larger than 3 mm, in particular for high superficial gas velocities. Deckwer et al. (1980) and Kolbel et al. (1960) have reported that the heat transfer coefficient increases with increasing solid concentrations, because of the changes in the thermo physical properties of the slurry when adding solids. On the contrary, Li and Prakash (1997) have noted that heat transfer coefficient decreases by increasing solid concentration, because of the decrease in turbulence as a result of increase in the viscosity of the medium with increasing solid concentration (Nigar et al., 2005).

2.2.2.4. Effect of Column Dimensions and Operating Conditions on Heat Transfer Coefficient

Saxena et al. (1990) have investigated the impact of column diameter on heat transfer. They have found that the measured heat transfer coefficients in a slurry bubble column with a diameter of (30.5 cm) were larger than that with a column diameter of (10.8 cm), because of the lower mixing rate in the smaller diameter column. The impact of the bed temperature on heat transfer coefficient has been studied by Saxena et al. (1990). They have found that the heat transfer coefficient will increase by increasing temperature, because of the reduction in liquid viscosity that leads to the increase in turbulence. Chen et al. (2003) have reported that increasing the operating pressure will lead to the increase of the heat transfer coefficient (Nigar et al., 2005)

Summary

The following summary are made from the literature survey of the heat transfer coefficients in bubble column reactors;

- The heat transfer coefficient increases with increasing system temperature, pressure, liquid viscosity, and/or superficial gas velocity.
- The decreasing rate of heat transfer coefficients with superficial gas velocity is lower at a higher superficial gas velocity.

2.3. Direct Contact Heat Transfer

Wikle et al. (1963) were the first authors who studied direct-contact heat exchangers which can be used in different applications such as; water desalination (Letan, 1988; Sideman and Gat, 1966), energy recovery from industrial waste (Shimizu and Mori, 1988), crystallization (Core and Mulligan, 1990; Letan, 1988), ice-slurry production (Wijeysundera et al., 2004), and thermal energy storage (Core and Mulligan, 1990; Wright, 1988) (Lemenand et al., 2010). Direct-contact gas-liquid heat transfer, in which a gas is injected into a stagnant pool of liquid, involves a complex phenomenon of bubble formation and gas motion through the

liquid layer. The book by Clift et al. (1978) contains an extensive amount of information on flows past bubbles, drops and particles.

Smith et al. (1982) have developed an analytical model for calculating direct contact volumetric heat-transfer coefficients in evaporation process. Heat transfer has been modeled using single droplet correlations for the Nusselt number. The analytical results have shown good agreement with data obtained from an experimental direct contact evaporator using cyclopentane and water.

Ghaz (1991) has presented results of experiments on direct-contact heat transfer between stagnant water maintained at a constant temperature and air bubbling through the water. He has found a correlation for the Nusselt number and the overall heat transfer between the water and air.

Jaber (2009) has investigated numerically the heat transfer in a direct contact heat exchanger, between CuCl droplets and air. His numerical results can be used in the scale-up analysis of the Cu-Cl cycle. Sheoran et al. (2010) have proposed a direct contact heat exchanger for high temperature thermal storage for solar power generating plants. They have used high pressure gas as the working fluid in the solar plant. The gas was circulated through solar receivers and was then bubbled through an immiscible molten salt solution, which acted as the thermal storage media. High heat transfer rates could be achieved between the gas and the molten salt. A higher heat exchange rate between the working fluid of the solar power system and the thermal storage media was important to maximise the thermal efficiency of the power plant.

Summary

It can be concluded from the direct contact heat transfer literature survey, that there is no general model that can be used to predict the volumetric heat transfer coefficient. Because of the direct dependence of heat transfer on hydrodynamic studies and because of the complexity of the bubble behavior, empirical equations from experimental studies are important to describe the direct contact heat transfer. In this thesis, experimental studies are carried out to investigate the direct contact heat transfer between gas bubbles and slurry system

under the operating conditions of the oxygen reactor. These experimental studies are carried out with alternative materials rather than the actual materials of the oxygen reactor. The selection of the alternative materials is based on the dimensional analysis to give similar behaviors of the hydrodynamic and heat transfer studies.

2.4. Computational Fluid Dynamics (CFD) Model

There are different studies regarding the modeling by CFD simulation in multiphase flow (Chen and Fan, 2004; Jakobsen et al., 1997; Joshi, 2001; Joshi et al., 2002; Laı´n, 2002; Sokolichin et al., 2004). In the literature, there is no universal agreement that indicates that the CFD models are capable of predicting the experimental results of multiphase flow regimes (Sokolichin et al., 2004). For instance, Delnoij et al. (1997a, b, c) have used Eulerian-Lagrangian approach in a flat bubble column to model two-phase flow by using laminar flow model, as well as drag, lift, virtual-mass, and hydrodynamic-interaction forces (Sarah et al., 2005). Sokolichin and Eigenberger (1999) have obtained same results by using finer grid size and neglecting the effects of virtual-mass and lift forces, as well as bubble-bubble interactions. Deen et al. (2001) have found that using the virtual mass force will not influence the results. Krishna and Van Baten (2001) have studied high pressure turbulent flow simulations and took into consideration the drag force only. They have found that there is high uncertainty when adding the effects of lift forces of small and large bubbles. Moreover, they have noted that there is no effect of the virtual mass force on the results of the simulations.

Table 2.8 summarizes the approaches and physical models used in the literature for different systems (Mahajan, 2010; Sarah et al., 2005). From the table, it is concluded that most of the studies have investigated one flow regime (such as churn-turbulent flow).

Table 2.8 Recent applications of CFD in modeling hydrodynamics (Mahajan, 2010; Sarah et al., 2005).

Author	Multiphase Approach	Model
Laı´n et al. (2002)	Euler–Lagrange	2-D axisymmetric standard $k-\varepsilon$ model
Sokolichin and Eigenberger (1994)	Euler–Euler	Laminar 2-D
Sokolichin et al. (1997)	Euler–Euler Euler–Lagrangian	Laminar 2-D
Sanyal et al. (1999)	Euler–Euler	2-D axisymmetric standard $k-\varepsilon$ model
Buscaglia et al. (2002)	Mixture equations, Reynolds Averaged Navier-Stokes (RANS)	2-D axisymmetric standard $k-\varepsilon$ model
Lapin et al. 1994	Euler–Euler Euler–Lagrange	Population balance 2-D
Delnoij et al. (1997a) Delnoij et al. (1997b)	Euler–Lagrange	Laminar 2-D
Sokolichin and Eigenberger (1999)	Euler–Euler	2-D, 3-D, Laminar, and standard $k-\varepsilon$ model
Mudde and Simonin (1999)	Euler–Euler	2-D, 3-D, standard $k-\varepsilon$ model low Reynolds $k-\varepsilon$ model
Buwa et al. (2002)	Euler–Euler	3-D, standard $k-\varepsilon$ model
Michele and Hempel (2002)	Euler–Euler	3-D, standard $k-\varepsilon$ model
Deen et al. (2001)	Euler–Euler	3-D, standard $k-\varepsilon$ model and Large Eddy Simulation (LES) model
Monahan and Fox (2002)	Euler–Euler	2-D, Laminar
Delnoij et al. (1999)	Euler–Lagrange	Laminar 3-D
Krishna et al. (1999)	Three-phase Euler–Euler	3-D cylindrical standard $k-\varepsilon$ model
Pfleger et al. (1999)	Euler–Euler	2-D, 3-D standard $k-\varepsilon$ model
Lopes and Quinta-Ferreira (2007)	Euler-Euler	3-D Eulerian $k-\varepsilon$ fluid model

Law et al. (2006) have determined the average gas holdup by using 2-D and 3-D models for a bubble column. They have examined the influence of various cell resolutions in calculating the average gas holdup by using FLUENT. They have found that there is a good agreement between the 2-D simulations and the experiments of Rampure et al. (2003) with a cell size of 0.67 cm. Also, they have reported that if the sizes of the cells are smaller than the size of the bubble, this will lead to unreasonable results. Moreover, they have found that both 3-D and 2-D simulations will predict the same results if their resolutions are comparable.

Rampure et al. (2003) have investigated the setup of FLUENT by carrying out experiments on a cylindrical column with two and three phase systems to measure gas holdup. They have found that the experimental results were lower than the CFD results and the agreement of the results was acceptable (Studely, 2010). Krishna et al. (2001) have investigated experimentally gas holdups for small and large bubbles with different systems and different column diameters. Also, they have determined the overall gas holdup by using CFD in an Eulerian framework and compared the CFD results with the experimental results for three different column diameters. They have reported that the results were in a good agreement (Shaikh, 2007).

Summary

From the literature review of CFD, it can be summarized as follows:

- Effects of lift and virtual mass forces are small compared with the drag force, so they can be neglected in the CFD simulation.
- The majority of literatures have used 2-D Euler-Euler approach and the standard $k-\varepsilon$ turbulence model.
- Most of the literature studies have performed their studies in churn-turbulent flow regime.
- The 2-D simulations can predict same results of 3-D simulations when they have comparable resolution.

In this thesis, the effect of lift and virtual mass forces are neglected in the simulation.

2.5. Summary of the Literature Survey

From the above review of the literatures, it can be concluded that the thermal hydraulics of the oxygen SBCR with direct contact heat transfer in the Cu-Cl cycle, has not been studied before. It is also found that the previous works on slurry bubble column reactors have investigated the hydrodynamics and heat transfer of the reactors in conditions that are different from the oxygen reactor operating conditions. This thesis fills the above gabs by examining the hydrodynamics and heat transfer of the slurry bubble column reactor at the operating conditions of the oxygen reactor in the CuCl cycle. The studies of the thermal hydraulics of the oxygen SBCR are performed experimentally by using alternative materials that are suitable for use in the laboratory and mimic the actual materials of the oxygen reactor, and numerically by using CFD simulations. Also, in this thesis, the flow regime transition points of the oxygen reactor are examined experimentally to specify at which regime the industrial oxygen reactor is working.

In the previous studies of the heat transfer in SBCRs, it has been shown that the heat is provided indirectly either through the wall of the reactor or by using an internal object, and gas bubbles are used to enhance the turbulence inside the reactor to increase the rate of the heat transfer. In this thesis, gas bubbles at high temperature are used to transfer heat directly to the slurry in addition to their role in enhancing the turbulence inside the reactor.

As shown from the literature survey, most of the empirical equations of the gas holdup and heat transfer coefficient have been formulated in terms of the physical properties of the gas and liquid. In this thesis, new forms of empirical equations are obtained, where the overall gas holdup and the volumetric heat transfer coefficient for the direct contact heat transfer, are correlated solely to the design and input parameters of the reactor, such as the rector dimensions, input velocity of the gas and input concentration of the solid particles. Moreover, the empirical equations are obtained for different flow regimes of the SBCR. The other new contribution of this thesis is obtaining a simple correlation to calculate the number of oxygen reactors that have specific dimensions in terms of the superficial gas velocity of the oxygen gas and the oxygen production rate.

The work of this thesis takes into consideration the advantages of the previous results in the literature survey for experimental setup. For example, the reactor diameter is specified to be larger than 15 cm to neglect its effect on the thermal hydraulics. As well, the sparger hole diameter is designed to be larger than 2 mm and the reactor aspect ratio larger than 5. Also, this thesis benefits from the previous results in CFD simulations to model the CFD analysis of this work.

CHAPTER 3
EXPERIMENTAL WORK

In this chapter, the details of the experimental setup and procedure are examined. In the actual oxygen reactor, the solid Cu_2OCl_2 decomposes thermally to O_2 gas and molten CuCl salt. The stoichiometric O_2 gas can be heated outside the oxygen reactor and re-injected in the reactor from the bottom to provide the necessary heat for the endothermic chemical reaction (decomposition process). In this way, to scale up the oxygen reactor, it is necessary to study the hydrodynamic and heat transfer between the oxygen gas and molten CuCl. In this experimental work, the hydrodynamic and heat transfer behaviors are studied by using alternative materials that simulate the actual materials hydrodynamically and thermally, where a hot gas is injected into a cold liquid to transfer the heat from the gas to the liquid. In this case, the hot gas simulates the oxygen gas and the cold liquid simulates the molten CuCl without the need of the chemical reaction.

3.1. Material Simulation of the Oxygen Reactor

3.1.1. Introduction

As mentioned in Chapter 1, in the oxygen reactor, an intermediate compound, solid copper oxychloride (Cu_2OCl_2, Melanothallite), is decomposed into oxygen gas (O_2) and molten cuprous chloride (CuCl, Nantokite) at 530^{o}C according to the following reaction;

$$Cu_2OCl_2(s) \rightarrow 2CuCl(l) + \frac{1}{2}O_2(g) \qquad (T = 530°C)$$

There are some challenges in using the products of the oxygen reactor in the lab for experiments, such as;

- The cuprous chloride or Nantokite (CuCl) has a high melting temperature of 430^{o}C and its color after melting is non-transparent dark grey, which makes it difficult to see oxygen bubbles inside it. Also the cuprous chloride molten salt is very corrosive.
- Oxygen gas is a strong oxidizing agent which will quickly combust materials.

Because of the above challenges, alternative materials of the liquid and gas have to be used for the experimental works. These materials have to be suitable for use in the lab and must give similar effects of the actual materials in hydrodynamic and heat transfer studies. To choose the alternative materials, dimensional analysis can be used by fixing the reactor and sparger dimensions and changing the materials of the system. It can be imagined that two experiments are done in the same reactor and sparger. The first experiment is imagined to be done with the actual materials and the second experiment is with the alternative materials. In this case, dimensional analysis, using Buckingham pi theorem, can be used to find the dimensionless groups that are used for the similarity between the actual and alternative materials.

3.1.2. Dimensional Analysis of Materials

In this section, dimensional analysis is used to define alternative materials for the molten CuCl and oxygen gas in the oxygen reactor. In the studies of the oxygen reactor, the interested particular physical quantity in heat transfer studies, is the volumetric heat transfer coefficient (U_V). This means that the "dependent variable" in the studies of the heat transfer in the oxygen reactor is (U_V).

The first step in dimensional analysis is to specify the independent parameters (Sonin, 2001) that have significant effect on the value of (U_V). A total of 14 parameters ($n = 14$) are involved in the problem of U_V. These parameters include gas and liquid properties (e.g., density, dynamic viscosity, surface tension, thermal conductivity, and specific heat), reactor geometry (e.g., reactor height and diameter), sparger size (e.g., sparger hole diameter) and flow conditions (e.g., superficial gas velocity). The functional equation of the volumetric heat transfer coefficient in terms of the complete independent parameters can be written as;

$$U_V = f\left(\rho_l, \rho_g, \mu_l, \mu_g, \sigma, U_{gs}, C_{p,l}, C_{p,g}, k_l, k_g\ D_R, H_R, d_o\right), \qquad (3.1)$$

where ρ is the density, μ is the dynamic viscosity, σ is the surface tension, U_{gs} is the superficial gas velocity, C_p is the specific heat, k is the thermal conductivity, D_R and H_R are the reactor diameter and height respectively, d_o is the hole diameter of

the sparger and the subscripts l and g denotes to the liquid and gas respectively. The set of parameters in the right side of Eq. (3.1) is complete and independent. By using Buckingham's pi theorem, Eq. (3.1) can be converted in terms of dimensionless groups to (see details in Appendix I);

$$Nu_V = f\left(\frac{\rho_g}{\rho_l}, \frac{\mu_g}{\mu_l}, \frac{k_g}{k_l}, \frac{C_{p,g}}{C_{p,l}}, Re_l, We_l, Pr_l, \frac{H_R}{D_R}, \frac{d_o}{D_R}\right) \tag{3.2}$$

Since the objective of this dimensional analysis is to choose alternative materials for the actual oxygen reactor materials, then, the dimensions of the reactor and sparger (e.g. H_R, D_R and d_o) can be fixed in the dimensional analysis and the materials properties are changed. Thus, the number of parameters that actually vary from case to case will be 11, not 14, and the dimensionless groups that can be omitted from Eq. (3.2) are $\frac{H_R}{D_R}$ and $\frac{d_o}{D_R}$. In this case Eq. (3.2) will be;

$$Nu_V = f\left(\frac{\rho_g}{\rho_l}, \frac{\mu_g}{\mu_l}, \frac{k_g}{k_l}, \frac{C_{p,g}}{C_{p,l}}, Re_l, \frac{Re_l^2}{We_l}, Pr_l\right) \tag{3.3}$$

The functional equation (Eq. (3.3)) can be written as;

$$Nu_V = C\left(\frac{\rho_g}{\rho_l}\right)^a \left(\frac{\mu_g}{\mu_l}\right)^b \left(\frac{k_g}{k_l}\right)^c \left(\frac{C_{p,g}}{C_{p,l}}\right)^d (Re_l)^e \left(\frac{Re_l^2}{We_l}\right)^f (Pr_l)^g, \tag{3.4}$$

where C, a, b, c, d, e, f and g are constants that can be determined from experiments. From Eq. (3.4), it can be seen that Nu_V depends on both hydrodynamic and heat transfer parameters. For hydrodynamic studies, the effect of heat transfer parameters, such as k_g, k_l, $C_{p,g}$, $C_{p,l}$ and U_V, are neglected. By repeating the same procedure of dimensional analysis of Nu_V on gas holdup (α_g) and flow regime transition Reynolds number $\left(Re_{g-trans}\right)$, they can be calculated as;

$$\alpha_g = C\left(\frac{\rho_g}{\rho_l}\right)^a \left(\frac{\mu_g}{\mu_l}\right)^b (Re_l)^c \left(\frac{Re_l^2}{We_l}\right)^d, \tag{3.5}$$

$$Re_{g-trans} = C \left(\frac{\rho_g}{\rho_l}\right)^a \left(\frac{\mu_g}{\mu_l}\right)^b (Re_l)^c \left(\frac{Re_l^2}{We_l}\right)^d, \quad (3.6)$$

where the constant C and the exponents a, b, c and d have different values in Eq. (3.4), (3.5) and (3.6) and;

$$Re_{g-trans} = \frac{\rho_g \, U_{g-trans} \, D_R}{\mu_g} \quad (3.7)$$

From Eq. (3.5) and (3.6), it can be seen that these equations have the same form of Eq. (3.4) when omitting heat transfer dimensionless groups $\left(\frac{k_g}{k_l}, \frac{C_{p,g}}{C_{p,l}}, Pr_l, \text{and } U_V\right)$. In the oxygen reactor, in order to find alternative materials that have similar effects of the actual materials for heat transfer and hydrodynamic studies, each dimensionless group in Eq. (3.4) for heat transfer and Eq. (3.5) and (3.6) for hydrodynamic, must have the same value for both the actual and alternative materials, except Re_l which is adjustable by U_{gs}.

After checking the physical properties of many liquids and gases, it was found that the alternative materials that can be used in the experiments instead of CuCl molten salt at 530°C and oxygen gas at 600°C are liquid water at 22°C and helium gas at 90°C respectively. The advantages of these materials are the availability and the safe usage in the lab. The temperature of oxygen gas is used here as 600°C by putting into consideration that oxygen gas is heated to that temperature by using CANDU-SCWR.

3.1.3. Properties of Actual and Experimental Materials

3.1.3.1. Gas Phase

Density

The densities of the gases are calculated from the ideal gas law;

$$\rho = \frac{P}{R\,T}, \quad (3.8)$$

where P is the pressure, R is the gas constant and T is the absolute gas temperature. The gas pressure required at the inlet of the reactor must be higher

than the hydrostatic pressure of the liquid inside the reactor. Since the height of the experimental reactor is small (<1m), the effect of the hydrostatic pressure is neglected and the pressure of the gas is considered as atmospheric pressure which is the pressure of the reactor system.

Dynamic viscosity, specific heat and thermal conductivity

The dynamic viscosities, specific heats and the thermal conductivities of the gases are considered as polynomial functions of temperature only, because of the small effect of pressure on them. By assuming that the physical property of the gas is denoted by γ, the polynomial function with the absolute temperature (T) is expressed by;

$$\gamma = a_0 + a_1 T + a_2 T^2 + a_3 T^3 + a_4 T^4 + a_5 T^5 + a_6 T^6 \qquad (3.9)$$

Table (3.1) indicates the values of polynomial coefficients for each gas and physical property. Table (3.2) shows the values of the physical properties at the atmospheric pressure of both oxygen gas at 600°C and helium gas at 90°C.

Table 3.1 Coefficients of Eq. (3.9) for different physical properties of each gas.

	Oxygen Gas			**Helium Gas**		
Coefficient	**Dynamic Viscosity** $(\mu \times 10^{-6})$ **(Pa.s)**	**Specific Heat** (C_p) **(kJ/Kg.K)**	**Thermal Conductivity** (k) **(W/m.K)**	**Dynamic Viscosity** $(\mu \times 10^{-6})$ **(Pa.s)**	**Specific Heat** (C_p) **(kJ/Kg.K)**	**Thermal Conductivity** (k) **(W/m.K)**
a_0	-0.398	0.88	-7.673 e-4	0.394	5.193	-7.761 e-3
a_1	0.088	-1 e-7	1.036 e-4	0.172	0	8.662 e-4
a_2	-7.06 e-5	5.4 e-7	-4.62 e-8	-0.0014	0	-1.556 e-6
a_3	4.629 e-8	-3.3 e-10	1.52 e-11	8.02 e-6	0	1.401 e-9
a_4	-1.7 e-11	0	0	-2.4 e-8	0	0
a_5	2.534 e-15	0	0	3.6 e-11	0	0
a_6	0	0	0	-2.1 e-14	0	0
Reference	Lemmon and Jacobsen, 2004	Borgnakke and Sonntag, 2009	Lemmon and Jacobsen, 2004	Petersen, 1970	Borgnakke and Sonntag, 2009	Petersen, 1970

Table 3.2 Physical properties of the actual and experimental materials (Lemmon and Jacobsen, 2004, Borgnakke and Sonntag, 2009, Petersen, 1970).

Physical Property	**Oxygen gas (T=600ºC)**	**Helium gas (T=90ºC)**
Gas constant (R) (J/kg.K)	259.8	2077
Density (ρ) (kg/m^3)	0.4467	0.1344
Dynamic viscosity (μ) (Pa.s)	4.45E-05	2.267E-05
Specific heat (C_p) (J/kg.K)	1071.9	5193
Thermal conductivity (k) (W/m.K)	0.0645	0.1687

3.1.3.2. Liquid Phase

Density

The density of the molten salt CuCl (see Fig. 3.1 for solid CuCl) as a function of temperature T is (Zamfirescu et al., 2010);

$$\rho_{CuCl} = \rho_m - \rho_m \, \beta (T - T_m), \tag{3.10}$$

where $\rho_m = 3692$ kg/m^3 is the density at the melting point $T_m = 430$ºC, $\beta = 2.083 \times 10^{-7} \frac{1}{^oC}$ and $T = 430 - 585$ºC. The density of the liquid water as a function of temperature T is (McCutcheon et al., 1993);

$$\rho_{H_2O} = 1 - \frac{(T + 288.94)\,(T - 3.99)^2}{508929\,(T + 68.13)}, \tag{3.11}$$

where T in ºC and ρ in g/cm^3.

Dynamic viscosity

The dynamic viscosity of the molten salt CuCl (Zamfirescu et al., 2010) and the water (Reid et al., 1987) as a function of temperature T are respectively;

$$\mu_{CuCl} = 0.365 \, e^{-6.95 + \left(\frac{1418}{T}\right)}, \tag{3.12}$$

$$\mu_{H_2O} = 0.001 \, e^{\left(-24.71 + \frac{4209}{T} + 0.04527\,T - 0.00003376\,T^2\right)}, \quad 0 \le T \le 370\ ^oC \tag{3.13}$$

where μ in Pa.s and T is the absolute temperature in Kelvin.

Specific heat

The specific heat of the molten salt CuCl (liquid) is constant and is equal to 64.4 J/mol.K (650.8 J/kg.K). This constant specific heat is for a temperature range from the melting point, 683 K up to the boiling point, 1482 K (Zamfirescu et al., 2010). The specific heat of the water as a polynomial function of temperature T is (Osborne et al., 1939);

$$C_{p,H_2O} = 4217.4 - 3.720283\,T + 0.1412855\,T^2 - 2.654387 \times 10^{-3}\,T^3 + 2.093235 \times 10^{-5}\,T^4, \quad (3.14)$$

where C_{p,H_2O} in J/kg.K and T in ^oC.

Thermal conductivity

The thermal conductivity of the molten salt CuCl (k_{CuCl}) at the melting temperature is 0.21 W/m.K, and at 900 K, $k_{CuCl} = 0.19$ W/m.K (Zamfirescu et al., 2010). The thermal conductivity of the liquid water as a function of the absolute temperature is (Ramires et al., 1994);

$$k_{H_2O} = 0.606\left(-1.48 + 4.123\,\frac{T}{298} - 1.639\,\left(\frac{T}{298}\right)^2\right) \quad (3.15)$$

Eq. (3.15) is used for $274 \leq T \leq 370\ K$.

(a) (b)

Fig. 3.1 a) CuCl solid powder before melting b) CuCl after melting and solidification (Marin, 2012).

Surface tension

The surface tension of molten CuCl in contact with air is equal to 0.092 N/m at the melting temperature of CuCl (450^{o}C) (Janz, 1988). Since the surface tension decreases approximately linearly with temperature and is equal to zero at the critical temperature of the liquid, a linear function of CuCl surface tension with temperature can be derived as follows;

$$\sigma_{CuCl} = 0.115 - 5.076 \times 10^{-5}\, T \qquad (3.16)$$

The predicted value of the critical temperature that is used in deriving Eq. (3.16) with 50% accuracy is equal to 2435 K (Rowley et al., 2004; Zamfirescu et al., 2010). The surface tension of water in contact with air as a function of the absolute temperature is (Vargaftik et al., 1983);

$$\sigma_{H_2O} = 0.236 \left[\frac{647.15 - T}{647.15}\right]^{1.256} \left[1 - 0.625 \left(\frac{647.15 - T}{647.15}\right)\right] \qquad (3.17)$$

There is no change in the value of the surface tension of pure liquid light water (H_2O) in the presence of the non-polar (i.e. non-interacting) helium gas in comparison to air or other relatively inert gases. At the atmospheric pressure, helium has a quite low solubility in water (8.53 mL/L at 21.7 ^{o}C or 0.00152 g/L at 20^{o}C). Therefore, helium gas is not able to induce measurable surface tension changes in the polar liquid water of more than 0.1 mN/m under STP, which is by the way, the repeatability and reproducibility of most simple tensiometers or pendant drop devices (Morrison and Johnstone, 1954).

3.1.3.3. Solid Phase

Density

The density of the solid copper oxychloride as a function of temperature is (Zamfirescu et al., 2010);

$$\rho_{Cu_2OCl_2} = \rho_r\, e^{\left(a\,\Delta T + b\,\Delta T^2\right)}, \qquad (3.18)$$

where;

$a = -2.660831725 \times 10^{-24}$

$b = -1.221274397 \times 10^{-13}$

$\Delta T = T - T_r$

$\rho_r = \rho\,(T_r) = 4080\ kg/m^3,\ T_r = 298.15\ K$

The density of the solid Alumina (Al_2O_3) as a function of absolute temperature is (Auerkari, 1996);

$$\rho_{Al_2O_3} = 4136\ e^{4.153\times10^{-4} - 3.107\times10^{-5}\ T + 1.082\times10^{-7}\ T^2} \qquad (3.19)$$

Specific heat

The specific heat of the solid copper oxychloride as a polynomial function of temperature is (Zamfirescu et al., 2010);

$$C_{p,Cu_2OCl_2} = 53.7 + 0.334\ T - 5.221\ T^2 + 2.999 \times 10^{-7}\ T^3, \qquad (3.20)$$

where C_{p,Cu_2OCl_2} is in kJ/kmol.K, T is the absolute temperature in Kelvin. Eq. (3.20) is used for a temperature range of 298-675 K. The specific heat of the solid alumina as a function of absolute temperature is (Auerkari, 1996);

$$C_{p,Al_2O_3} = 1.045 + 1.742 \times 10^{-4}\ T - \frac{2.796 \times 10^4}{T^2}, \qquad (3.21)$$

where C_{p,Al_2O_3} in kJ/kg.K and T in Kelvin. Eq. (3.21) is used for a temperature range of 25-1500°C.

Thermal conductivity

The thermal conductivity of the solid copper oxychloride is averaged from CuO and $CuCl_2$ to be 0.451 W/m.K (Marin, 2012). The thermal conductivity of the solid alumina as a function of temperature is (Auerkari, 1996);

$$k_{Al_2O_3} = 5.5 + 34.5\ e^{-0.003\ T}, \qquad (3.22)$$

where $k_{Al_2O_3}$ in W/m.K and T in ^oC. Eq. (3.22) is used for a temperature range of 25-1300^oC.

Kinds of alumina

Three different types of alumina spherical particles supplied by FISHER SCIENTIFIC (CANADA) have been used in the experimental studies, to study the effects of solid particle concentration and diameter on the scale up of SBCR;

a) Basic Alumina with a mesh of 60-325.
b) Adsorption Alumina with a mesh of 80-200.
c) Activated Alumina with a mesh of 8-14.

Particles sizes have been analyzed for the first two types of alumina by using wet operation in a MICROTRAC S3500 Particle Size Analyzer. Each type of alumina has been tested nine times and the mean diameter of the volume distribution has been calculated by using MICROTRAC FLEX software. Fig. 3.2 shows the particle size distribution of both Basic and Adsorption Alumina. The average particle size of the Activated Alumina has been measured by using a digital Vernier caliper for 30 different samples. The alumina solid particles have reasonable rigidity that do not form agglomerates. Table 3.3 shows the images of the three different types of alumina with the mean diameter of the volume distribution and the accuracy and percentage error of each type within the instrument precision.

Table 3.3 Three different types of alumina particles with different sizes.

		
Basic Alumina	Adsorption Alumina	Activated Alumina
$d_m = 113.7\ \mu m$	$d_m = 116.3\ \mu m$	$d_m = 1.953\ mm$
Error = 2.946%	Error = 1.91%	Error = 1.02%

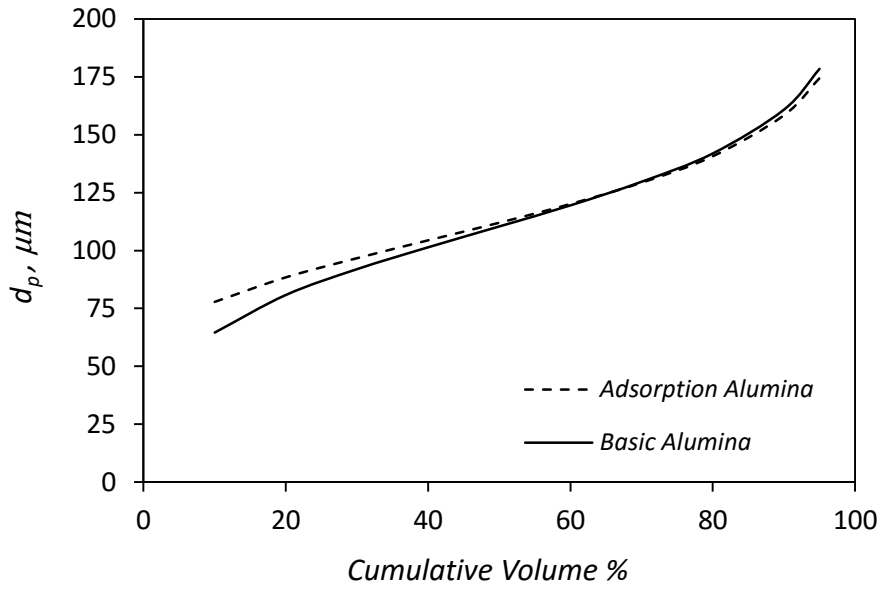

Fig. 3.2 Particle size distribution of Basic and Adsorption Alumina.

Table 3.4 indicates the physical properties of both the actual and experimental fluids and Table 3.5 shows the values of each dimensionless group of Eq. (3.4) for both the actual and experimental fluids in addition to the percentage of error that is calculated for each dimensionless group. From Table 3.5, it can be shown that the maximum percentage error that is produced from using water liquid and helium gas instead of molten CuCl and oxygen gas is coming from the specific heat and is equal to 24.576%.

Table 3.4 Physical properties of the actual and experimental materials (Zamfirescu et al., 2010; Lemmon and Jacobsen, 2004; Borgnakke and Sonntag, 2009; Ramires et al., 1994; Helge, 1970).

Physical Property	Actual Materials		Experimental Materials	
	CuCl molten salt (T=530°C)	Oxygen gas (T=600°C)	Water (T=22°C)	Helium gas (T=90°C)
Density (ρ)	3692	0.4467	997.8	0.1344
Dynamic viscosity (μ)	0.002045	4.45E-05	0.000975	2.267E-05
Specific heat (C_p)	650.85	1071.9	4180.6	5193
Thermal conductivity (k)	0.2	0.0645	0.6	0.1687
Surface tension (σ)	0.0867	-	0.0724	-

Table 3.5 Dimensionless groups of the actual and experimental materials and the percentage of error.

Dimensionless Group	Actual Materials	Experimental Materials	Error%
$\frac{\rho_g}{\rho_l}$	0.000121	0.000135	11.311
$\frac{\mu_g}{\mu_l}$	0.021756	0.023	6.908
$\frac{C_{p,g}}{C_{p,l}}$	1.647	1.242	24.576
$\frac{k_g}{k_l}$	0.32	0.28	13
Pr_l	6.66	6.779	1.83
$\frac{Re_l^2}{We_l}$	76473868 ($D_R = 1m$)	76085070 ($D_R = 1m$)	0.508

3.1.3.4. Slurry Properties

The thermo physical properties of the slurry mixture can be calculated from the volumetric solid concentration (C_s). For example, the average density of the slurry ρ_{sl} can be calculated as follows;

$$\rho_{sl} = \rho_s \, C_s + \rho_l \, (1 - C_s), \qquad (3.23)$$

where ρ_s and ρ_l are the densities of solid and liquid respectively. The average specific heat of the slurry is;

$$C_{p,sl} = \frac{\rho_s \, C_{p,s} \, C_s + \rho_l \, C_{p,l} \, (1 - C_s)}{\rho_{sl}}, \tag{3.24}$$

where $C_{p,s}$ and $C_{p,l}$ are the specific heats of the solid and liquid respectively. The effective thermal conductivity of the slurry k_{sl} is calculated from (Boomsma and Poulikakos, 2001);

$$k_{sl} = k_s \, C_s + k_l \, (1 - C_s), \tag{3.25}$$

where k_s and k_l are the thermal conductivities of the solid and liquid respectively.

The slurry dynamic viscosity (μ_{sl}) can be related to the viscosity of the liquid phase as;

$$\mu_{sl} = \mu_r \, \mu_l, \tag{3.26}$$

where μ_r is the relative dynamic viscosity (dimensionless), μ_l is the dynamic viscosity of the liquid (CuCl molten salt). There are different equations to calculate the relative viscosity as a function of volumetric solid concentration (C_s). The volumetric solid concentration can be expressed as;

$$C_s = \frac{V_s}{V_{sl}}, \tag{3.27}$$

where V_s and V_{sl} are the volumes of solid particles and slurry respectively. For very low solid concentrations, Einstein's equation can be used (Einstein, 1906);

$$\mu_r = 1 \tag{3.28}$$

For higher solid concentrations, the equation of Guth and Simba (1936) can be used;

$$\mu_r = 1 + 2.5 \, C_s + 14.1 \, C_s^2 \tag{3.29}$$

3.2. Experimental Setup

The schematic of the SBC setup is illustrated in Fig. 3.3. All experiments were performed in a stainless steel column of 21.6 cm (8.5 in) inner diameter, 91.5 cm (36 in) height and 6 mm (0.25 in) thickness. The diameter of the column was

chosen to be larger than 15 cm, to minimize its effect on hydrodynamic studies as mentioned in Chapter 2. To study the effect of the column height on hydrodynamics, the height was chosen to be less than 1 m, because its effect can be neglected when it is higher than 1 m as indicated in Cahpter 2. To enable viewing the behavior of the bubbles inside the column, the reactor was provided with two windows, located in the middle of the second section from the bottom of the reactor. A ball valve was installed at the bottom of the column to drain the slurry and clean the column. The column wall was insulated by a thermal insulation to reduce heat losses from the column wall.

There are four pressure transducers mounted to pressure taps at different heights of the reactor to measure the hydrostatic pressure head at these heights. The locations of the pressure transducers are 21 cm (8.25 in), 42.5 cm (16.75 in), 61.6 cm (24.25 in) and 80.6 cm (31.75 in) above the bottom of the column (Figs. 3.3-3.5). Pressure transducers provide quasi-instantaneous pressure signals which are used for gas holdup measurements. Six thermocouples, type K, were mounted at different heights inside the column to measure the temperature at these heights. These distances are, 15.2 cm (6 in), 25.4 cm (10 in), 37.5 cm (14.75 in), 47.6 cm (18.75 in), 61.6 cm (24.25 in) and 80.6 cm (31.75 in), from the bottom of the column (Fig. 3.4). For more details about pressure transducers and thermocouples, see Appendix II.

Helium gas is injected into the bottom of the column through a six-arm spider-type gas sparger. The orifice diameter of the gas sparger was designed to be 3 mm to reduce the effect of the orifice diameters (that are larger than 2 mm) on gas holdup. The helium volumetric flow rate is measured using a digital flow meter that is connected to a pressure regulator to control the flow rate. For more details about the digital flow meter and pressure regulator, see Appendix II.

A stainless steel helical tube inside an electrical furnace was installed in place after the flow meter to heat the helium gas to a certain temperature before entering the reactor column. A one-way valve was mounted before and near the inlet of the column to allow helium gas to enter the column without backflow of water. Analog pressure gages and thermocouples of type K, were installed at the

inlet and outlet of the column to measure the pressure and temperature of helium gas at these locations. For more details about analog pressure gages, see Appendix II. Helium gas that exit from the column is vented through a ventilation hood. The National Instrument Field Point modules and LabView software were used for online data acquisition to monitor the readings from the thermocouples and pressure transducers.

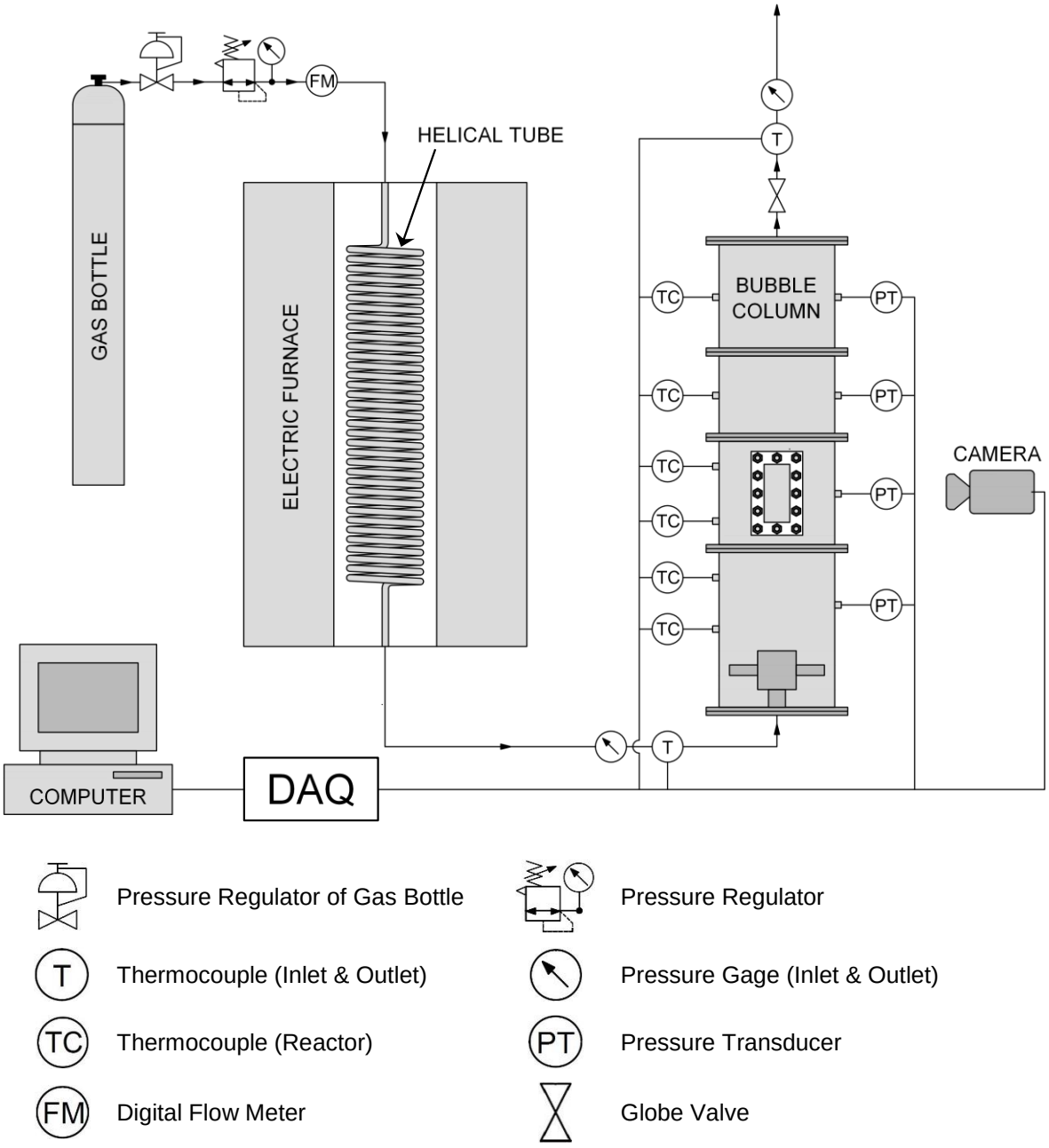

Fig. 3.3 Schematic diagram of the experimental setup.

3.2.1. Reactor Column Specifications

The reactor column was constructed from stainless steel and it consisted of four sections provided with flanges for easy construction and flexibility and also for easy installation and removal for cleaning purposes. The first (bottom) section is 31.8 cm (12.5 in) in height, the second and fourth (upper) sections are 21.6 cm (8.5 in) in height and the third section is 16.5 cm (6.5 in) in height. Two windows were provided in the second section of the column. These windows were placed in opposite directions to allow the light to penetrate through one of the windows for a clear vision. The inside dimensions of the window are 5.1×11.4 cm (2×4.5 in) and the outside dimensions are 10.2×16.5 cm (4×6.5 in). Fig. 3.4 shows three different views of the slurry bubble column (SBC), where the windows can be seen. Fig. 3.5 shows the pictures of front and side views of the SBC.

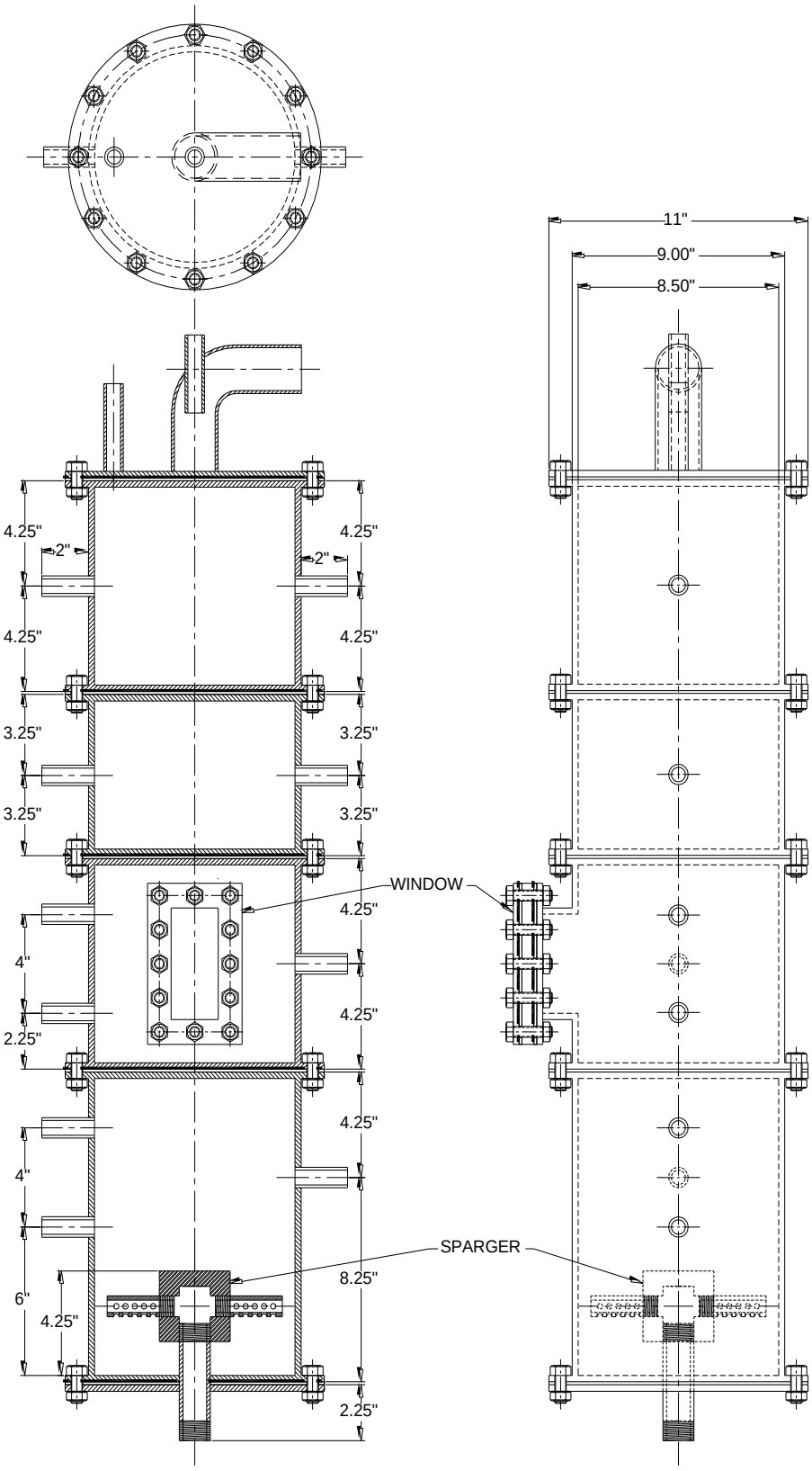

Fig. 3.4 Reactor column dimensions.

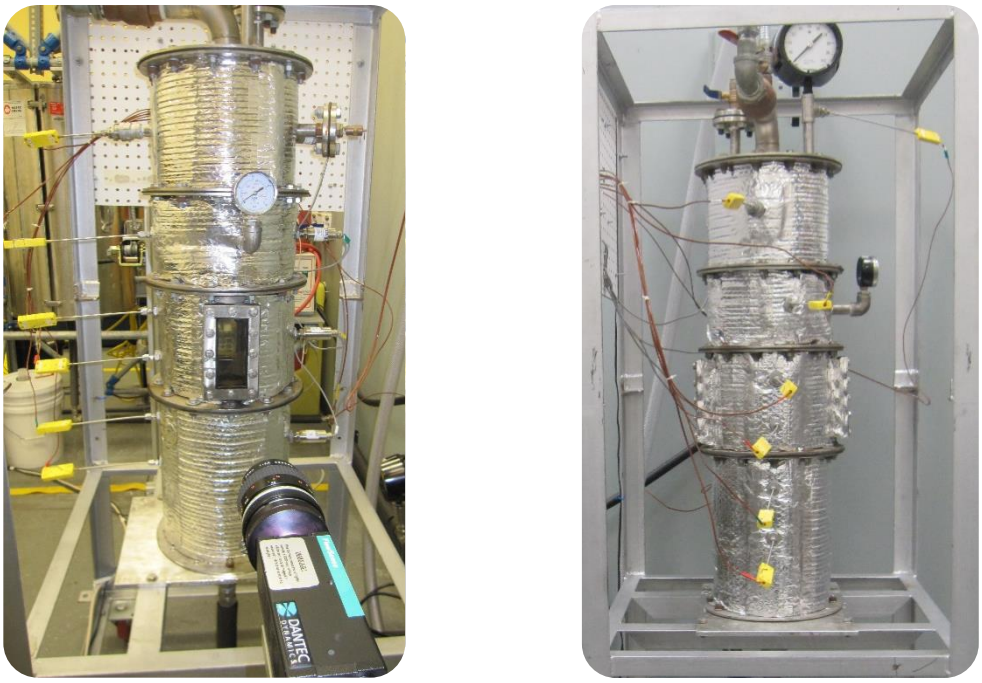

(a) (b)

Fig. 3.5 a) Front view of the SBC b) Side view of the SBC.

3.2.2. Helical Tube Specifications

The specifications of the helical tube are shown in Table 3.6 and the dimensions of the helical tube are shown in Fig. 3.6.

Table 3.6 Characteristics of the helical tube.

Material	Stainless steel 304/304L
Outside diameter	1.3 cm (0.5 in)
Wall thickness	1.6 mm (0.065 in)
Coil diameter	12.7 cm (5 in)
Coil length	6.096 m (240 in)
Coil pitch	1.9 cm (0.75 in)

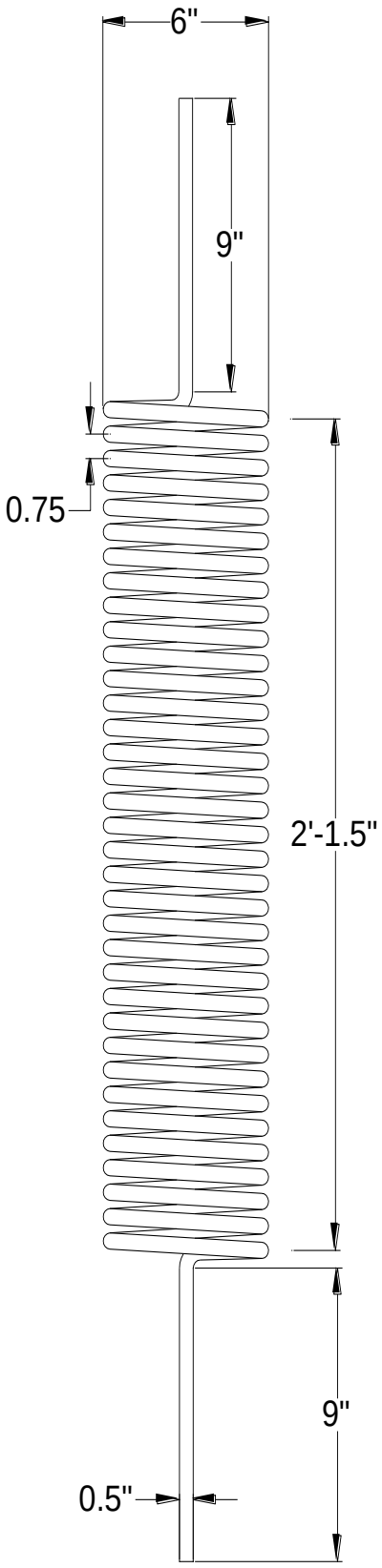

Fig. 3.6 Dimensions of the helical tube.

3.2.3. Furnace Specifications

The specifications of the electrical furnace are shown in Table 3.7. Fig. 3.7 shows the dimensions of the furnace and Fig. 3.8 shows the helical tube inside the electrical furnace.

Table 3.7 Characteristics of the electrical furnace.

Overall Dimension	22” Diameter X 36” Height
Heated Chamber	8.25” ID X 30” Height
Total Power	13605 Watts, 208 Volts, 65.4 Amps, 60 Hz
Zone 1	10” Length, 4535 Watts, 208 Volts, 21.8 Amps
Zone 2	10” Length, 4535 Watts, 208 Volts, 21.8 Amps
Zone 3	10” Length, 4535 Watts, 208 Volts, 21.8 Amps
Max. Temp.	1200 ^{O}C
Shell	Stainless Steel
Heater	Nickel-Chrome alloy wire helically wound and held in the ceramic refractory forms
Thermocouple Type	Type K Dual, Thermocouple Port at Center of Each Heated Zone

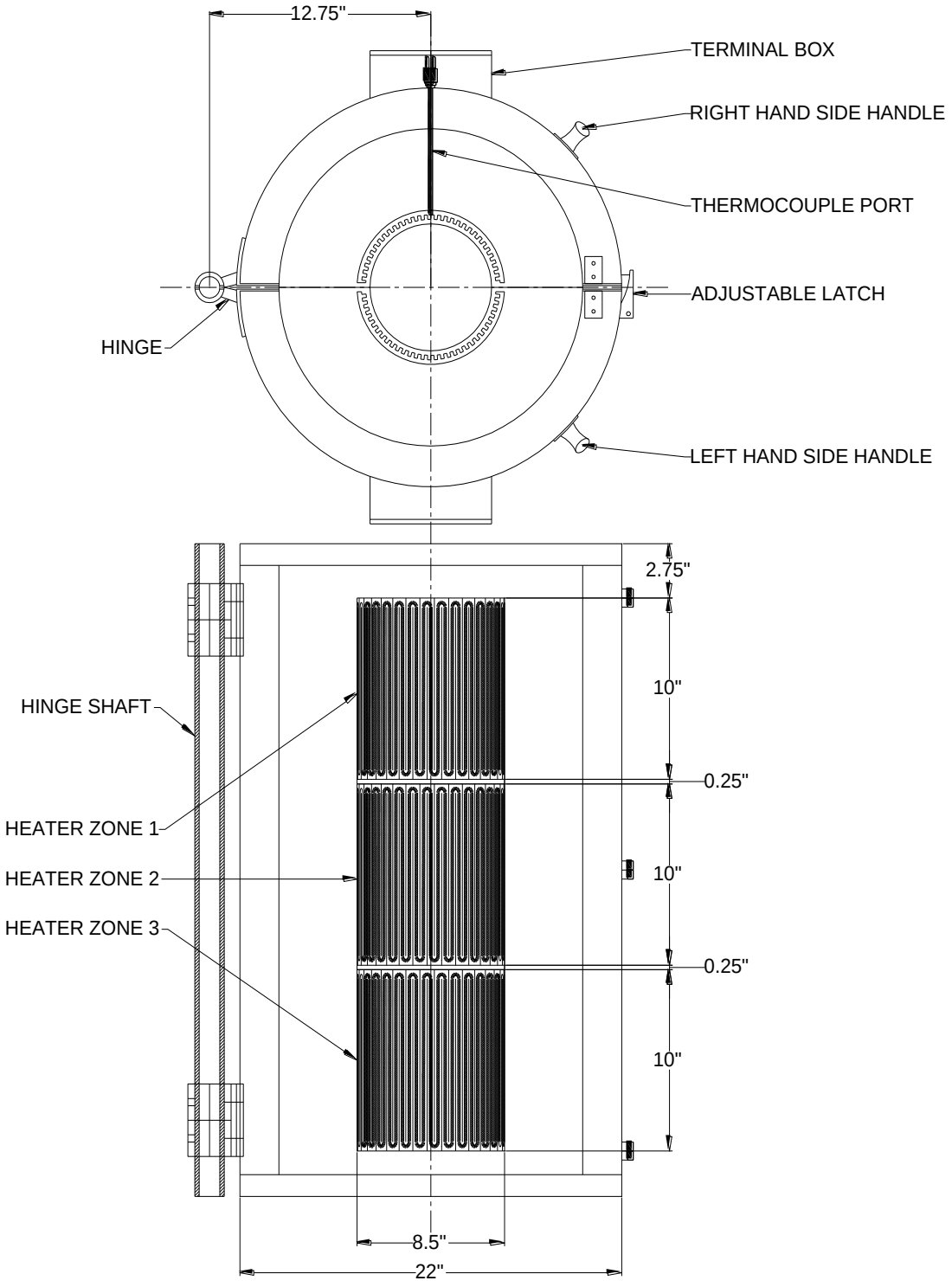

Fig. 3.7 Dimensions of the electrical furnace.

Fig. 3.8 Picture of the helical tube inside the electrical furnace.

3.2.4. Gas Distributer (Sparger)

A spider-type gas sparger with six arms is located at the bottom of the column. Each arm was made of stainless steel tube of 7.9 cm (3.125 in) long and 1.3 cm (0.5 in) inside diameter. Each arm has 4 openings of 3 mm diameter on each side of the arm except the top side to prevent blocking orifices by solid particles. There are a total of 72 openings on the gas sparger. The holes were located at 4.4 cm (1.75 in), 5.2 cm (2.06 in), 6 cm (2.375 in) and 6.8 cm (2.6875 in) from the center of the column. The gas sparger is screwed to a 2.54 cm inside diameter pipe and its maximum height from the bottom of the column is about 10.8 cm (4.25 in). A schematic of the spider-type gas sparger is given in Fig. 3.9 and the picture of the spider-type gas sparger is given in Fig. 3.10.

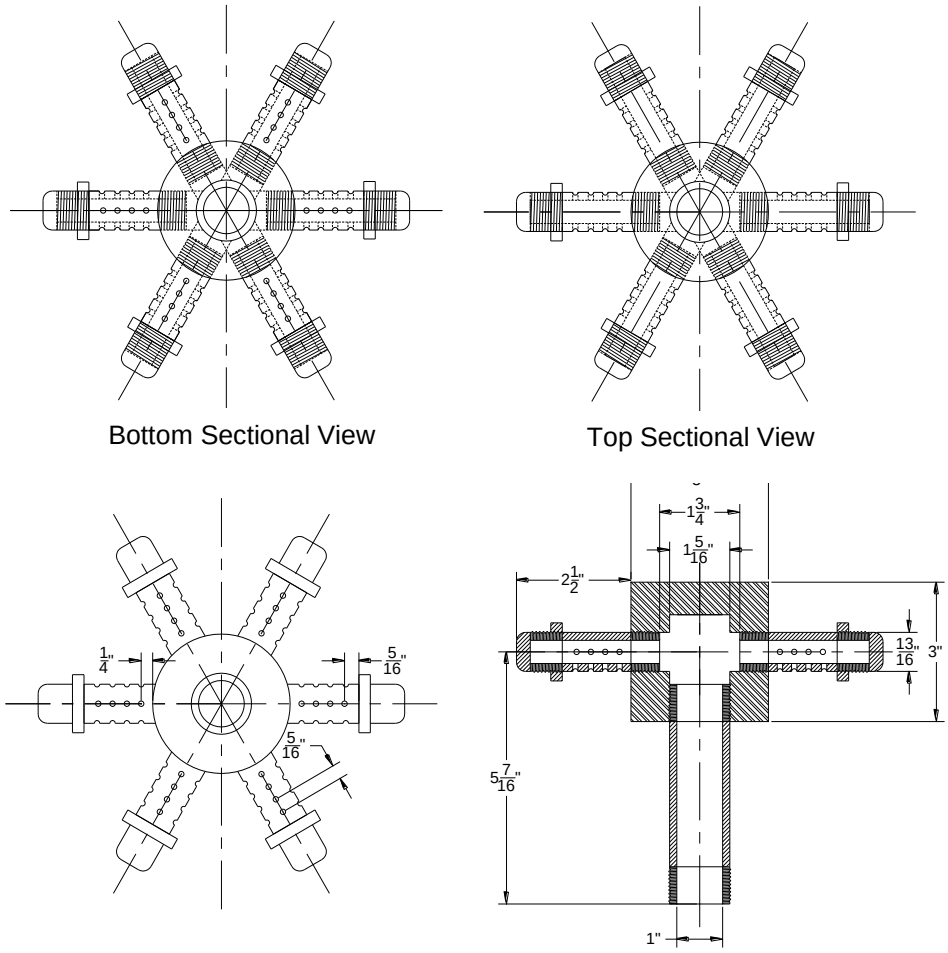

Fig. 3.9 Dimensions of the sparger.

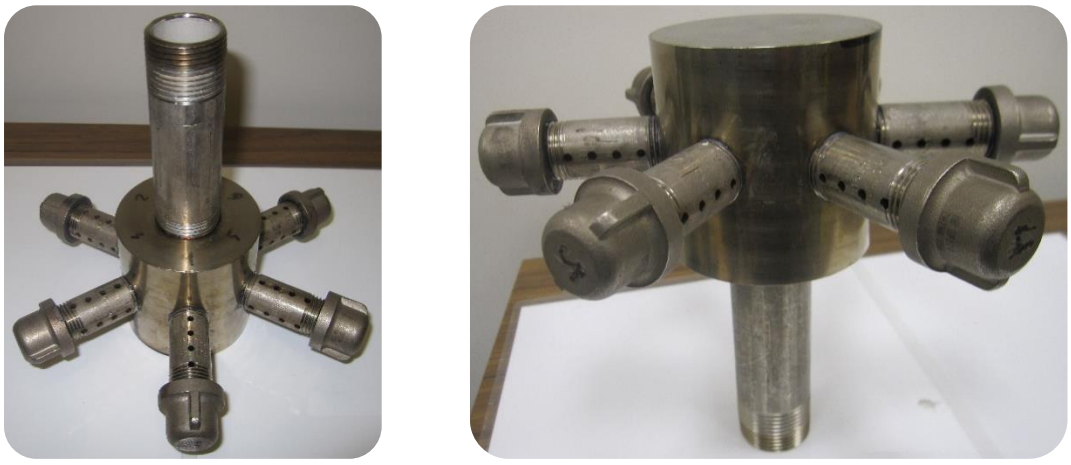

(a) (b)

Fig. 3.10 Picture of the sparger a) from the bottom, b) from the side.

3.3. Experimental Procedure

In all experiments that were performed at operating pressure of 0.1MPa, the column was first filled with tap water at about 22^{o}C to a specified level (45, 55, and 65 cm). Helium gas with oil free was then introduced into the column and the gas flow rate was adjusted by using a pressure regulator with a digital flow meter. Helium gas was heated to about 90^{o}C before entering the column by using a helical tube inside an electric furnace. The system was given some time (about 5 min.) to reach the steady state condition, then the experimental measurements process was commenced by measuring the hydrostatic pressures at different locations in the column, the temperatures at various points in the column as well as the inlet and outlet pressures and temperatures of the helium gas. Since single-sample data are those in which some uncertainties may not be discovered by repetition, each experimental run with a fixed static liquid level and solid concentration was repeated three times and the mean values of the gas holdup and volumetric heat transfer coefficient were calculated. The relative standard deviation for gas holdup is less than 6% and for volumetric heat transfer coefficient is less than 10%. This procedure was repeated for different static water heights (45, 55 and 65 cm), different solid concentrations (0, 5 and 10 %) and different gas flow rates ranging from 20 to 320 SLPM which covers the bubbly flow regime and part of the churn turbulent flow regime. The static water heights of 45, 55, and 65 cm were selected to give aspect ratios of 2, 2.5, and 3 respectively, because the effect of the column height on gas holdup is negligible for a height larger than 1 m and aspect ratios larger than 5. The solid concentrations of 5, and 10 vol. % were selected because it has been found that for solid concentration less than 5 vol. %, the effect of solid concentration is negligible (see Chapter 2). Before inserting solid particles into the column, they were washed with tap water and then mixed with the water for about 1 hr to ensure that they were completely wetted.

CHAPTER 4
CFD SIMULATION OF THE MULTIPHASE FLOW IN THE OXYGEN REACTOR

4.1. Approaches to Multiphase Modeling

In multiphase flows, there are two methods that can be used for numerical solution: the Euler-Lagrange method and the Euler-Euler method. The computational effort of the Eulerian-Lagrangian method is high due to the study of each single bubble effect. Therefore, the Euler-Lagrange method can be used for small volume fraction of gas phase in which the bubble-bubble interactions can be neglected. In this way, this method is not preferred for significant gas volume fraction such as in bubble column reactors (Mahapatra and Rakh, 2007). Therefore, the more common method used in CFD of multiphase flow is the Eulerian-Eulerian method. This method includes three different models: the volume of fluid (VOF) model, the mixture model, and the Eulerian model (ANSYS, 2012).

In bubble column reactors, both mixture and Eulerian models can be used. The mixture model can be used for simpler problems where the interphase drag laws are not required and the computational effort is less. The Eulerian model can be used for more accurate results but with more computational effort. Mostly, the interphase drag law of Schiller-Naumann can be used in the Eulerian model (ANSYS, 2012). In this thesis, the Eulerian model is used, because of its accuracy.

4.2. Eulerian Model Theory

4.2.1. Volume Fraction Equation

Oxygen production reactor can be described by two phases: the slurry continuous (primary) phase and the dispersed (secondary) gas phase. The volumes of gas phase V_g and slurry phase V_{sl} are respectively defined by (ANSYS, 2012);

$$V_g = \int_V \alpha_g \, dV \qquad and \qquad V_{sl} = \int_V \alpha_{sl} \, dV, \tag{4.1}$$

where α_g and α_{sl} are the gas and slurry phasic volume fractions (phase holdups) respectively, which must satisfy the relation;

$$\alpha_g + \alpha_{sl} = 1 \qquad (4.2)$$

The effective densities of gas phase $\hat{\rho}_g$ and slurry phase $\hat{\rho}_{sl}$ are respectively;

$$\hat{\rho}_g = \alpha_g \, \rho_g \qquad and \qquad \hat{\rho}_{sl} = \alpha_{sl} \, \rho_{sl}, \qquad (4.3)$$

where ρ is the physical density and the subscripts g and sl denote to the gas and slurry phase respectively.

4.2.2. Conservation Equations

Conservation of mass

The flow in the oxygen bubble column reactor is incompressible and Newtonian. The general forms of the continuity equation for gas and slurry phases are (ANSYS, 2012);

$$\nabla . \boldsymbol{V_g} = 0 \qquad (gas\ phase), \qquad (4.4)$$

$$\nabla . \boldsymbol{V_{sl}} = 0 \qquad (slurry\ phase), \qquad (4.5)$$

where $\boldsymbol{V}$ is the velocity field, and the subscripts $\boldsymbol{g}$ and $\boldsymbol{sl}$ denote to gas and slurry phase respectively. In 2D Cartesian coordinates (x, y), Eq. (4.4) and (4.5) are written as (Bejan, 2004);

$$\frac{\partial v_{x,g}}{\partial x} + \frac{\partial v_{y,g}}{\partial y} = 0 \qquad (gas\ phase) \qquad (4.6)$$

$$\frac{\partial v_{x,sl}}{\partial x} + \frac{\partial v_{y,sl}}{\partial y} = 0 \qquad (slurry\ phase) \qquad (4.7)$$

Conservation of momentum

The momentum equations for the gas and slurry phases are (Batchelor, 1967);

$$\rho_g \alpha_g \frac{D\boldsymbol{V_g}}{Dt} = -\alpha_g \nabla P + \alpha_g \, \mu_{g,eff} \, \nabla^2 \boldsymbol{V_g} + \alpha_g \, \rho_g \, \boldsymbol{g} + M_{i,g} \qquad (gas\ phase), \qquad (4.8)$$

$$\rho_{sl} \alpha_{sl} \frac{D\boldsymbol{V_{sl}}}{Dt} = -\alpha_{sl} \nabla P + \alpha_{sl} \, \mu_{sl,eff} \, \nabla^2 \boldsymbol{V_{sl}} + \alpha_{sl} \, \rho_{sl} \, \boldsymbol{g} + M_{i,sl} \, (slurry\ phase), \quad (4.9)$$

where P is the pressure (same pressure for all phases), μ_{eff} is the effective dynamic viscosity (for more details on effective dynamic viscosity, see (ANSYS, 2012)), $\boldsymbol{g}$ is the gravitational acceleration and M_i is the total interfacial force acting between the phases, which can be represented as;

$$M_{i,l} = -M_{i,g} = M_D + M_L + M_{VM}, \qquad (4.10)$$

where M_D is the drag force, M_L is the lift force and M_{VM} is the virtual mass force (for details about these forces, see (ANSYS, 2012)). Sokolichin et al. (2004) have reported that the lift force can be neglected without significant effects on the results. Rafique et al. (2004) have concluded that, in bubbly flow, the effect of the virtual mass force is insignificant compared with the drag force. In the CFD simulation of this thesis, the effects of the lift and virtual mass forces are neglected.

For gas-slurry system, the drag force can be expressed as (ANSYS, 2012);

$$M_D = \frac{\rho_g \, f}{6 \, \tau_b} \, d_b \, A_i \, \left(\boldsymbol{V_g} - \boldsymbol{V_{sl}}\right), \qquad (4.11)$$

where (ANSYS, 2012);

$$A_i \text{ (interfacial area)} = \frac{6 \, \alpha_g \left(1 - \alpha_g\right)}{d_b} \qquad (4.12)$$

$$\tau_b \text{ (particulate relaxation time)} = \frac{\rho_g \, d_b^2}{18 \, \mu_{sl}}, \qquad (4.13)$$

$$f \text{ (drag function)} = \frac{C_D \, Re}{24}, \qquad (4.14)$$

$$Re \text{ (Reynolds number)} = \frac{\rho_{sl} \left|\boldsymbol{V_g} - \boldsymbol{V_{sl}}\right| \, d_b}{\mu_{sl}}, \qquad (4.15)$$

$\left|\boldsymbol{V_g} - \boldsymbol{V_{sl}}\right|$ is the slip velocity of the gas and slurry phases, d_b, is the effective bubble diameter, which is recommended to be Sauter-mean diameter, and C_D, is the drag coefficient. In general, the most frequently used drag correlation in bubble

column reactors, is the Schiller-Naumann equation (ANSYS, 2012), which is (Schiller and Naumann, 1933);

$$C_D = \begin{cases} \dfrac{24\ (1 + 0.15\ Re_b^{0.687})}{Re_b} & Re_b \leq 1000 \\ 0.44 & Re_b > 1000 \end{cases} \tag{4.16}$$

In 2D Cartesian coordinates, Eq. (4.8) is written as follows;

$\underline{x}$ - direction

$$\rho_g \alpha_g \left(\frac{\partial v_x}{\partial t} + v_x \frac{\partial v_x}{\partial x} + v_y \frac{\partial v_x}{\partial y}\right) = -\alpha_g \frac{\partial P}{\partial x} + \alpha_g \frac{\mu_{g,eff}}{3} \frac{\partial(\nabla . \boldsymbol{V})}{\partial x} + \mu_{g,eff}\ \alpha_g \left[\frac{\partial^2 v_x}{\partial x^2} + \frac{\partial^2 v_x}{\partial y^2}\right] + \rho_g \alpha_g\ g_x + M_{i,g,x} \tag{4.17}$$

$\underline{y}$ - direction

$$\rho_g \alpha_g \left(\frac{\partial v_y}{\partial t} + v_x \frac{\partial v_y}{\partial x} + v_y \frac{\partial v_y}{\partial y}\right) = -\alpha_g \frac{\partial P}{\partial y} + \alpha_g \frac{\mu_{g,eff}}{3} \frac{\partial(\nabla . \boldsymbol{V})}{\partial y} + \mu_{g,eff}\ \alpha_g \left[\frac{\partial^2 v_y}{\partial x^2} + \frac{\partial^2 v_y}{\partial y^2}\right] + \rho_g \alpha_g\ g_y + M_{i,g,y} \tag{4.18}$$

Note that the 2D Cartesian coordinate's form of Eq. (4.9) is similar to that of Eq. (4.8), so it is not repeated here.

Conservation of energy

The conservation of energy equations for gas and slurry phases can be written as (ANSYS, 2012);

$$\alpha_g\ \rho_g \frac{Dh_g}{Dt} = \alpha_g \frac{\partial P}{\partial t} + \bar{\bar{\tau}}_g : \nabla \boldsymbol{V_g} - \nabla . \boldsymbol{q_g} + S_g + Q_{g,sl}, \tag{4.19}$$

$$\alpha_{sl}\ \rho_{sl} \frac{Dh_{sl}}{Dt} = \alpha_{sl} \frac{\partial P}{\partial t} + \bar{\bar{\tau}}_{sl} : \nabla \boldsymbol{V_{sl}} - \nabla . \boldsymbol{q_{sl}} + S_{sl} - Q_{g,sl}, \tag{4.20}$$

where h is the specific enthalpy of each phase, $\bar{\bar{\tau}}:\nabla \boldsymbol{V}$ is the viscous stress tensor contracted with the velocity gradient, $\boldsymbol{q}$ is the heat flux which can be written as $(-k\,\nabla T)$, S is a source term (due to the decomposition process) and $Q_{g,sl}$ is the intensity of heat transferred from gas to slurry phases. The specific enthalpy can be expressed in terms of the temperature and specific heat as (Bejan, 1997);

$$dh = C_P\, dT + \frac{1}{\rho}(1 - \beta\, T)\, dP \tag{4.21}$$

For Incompressible liquid $(\beta = 0)$ and Eq. (4.21) will be;

$$dh = C\, dT + \frac{dP}{\rho} \tag{4.22}$$

Substitute Eq. (4.22) and the definition of $(\boldsymbol{q} = -k\,\nabla T)$ into Eqs. (4.19) and (4.20) and rearrange to get;

$$\alpha_g\, \rho_g\, C\, \frac{DT_g}{Dt} = \bar{\bar{\tau}}_g:\nabla \boldsymbol{V_g} + \nabla.\left(k_g\, \nabla T\right) + S_g + Q_{g,sl} \tag{4.23}$$

$$\alpha_{sl}\, \rho_{sl}\, C\, \frac{DT_{sl}}{Dt} = \bar{\bar{\tau}}_{sl}:\nabla \boldsymbol{V_{sl}} + \nabla.\,(k_{sl}\, \nabla T) + S_{sl} - Q_{g,sl} \tag{4.24}$$

In 2D Cartesian coordinates, Eqs. (4.23) and (4.24) are written as;

$$\alpha_g \rho_g C \left(\frac{\partial T_g}{\partial t} + v_{x,g}\frac{\partial T_g}{\partial x} + v_{y,g}\frac{\partial T_g}{\partial y}\right) = \bar{\bar{\tau}}_g:\nabla \boldsymbol{V_g} + k_g\left(\frac{\partial^2 T_g}{\partial x^2} + \frac{\partial^2 T_g}{\partial y^2}\right) + S_g + Q_{g,sl} \tag{4.25}$$

$$\alpha_{sl} \rho_{sl}\, C \left(\frac{\partial T_{sl}}{\partial t} + v_{x,sl}\frac{\partial T_{sl}}{\partial x} + v_{y,sl}\frac{\partial T_{sl}}{\partial y}\right) = \bar{\bar{\tau}}_{sl}:\nabla \boldsymbol{V_{sl}} + k_{sl}\left(\frac{\partial^2 T_{sl}}{\partial x^2} + \frac{\partial^2 T_{sl}}{\partial y^2}\right) + S_{sl} + Q_{sl,g} \tag{4.26}$$

4.3. Modeling of Turbulence

The standard $k-\varepsilon$ model that was proposed by Launder and Spalding (Launder and Spalding, 1972) is widely used in the CFD simulations of hydrodynamics and heat transfer, because of its reasonable accuracy and simplicity, where it solves two transport equations separately in which the turbulent velocity and length scales are determined independently. The derivation of the standard $k-\varepsilon$ model was based on the assumption that the flow is fully turbulent, and the effects of molecular viscosity are negligible (ANSYS, 2012). On the other hand, $k-\omega$ model shows better performance for low Reynolds number flows, but the negative aspect of this model is its relatively strong sensitivity of the solution to the values of k and ω outside the shear layer (free stream sensitivity). For this reason, the use of the standard $k-\omega$ model is not generally recommended in ANSYS FLUENT (ANSYS, 2012). Since the CFD simulations of this thesis are for churn turbulent flow only, the most suitable turbulence model that can be used is the standard $k-\varepsilon$ model. The standard $k-\varepsilon$ model comprises three turbulence sub models: the mixture turbulence model, the dispersed turbulence model, and a per-phase turbulence model (ANSYS, 2012). The mixture turbulence model can be used for stratified multiphase flow, and when the densities of phases are comparable. Since the density ratio between oxygen gas and molten CuCl is very big, mixture model cannot be used in this work. The advantage of the dispersed turbulence model is the less computational efforts needed than the per-phase turbulence model (ANSYS, 2012), therefore, the $k-\varepsilon$ dispersed turbulence model is used in this work for modeling the turbulence in the bubble column reactor.

4.4. Domain Description

The theoretical model of the multiphase oxygen SBC that was described above was based on using 2D-CFD simulations which were run using the ANSYS FLUENT V.13 software for a column with an overall diameter of 21.6 cm and three different heights of static liquid (45, 55, and 65 cm). First, ANSYS WORKBENCH V.13 was implemented to draw 2D geometries of the SBC and to create meshing. Quadratic mapped mesh was used for the area of the SBC and a very fine mesh

was used near the wall. The size of the mesh was selected so that to get the grid independence of α_g and U_V. After investigating the grids for different H and U_{gs}, it has been found that the most unfavourable situation is for $H = 65\ cm$ and $U_{gs} = 0.15\ m/s$. Table 4.1 shows the grid independence study that was used to select the optimum grid distribution of the SBC problem. From Table 4.1, it can be seen that the optimum grid is when the number of cells is 20,203 cells, because this will provide minimum relative errors of 0.43% and 0.25% for the values of α_g and U_V respectively, when compared with the grid of 56,341 cells. When using the grid of 56,341 cells, the memory requirement of the computer as well as the calculation time will increase significantly because the number of cells is more than twice of that of 20,203. Since the relative errors of α_g and U_V between the two grids are very small, it is preferred to use the grid of 20,203 cells and reduce the memory requirement of the computer and the calculation time. Fig. 4.1 shows the geometry and mesh used for the SBC with 21.6 cm inside diameter and 65 cm static liquid height (these dimensions are the same as the experimental system and the rationale for selecting them is stated in Chapter 2). The quantities of interest that were monitored during the CFD simulation were the overall gas holdup, inlet gas temperature, outlet gas temperature and slurry average temperature. The convergence criteria of the simulation was to ensure that the quantities of interest reached a steady state simulation and the residual RMS error values were less than 10^{-4}. Table 4.2 summarizes the setup of the SBC problem in ANSYS FLUENT.

Table 4.1 Grid independence test for a helium-water BC ($H = 65\ cm$, $U_{gs} = 0.15\ m/s$).

Total Cells	3,704	20,203	34,288	56,341
$\alpha_g\ (\%)$	22.3	23	22.8	23.1
$U_V\ (W/m^3.K)$	808.2	825.5	820.8	827.6

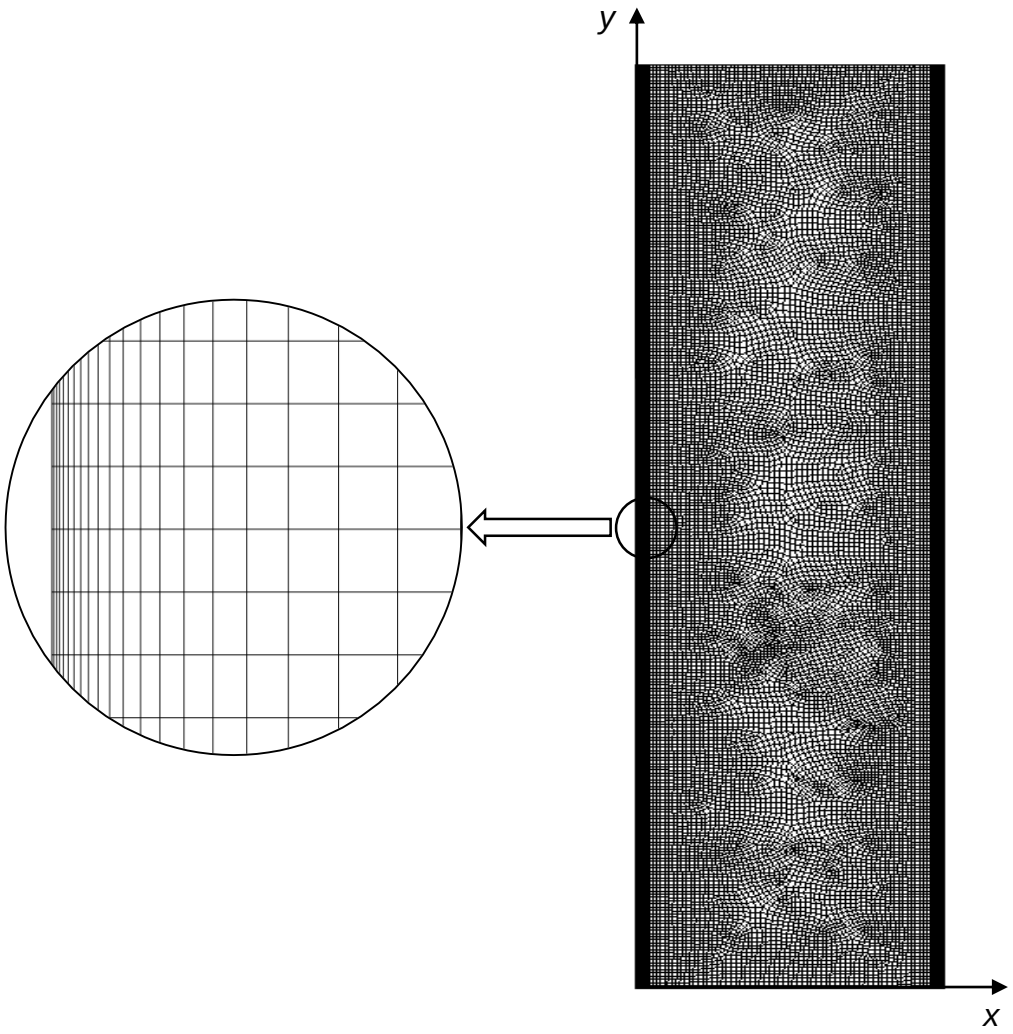

Fig. 4.1 Domain and detailed mesh used for the SBC in ANSYS WORKBENCH V.13.

Table 4.2 Summary of the SBC problem setup in ANSYS FLUENT.

General	*Solver Type*	Pressure-Based	
	Velocity Formulation	Absolute	
	Time	Steady	
	Gravity	ON	
	2D Space	Planar	
Models	Multiphase-Eulerian		
	Energy-On		
	Viscous-Standard $k-\varepsilon$, Standard Wall Function, Dispersed		
Materials	Water liquid		
	Helium gas		
Phases	Primary phase=liquid phase		
	Secondary Phase=gas phase		
Bubble Diameter	Sauter-mean diameter		
Solution Methods	*Scheme*	Phase-Coupled SIMPLE	
	Spatial Discretization	Gradient	Least Squares Cell Based
		Momentum	Second Order Upwind
		Volume Fraction	First Order Upwind
		Turbulent Kinetic Energy	Second Order Upwind
		Turbulent Dissipation Rate	Second Order Upwind
		Energy	Second Order Upwind
		Interfacial Area Concentration	Second Order Upwind
Number of Iterations	100,000		

Boundary conditions

The boundary conditions of the SBC can be represented by inlet, outlet and wall boundary conditions. The inlet volume fraction of the gas is equal to 1 and the inlet velocity of the gas is considered uniform and equal to the volumetric flow rate of the gas divided by the total cross-sectional area of the sparger's orifices.

According to Akhtar et al. (2006), the pressure boundary condition can be applied at the outlet of the column because it will produce better convergence. In all simulations, the outlet pressure is equal to atmospheric pressure. The no-slip boundary conditions are applied at the walls of the SBC. Symmetry conditions were not used in the simulations to be able to obtain better behaviors of

hydrodynamics and heat transfer. Because of the estimation difficulty of the liquid turbulence at the inlet and outlet boundary conditions of the liquid phase, iterations were used to specify the turbulent kinetic energy and dissipation rate.

4.5. Summary

From this chapter, the following points can be summarized for the CFD simulation of the multiphase flow in the oxygen bubble column reactor;

- An Eulerian multiphase flow model is used.
- Two phases are used in the simulation. The continuous phase is the slurry phase and the dispersed phase is the gas phase.
- The only force that is considered for the interphase momentum exchange is the drag force.
- The standard $k-\varepsilon$ dispersed model is chosen for modeling the turbulence in the bubble column reactor.

CHAPTER 5
EXPERIMENTAL RESULTS AND DISCUSSION

5.1. Introduction

In the oxygen reactor, since the materials of the inventories and the operating conditions are fixed, scale up analysis will include only the effects of gas flow rates, reactor dimensions, solid concentrations and solid particles sizes, on the reactor hydrodynamic and heat transfer. This chapter examines experimentally, the effects of superficial gas velocity (U_{gs}), static liquid height (H), solid particles concentration (C_s) and solid particle size (d_p), on the hydrodynamic and heat transfer studies of the oxygen SBCR. These effects are formulated in the forms of empirical equations, which include, the overall gas holdup (α_g), and the volumetric heat transfer coefficient (U_V).

5.2. Results of Hydrodynamic Studies

5.2.1. Overall Gas Holdup in the Water-Helium-Alumina SBCs

5.2.1.1. Calculation of the Gas Holdup (α_g)

The change of the pressure drop along the height of the bubble column, which is due to the passage of gas bubbles throughout the slurry phase, can be expressed as (Behkish, 2004);

$$\frac{dP}{dh} = -\rho_F \, g, \tag{5.1}$$

where ρ_F is the density of the multiphase system. The above expression can be integrated as follows (Behkish, 2004);

$$\int_{P_1}^{P_2} dP = -\int_{H_1}^{H_2} \rho_F \, g \, dh, \tag{5.2}$$

where H_1 and H_2 are the lower and higher positions of the pressure taps respectively, and P_1 and P_2 are the corresponding pressures measured at these positions by using pressure transducers. Eq. (5.2) hence gives (Behkish, 2004);

$$(P_1 - P_2) = \rho_F \, g \, (H_2 - H_1) \tag{5.3}$$

Eq. (5.3) can be rewritten in terms of ΔH, which is the distance between pressures taps, as (Behkish, 2004);

$$(P_1 - P_2) = \rho_F \, g \, \Delta H, \tag{5.4}$$

where $\Delta H = H_2 - H_1$

The density of the multiphase system ρ_F can be written in terms of the gas holdup (α_g) as follows;

$$\rho_F = \alpha_g \, \rho_g + \left(1 - \alpha_g\right) \rho_{sl}, \tag{5.5}$$

where ρ_g and ρ_{sl} are the gas and slurry densities respectively. By substituting Eq. (5.5) into Equation (5.4) and solving for α_g, the following expression for the gas holdup can be obtained;

$$\alpha_g = \left(\frac{\rho_{sl}}{\rho_{sl} - \rho_g}\right)\left(1 - \frac{P_1 - P_2}{\rho_{sl} \, g \, \Delta H}\right) \tag{5.6}$$

If $\rho_{sl} \gg \rho_g$, the above expression is reduced to;

$$\alpha_g = 1 - \frac{P_1 - P_2}{\rho_{sl} \, g \, \Delta H} \tag{5.7}$$

In the water-helium SBC, the gas holdup α_g is calculated from Eq. (5.7) for different U_{gs}, H, C_s and d_p. The results of this section and sections (5.2.1.2 - 5.2.1.6) have been published as a journal paper (Abdulrahman, 2016c).

5.2.1.2. Effect of Superficial Gas Velocity (U_{gs}) on α_g

To study the effect of U_{gs} on α_g, experiments were conducted for a range of U_{gs} from 0.01 to 0.15 m/s. For each velocity, the readings for pressures were noted down and the gas holdup was calculated from Eq. (5.7). Fig. 5.1 represents the plot of α_g variation with U_{gs} in the water-helium BC with $C_s = 0$ and $H = 65\ cm$. From this figure, it can be seen that α_g increases with U_{gs}. This is because of the

reduction in the hydrostatic pressure which reduces the pressure drop of the bed. The observed pressure drop recorded in pressure transducers for liquid bed, was found to be larger than that for gas-liquid system. The pressure drop decreases further with increasing the gas flow rate, because of the reduction in the hydrostatic pressure.

As seen from Fig. 5.1, the rate of increase in α_g, is higher at low U_{gs}, where the regime represents the bubbly flow regime. This corroborates the findings of Krishna et al. (1991) and Reilly et al. (1994). In the lower range of U_{gs}, as in the bubbly flow regime, when the gas velocity increases, the number of bubbles will increase with keeping the size of the bubble as approximately the same. Thus, the gas holdup will increase. When the velocity of the gas increases, as in the churn-turbulent flow regime, the size of the bubble increases because of the bubble coalescence, where the increase of bubble-bubble collisions results in increasing the rate of gas bubble coalescence. In this case, the large bubble holdup increases but the small bubbles holdup does not change with increasing U_{gs}. Since the large bubbles move faster than the small bubbles, this leads to a relative decrease in the gas holdup, but the overall gas holdup increases.

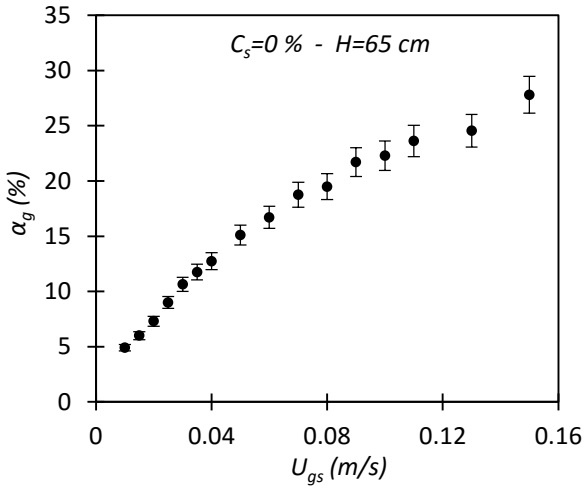

Fig. 5.1 Variation of α_g with U_{gs} for the helium-water BC with $C_s = 0\%$ and $H = 65\ cm$.

5.2.1.3. Effect of Static Liquid Height (H) on α_g

Figures 5.2 and 5.3 illustrate the effect of static liquid height (H) on the overall gas holdup (α_g) of the water-helium system with 0% and 5% concentration of solid particles (the rationale for selecting specific solid concentrations in the experiments is stated in Chapter 3). As can be seen in these figures, the overall gas holdups show a decreasing trend with height at any given U_{gs}, which agrees with the results of the literature (Jordan and Schumpe, 2001). For $C_s = 0\%$ and when H increases from 45 to 65 cm, the rate of decrease of the gas holdup is about 40% when $U_{gs} = 0.01\ m/s$ and is about 19% when $U_{gs} = 0.15\ m/s$. This decrease is due mainly to the decrease of the small bubbles gas holdup (Jordan and Schumpe, 2001). Also, for a given U_{gs}, the hydrostatic pressure and the pressure drop increases by increasing H, which leads to the decrease of α_g.

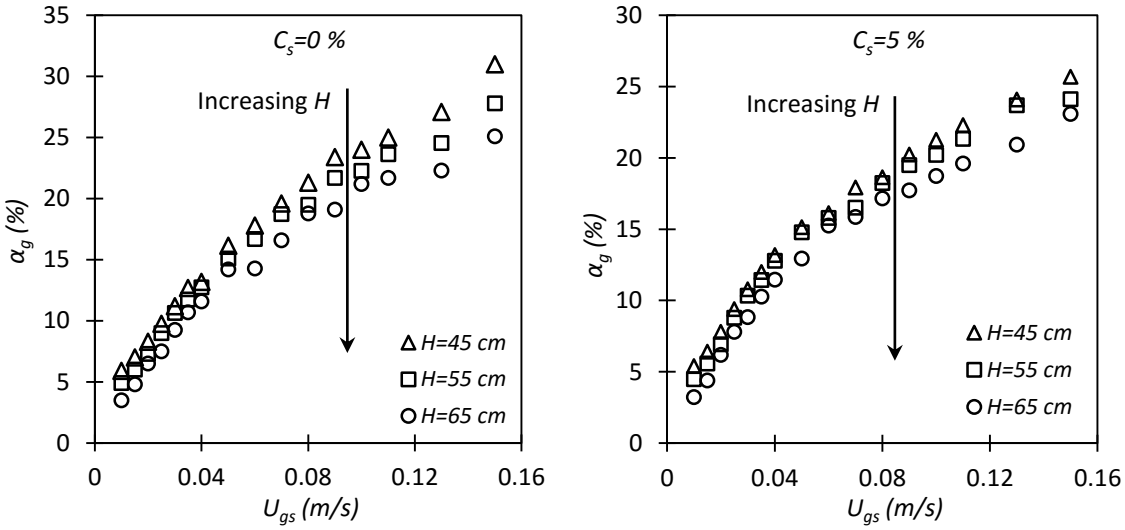

(a) (b)

Fig. 5.2 Variation of α_g with U_{gs} for the helium-water-alumina SBC for different H and a) $C_s = 0\%$, b) $C_s = 5\%$.

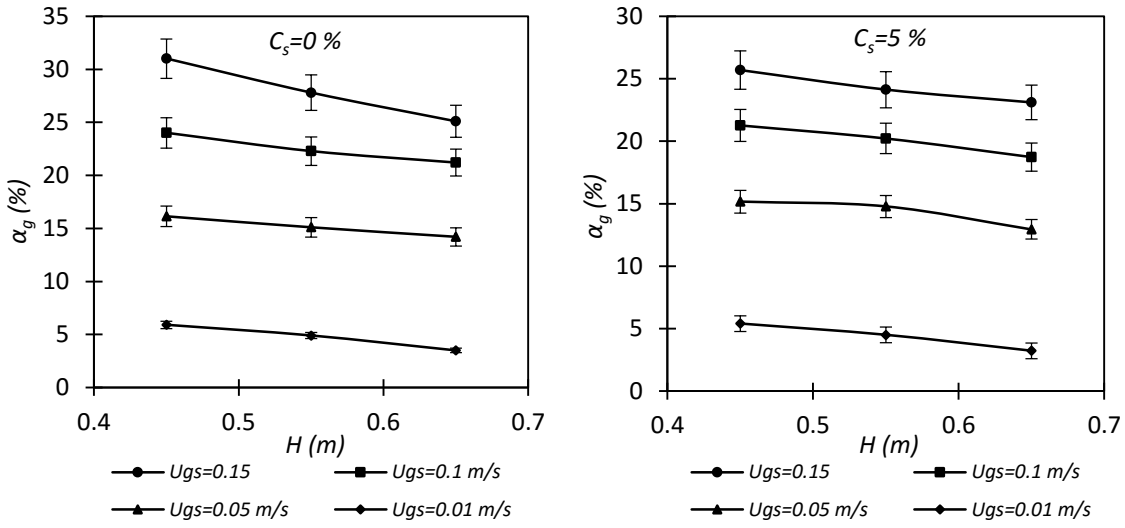

(a) (b)

Fig. 5.3 Variation of α_g with H of the helium-water-alumina SBC for different U_{gs} and a) $C_s = 0\%$, b) $C_s = 5\%$.

5.2.1.4. Effect of Solid Concentration (C_s) on α_g

Note that the solid concentration is expressed throughout this thesis in volume fraction of solids in the slurry without gas. The effects of solid concentration on overall gas holdup are shown in Figs. 5.4 and 5.5. As can be seen from these figures, the increase in solid concentration will decrease the overall gas holdup at all static liquid heights, which agrees with the results of literature (Deckwer, 1992; Fan et al., 1999; Inga and Morsi, 1999; Krishna and Sie, 2000; Krishna et al., 1997). For instance, in the case of $H = 45\ cm$ in the water-helium-alumina SBC, α_g in the absence of solid particles is equal to *31%* at $U_{gs} = 0.15\ m/s$, while at $C_s = 5\%$, it is equal to *25.7%* and at $C_s = 10\%$ is equal to *23.92%* at similar U_{gs}.

These behaviors can be interpreted on the basis that the slurry dynamic viscosity increases by increasing solid loading. This will enhance the formation of larger gas bubbles, and will decrease the break-up rate of the bubbles due to the enhancing of stabilities at interface. Therefore, by adding solids, more large bubbles will be created, which will rise faster and lead to a reduction in gas holdup.

It can also be seen from Figs. 5.4 and 5.5 that the rate of increase of α_g with U_{gs} decreases with increasing C_s. For instance, when $H = 45\ cm$, in the case of $C_s = 5\ \%$, the rate of gas holdup increase is about 20.8% when U_{gs} increases from

0.1 to 0.15 m/s, while in the case of $C_s = 10\ \%$, the increasing rate of α_g is about 16.7% in the same range of U_{gs}. This observation agrees with the literature findings (Lee et al., 1999). Furthermore, the decreasing rate of α_g values with C_s decreases by increasing C_s. For example, when $H = 45\ cm$ and $U_{gs} = 0.1\ m/s$, the value of α_g decreases by 9.1% for $C_s = 0 - 5\%$, while α_g only decreases by 2.8% for $C_s = 5 - 10\%$ at the same value of U_{gs}.

From above results, it can be concluded that the reduction in the overall gas holdup for helium-water system with the increase of solid concentration, is mainly because of the decrease in the gas holdup of small bubbles. When the solid concentration is high, the volume fraction of small bubbles gas holdup becomes so small that it can be neglected. Under these conditions, the increase of α_g with U_{gs} is mainly refered to the increase of large bubbles gas holdup. Krishna et al. (1997) have reported that in the heterogeneous flow regime, the change in the gas holdup of large bubbles is insignificant, while the gas holdup of small bubbles decreases significantly with increasing solid concentration (Behkish, 2004).

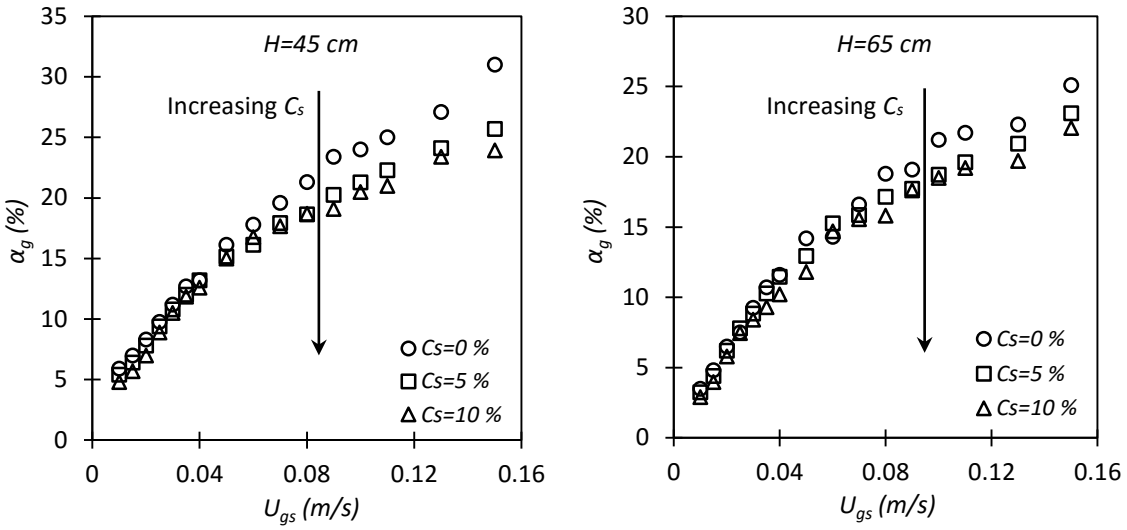

(a) (b)

Fig. 5.4 Variation of α_g with U_{gs} of the helium-water-alumina SBC with different C_s and a) $H = 45\ cm$, b) $H = 65\ cm$.

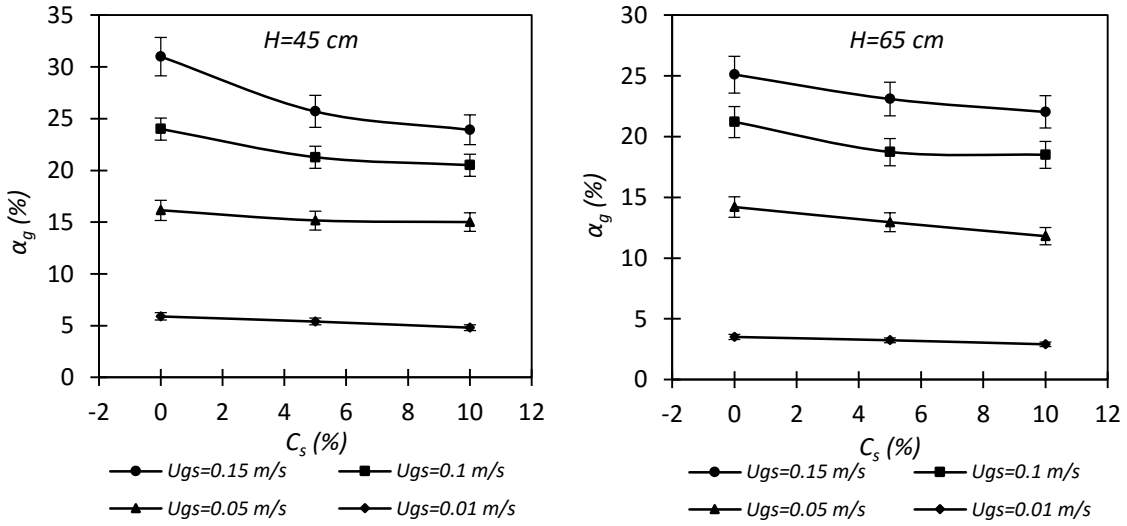

(a) (b)

Fig. 5.5 Variation of α_g with C_s of the helium-water-alumina SBC for different U_{gs} and a) $H = 45\ cm$, b) $H = 65\ cm$.

5.2.1.5. Effect of Solid Particle Size (d_p) on α_g

The effect of solid particle size (d_p) on overall gas holdup (α_g) of a helium-water-alumina SBC, with $C_s = 2\%$ and $H = 45\ cm$, is shown in Fig. 5.6. As can be seen from this figure, the change of α_g with d_p is negligible. This can be approved by using a nonlinear regression, where it is found that the overall gas holdup is proportional inversely with the size of solid particles according to the following equations;

$$\alpha_g \propto \left(\frac{D_R}{d_p}\right)^{0.0356}, (R^2 = 0.982), (homogeneous\ flow\ regime), \quad (5.8)$$

$$\alpha_g \propto \left(\frac{D_R}{d_p}\right)^{0.0138}, (R^2 = 0.991), (heterogeneous\ flow\ regime), \quad (5.9)$$

where d_p is the solid particle diameter in meters. From Eqs. (5.8) and (5.9), it can be seen that the exponent of the d_p is very small as a function with the gas holdup and the effect of the solid particle diameter can be neglected. The reason of this behavior is that, when the size of the solid particle increases, the number of particles decreases when keeping C_s as constant. Because of that, there is no significant effect of the solid particle diameter on the overall gas holdup for constant C_s.

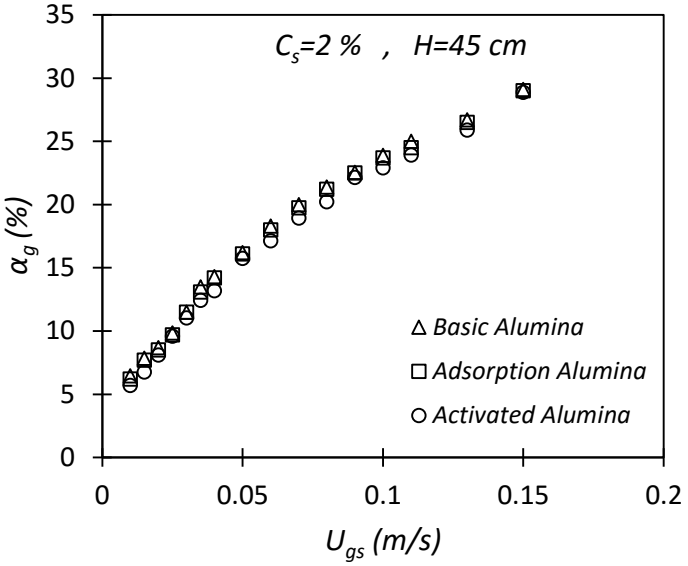

Fig. 5.6 Variation of α_g with U_{gs} for different solid particle sizes.

5.2.1.6. Comparison of α_g with Literature Data

The experimental results of this study was compared with the literature data of water-helium BCs. Fig. 5.7 shows the comparison of α_g between this study and the previous studies of Krishna et al. (1991) and Reilly et al. (1994), and Table 5.1 shows the experimental conditions of each study. From Table 5.1, it can be seen that, in the previous studies, both the liquid and gas phases have the same temperatures, which means that there is no heat transfer between the gas and liquid phases. In this thesis, the hydrodynamics of the helium-water system is investigated when there is direct contact heat transfer between the two phases. Fig. 5.7 shows that the gas holdup values obtained by Krishna et al. (1991) are in good agreements with this experimental study, with a maximum relative error less than 25%, because the reactor dimensions of their system are close to those of this study, but the gas temperature is different. A comparison between the data of Reilly et al. (1994) and those obtained in this study shows a fair agreement with a maximum relative error less than 44%, because of the difference in the reactors heights and gas temperatures. In general, the difference between α_g values in the previous and current studies is due mainly to the heat transfer between gas and liquid phases, where in the previous studies there were no heat transfer between

both phases, while in this study, direct contact heat transfer occurs between helium gas and liquid water. The heat transfer between both phases affects the sizes and speeds of the bubbles which is then affects the results of the overall gas holdup and the flow regime transition point.

Table 5.1 Experimental conditions of the compared studies.

Author	**Reactor dimensions (D_R x H_R)**	**Water liquid conditions**	**Helium gas conditions**
Krishna et al. (1991)	16cm × 120 cm	Pressure=0.1MPa Ambient Temperature	Pressure=0.1MPa Ambient Temperature
Reilly et al. (1994)	15cm × 270 cm	Pressure=0.1MPa Ambient Temperature	Pressure=0.1MPa Ambient Temperature
This study	21.6cm × 91.5 cm	Pressure=0.1MPa Ambient Temperature	Pressure=0.1MPa Temperature=90°C

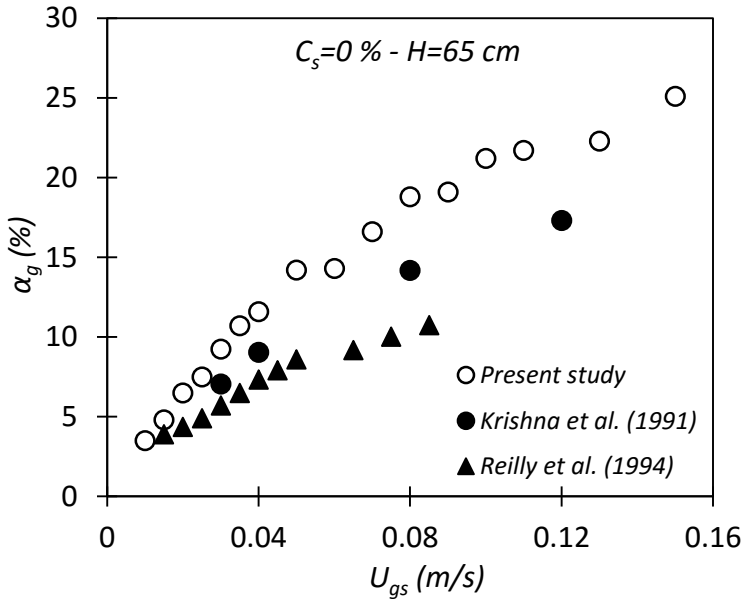

Fig. 5.7 Comparison of experimental gas holdup between the present study and the studies of Krishna et al. (1991) and Reilly et al. (1994).

5.2.1.7. Gas Holdup of the Oxygen Reactor

In Eq. (3.5), since each dimensionless group has approximately the same value for both helium-water and oxygen-CuCl molten salt systems, the overall gas holdup of both systems is equal, i.e.;

$$\left(\alpha_g\right)_{CuCl-O_2} = \left(\alpha_g\right)_{H_2O-He} \tag{5.10}$$

From Eq. (5.10), it can be concluded that both helium-water and oxygen-molten salt systems are similar hydrodynamically. That means, the hydrodynamic experiments that can be examined in helium-water system will give the nearly same results for the oxygen-CuCl molten salt system.

5.2.1.8. Summary of Overall Gas Holdup Results

The following points are summarized from the results of overall gas holdup $\left(\alpha_g\right)$;

- The overall gas holdup $\left(\alpha_g\right)$ increases by increasing U_{gs}, and the rate of increase in α_g with U_{gs} is higher in the bubbly flow regime than in the churn-turbulent flow regime.
- The overall gas holdup $\left(\alpha_g\right)$ decreases by increasing H at any given U_{gs}.
- The overall gas holdup $\left(\alpha_g\right)$ decreases by increasing C_s at all static liquid heights, and the rate of increase of α_g with U_{gs} decreases with increasing C_s. Also, the decreasing rate of α_g values with C_s decreases by increasing C_s.
- The effect of the solid particle size on α_g is negligible.

5.2.2. Flow Regimes Transitions

When the transition from one regime to another takes place, the behavior in the hydrodynamic of the system will be changed significantly. Since the flow regime transition depends on several parameters, the boundaries between the regimes are not exact and depend on the experimental setup and system used. It was found from the literature survey of this thesis that the slug flow regime usually occurs when the reactor diameter is small (less than 0.15 m). Also, it was shown that the column diameter has an insignificant effect on transition velocity when it is

beyond 0.15 m. Since the diameter of the experimental and industrial oxygen reactors are more than 0.15 m (where the diameter of the experimental reactor is 0.216 m and the diameter of the industrial oxygen reactor is in meters), it can be inferred that the regime of slug flow will not exist in both experimental and actual systems. Thus, in the oxygen reactor system, there is only one transition velocity, which is the transition velocity between the bubbly and churn-turbulent flow regimes and this velocity is independent of the reactor diameter. The results of this section and sub-sections (5.2.2.1 - 5.2.2.5) have been published as a journal paper (Abdulrahman, 2016d).

5.2.2.1. Calculation of the Transition Velocity $(U_{g-trans})$

In general, the evolution of global hydrodynamic parameter technique is used to specify the point of flow regime transition (Shaikh and Al-Dahhan, 2007). Typically, the flow regime can be specified from the plot of the overall gas holdup versus the superficial gas velocity. In the homogeneous regime, where the gas velocities are low, the relationship between α_g and U_{gs} is almost linear and has a slope greater than or closer to one and the line passes through the origin. In the heterogeneous regime, where the velocities of the gas are high, the relationship between α_g and U_{gs} deviates from linearity, because of the intense nonlinear interaction of bubbles, and has a slope less than one. From the slope variation of the gas holdup curve, the regime transition point can be identified (Shaikh and Al-Dahhan, 2007).

Based on design and operating conditions, gas holdup curve may looks like an S-shaped curve. In this case, the transition velocity will be this that correspond to the maximum value of α_g (Rados, 2003). However, it will be difficult to specify the transition point when the slope of the curve is changed gradually or the maximum value of the gas holdup curve is not shown. In this case, it is preferred to use the drift flux method proposed by Wallis (1969) which can give reliable results (Ruzicka et al., 2001b). In this method, the experimental gas holdup (α_g) is plotted versus the experimental drift flux, j_E, which is given by (Shaikh and Al-Dahhan, 2007);

$$j_E = U_{gs}(1 - \alpha_g) \pm U_{ls}\,\alpha_g, \tag{5.11}$$

where U_{gs} and U_{ls} are the superficial gas and liquid velocities respectively. The positive or negative sign represents the flow direction of the slurry relative to the gas flow direction, where the positive sign is used for counter-current flow and the negative sign is used for co-current flow (Shaikh and Al-Dahhan, 2007). In this study, since the liquid phase is stagnant, U_{ls} is neglected and Eq. (5.11) can be written as;

$$j_E = U_{gs}(1 - \alpha_g) \tag{5.12}$$

The theoretical drift flux velocity is defined as (Shaikh and Al-Dahhan, 2007);

$$j_T = u\,\alpha_g(1 - \alpha_g), \tag{5.13}$$

where u is determined from (Ruzicka et al., 2001b);

$$u = u_o\left(1 - \frac{a\,\alpha_g}{1 - \alpha_g}\right), \tag{5.14}$$

Eq. (5.14) is used for homogeneous regime, where the values of the bubble terminal velocity (u_o) and the bubble drift coefficient (a) can be obtained from the experimental data of α_g and U_{gs}. By using the basic relation;

$$\alpha_g = \frac{U_{gs}}{u}, \tag{5.15}$$

Eq. (5.14) will be;

$$\frac{U_{gs}}{\alpha_g} = u_o - (a\,u_o)\frac{\alpha_g}{1 - \alpha_g} \tag{5.16}$$

To find the transition velocity $(U_{g-trans})$, both the experimental and theoretical drift flux velocities (Eq. (5.12) and (5.13)) are drawn in the same graph as a function of α_g. In the bubbly flow regime, both the experimental and theoretical drift flux velocities are equal $(j_E = j_T)$, and the transition begins where the experimental data (j_E) departs from the theoretical curve (j_T). The transition point

from bubbly to churn turbulent flow regime can be specified from the slope variation of the curve. In general, the slope variation of the drift flux curve is sharper than that of the gas holdup curve (Shaikh, 2007). In this thesis, the drift flux method is used to specify the transition velocity between homogeneous and heterogeneous flow regimes of the water-helium system.

5.2.2.2 Transition Velocity of Water-Helium System

Figure 5.1 shows the evolution of the overall α_g with U_{gs} in a water-helium system at $C_s = 0\ \%$ and $H = 65\ cm$. From this figure, it can be seen that the slope variation is gradual, which makes it difficult to specify the transition point from this curve. In this case, a drift flux plot versus the overall gas holdup is used to indicate the regime transition point of the water-helium system. Fig. 5.8 shows the drift flux based on the overall gas holdup, for water-helium system with $C_s = 0\ \%$ and $H = 65\ cm$. The theoretical drift flux was determined from Eq. (5.13). From Fig. 5.8, it can be seen that the experimental data separate from the theoretical curve at around 2 – 2.5 cm/s (represented by void triangles), indicating the regime transition point, from bubbly to churn-turbulent flow around these velocities.

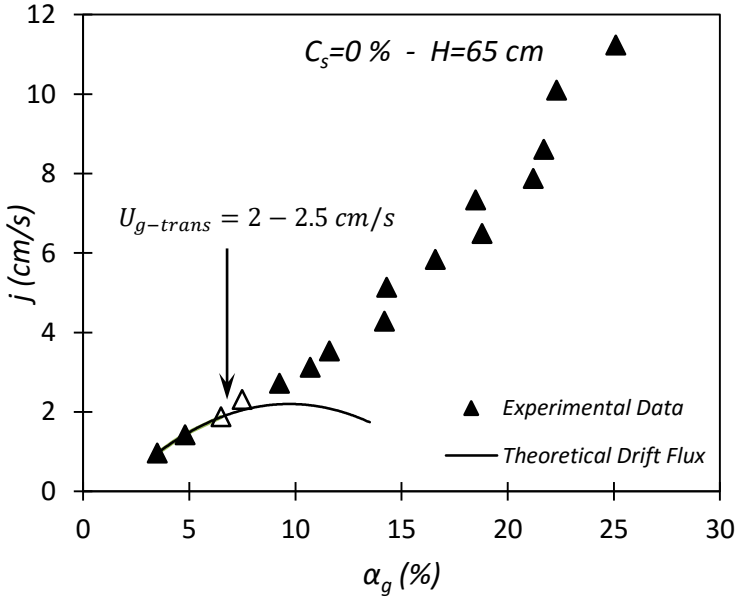

Fig. 5.8 Plot of drift flux based on α_g in the helium-water system with $C_s = 0\%$ and $H = 65\ cm$. The theoretical drift flux was determined from Eq. (5.13).

5.2.2.3. Effect of Static Liquid Height (H) on $U_{g-trans}$

Figs. 5.9 and 5.10 show the effect of the static liquid height (H) on the transition superficial gas velocity ($U_{g-trans}$) of the water-helium-alumina system. From these figures, it can be shown clearly that $U_{g-trans}$ (represented by void markers) decreases with H, which is in agreement with the literature findings (Ruzicka et al., 2001b; Sarrafi et al., 1999; Wilkinson, 1991). The rate of decrease of $U_{g-trans}$ ranges from about 11% to 23% when H increases from 45 cm to 65 cm. This decrease is due mainly to the gravity effect.

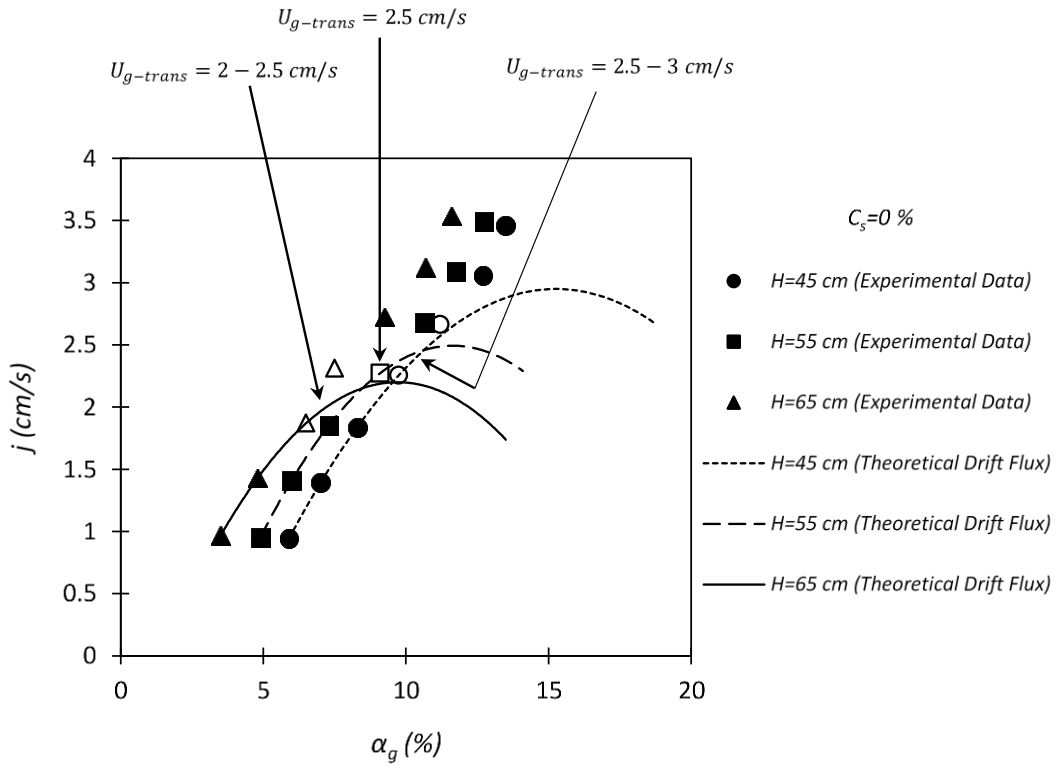

Fig. 5.9 Transition superficial gas velocities from the plot of the drift flux versus α_g of the helium-water system with $C_s = 0\%$ and different H. The theoretical drift flux was determined from Eq. (5.13).

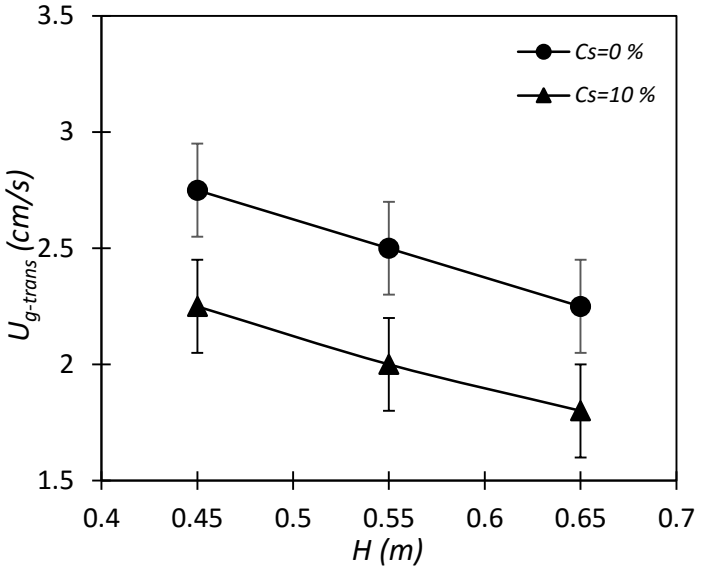

Fig. 5.10 The transition superficial gas velocity versus H of the helium-water system with different C_s values.

5.2.2.4. Effect of Solid Concentration (C_s) on $U_{g-trans}$

The effect of C_s on U_{gs} is shown in Figs. 5.11 and 5.12. Fig. 5.11 shows the plot of the drift flux versus the overall gas holdup in the water-helium-alumina system with $H = 45\ cm$. From Fig. 5.11, it can be observed that, the point at which the theoretical drift flux separates from the experimental one (void markers), shifts towards lower U_{gs} with an increase in C_s. This advance of the flow regime transition is caused by the relatively early formation of the large bubbles at higher solids concentrations. The high rise velocity of the large bubbles, results in lower gas holdup.

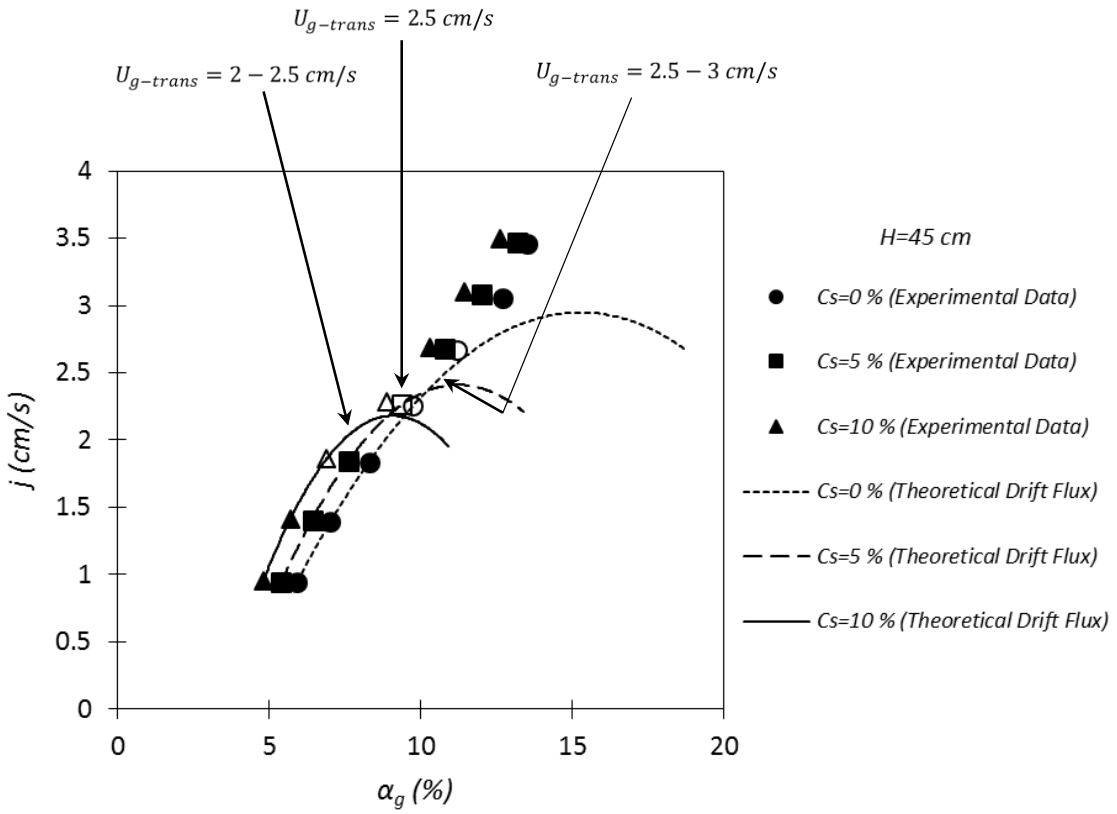

Fig. 5.11 Effect of solids loading on thedrift flux plot in the helium-water-alumina SBC. The theoretical drift flux was determined from Eq. (5.13).

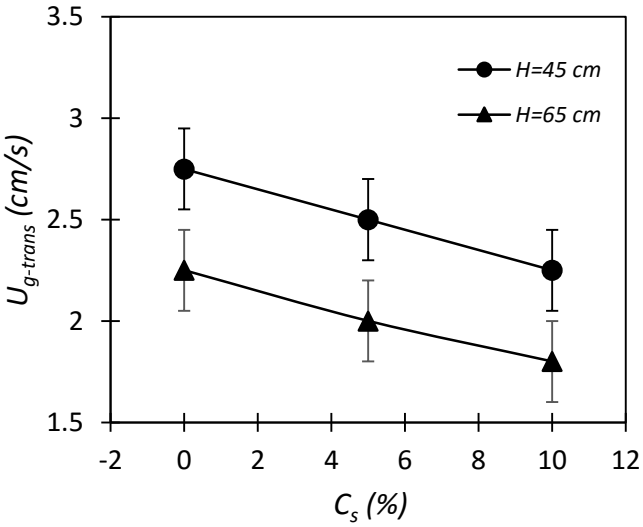

Fig. 5.12 The transition superficial gas velocity versus C_s of the helium-water system with different H values.

5.2.2.5. Comparison of $U_{g-trans}$ with Literature Data

In this section, the experimental results of the transition velocity of this thesis are compared with the previous experimental data of Krishna et al. (1991) and Reilly et al. (1994) (the details of the previous works are stated in Chapter 2). The experimental data of Krishna et al. (1991) are fitted by using the second order polynomial, with $R^2 = 0.9887$, to the following equation (see Fig. 5.13);

$$U_{g-trans} = -0.0001\ \rho_g^2 + 0.0072\ \rho_g - 0.0002, \qquad (5.17)$$

where $U_{g-trans}$ in m/s and ρ_g in Kg/m^3. By substituting the value of the helium gas density at 90ºC $\left(\rho_g = 0.1344\ kg/m^3\right)$ into Eq. (5.17), the transition velocity of water-helium system, with a reactor diameter of 16 cm and a height of 120 cm, will be 0.000766 m/s. This value represents the transition velocity of the system studied by Krishna et al. (1991).

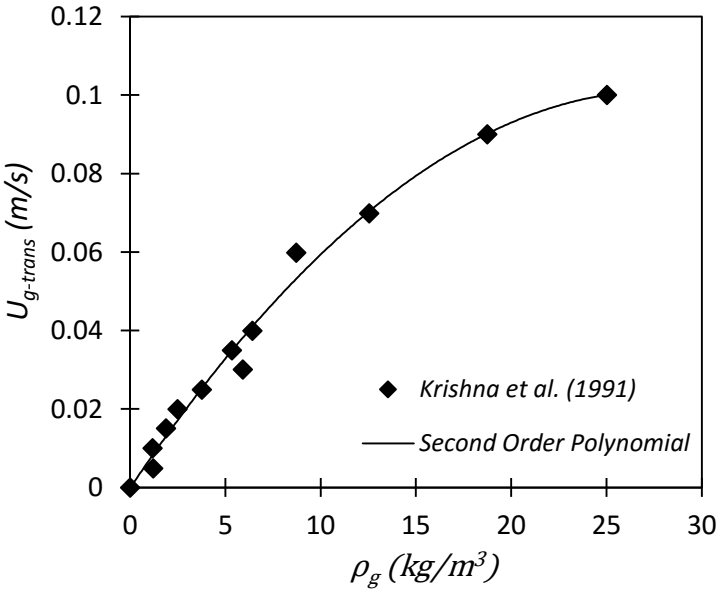

Fig. 5.13 Regime transition velocity $\left(U_{g-trans}\right)$ versus gas density $\left(\rho_g\right)$ in water.

Table 5.2 shows the comparisons in the transition velocities between the experimental studies of this thesis (at zero solid concentration) and the above previous studies. From this table, it can be seen that, the study of Krishna et al. (1991) have under predicted the transition velocity compared to that of Reilly et al.

(1994). It is noted that the experimental value of the transition velocity is closer to that of Reilly et al. (1994) and the percentage of error is due to the differences in the static liquid heights and gas temperatures between both systems, where the height of the experimental work is 65 cm and of Reilly et al. (1994) is 270 cm, and the helium gas temperature of this work is 90 ^{o}C and of Reilly et al. (1994) is ambient temperature.

Table 5.2 Comparison of transition velocities between the present experimental study and previous studies in a water-helium system.

Present Experimental Study	**Krishna et al. (1991)**		**Reilly et al. (1994)**	
$U_{g-trans}$ (cm/s)	$U_{g-trans}$ (cm/s)	Relative Max. Error (%)	$U_{g-trans}$ (cm/s)	Relative Max Error (%)
2 - 2.5	0.0766	96	1.22	39

5.2.2.6. The Transition Velocity of the Oxygen Reactor

The transition velocity of the actual materials of the oxygen reactor (i.e. molten CuCl and O_2 gas), can be obtained by using Eq. (3.6), where $Re_{g-trans}$ of both H_2O-He and CuCl-O_2 systems are equal.

$$\left(Re_{g-trans}\right)_{H_2O-He} = \left(Re_{g-trans}\right)_{CuCl-O_2} \tag{5.20}$$

From Eq. (5.20), the transition velocity of the actual materials can be expressed as;

$$\left(U_{g-trans}\right)_{CuCl-O_2} = \frac{\rho_{He}}{\rho_{O_2}} \frac{\mu_{O_2}}{\mu_{He}} \left(U_{g-trans}\right)_{H_2O-He}, \tag{5.21}$$

where ρ_{He} and ρ_{O_2} are the densities of helium and oxygen gases respectively and μ_{He} and μ_{O_2} are the dynamic viscosities of helium and oxygen gases respectively. From Eq. (5.21), the flow regime transition velocity of CuCl-O_2 system, with a reactor diameter of 21.6 cm and a height of 45 cm, can be calculated as $\left(U_{g-trans}\right)_{CuCl-O_2} = 0.0148 - 0.0178\, m/s$. Fig. 5.14 shows the transition velocities

of the actual materials of the oxygen reactor for different static liquid heights and solid concentrations.

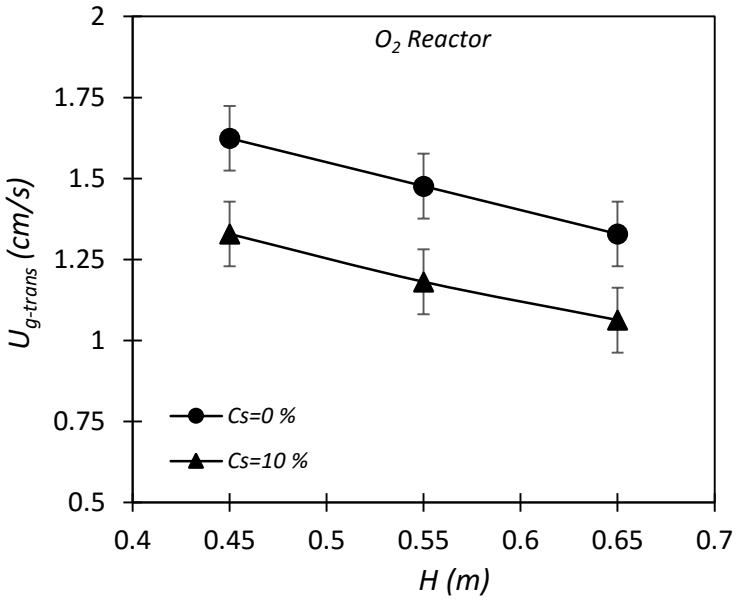

Fig. 5.14 The transition velocity versus H for the actual materials of the oxygen reactor for different C_s values.

5.2.2.7. Superficial Gas Velocity of a Stoichiometric Oxygen Gas

In order to know the flow regime of the oxygen reactor, it is necessary to calculate the superficial gas velocity of the stoichiometric oxygen gas, which is produced from the thermal decomposition process of the copper oxychloride solid particles inside the oxygen reactor at 530°C. The superficial gas velocity of the stoichiometric oxygen gas depends on the oxygen (or hydrogen) production rate and the diameter of the oxygen reactor. Fig. 5.15 shows the values of the superficial oxygen gas velocity for different reactor diameters and oxygen production rates. From this figure, it can be seen that the superficial oxygen gas velocity decreases by increasing the reactor diameter and decreasing the oxygen production rate. The minimum value of the superficial oxygen gas velocity is about 1.5 m/s when the reactor diameter is 4m and the oxygen production rate is 800 tonne/day. This minimum value is higher than the transition velocity of the oxygen reactor system with $C_s = 0\ \%$ and $H = 45\ cm$, by more than 80 times. Since the

transition velocity of the oxygen reactor decreases by increasing C_s and/or increasing H, and since these parameters are large in the actual oxygen reactor, therefore, it is expected that the minimum stoichiometric superficial oxygen gas velocity will be too much higher than the transition velocity of the oxygen reactor system. From that, it can be concluded that bubbly flow regime will never be existing in the oxygen reactor system and the only regime that will be available in the oxygen reactor is the churn-turbulent flow regime.

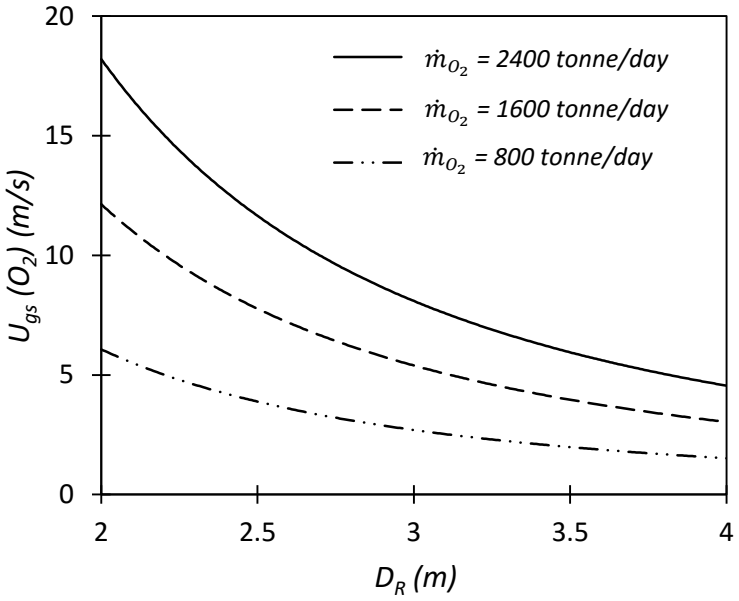

Fig. 5.15 Values of the superficial stoichiometric oxygen gas velocity for different reactor diameters (D_R) and oxygen production rates $(\dot{m}_{O_2})$.

5.2.2.8. Summary of Transition Velocity Results

From the results of the transition velocity, the following points can be concluded;

- In the oxygen reactor system, there is only one transition velocity, which is the transition velocity between the bubbly and churn-turbulent flow regimes, and this velocity is independent of the reactor diameter. The slug flow regime does not exist in the oxygen reactor.
- The transition velocity $(U_{g-trans})$ decreases by increasing H.
- The transition velocity $(U_{g-trans})$ decreases by increasing C_s.

- Bubbly flow regime will never be existing in the oxygen reactor system and the only regime that will be available in the oxygen reactor is the churn-turbulent flow regime.

5.2.3. Dimensional Analysis of Gas Holdup

In this section, dimensional analysis is used to define the effects of gas velocity, reactor height, and solid concentration in the water-helium SBC. In the hydrodynamic studies of the SBC, the interested particular physical quantity, is the gas holdup (α_g). Possible variables on which α_g in the water-helium-alumina system may depend are; gas properties (e.g., gas density (ρ_g) and gas viscosity (μ_g)), liquid properties (e.g., liquid density (ρ_l) and liquid viscosity (μ_l)), surface tension (σ), SBC geometry (e.g., reactor height (H_R), reactor diameter (D_R) and sparger hole diameter (d_o)), solid particles properties (e.g., solid density (ρ_s), solid concentration (C_s) and solid particle size (d_p)) and flow conditions (e.g., superficial gas velocity (U_{gs})). The height of the reactor (H_R) is considered as the same of the static liquid height. The equation of α_g can be written in the following form;

$$\alpha_g = f(\rho_s, \rho_l\, \rho_g, \mu_l, \mu_g, \sigma, U_{gs}, D_R, H_R, d_o, C_s, d_p) \tag{5.22}$$

The dimensional analysis carried out by Buckingham's pi theorem, indicates that the gas holdup may be simplified in terms of dimensionless groups as;

$$\alpha_g = f\left(\frac{\rho_s}{\rho_l}, \frac{\rho_g}{\rho_l}, \frac{\mu_g}{\mu_l}, Re_l, \frac{Re_l^2}{We_l}, \frac{H_R}{D_R}, \frac{d_o}{D_R}, \frac{d_p}{D_R}, C_s\right), \tag{5.23}$$

where;

$$Re_l = \frac{\rho_l\, U_{gs}\, D_R}{\mu_l}, \tag{5.24}$$

$$We_l = \frac{\rho_l\, {U_{gs}}^2\, D_R}{\sigma} \tag{5.25}$$

Since the materials of the oxygen reactor inventories and the reactor operating conditions are not changed during the reactor operation, the materials

properties $\left(\rho_{sl}, \rho_g, \mu_{sl}, \mu_g, \sigma\right)$ can be fixed in the dimensional analysis. Also, the sparger hole diameter (d_o) is fixed in this study, because the gas sparger has insignificant influence on gas holdup if the hole diameters are larger than 2mm, and the hole diameter that is used in the experimental study of this work is 3mm. Moreover, the effect of the solid particle diameter on gas holdup is negligible, as it was shown in Fig. 5.6. In this case, the dimensionless groups $\left(\frac{\rho_g}{\rho_{sl}}, \frac{\mu_g}{\mu_{sl}}, \frac{d_o}{D_R}, \frac{d_p}{D_R} \text{ and } \frac{Re_l^2}{We_l}\right)$ can be omitted, and Eq. (5.23) will be;

$$\alpha_g = f\left(Re_l, \frac{H_R}{D_R}, C_s\right) \tag{5.26}$$

The functional equation (Eq. (5.26)) can be written as;

$$\alpha_g = C\left(\frac{H_R}{D_R}\right)^a (Re_l)^b (1 - C_s)^c, \tag{5.27}$$

where the constant C and the exponents a, b and c are the pending coefficients that can be determined from experiments. In Eq. (5.27), the term $(1 - C_s)$ was used instead of (C_s) to avoid getting values of infinity when using zero concentration of solid particles.

Since the hydrodynamics of the homogeneous flow regime is different than that of the churn-turbulent flow regime, two empirical equations of gas holdup can be obtained from the experimental studies. One for the homogeneous flow regime which include the experimental data for $U_{gs} < U_{g-trans}$, and the other for churn-turbulent flow regime which include the experimental data for $U_{gs} > U_{g-trans}$. Different experiments were performed for different U_{gs}, H_R, and C_s to measure the pressures from pressure transducers and then calculate α_g from Eq. (5.7). The pending coefficients in Eq. (5.27) are obtained by non-linear regressions for both homogeneous and churn-turbulent flow regimes, as shown in the following equations;

Homogeneous flow regime;

$$\alpha_g = 0.083 \left(\frac{D_R}{H_R}\right)^{1.023} (Re_l)^{0.645} (1 - C_s)^{1.822}, (R^2 = 0.953) \qquad (5.28)$$

Churn-turbulent flow regime;

$$\alpha_g = 0.085 \left(\frac{D_R}{H_R}\right)^{0.433} (Re_l)^{0.594} (1 - C_s)^{1.196}, (R^2 = 0.982) \qquad (5.29)$$

The empirical equations (5.28) and (5.29) are used for; $\frac{H_R}{D_R} \leq 4$, $C_s \leq 15$ % and $U_{gs} \leq 0.15\ m/s$. To check the validity of Eqs. (5.28) and (5.29), the gas holdup (α_g) is calculated by these equations, under the same experimental conditions, and is plotted with the experimental data (see Fig. 5.16). It is found that the empirical α_g values agree well with the experimental values, and the maximum relative error is less than 12.5% for the homogeneous flow regime and less than 15.5% for the heterogeneous flow regime. Therefore, Eqs. (5.28) and (5.29) can be used to specify gas holdup in the helium-water-alumina system.

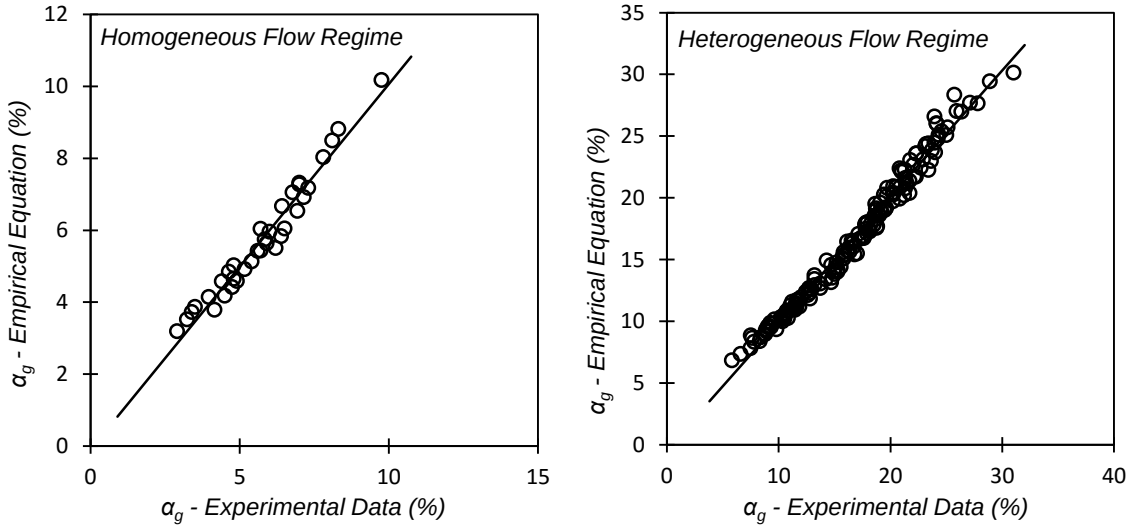

(a) (b)

Fig. 5.16 Empirical equation versus experimental data of α_g (a) Eq. (5.28) and (b) Eq. (5.29), for different H and C_s.

5.3. Results of Heat Transfer Studies

5.3.1. Calculation of the Volumetric Heat Transfer Coefficient

When the area between the two separate fluids (i.e. gas and liquid) is known, the heat power exchanged can be calculated as;

$$\dot{Q} = U_A \, A_i \, \Delta T_{lm}, \tag{5.30}$$

where U_A ($W/m^2.{}^oC$) is the overall heat transfer coefficient based on the fluid interface area A_i (m^2), and ΔT_{lm} (^oC) is the LMTD which can be expressed as;

$$\Delta T_{lm} = \frac{T_{g,in} - T_{g,out}}{ln\left(\frac{T_{g,in} - \bar{T}_{sl}}{T_{g,out} - \bar{T}_{sl}}\right)} \tag{5.31}$$

In Eq. (5.31), $T_{g,in}$ and $T_{g,out}$ are the inlet and outlet gas temperatures respectively, and $\bar{T}_{sl}$ is the average temperature of the slurry.

There are several problems exist with the approach of Eq. (5.30). First, the area-based heat transfer coefficient on the fundamental bubble level may be difficult to estimate. Second, the area of that interface can also be difficult to determine. Third, even if the area is known, it is usual for it to vary considerably throughout the reactor. A more easily evaluated approach that has been used in many studies reported in the literature is to replace the area-based heat transfer characteristics with volume-based values. In this case, the heating power exchanged is expressed as (Robert, 2003);

$$\dot{Q} = U_V \, V_R \, \Delta T_{lm}, \tag{5.32}$$

where V_R is the total internal volume of the reactor and U_V is the volumetric heat transfer coefficient. Although the latter can suffer from imprecision about details of the heat transfer variations as indicated in the area-based approach, the assumption made here is that the result is a composite for the overall situation. The volume V_R includes the total volume of the slurry and gas. It changes with the gas flow rate and static liquid height and can be calculated from the gas holdup by using Eq. (1.5).

The exchanged heating power $\dot{Q}$ can be determined from the heating power exchanged by the gas phase, which is expressed as;

$$\dot{Q} = \dot{m}_g \, C_{p,g} \left(T_{g,in} - T_{g,out}\right), \tag{5.33}$$

where $\dot{m}_g$ (kg/s) is the gas mass flow rate and $C_{p,g}$ (J/kg.^{o}C) is the gas specific heat at constant pressure. Substitute Eq. (5.31) and (5.33) into Eq. (5.32) and solve for U_V to get;

$$U_V = \frac{\dot{m}_g \, C_{p,g}}{V_R} \, ln\left(\frac{T_{g,in} - \bar{T}_{sl}}{T_{g,out} - \bar{T}_{sl}}\right), \tag{5.34}$$

where $T_{g,in}$ and $T_{g,out}$ are the inlet and outlet thermocouples readings that represent the inlet and outlet gas temperatures respectively and $\bar{T}_{sl}$ is the average temperature of the slurry, which is calculated from the thermocouples (that are submerged in the slurry) after stopping the gas injection into the reactor for few seconds.

The experimental data of the volumetric heat transfer coefficient was correlated using a priori information, such as, gas physical properties and reactor dimensions. Hence helium gas properties such as density and specific heat are calculated at the average gas temperature ($\bar{T}_g$), where;

$$\bar{T}_g = \frac{T_{g,in} + T_{g,out}}{2} \tag{5.35}$$

The results of this section and sub-sections (5.3.1 – 5.3.5) have been published as a journal paper (Abdulrahman, 2015).

5.3.2. Effect of Superficial Gas Velocity (U_{gs}) on U_V

To study the effect of U_{gs} on U_V, experiments were conducted for a range of U_{gs} from 0.01 to 0.15 m/s. For each velocity, the readings for thermocouples were noted down and U_V was calculated from Eq. (5.34). Fig. 5.17 represents the variation of U_V with U_{gs}, in the water-helium BC with $C_s = 0$ % and $H = 65\ cm$. From this figure, it can be seen that U_V increases by increasing U_{gs}. This behavior is due

to the increase in the gas flow rate which results in higher relative velocities between gas bubbles and liquid, and hence higher heat transfer rates. The results show that (U_V) increases by about 44%, when increasing U_{gs} velocity from 0.1 to 0.15 m/s.

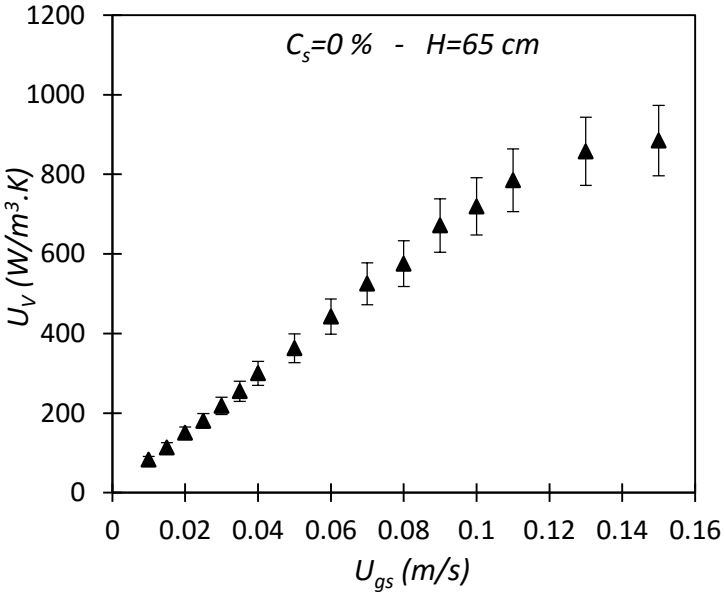

Fig. 5.17 Volumetric heat transfer coefficient versus U_{gs} in the helium-water BC with $C_s = 0\%$ and $H = 65\ cm$.

5.3.3. Effect of Static Liquid Height (H) on U_V

Figures 5.18-5.19 illustrate the effect of H on U_V of the water-helium system with $C_s = 0\ \%$ and $C_s = 5\ \%$. As can be seen in these figures, U_V shows a decreasing trend with H at any given U_{gs}. When $C_s = 0\ \%$, the rate of decrease of U_V is from 39-82% (for $U_{gs} = 0.01\ to\ 0.15\ m/s$), when H increases from 45 to 65 cm. This decrease is due mainly to the increase of slurry volume. Also, for a given U_{gs}, the hydrostatic pressure increases by increasing H which leads to the decrease of slurry mixing rate.

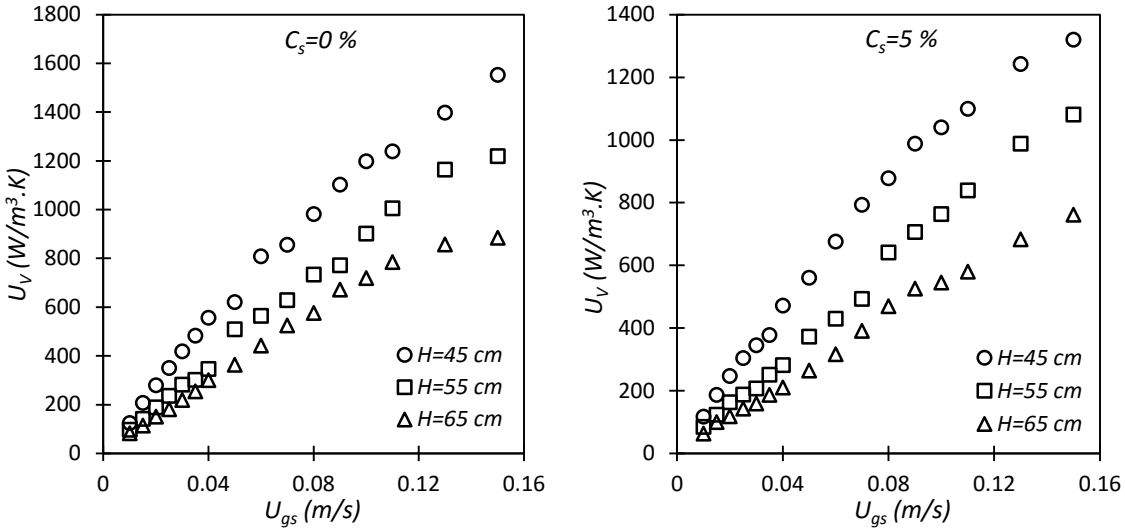

(a) (b)

Fig. 5.18 Volumetric heat transfer coefficient versus U_{gs} of the helium-water-alumina SBC for different H and a) $C_s = 0\%$, b) $C_s = 5\%$.

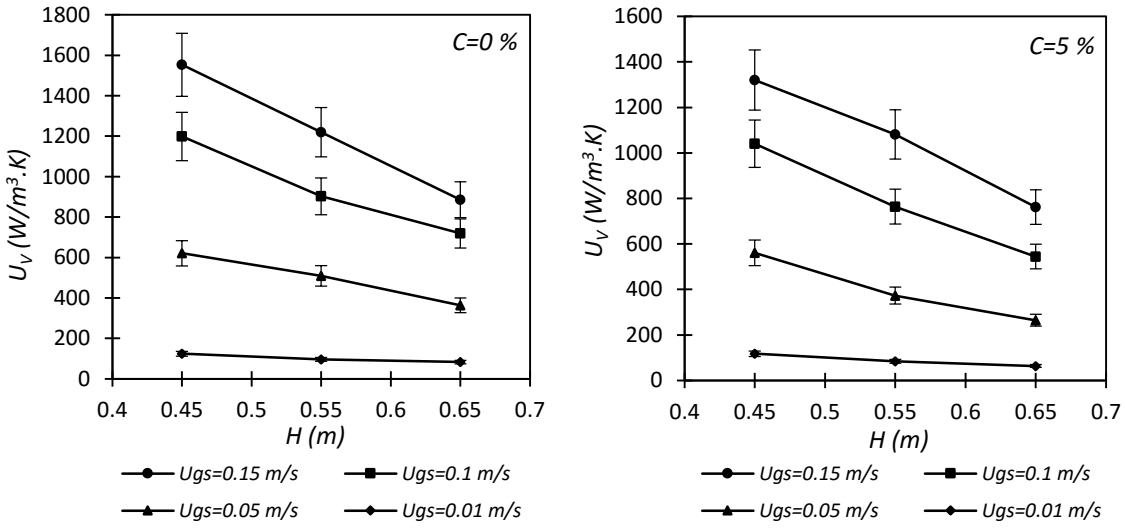

(a) (b)

Fig. 5.19 Volumetric heat transfer coefficient versus H of the helium-water-alumina SBC for different U_{gs} and a) $C_s = 0\%$, b) $C_s = 5\%$.

5.3.4. Effect of Solid Concentration (C_s) on U_V

Figures 5.20 and 5.21 show the effect of C_s on U_V versus U_{gs} for different H. From these figures, it can be seen that U_V decreases by increasing C_s at all static liquid heights. For instance, in the case of $H = 45\ cm$ and $C_s = 0\ \%$, in the water-helium-alumina SBC, U_V is equal to 1552.6 W/m^3.K at $U_{gs} = 0.15\ m/s$, while at $C_s = 5\%$, it is equal to 1319.8 W/m^3.K and at $C_s = 10\%$ is equal to 1221.9 W/m^3.K at the same U_{gs}. These behaviors can be attributed to the fact that increasing C_s leads to the increase of large bubbles and decrease of gas holdup, which leads to the decrease of the heat transfer rate between the gas and slurry.

It can also be noted from Figs. 5.20 and 5.21, that the rate of decrease of U_V values with C_s is approximately the same for different U_{gs}. For example, when $H = 45\ cm$ and $U_{gs} = 0.01\ m/s$, the value of U_V decreases by 21.8% for $C_s = 0 - 10\%$, and U_V decreases by 21.3% when $U_{gs} = 0.15\ m/s$ at the same value of H.

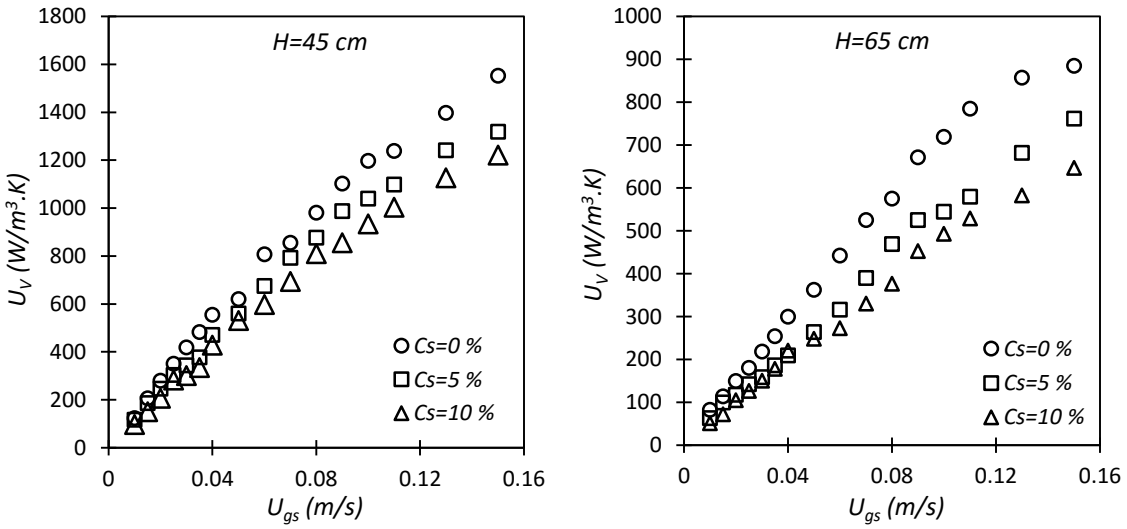

Fig. 5.20 Volumetric heat transfer coefficient versus U_{gs} of the helium-water-alumina SBC for different C_s and a) $H = 45\ cm$, b) $H = 65\ cm$.

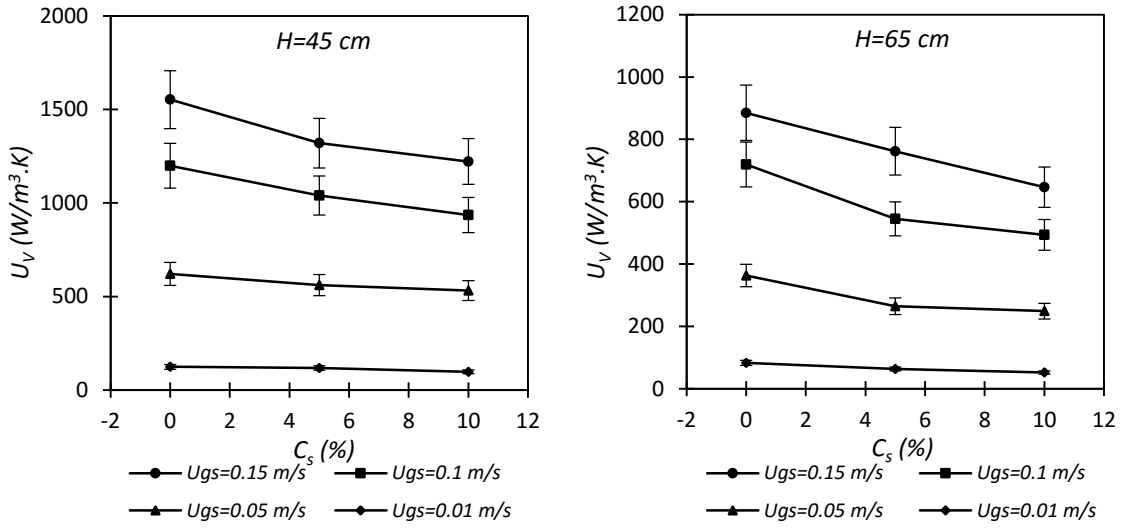

Fig. 5.21 Volumetric heat transfer coefficient versus C_s of the helium-water-alumina SBC for different U_{gs} and a) $H = 45\ cm$, b) $H = 65\ cm$.

5.3.5. Dimensional Analysis of Volumetric Heat Transfer Coefficient

In this section, the dimensional analysis of the volumetric heat transfer coefficient is studied by following the same procedure of the dimensional analysis for α_g. In the heat transfer studies of the SBC, the interested particular physical quantity, is the volumetric heat transfer coefficient (U_V). The conceivable variables on which U_V in the water-helium-alumina system may depend are the same of that in gas holdup in addition to the heat transfer parameters, such as the thermal conductivity and the specific heat of each phase (gas, liquid and solid). Therefore, U_V can be written in the following form;

$$U_V = f\left(\rho_s, \rho_l, \rho_g, \mu_l, \mu_g, k_s, k_l, k_g, C_{p,s}, C_{p,l}, C_{p,g}, \sigma, U_{gs}, D_R, H_R, d_o, C_s, d_p\right) \qquad (5.36)$$

By using Buckingham's pi theorem, the volumetric heat transfer coefficient may be simplified in terms of dimensionless groups as;

$$Nu_V = f\left(\frac{\rho_s}{\rho_l}, \frac{\rho_g}{\rho_{sl}}, \frac{\mu_g}{\mu_l}, \frac{k_s}{k_l}, \frac{k_g}{k_l}, \frac{C_{p,s}}{C_{p,l}}, \frac{C_{p,g}}{C_{p,l}}, Re_l, \frac{Re_l^2}{We_l}, Pr_l, \frac{H_R}{D_R}, \frac{d_o}{D_R}, \frac{d_p}{D_R}, C_s\right), \qquad (5.37)$$

where;

$$Nu_V = \frac{U_V\, D_R^2}{k_l} \tag{5.38}$$

$$Re_l = \frac{\rho_l\, U_{gs}\, D_R}{\mu_l} \tag{5.39}$$

$$We_l = \frac{\rho_l\, {U_{gs}}^2\, D_R}{\sigma} \tag{5.40}$$

$$Pr_l = \frac{C_{p,l}\, \mu_l}{k_l} \tag{5.41}$$

By fixing the materials properties $\left(\rho_s, \rho_l, \rho_g, \mu_l, \mu_g, k_s, k_l, k_g, C_{p,s}, C_{p,l}, C_{p,g}, \sigma\right)$, the sparger hole diameter (d_o), and the solid particle size (d_p), the dimensionless groups $\left(\frac{\rho_s}{\rho_l}, \frac{\rho_g}{\rho_l}, \frac{\mu_g}{\mu_l}, \frac{k_s}{k_l}, \frac{k_g}{k_l}, \frac{C_{p,s}}{C_{p,l}}, \frac{C_{p,g}}{C_{p,l}}, \frac{d_o}{D_R}, \frac{d_p}{D_R}, Pr_l \text{ and } \frac{Re_l^2}{We_l}\right)$ can be omitted, and Eq. (5.37) will be;

$$Nu_V = f\left(Re_l, \frac{H_R}{D_R}, C_s\right) \tag{5.42}$$

The functional equation (Eq. (5.42)) can be written as;

$$Nu_V = C\, \left(\frac{H_R}{D_R}\right)^a\, (Re_l)^b\, (1 - C_s)^c, \tag{5.43}$$

where the constant C and the exponents a, b and c are the pending coefficients that can be determined from experiments.

Different experiments were performed for different U_{gs}, H_R and C_s to measure the temperatures from thermocouples and then calculate Nu_V from Eq. (5.34 & 5.38). Then the pending coefficients in Eq. (5.43) are obtained by non-linear regressions as shown in the following equations;

Homogeneous flow regime;

$$Nu_V = 0.0165\, \left(\frac{D_R}{H_R}\right)^{1.71}\, Re_l\, (1 - C_s)^{3.32}, \;\; R^2 = 0.99 \tag{5.44}$$

Churn-turbulent flow regime;

$$Nu_V = 0.0315 \left(\frac{D_R}{H_R}\right)^{1.765} (Re_l)^{0.93} (1 - C_s)^{2.94}, \;\; R^2 = 0.99 \qquad (5.45)$$

The empirical equations (5.44) and (5.45) are used for; $\frac{H_R}{D_R} \leq 4$, $C_s \leq 15\ \%$ and $U_{gs} \leq 0.15\ m/s$. To check the validity of Eqs. (5.44) and (5.45), Nu_V is calculated by these equations, under the same experimental conditions, and is plotted with the experimental data (see Fig. 5.22). It is found that the calculation values have good agreements with the experimental data, and the maximum relative error is less than 12.1% for homogeneous flow regime and less than 15% for heterogeneous flow regime. Therefore, Eqs. (5.44) and (5.45) can be used to specify the volumetric heat transfer coefficient in the water-helium-alumina system.

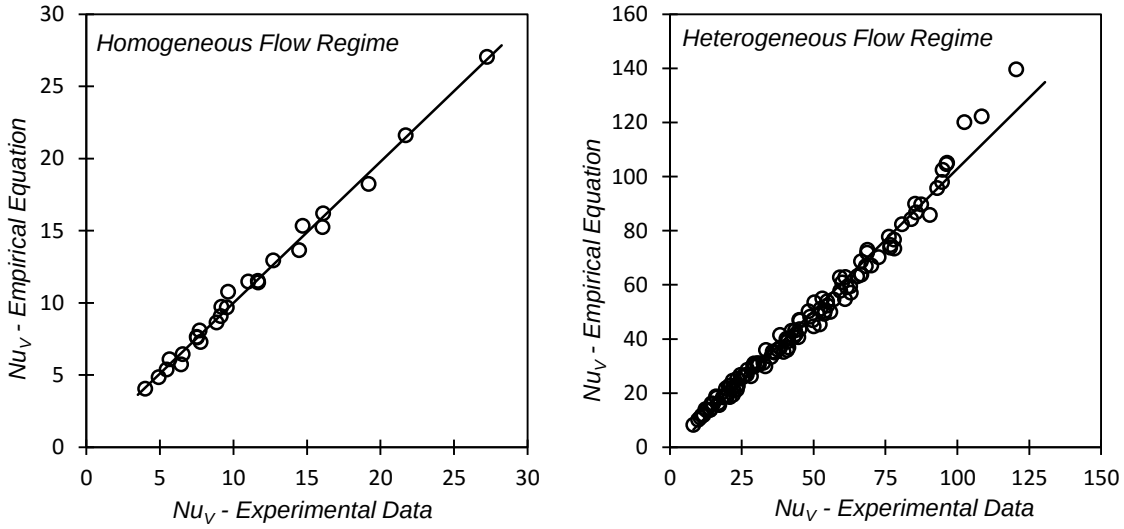

(a) (b)

Fig. 5.22 Empirical equation versus experimental data of Nu_V (a) Eq. (5.44) and (b) Eq. (5.45), for different H and C_s values.

5.3.6. Volumetric Heat Transfer Coefficient of the Oxygen Reactor

The volumetric heat transfer coefficient of the actual materials of the oxygen reactor (i.e. molten CuCl and O_2 gas), can be obtained by using Eq. (3.4), where Nu_V of both H_2O-He and CuCl-O_2 systems are equal.

$$(Nu_V)_{H_2O-He} = (Nu_V)_{CuCl-O_2} \tag{5.46}$$

By substituting Eq. (5.38) into Eq. (5.46), then;

$$(U_V)_{CuCl-O_2} = \frac{(k_{sl})_{CuCl-O_2}}{(k_{sl})_{H_2O-He}} (U_V)_{H_2O-He} \tag{5.47}$$

where $(k_{sl})_{CuCl-O_2}$ and $(k_{sl})_{H_2O-He}$ are the slurry thermal conductivities of the CuCl-O_2 and H_2O-He systems respectively, and $(U_V)_{CuCl-O_2}$ and $(U_V)_{H_2O-He}$ are the volumetric heat transfer coefficients of the CuCl-O_2 and H_2O-He systems respectively. Fig. 5.23 shows the volumetric heat transfer coefficients of O_2-CuCl system for different static liquid heights and solid concentrations.

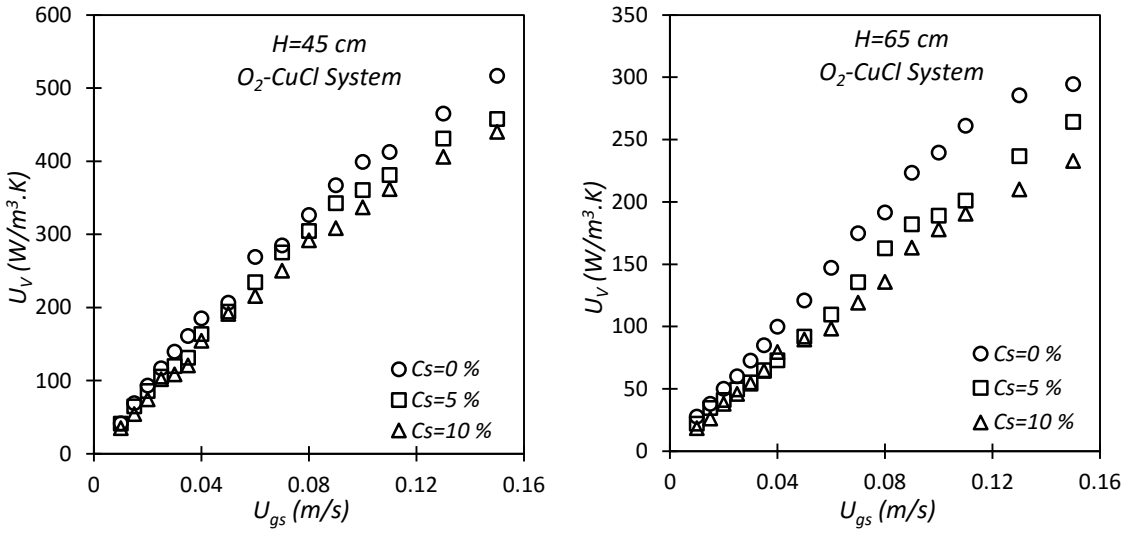

(a) (b)

Fig. 5.23 Volumetric heat transfer coefficient of O_2-CuCl system for different C_s values and a) $H = 45\ cm$, b) $H = 65\ cm$.

5.3.7. Summary of Heat Transfer Results

From the study of direct contact heat transfer in the SBC, the following points are concluded;

- The volumetric heat transfer coefficient (U_V) increases by increasing U_{gs}.
- U_V decreases by increasing H at any given U_{gs}.
- U_V decreases by increasing C_s at all static liquid heights.

- The rate of decrease of U_V values with C_s is approximately the same for different U_{gs}.

5.3.8. Uncertainty Analysis

Uncertainty analysis is the process of identifying and quantifying errors. In the experimental work of this thesis, there are two main types of uncertainties, systematic and random uncertainties. Systematic uncertainties (or fixed uncertainties) are those which cause repeated readings to be in uncertainty by roughly the same amount. These uncertainties are related to the calibration errors in the measuring instruments or in the experimental techniques. For example, the measurement of the fluid temperature in the SBC system with a thermocouple probe. It is well known that heat may be conducted from the stem of the thermocouple, out of the body, and into the surroundings, which may influence the temperature of the stem of the thermocouple. Therefore, the reading temperature of the thermocouple is not the true temperature of the fluid, and it will not make any difference how many readings are taken. Therefore, there will always be an uncertainty resulting from the heat-transfer condition of the stem of the thermocouple. This is a systematic uncertainty. In addition to uncertainties of measuring instruments, there are other sources of systematic uncertainties in the experimental system that increase the frictional and form losses and the losses of heat transfer such as; the sparger, helical tube and the connecting pipes and fittings. Random uncertainties are related to the changes in the conditions of the performed experiments. Common sources of random errors in the experimental works are; operating conditions fluctuations, random electronic fluctuations in the instruments and vibrations produced in the system.

Error Propagation

Error propagation is a method of calculating the uncertainty of a result that depends on several variables that have their own uncertainties. Kline and McClintock (1953) have presented a precise method to determine the uncertainty in experimental results (σ_f) (Bevington and Keith, 2003);

$$\sigma_f^2 = \sigma_x^2 \left(\frac{\partial f}{\partial x}\right)^2 + \sigma_y^2 \left(\frac{\partial f}{\partial y}\right)^2 + \sigma_z^2 \left(\frac{\partial f}{\partial z}\right)^2 + \dots , \quad (5.48)$$

where;

f is the result that is required to calculate its uncertainty such as; α_g and U_V.

$x, y, z, \dots$ are the physical variables that the results depend on, such as; P_1 and P_2 for the result of α_g, and $\dot{m}_g$, $T_{g,in}$, $T_{g,out}$ and $\bar{T}_{sl}$ for the result of U_V.

$\sigma_x, \sigma_y, \sigma_z, \dots$ are uncertainties of the physical variables $x, y, z, \dots$ respectively.

From Eqs. (5.7) and (5.48), the maximum value of gas holdup systematic uncertainty is calculated to be $\mp 0.166\%$. By using Eqs. (5.34) and (5.48), the maximum value of the volumetric heat transfer coefficient systematic uncertainty is calculated to be ∓ 29 W/m^3.K. The above systematic uncertainties are due to the calibration errors in the pressure transducers and thermocouples. As indicated in Section 3.3, the random uncertainties of the gas holdup and the volumetric heat transfer coefficient are less than 6% and 10% respectively. These uncertainties are mainly due to the fluctuations in the operating conditions. Examples of systematic and random uncertainties calculations for each of the gas holdup and volumetric heat transfer coefficient are shown in Appendix III. By taking into consideration the above uncertainties, the value of the gas holdup at $H_R = 45cm$, $C_s = 0\%$ and $U_{gs} = 0.05m/s$ can be calculated as $(16.14 \mp 1.14)\%$. In the same way, the value of the volumetric heat transfer coefficient at $H_R = 45cm$, $C_s = 0\%$ and $U_{gs} = 0.05m/s$ can be calculated as (620 ∓ 91).

CHAPTER 6
CFD SIMULATIONS RESULTS OF HELIUM-WATER-ALUMINA SYSTEM

6.1. Introduction

In this chapter, the results of the CFD models for a SBC are introduced. These results include both hydrodynamic and heat transfer studies for steady-state conditions. The effects of superficial gas velocities (U_{gs}), static liquid heights (H) and solid concentrations (C_s) on hydrodynamic and heat transfer are investigated in this chapter. Some assumptions are made in the CFD simulations. First, the slurry is assumed to be perfectly mixed. This is true if Stokes number (Stk) of solid particles is small $(Stk \ll 1)$. Table 6.1 shows stokes numbers of the solid particles used in the experimental work and the actual oxygen reactor by using the following equation (Tropea, Yarin, & Foss, 2007);

$$Stk = \frac{\rho_s \, d_p^2 \, U_l}{18 \, \mu_l \, D_R}, \qquad (6.1)$$

where ρ_s and d_p are the density (Kg/m^3) and diameter (m) of the solid particles respectively, μ_l is the dynamic viscosity of the surrounding liquid, D_R is the reactor diameter, and U_l is the liquid velocity which is taken here as the same value of the largest superficial gas velocity $(U_{gs} = 0.15\ m/s)$. In this way, it can be ensured that the Stokes number will not exceed the values in Table 6.1. From Table 6.1, it can be seen that the Stokes number of Activated alumina with water is not much smaller than one. In this case, the accuracy error will by higher, where it has been found that, if $Stk \ll 0.1$, accuracy errors are below 1% (Tropea, Yarin, & Foss, 2007). The second assumption is that, 2D plane approaches are used. This is possible for shallow bubble columns (initial liquid height is less than 4 column diameters), because these columns do not exhibit bubble plume oscillation and can be modeled as 2D plane (Chen et al., 2005).

Table 6.1 Stokes number of the experimental and actual systems materials.

System	Stk
Basic Alumina and Water	≤ 0.0021
Adsorption Alumina and Water	≤ 0.0022
Activated Alumina and Water	≤ 0.62
Copper Oxychloride and Cuprous Chloride	≤ 0.29

6.2. Results of Overall Gas Holdup (α_g) in the Water-Helium-Alumina SBCs

6.2.1. Effect of Static Liquid Height (H) on α_g

Figures 6.1-6.3 show the effect of superficial gas velocity (U_{gs}) and static liquid height (H), on the numerical overall gas holdup (α_g) of the helium-water-alumina SBC, for different solid particle concentrations (C_s). From these figures, it can be seen that α_g increases by increasing U_{gs} and/or decreasing H. Figs. 6.4 and 6.5 show the effect of U_{gs} and H on the contours of α_g. It can be seen in these figures that the radial distribution of the gas holdup is unequal, where the gas holdup is high in the center and low in the wall region. This behavior is due to the gradient of buoyancy forces between the column center and the wall region as indicated by Shaikh and Al-Dahhan (2007).

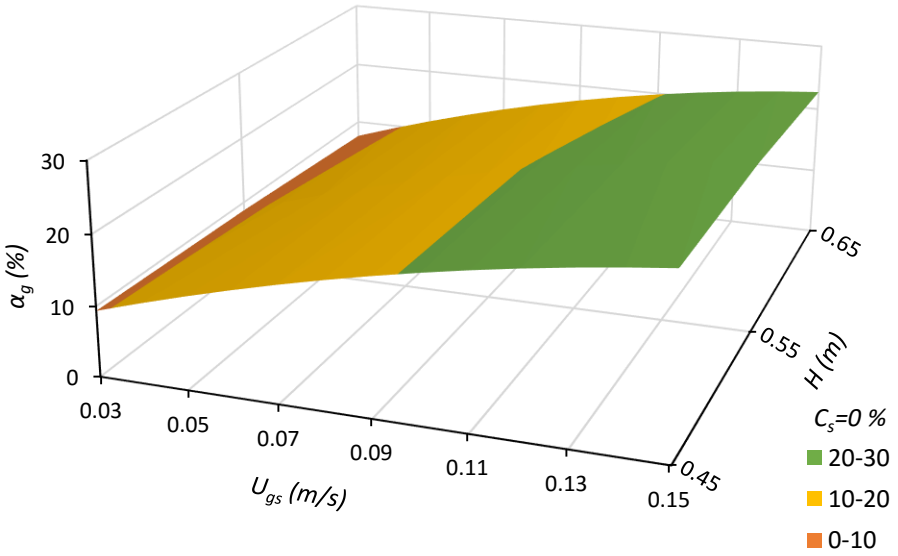

Fig. 6.1 α_g of the CFD model versus U_{gs} and H of the helium-water BC.

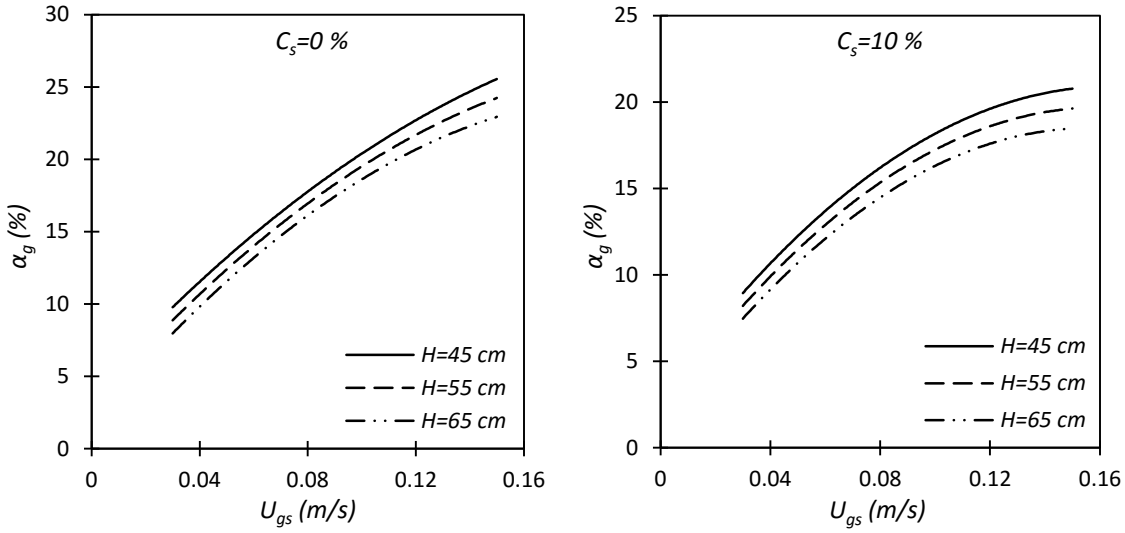

(a) (b)

Fig. 6.2 Effect of the static liquid height on the α_g of the CFD model versus U_{gs} of the helium-water-alumina SBC for a) $C_s = 0\%$ and b) $C_s = 10\%$.

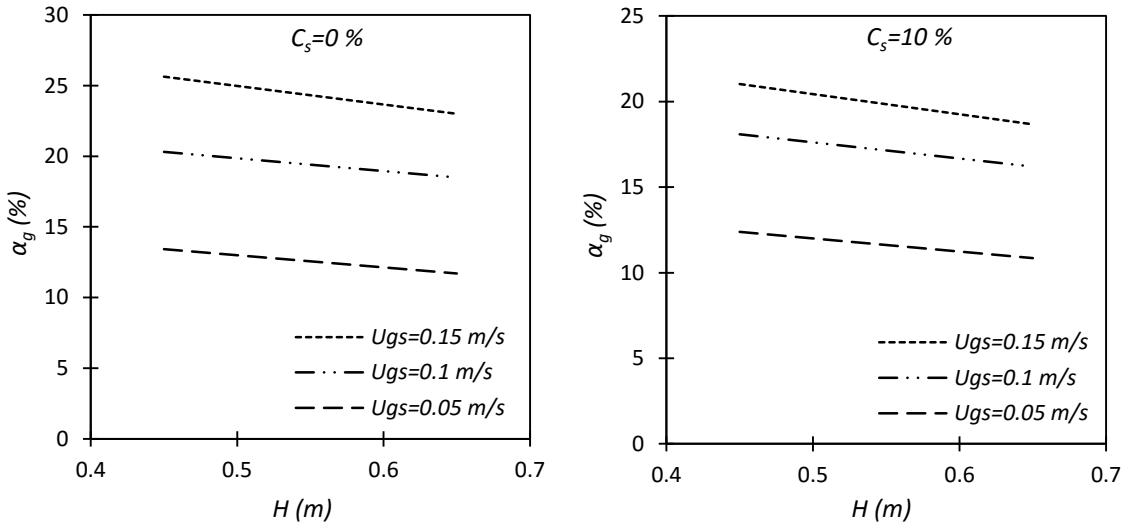

(a) (b)

Fig. 6.3 α_g of the CFD model versus H of the helium-water-alumina SBC for different U_{gs} and a) $C_s = 0\%$ and b) $C_s = 10\%$.

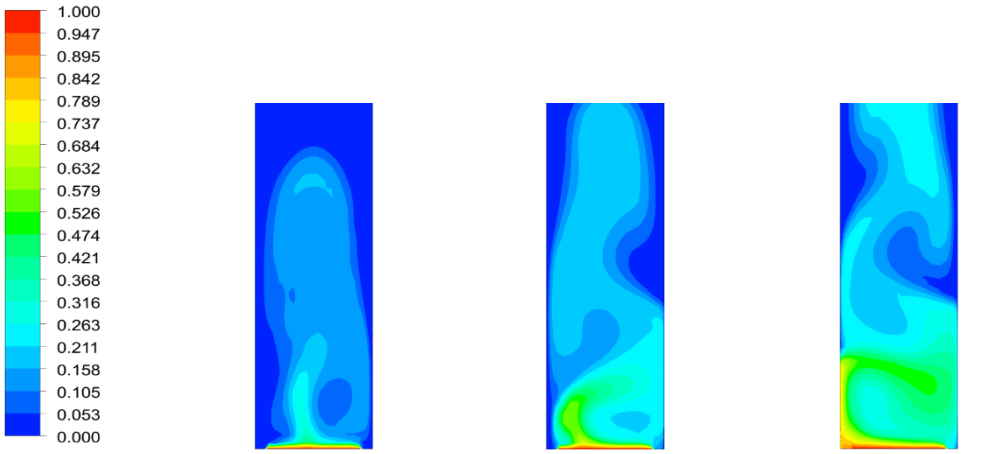

Fig. 6.4 Contours of gas holdup of a helium-water BC with $C_s = 0\%$, $H = 65\ cm$ and different U_{gs}.

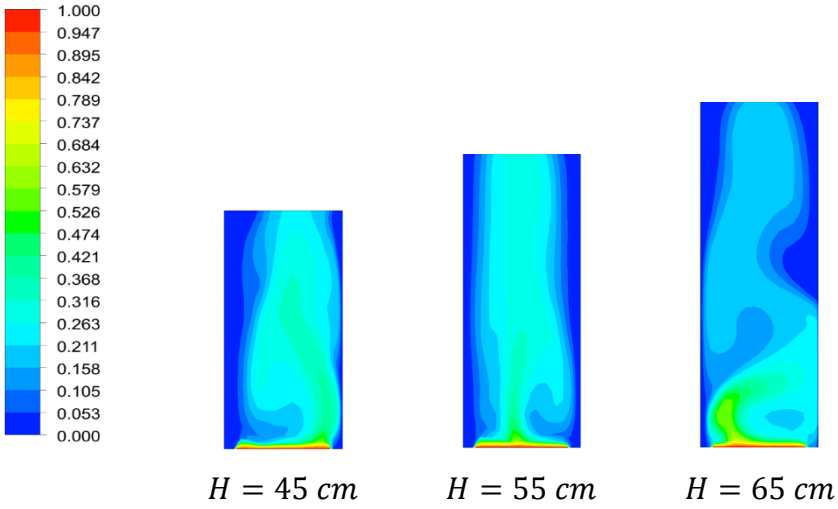

Fig. 6.5 Contours of the α_g of the helium-water BC with $C_s = 0\ \%$, $U_{gs} = 0.1\ m/s$ and different H.

6.2.2. Effect of Solid Particle Concentration (C_s) on α_g

Figures 6.6-6.9 show the plots and contours of the numerical α_g as a function of U_{gs} and C_s of helium-water-alumina SBC. From these figures, it can be seen that α_g decreases by increasing C_s, which is the same trend of the experimental results.

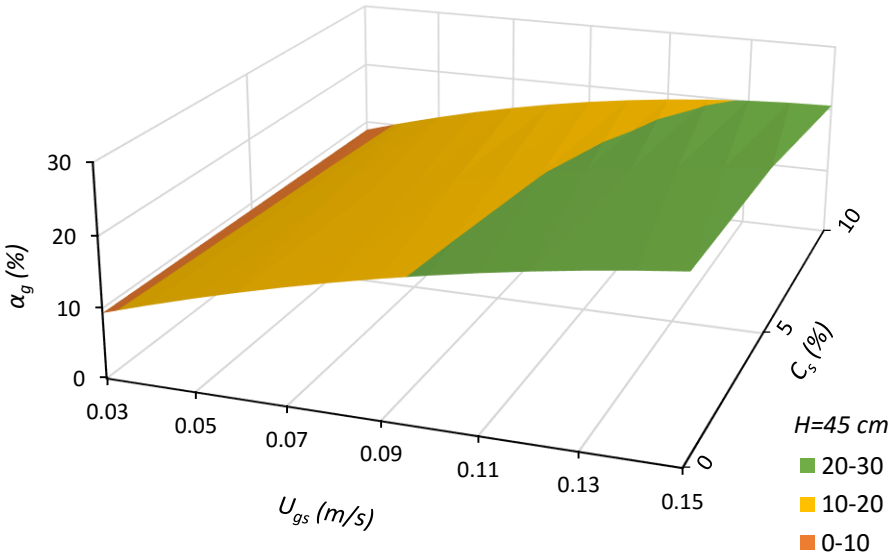

Fig. 6.6 α_g of the CFD model versus U_{gs} and C_s of the helium-water-alumina SBC.

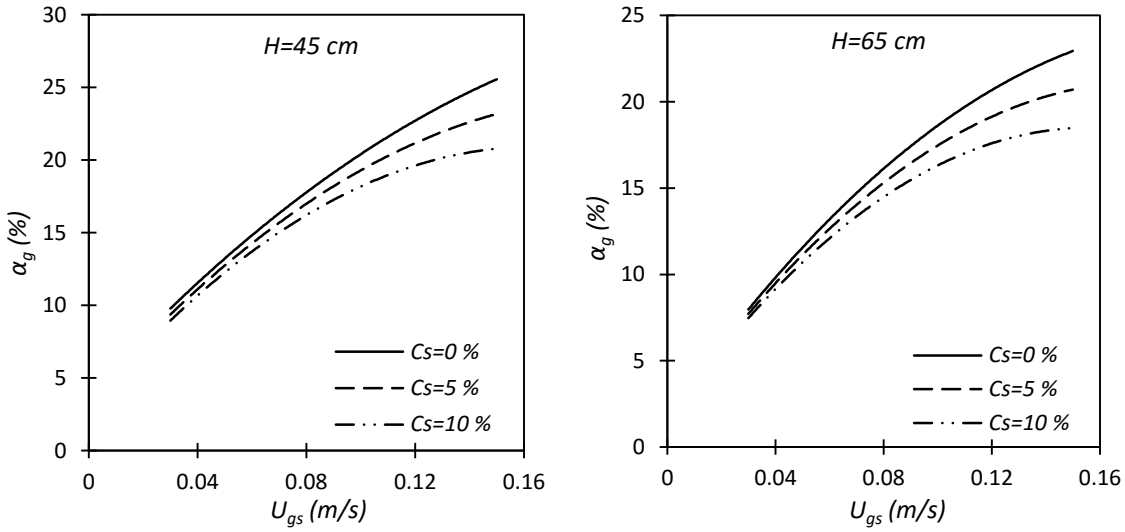

(a) (b)

Fig. 6.7 Effect of C_s on α_g versus U_{gs} of the helium-water-alumina SBC for a) $H = 45\ cm$, b) $H = 65\ cm$.

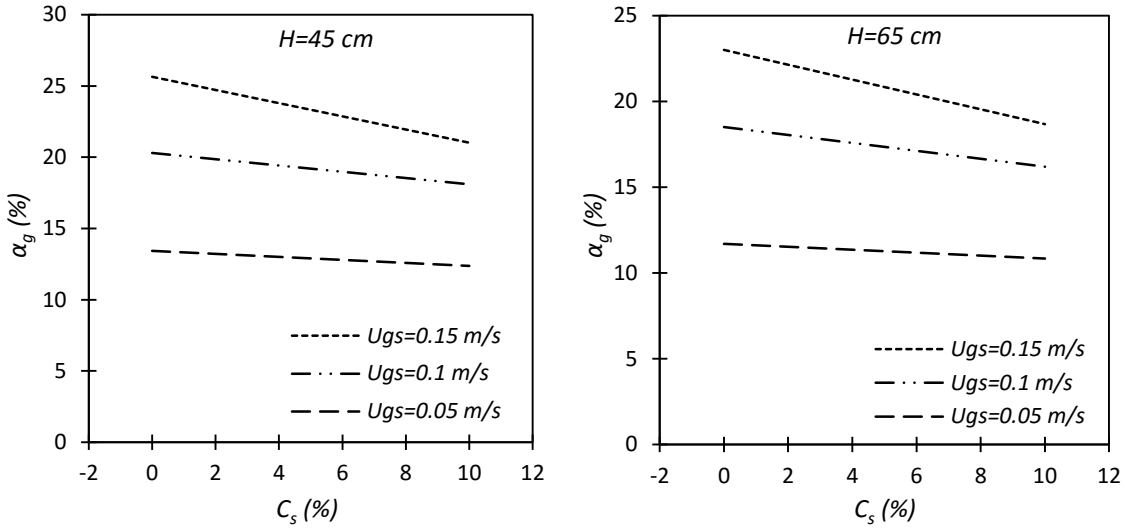

Fig. 6.8 α_g of the CFD model versus C_s of the helium-water-alumina SBC for a) $H = 45\ cm$, b) $H = 65\ cm$.

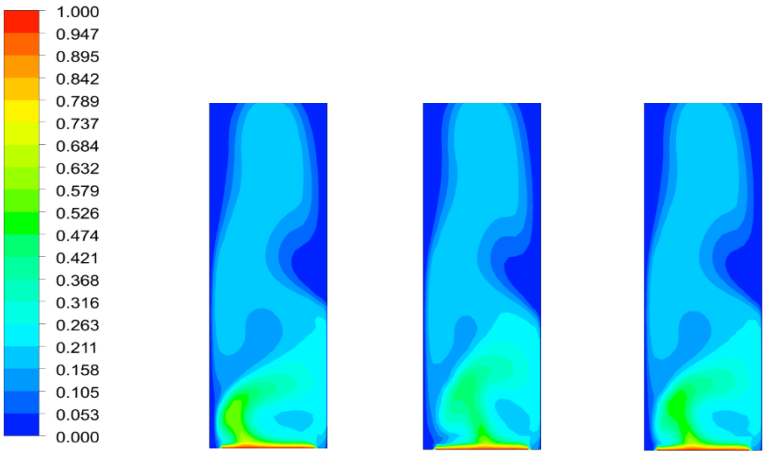

Fig. 6.9 Contours of α_g of the helium-water BC with $H = 65\ cm$, $U_{gs} = 0.1\ m/s$ and different C_s.

6.2.3. Comparison of Numerical α_g with the Experimental Data

To validate the numerical (CFD) data of hydrodynamic studies produced in the helium-water-alumina SBC, a comparison is made with the experimental data obtained in Chapter 5. Fig. 6.10 compares between the CFD simulations and experimental results of α_g versus U_{gs} for different H and C_s. In general, it can be

seen that all profiles of α_g calculated from CFD models under-predict the experimental data with a maximum relative error of less than 28.5%. Considering the complexity of the multi-phase flow in bubble columns, the agreement is satisfactory and encouraging.

The reduction in the results of CFD models is caused by the use of a 2D-plane mesh producing lower gas flow rates when compared with the 3D column. Also, the CFD model applied the source for the gas phase across the base of the column, ignoring the effect of the sparger height and therefore over-estimating the static liquid height (H). Due to that, the overall gas holdup is under-estimated when compared with the experimental flows. Another reason for the reduction of α_g is that the turbulent nature of the flow demands the use of a very fine mesh to realize all the vortical structures in the flow, especially for the smaller eddies (Sokolichin and Eigenberger, 1999).

The ability of the CFD model to account for H and C_s effects on α_g versus U_{gs} is also assessed by comparison to the experimental data of this thesis as shown in Figs. 6.11-6.14. Fig. 6.11 shows that, at a specific C_s, the curves of α_g versus U_{gs} at different values of H, are approximately parallel to each other, which means that the values of α_g versus U_{gs} decreases almost with a constant value by increasing H. In other words, the rate of decrease of α_g versus H is higher at lower U_{gs}. This behavior of α_g versus U_{gs} is also shown in Fig. 6.12 with α_g versus H, where the curves are approximately parallel to each other for different values of U_{gs}. The above experimental behaviors of α_g versus U_{gs} and H are correctly predicted by the CFD model.

Fig. 6.13 shows that at a specific H, the curves of α_g versus U_{gs} for different values of C_s, are not parallel to each other. This means that the rate of decrease of α_g with C_s increases by increasing U_{gs}, where at low U_{gs}, the effect of C_s is insignificant and it increases by increasing U_{gs}. In the same way, Fig. 6.14 shows that at a specific H, the rate of increase of α_g with U_{gs} decreases by increasing C_s. The CFD model correctly predicted the above experimental behaviors of α_g versus U_{gs} and C_s.

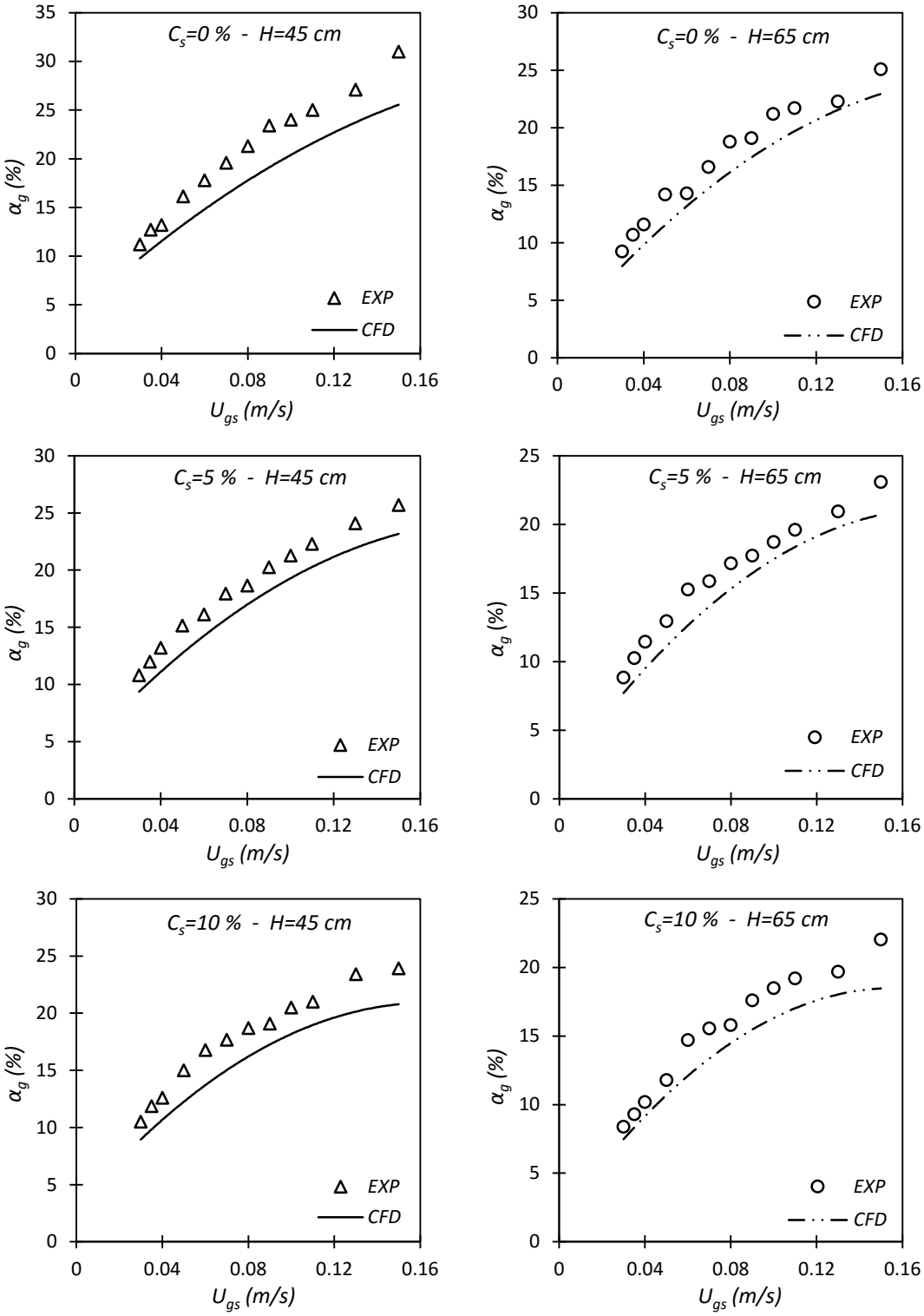

Fig. 6.10 Comparison of α_g versus U_{gs} between CFD and experimental results for different C_s and H of the helium-water-alumina SBC.

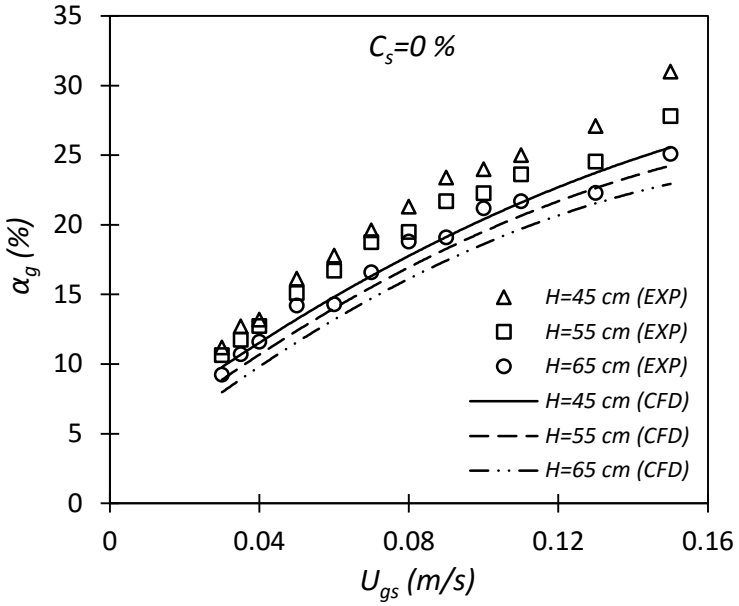

Fig. 6.11 Effect of H on α_g versus U_{gs} of the helium-water BC for the experimental data and CFD model.

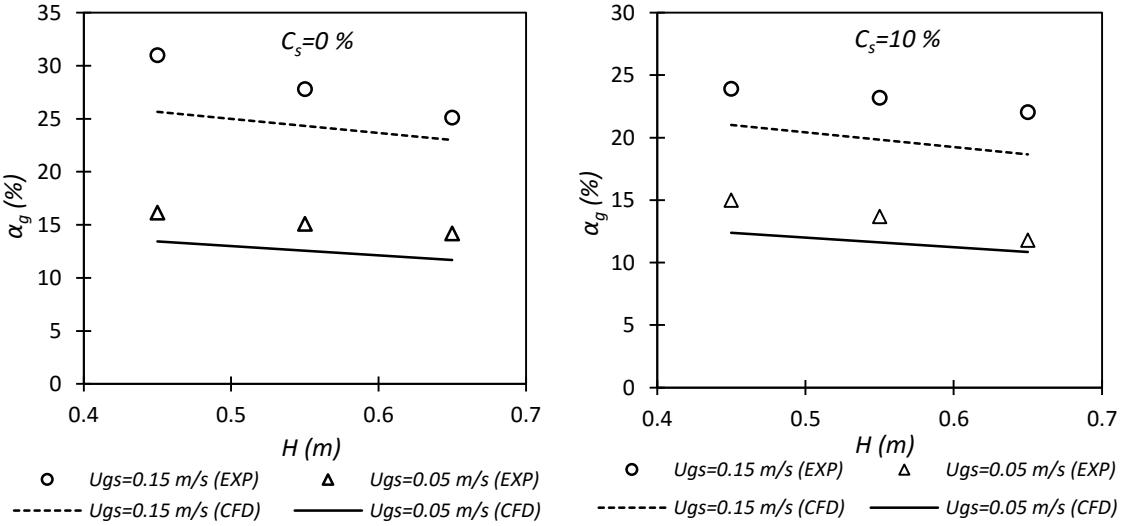

(a) (b)

Fig. 6.12 Comparison between CFD and experimental α_g versus H of the helium-water-alumina SBC for different U_{gs} and a) $C_s = 0\%$, b) $C_s = 10\%$.

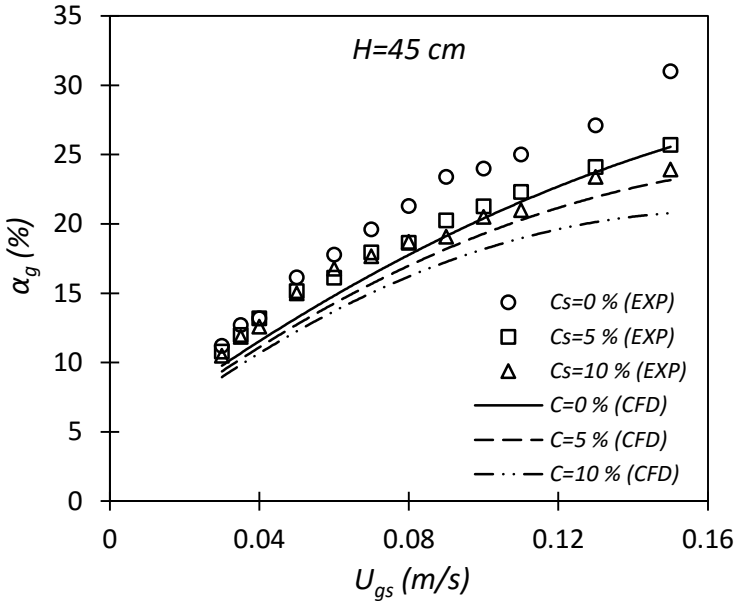

Fig. 6.13 Effect of C_s on α_g versus U_{gs} of the helium-water BC for the experimental data and CFD model.

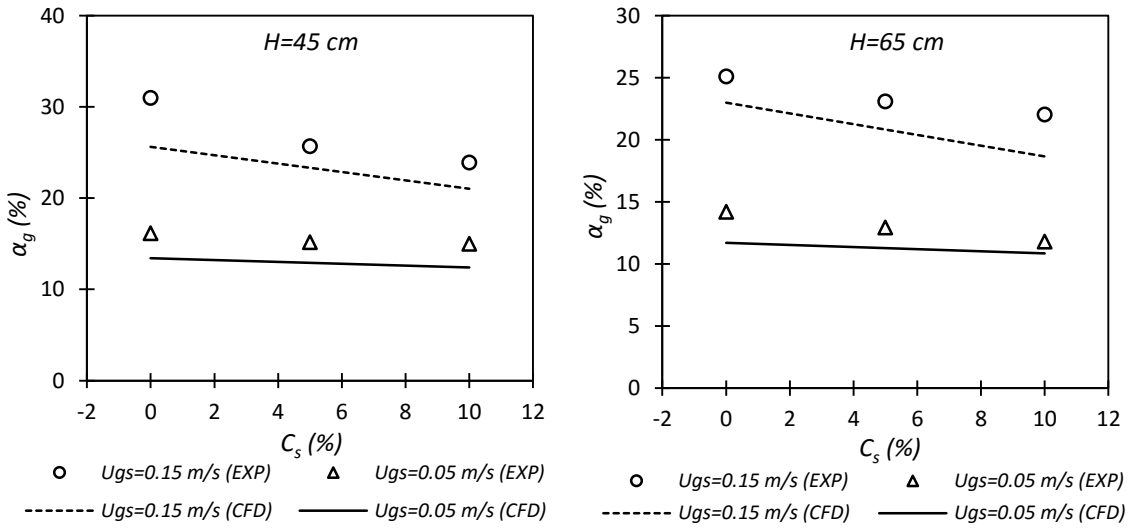

(a) (b)

Fig. 6.14 Comparison between CFD and experimental α_g versus C_s of the helium-water-alumina SBC for different U_{gs} and a) $H = 45\ cm$, b) $H = 65\ cm$.

6.3. Results of Volumetric Heat Transfer (U_V) Coefficient in the Water-Helium-Alumina SBCs

6.3.1. Effect of Static Liquid Height (H) on U_V

Figures 6.15 - 6.17 show the CFD volumetric heat transfer coefficient (U_V) versus U_{gs} and H of helium-water-alumina SBC for different C_s. From these figures, it can be seen that U_V increase by increasing U_{gs} and/or decreasing H, which is the same trend of the experimental results.

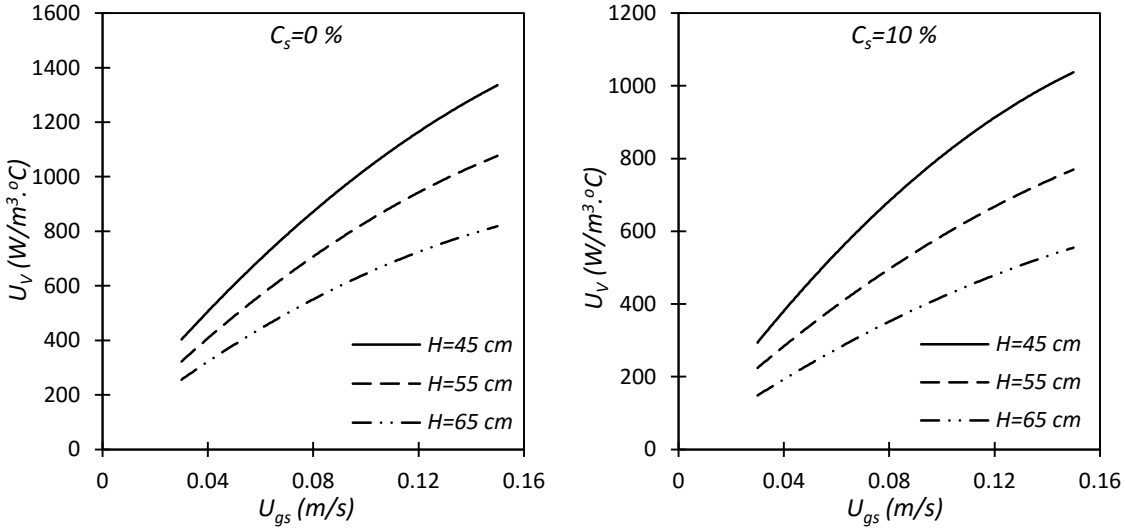

(a) (b)

Fig. 6.15 Effect of H on U_V of CFD model versus U_{gs} for a) $C_s = 0\%$, b) $C_s = 10\%$.

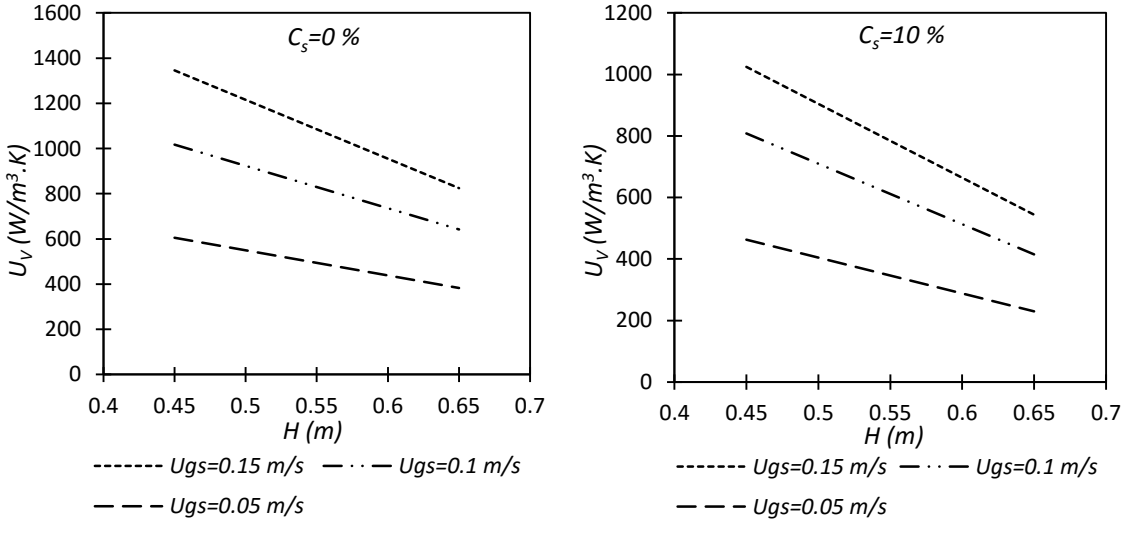

(a) (b)

Fig. 6.16 U_V of the CFD model versus H for a) $C_s = 0\%$, b) $C_s = 10\%$.

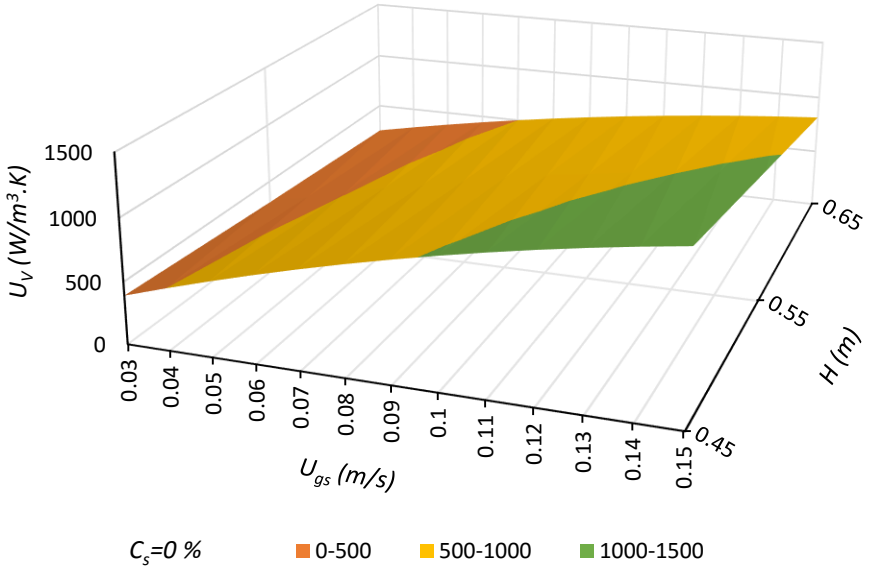

Fig. 6.17 U_V of the CFD model versus U_{gs} and H of helium-water BC.

6.3.2. Effect of solid particle concentration (C_s) on U_V

Figure 6.18 – 6.20 show U_V of helium-water-alumina SBC as a function of U_{gs} and C_s for different H. From these figures, it can be seen that U_V have the same behavior of the experimental results, where they decrease by increasing C_s.

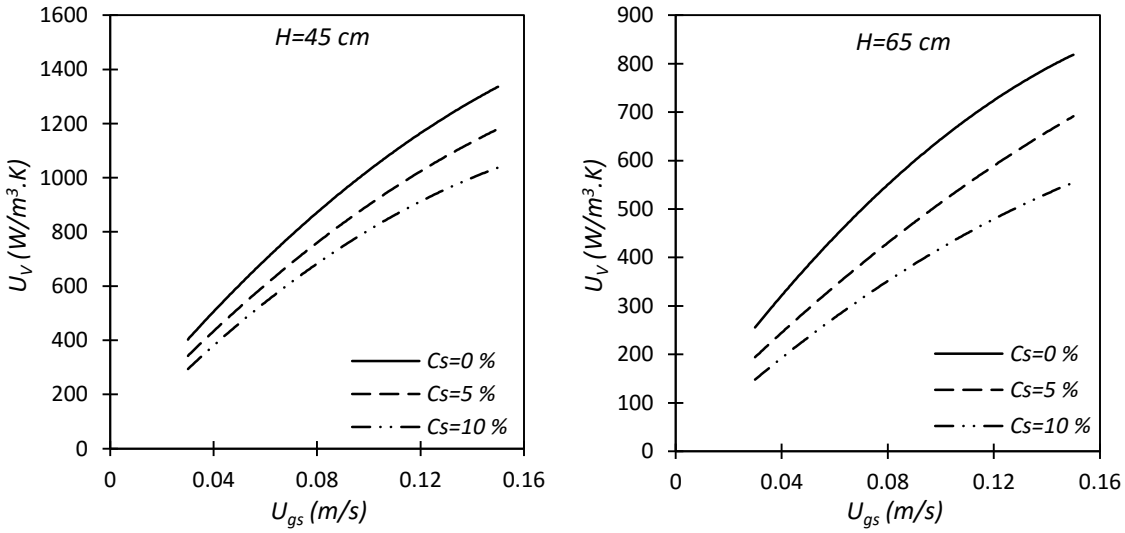

(a) (b)

Fig. 6.18 Effect of C_s on U_V of the CFD model versus U_{gs} for a) $H = 45\ cm$, b) $H = 65\ cm$.

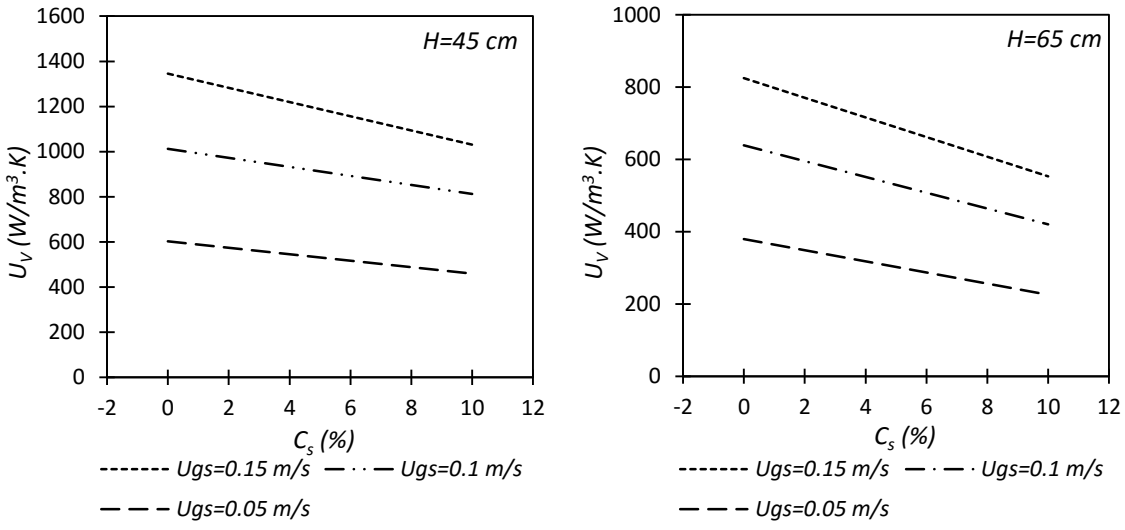

(a) (b)

Fig. 6.19 U_V of the CFD model versus C_s for different U_{gs} and a) $H = 45\ cm$, b) $H = 65\ cm$.

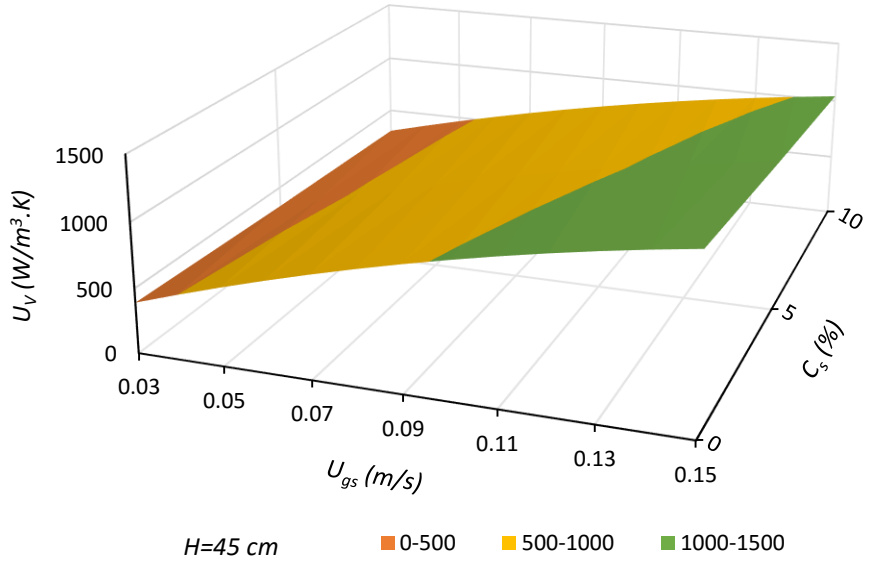

Fig. 6.20 U_V of the CFD model versus U_{gs} and C_s of the helium-water-alumina SBC.

6.3.3. Comparison of Numerical U_V with the Experimental Data

To validate the CFD data of heat transfer studies produced in the helium-water-alumina SBC, a comparison is made with the experimental data obtained in Chapter 5. Fig. 6.21 compares between the CFD simulations and experimental results of U_V versus U_{gs} for different H and C_s of helium-water-alumina SBC. From this figure, it can be seen that all profiles of U_V calculated from CFD models generally under-predict the experimental data at different values of U_{gs}, with a maximum relative error of less than 20%.

In general, the reduction in CFD values of U_V, is caused by the use of a 2D-plane mesh that produce lower gas flow rates and lower heat transfer rate when compared with the 3D column. Also, as in the gas holdup situation, the CFD model ignores the effect of the sparger height and therefore under-estimates the heat transfer rate compared with the experimental rates. This is due to the over-estimating of the static liquid height (H). Another reason of the reduction in values of U_V is that the theoretical gas density is calculated at the average gas temperature of Eq. (5.35). This temperature is more than the actual average gas temperature, because the gas transfers most of its heat near the bottom of the reactor. Because of that, the theoretical gas density and mass flow rate are lower than the actual ones, which leads to a reduction in U_V values.

The ability of the CFD model to account for H and C_s effects on U_V is also assessed by comparison to the experimental data of this thesis as shown in Figs. 6.22-6.25. Figs. 6.22 and 6.23 show that, at a specific C_s, the curves for different H are not parallel to each other, where the rates of decrease of U_V with H increase by increasing U_{gs}. For instance, for $C_s = 0\ \%$, U_V decrease by 35.5%, when H increases from 45 cm to 65 cm at $U_{gs} = 0.01\ m/s$, while they decrease by 38.7% at $U_{gs} = 0.15\ m/s$. The CFD model correctly predicted the behaviors of the experimental rates of decrease of U_V with H.

Figures. 6.24 and 6.25 show the behavior of U_V with C_s at a specific H. From these figures, it can be seen that the trends of the curves are similar to that in Figs. 6.22 and 6.23, but with lower rates of changes. For instance, for $H = 45\ cm$, U_V

decrease by 22.4%, when C_s increases from 0% to 10% at $U_{gs} = 0.01\, m/s$, while it decreases by 23.3% at $U_{gs} = 0.15\, m/s$. The experimental rates of decrease of U_V with C_s are predicted correctly by the CFD model.

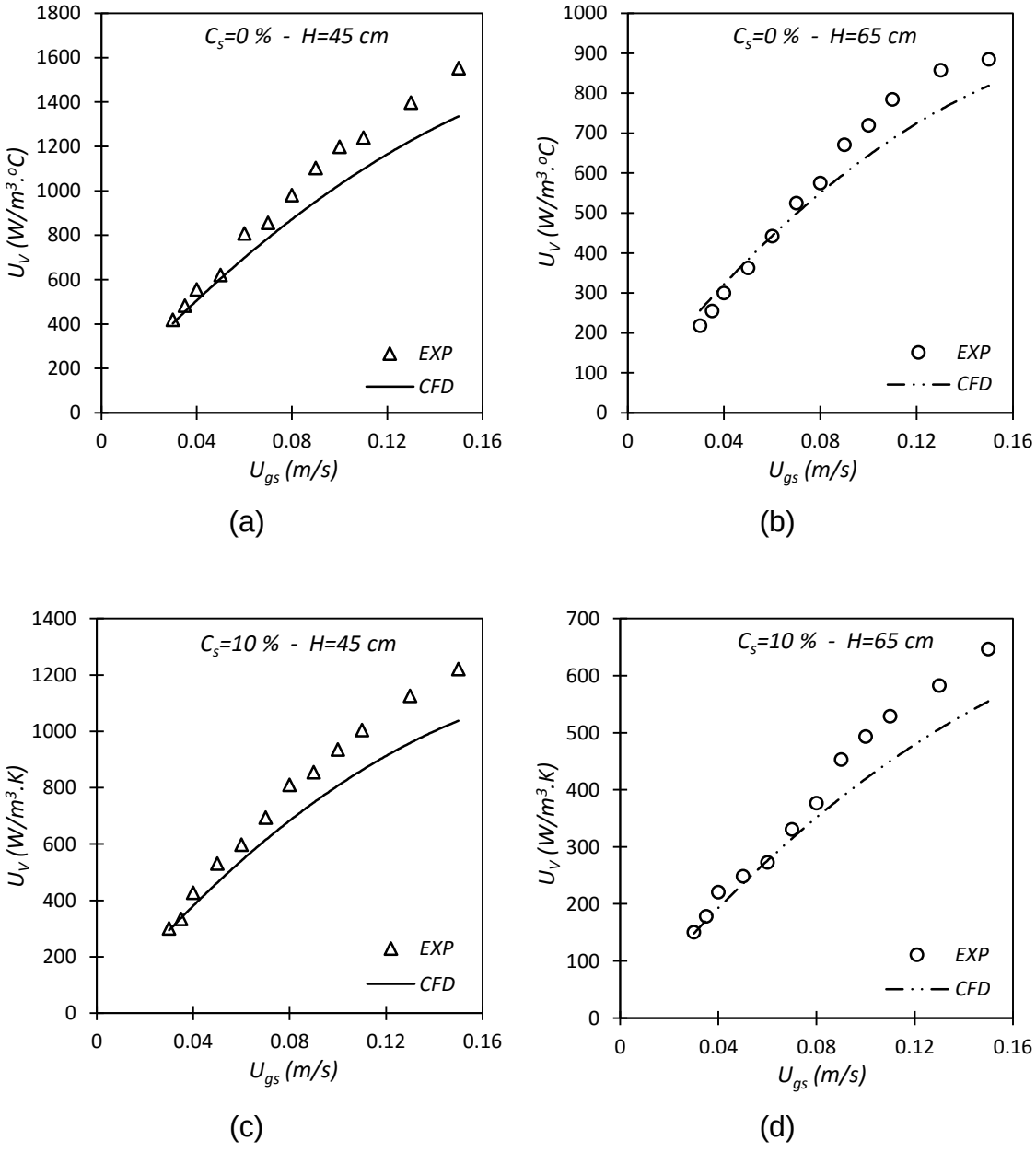

Fig. 6.21 Comparison of U_V versus U_{gs} between CFD and experimental results for a) $C_s = 0\%$ and $H = 45\ cm$, b) $C_s = 0\%$ and $H = 65\ cm$, c) $C_s = 10\%$ and $H = 45\ cm$, d) $C_s = 10\%$ and $H = 65\ cm$.

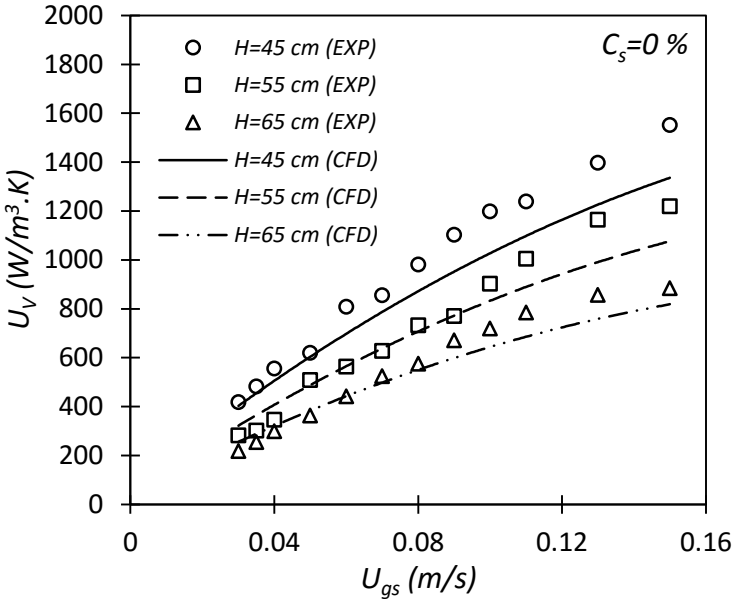

Fig. 6.22 Effect of H on U_V versus U_{gs} for experimental data and CFD model.

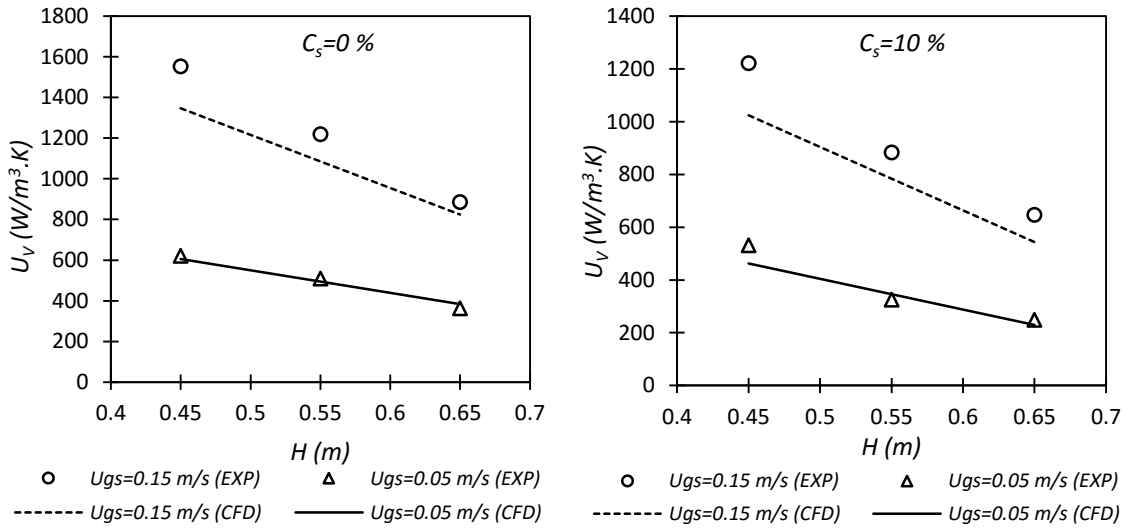

Fig. 6.23 Comparison between CFD and experimental U_V versus H for different U_{gs} and a) $C_s = 0\%$, b) $C_s = 10\%$.

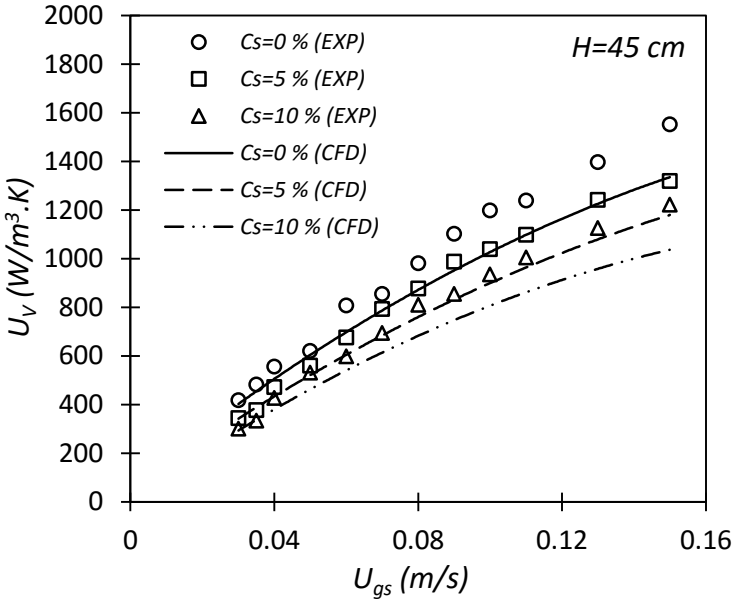

Fig. 6.24 Effect of C_s on U_V versus U_{gs} for experimental data and CFD model.

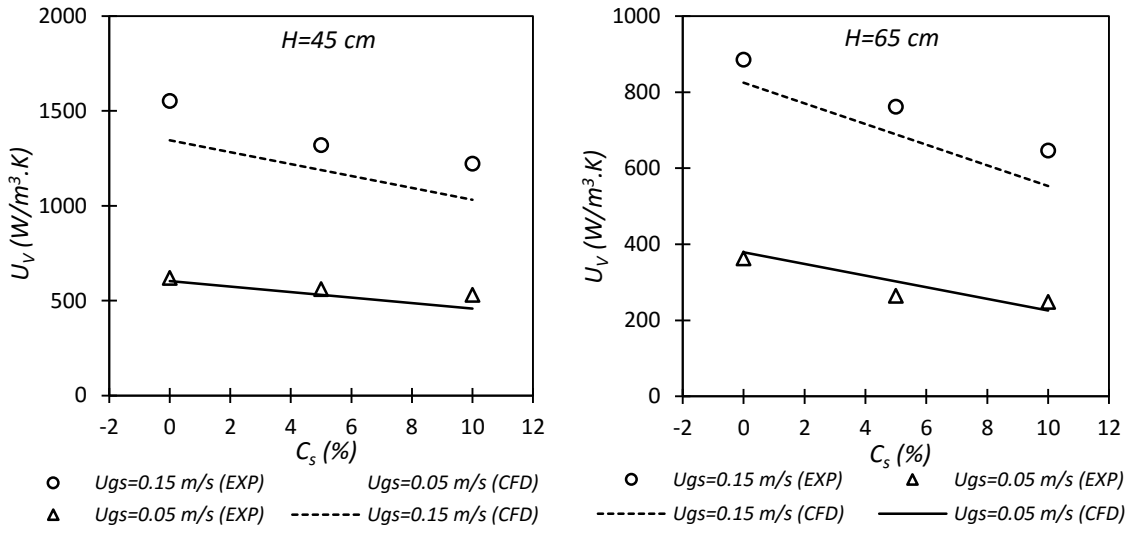

Fig. 6.25 Comparison between CFD and experimental U_V versus C_s for different U_{gs} and a) $H = 45\ cm$, b) $H = 65\ cm$.

6.3.4. Axial Variation of Gas Temperature (T_g)

In this section, the effect of axial variation on gas temperature (T_g) is briefly discussed. Figs. 6.26 and 6.27 show the axial gas temperature profiles of CFD model and contours of a helium-water BC with $C_s = 0\ \%$ and $H = 65\ cm$ for different U_{gs}. From these figures, it can be seen that T_g decreases dramatically near the bottom of the reactor (within the first quarter of the height (i.e., $h \approx 20\ cm$)). For the rest of the reactor (i.e., $h > 20\ cm$), the gas temperature decrease is negligible and the temperature can be considered as constant. This means that the majority of the heat transfer from gas to the slurry occurs at the base of the column, which reflects the fact that direct contact heat transfer between the gas and slurry is very efficient. In this thesis, to facilitate the explanation of the results, the height where the gas temperature starts to be approximately constant (i.e., $h \approx 20\ cm$) is called "*thermal effective height*". Figs 6.26 and 6.27 also shows that the effect of U_{gs} on T_g and the thermal effective height is insignificant and can be neglected, where the maximum relative difference in T_g is less than 1.23%.

Figures. 6.28 and 6.29 show the effect of H in the axial T_g profiles for helium-water BC with $C_s = 0\ \%$ and $U_{gs} = 0.1\ m/s$. From these figures, it can be seen that the effect of H on T_g is insignificant and can be neglected, where the maximum relative difference in T_g is less than 1%. Figures. 6.30 and 6.31 show the effect of C_s in the axial T_g profiles for helium-water BC with $H = 65\ cm$ and $U_{gs} = 0.1\ m/s$. From these figures, it can be seen that the effect of C_s on T_g is negligible, where the maximum relative difference in T_g is less than $2.66 \times 10^{-4}\ \%$.

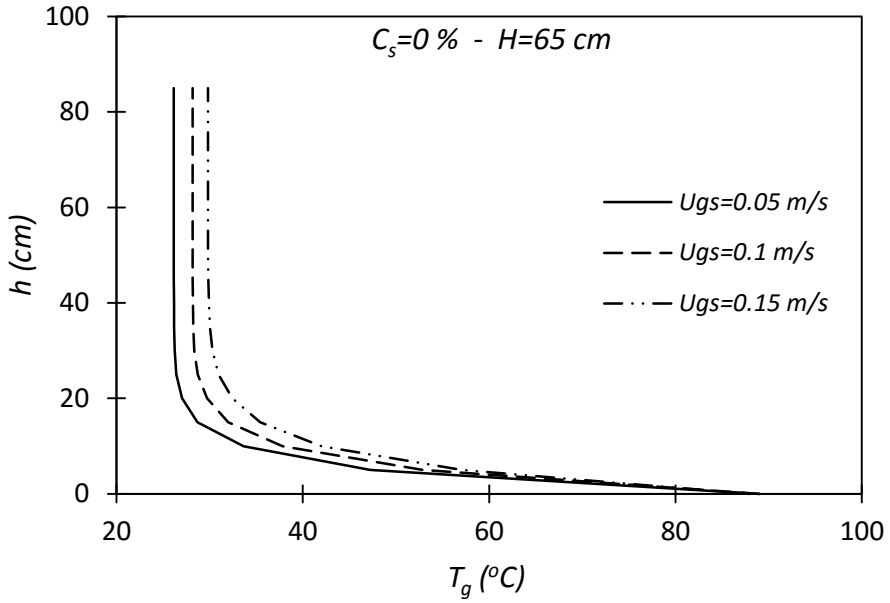

Fig. 6.26 Axial gas temperature profiles of the helium-water BC for different U_{gs}.

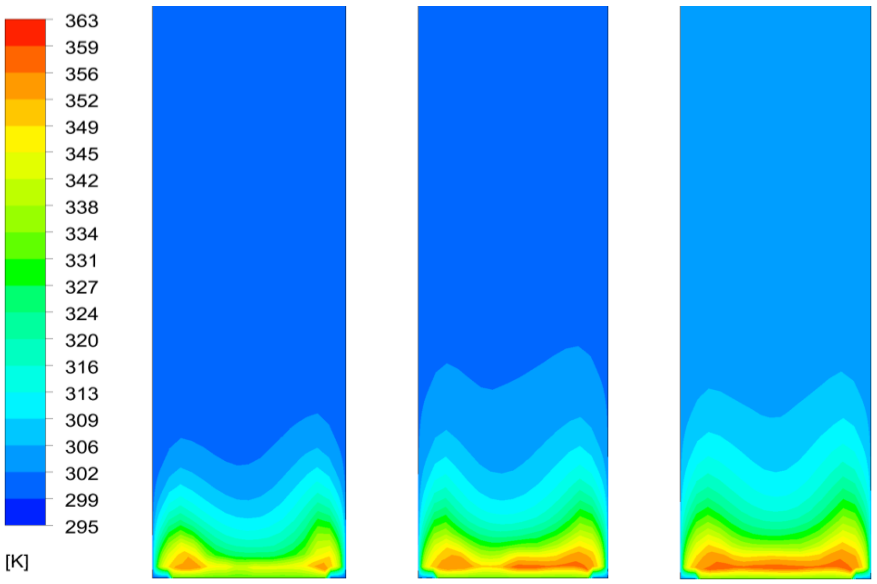

Fig. 6.27 Axial gas temperature contours for different $U_{gs}$of the helium-water BC with $C_s = 0$ and $H = 65\ cm$.

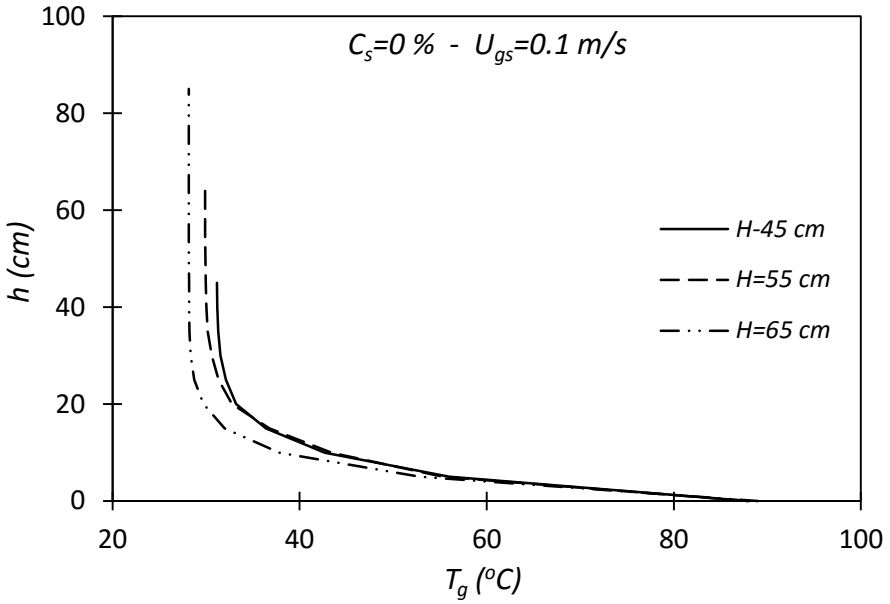

Fig. 6.28 Axial gas temperature profiles of the helium-water BC for different H.

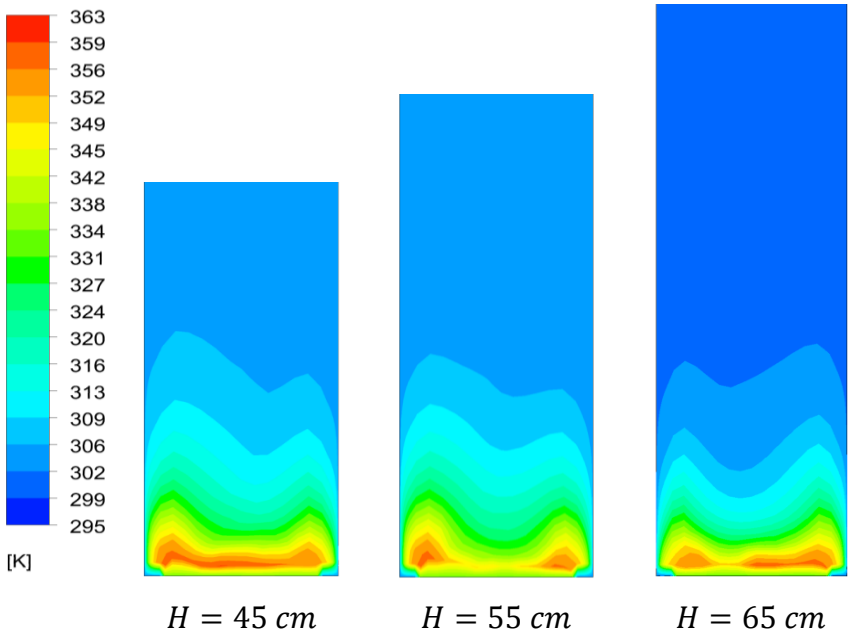

Fig. 6.29 Axial gas temperature contours for H of the helium-water BC with $C_s = 0\ \%$ and $U_{gs} = 0.1\ m/s$.

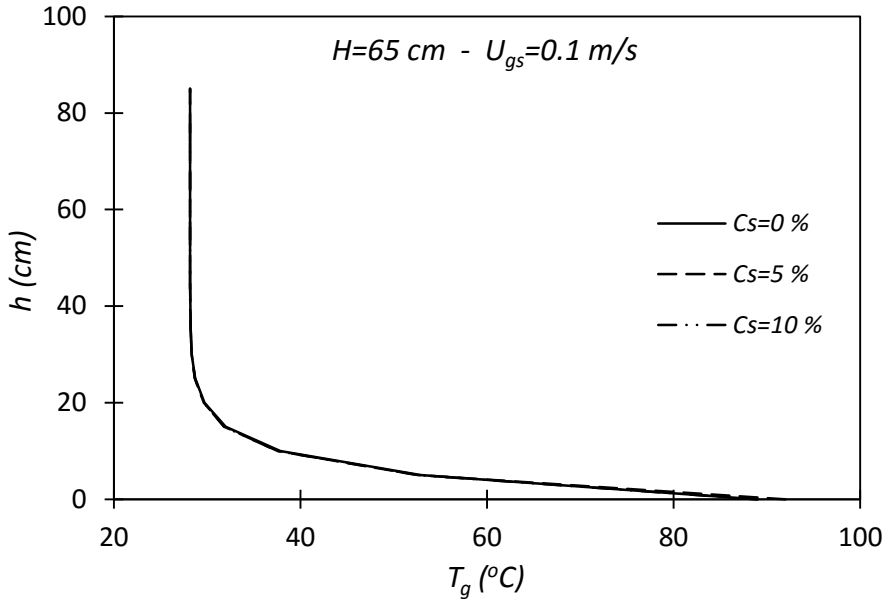

Fig. 6.30 Axial gas temperature profiles of the helium-water BC for different C_s.

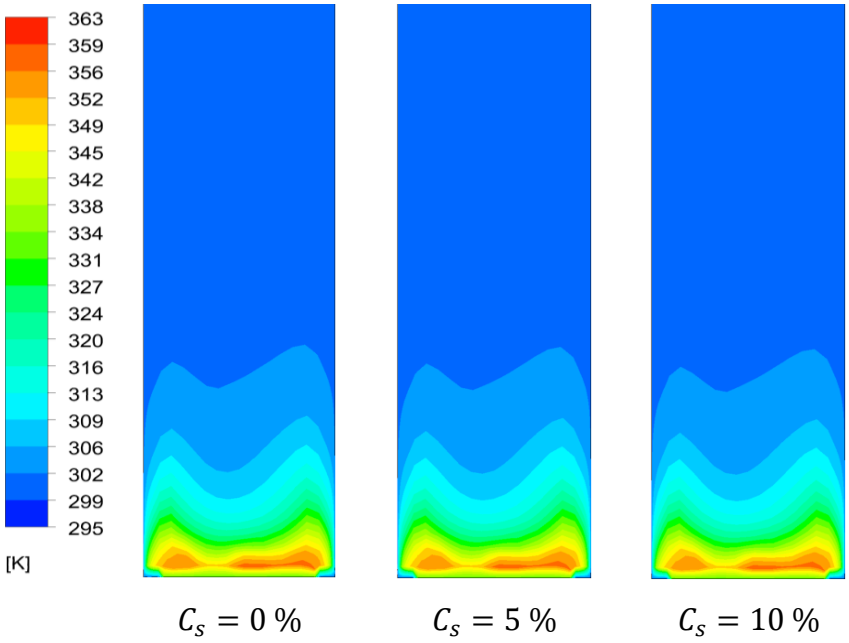

Fig. 6.31 Axial gas temperature contours for different C_s of the helium-water BC with $H = 65\ cm$ and $U_{gs} = 0.1\ m/s$.

6.4. Size of the Oxygen SBCR

In the oxygen reactor, since the flow is churn-turbulent as indicated in section 5.2.2.7, the empirical equation (Eq. (5.45)) is used to determine Nu_V. The volumetric heat transfer coefficient (U_V) is calculated by using Eqs. (5.38) and (5.47), and the amount of heat transferred by using direct contact heat transfer is calculated from Eq. (5.32). The size of the oxygen reactor is assumed to be 4m diameter and 8m height. From Fig. 5.15, for an oxygen production rate $\left(\dot{m}_{O_2}\right)$ of 800 tonne/day, the superficial gas velocity of the stoichiometric oxygen gas is 1.517 m/s.

By using above equations and values for the oxygen BCR and for $C_s = 0\ \%$, the amount of heat that can be transferred by using direct contact heat transfer configuration $\left(\dot{Q}_{DC}\right)$ is calculated to be 67.624 MW. The number of oxygen reactors (N) required for $\dot{m}_{O_2} = 800\ tonne/day$ can be calculated by dividing the amount of heat needed for the decomposition process $\left(\dot{Q} = 87\ MW\right)$ (Abdulrahman, 2016a; 2016b) to the amount of heat transferred $\left(\dot{Q}_{DC} = 67.624\ MW\right)$, i.e.;

$$N = \frac{\dot{Q}}{\dot{Q}_{DC}} = \frac{87}{67.624} = 1.28 \approx 2\ reactors \qquad (6.3)$$

Figs. 6.32 and 6.33 show the effect of reactor height (H_R) and solid particle concentration (C_s) respectively in the number of oxygen SBCRs (N) for different $\dot{m}_{O_2}$. It can be seen from Fig. 6.32 that increasing H_R will increase N insignificantly, where N increases from 1.27 to 1.286 by increasing H_R from 4 m to 8 m for $\dot{m}_{O_2} = 800\ tonne/day$ and $C_s = 0\ \%$. Fig. 6.32 also shows that the effect of $\dot{m}_{O_2}$ on N is negligible, where for $H_R = 8\ m$ and $C_s = 0\ \%$, the number of reactors (N) increases from 1.286 to 1.39 when $\dot{m}_{O_2}$ increases from 800 tonne/day to 2400 tonne/day.

Fig. 6.33 shows that increasing C_s will increase N, where N increases from 1.286 to 2.834 when C_s increases from 0% to 15% for $\dot{m}_{O_2} = 800\ tonne/day$ and a reactor height of 8 m. Fig. 6.33 also shows that the effect of $\dot{m}_{O_2}$ on N is negligible, where for $H_R = 8\ m$ and $C_s = 15\ \%$, the number of reactors (N) increases from 2.834 to 3.06 by increasing $\dot{m}_{O_2}$ from 800 tonne/day to 2400

tonne/day. From above calculations, it can be concluded that the effects of H_R and $\dot{m}_{O_2}$ on N can be neglected.

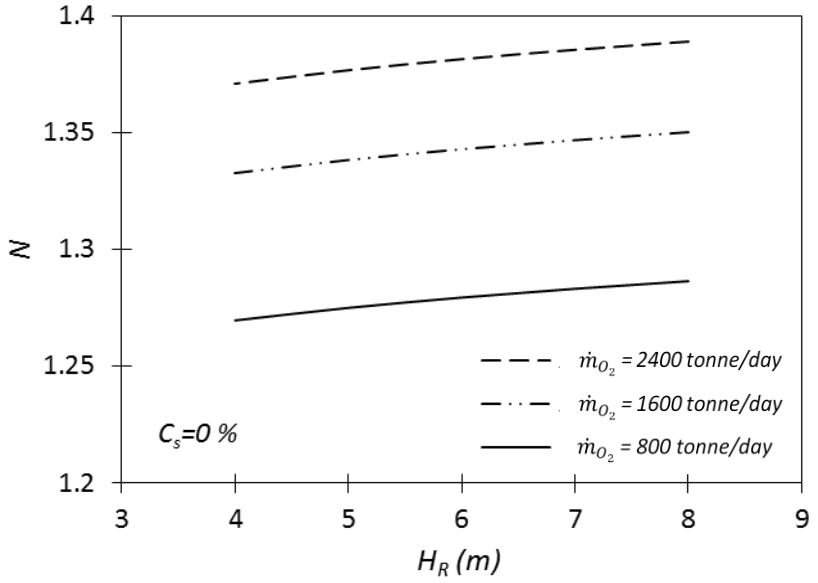

Fig. 6.32 Number of oxygen BCRs versus reactor height (H_R) for different $\dot{m}_{O_2}$ and $C_s = 0\ \%$.

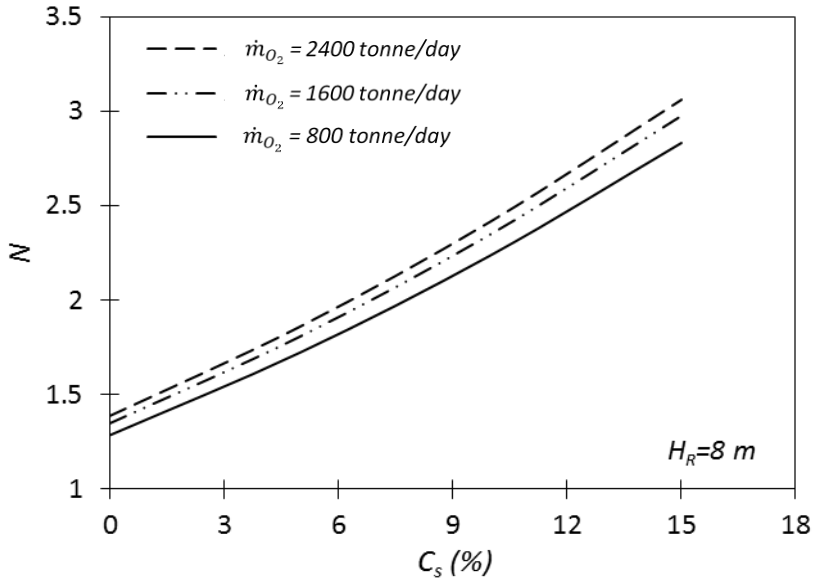

Fig. 6.33 Number of oxygen SBCRs versus solid particle concentration (C_s) for different $\dot{m}_{O_2}$ and $H_R = 8\ m$.

Above calculations of oxygen reactors numbers, depend on the amount of heat that can be transferred by using direct contact between the molten CuCl and the stoichiometric O_2 gas bubbles. For the oxygen reactor, it is preferable to inject the heated oxygen gas at the same speed of the stoichiometric oxygen gas. The question that can be asked is "How much heat can the stoichiometric O_2 gas carry?" The answer to that is by calculating the amount of heat that can be carried by the stoichiometric O_2 gas as follows;

$$\dot{Q}_{O_2} = \{\dot{m}\, C_p\, (T_{gin} - T_{gout})\}_{O_2}, \qquad (6.4)$$

where $\dot{Q}_{O_2}$ is the amount of heat carried by O_2 gas, $\dot{m}$ is the mass flow rate of the oxygen gas and C_p is the specific heat of the oxygen gas. For a CANDU-SCWR heat source, the inlet temperature of the oxygen gas (T_{gin}) is assumed to be 600°C and the outlet temperature (T_{gout}) is assumed to be 540°C. From Eq. (6.4), for the superficial gas velocity of the stoichiometric oxygen gas for $\dot{m}_{O_2} = 800\ tonne/day$ and $C_s = 0\ \%$, the amount of heat $(\dot{Q}_{O_2})$ is calculated as 0.55 MW and the number of reactors required in this case is about 158. This number of reactors is very big compared to that by using the amount of heat that can be transferred by direct contact.

As indicated in Eq. (6.4), the value of $\dot{Q}_{O_2}$ can be increased by either increasing $\dot{m}_{O_2}$ or $(T_{gin} - T_{gout})_{O_2}$. The temperature difference can be increased by using a higher temperature heat source rather than CANDU-SCWR, such as HTGR, where the inlet temperature can be taken as 900°C and the outlet temperature is the same as 540°C. In this case, the number of oxygen reactors will decrease to 35 when using the superficial gas velocity of a stoichiometric oxygen bubbles for $\dot{m}_{O_2} = 800\ tonne/day$ and $C_s = 0\ \%$. This number is still considered high compared with that calculated from the material balance of an earlier work by this author (Abdulrahman et al., 2013). The only option that is remaining to increase $\dot{Q}_{O_2}$, is to increase $\dot{m}_{O_2}$ by increasing the superficial gas velocity (U_{gs}) when fixing the reactor diameter (D_R). Fig. 6.34 shows the number of oxygen

reactors calculated from $\dot{Q}_{O_2}$ versus U_{gs} for different $\dot{m}_{O_2}$. From this figure, it can be seen that N decreases non-linearly with U_{gs}.

Since $\dot{Q}_{O_2}$ is less than $\dot{Q}_{DC}$, the number of oxygen reactors (N) will depend mainly on $\dot{Q}_{O_2}$ rather than $\dot{Q}_{DC}$. In this case, for a specific heat source such as CANDU-SCWR and a specific reactor diameter (D_R), the value of N will depend only on the superficial gas velocity (U_{gs}) and the oxygen production rate $(\dot{m}_{O_2})$. By using the power function of curve fitting for the curves in Fig. 6.34, the following equation can be obtained for the number of oxygen reactors (N) as a function of U_{gs} and $\dot{m}_{O_2}$ with $R^2 = 1$;

$$N = \frac{0.3012\,\dot{m}_{O_2}}{U_{gs}}, \tag{6.5}$$

where $\dot{m}_{O_2}$ is the oxygen production rate in tonne/day and U_{gs} is the superficial gas velocity in m/s.

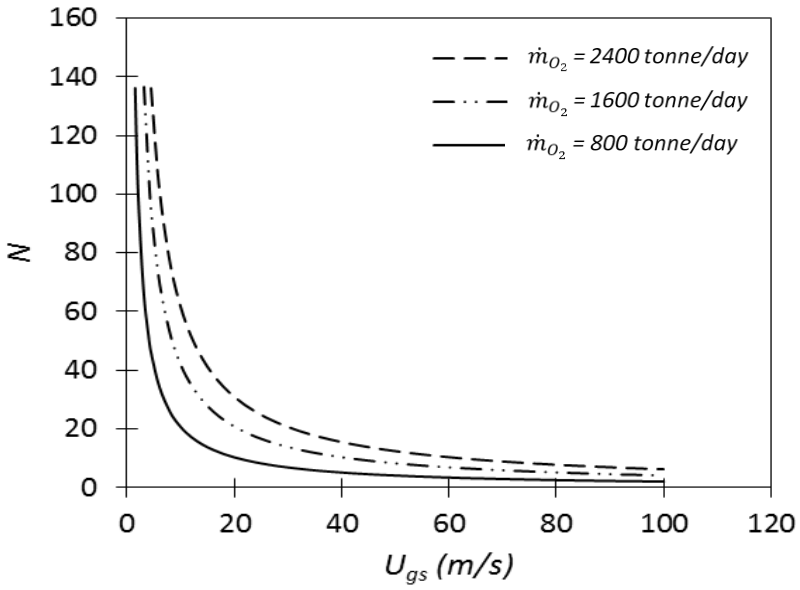

Fig. 6.34 Number of oxygen BCRs versus superficial gas velocity of oxygen gas for CANDU-SCWR and different oxygen production rates.

The size of the oxygen reactor from the perspective of material balance can be calculated by using the same method that is followed by Abdulrahman et al. (2013). The total volume of the oxygen reactor can be considered to be the sum of the volumes of the solid particles and molten salt. In this way, for a reactor diameter of 4 m and an aspect ratio of 2, the number of oxygen reactors obtained from the material balance, for $\dot{m}_{O_2} = 800\ tonne/day$ (equivalent to $\dot{m}_{H_2} = 100\ tonne/day$) and a residence time of 2 hours is 4. To keep the same number of the reactors by using direct contact heat transfer configuration in the oxygen SBCR, the superficial gas velocity has to be about 50 m/s. Fig. 6.35 shows a comparison in the number of oxygen reactors versus oxygen production rate between the material balance and the heat balance with a direct contact heat transfer configuration for the CANDU-SCWR heat source. The superficial gas velocity of the oxygen SBCR is assumed to be 50 m/s. It can be seen from Fig. 6.35, that the sizes of the oxygen reactor, calculated from the material balance and the heat balance by using a direct contact heat transfer configuration, are comparable.

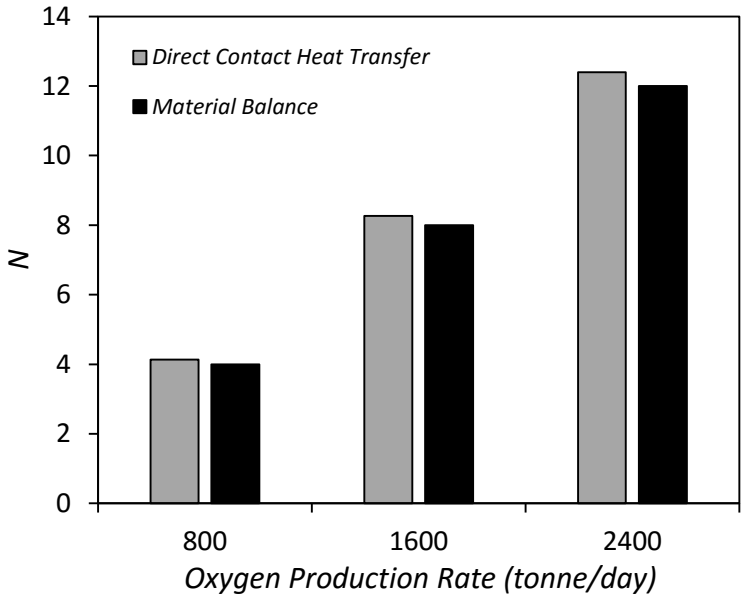

Fig. 6.35 Comparison in number of oxygen reactors (N) between the material balance and the heat balance with a direct contact heat transfer configuration.

6.5. Summary of the CFD Simulations Results

This chapter investigated the hydrodynamic and heat transfer results of the CFD models for a steady state SBC. The following points summarize the work of this chapter;

- This chapter examined the effects of superficial gas velocities (U_{gs}), static liquid heights (H) and solid concentrations (C_s) on overall gas holdup (α_g), and volumetric heat transfer coefficient (U_V).
- The slurry inside SBC is assumed to be perfectly mixed.
- 2D plane approaches were used to model SBC by CFD.
- Gas holdup distribution with reactor radius is unequal, where the gas holdup is high in the center and low in the wall region
- In general, all profiles of α_g and U_V calculated from CFD models, under-predicted the experimental data.
- The CFD model correctly predicted the experimental effects of H and C_s on α_g and U_V.
- The gas temperature (T_g) decreases dramatically near the bottom of the reactor (within the first quarter of the reactor height).
- The effects of U_{gs}, H and C_s on T_g are negligible.
- The number of oxygen reactors is calculated from the amount of heat carried by the oxygen gas rather than the amount of heat transferred by direct contact heat transfer. This number of reactors depends mainly on the oxygen production rate and the superficial gas velocity of the oxygen gas.

CHAPTER 7
CONCLUSIONS AND FUTURE WORKS

7.1. Conclusions

This thesis is aimed at making a contribution in the development of the thermochemical Cu-Cl cycle for hydrogen production. For this purpose, the scale-up of the multiphase oxygen production reactor has been examined. The oxygen reactor in the Cu-Cl cycle is characterized by the large amount of heat that is required for the thermal decomposition process inside the reactor. The research work presented in this thesis focused on the scale up analysis of the oxygen slurry bubble column reactor from the perspectives of the hydrodynamics and heat transfer. The main objectives set for the works in the oxygen SBCR are to advance the state of knowledge of key hydrodynamic and heat transfer parameters of the oxygen SBCR at simulated industrial conditions.

This research has made several original contributions to the scale-up analysis of the oxygen reactor. Two innovative techniques were successfully developed in this thesis research. The first innovative technique is using the stoichiometric oxygen gas produced from the decomposition process as a direct contact heat transfer medium. The stoichiometric oxygen gas produced at 530^{o}C is heated to about 600^{o}C by using CANDU-SCWR and re-injected into the oxygen reactor from the bottom to transfer heat directly to the slurry of molten CuCl and Cu_2OCl_2 solid particles.

The second innovative technique was used to overcome the obstacles of using the actual materials of the oxygen reactor (Oxygen gas and CuCl molten salt) in the experiments, by using the technique of material simulations. Material simulations were used to simulate the actual materials with alternative materials that can be safely used in the laboratory and mimic the behaviors of the actual materials from the perspectives of both hydrodynamic and heat transfer. The alternative materials were found to be helium gas at 90^{o}C and liquid water at 22^{o}C.

The investigations of this thesis have been performed experimentally and numerically by using CFD simulations. The experiments were performed on a new

system of the slurry bubble column with the simulated materials of helium gas and the slurry of water and alumina. In the experiments, it has been studied the effects of superficial gas velocity (U_{gs}), static liquid height (H), solid particles concentration (C_s) and solid particle size (d_p), on the overall gas holdup (α_g), flow regime gas transition velocity $(U_{g-trans})$ and volumetric heat transfer coefficient (U_V) of the helium-water-alumina SBC. New forms of empirical equations for the steady state of the overall gas holdup (α_g) and the volumetric heat transfer coefficient (U_V), were formulated for both bubbly and churn-turbulent flow regimes. These equations were formulated in terms of design parameters such as; reactor dimensions, and input parameters such as; Reynolds number and solid particles concentration. By using the results of the dimensional analysis in Eq. (5.10), (5.21), and (5.47), the results of α_g, $U_{g-trans}$, and U_V of the oxygen SBCR were obtained from the experimental results of the helium-water-alumina system. From the experiments, the following new foundations and conclusions were obtained;

a) In the oxygen reactor system, bubbly flow regime will never be existing and the only regime that will be available in the oxygen reactor is the churn-turbulent flow regime.
b) There is no significant effect of the solid particle diameter on the overall gas holdup when the solid concentration (C_s) is constant.
c) The volumetric heat transfer coefficient (U_V) increases by increasing U_{gs} and decreases by increasing H and/or C_s.
d) The decreasing rate of α_g values with C_s decreases by increasing C_s, while the rate of decrease of U_V values with C_s is approximately the same for different U_{gs}.

Two dimensional CFD simulations of helium-water-alumina system were developed to predict the values of the gas hold-up and the volumetric heat transfer coefficient at different superficial gas velocities, static liquid heights and solid concentrations. In this thesis, the multiphase Euler-Euler method was used for the numerical solutions and the standard $k-\varepsilon$ dispersed turbulence model was used

for modeling the turbulence in the bubble column reactor. The simulations in this research were based on the assumption of perfect mixing of the slurry, and the conservation equations associated with the volume fraction equation were solved together for the heterogeneous flow regime. The data of gas holdup and volumetric heat transfer coefficient were validated against the experimental data and showed good agreement. The validation of the CFD simulations with the experimental data demonstrates the applicability of the simulations for the oxygen slurry bubble column reactor systems. The CFD simulations were validated for superficial gas velocities up to 0.15 m/s, aspect ratios up to 4, and solid concentrations up to 15%. In addition to the gas holdup and volumetric heat transfer coefficient, CFD simulations predicted the new profiles of gas temperature at different superficial gas velocities, static liquid heights and solid concentrations. From the CFD simulations, the following points are concluded;

a) In general, the profiles of α_g and U_V determined from CFD simulations, under-predicted the experimental data.
b) The experimental effects of H and C_s on α_g and U_V were correctly predicted by CFD simulations.
c) The distribution of gas holdup along the cross-section of the column is unequal, where the gas holdup is higher at the center of the column and lower near the wall region.
d) The temperature of the gas (T_g) decreases dramatically near the bottom of the reactor (within the first quarter of the reactor height).
e) The effects of U_{gs}, H and C_s on T_g are negligible.

Another new and important foundation that was obtained in the study of this thesis, is that the thermal scale up analysis of the oxygen reactor with direct contact heat transfer, is based on the amount of heat carried by the oxygen gas rather than the amount of heat transferred by direct contact heat transfer. According to that, an innovative simple correlation (Eq. 6.5) was developed to calculate the number of oxygen reactors as a function of the superficial gas velocity of the oxygen gas and the oxygen production rate.

7.2. Recommendations for Future Research

This thesis provided useful information pertaining to hydrodynamic and heat transfer in multiphase flows in the oxygen reactor. The results of the experiments and analyses enable the integration of the oxygen reactor with the hydrolysis and electrolysis steps of the thermochemical Cu-Cl cycle for hydrogen production. Further recommendations for future works are presented in this section.

- In this thesis, empirical correlations for gas holdup and volumetric heat transfer coefficient in steady state churn-turbulent flows were obtained based on experimental results. However, this study didn't take into account the transient behavior of the churn-turbulent flows. Since the transient flow is a factor affecting the scale-up of the oxygen reactor, it should be considered in future investigations. Therefore, it is suggested that the experimental setup is modified to enable the investigation of how the transient flow affects the hydrodynamic and heat transfer parameters in the SBC.
- Regarding the SBCR systems, the statement by Fan et al. (1999) "*The studies of the regime transition in three-phase fluidized beds and slurry bubble columns are scarce*" is still valid (Mena et al., 2005). This thesis contributed experimentally to filling in this gap, by determining ranges of the transition velocities for helium-water-alumina SBCs. However, this study didn't determine the transition velocity numerically. Further theoretical and numerical studies are needed to determine the flow regime transition velocities.
- The numerical values of both gas holdup and volumetric heat transfer coefficient calculated from CFD simulations, noticeably under predicted the experimental data. Thus, CFD simulations of this thesis needs to be more developed. Three-dimensional mesh of the SBC system may provide a more representative gas holdup and volumetric heat transfer coefficient.
- From the previous studies of the kinetics and the current studies of the hydrodynamic and heat transfer in the oxygen reactor, the final conceptual design of the oxygen reactor can be represented by the schematic diagram in Fig. 7.1. This thesis investigated the scale up of the oxygen SBCR from the perspective of the hydrodynamic and heat transfer studies which is represented

by part A in Fig. 7.1. Further recommendations for future works can be extracted from Fig. 7.1;

a) In part A, there are two kinds of oxygen gas, the stoichiometric and injected oxygen gas, where the stoichiometric oxygen gas has lower speed and temperature than the injected one. This thesis investigated the effect of the injected gas only and didn't take into account the effect of the stoichiometric oxygen gas in the scale up of the oxygen reactor. Since the existence of the stoichiometric oxygen gas affects the scale-up of the oxygen reactor, it should be considered in future investigations. Therefore, it is suggested that the experimental setup is modified to enable the investigation of how stoichiometric oxygen gas bubbles affect the hydrodynamic and heat transfer parameters in the SBCR.
b) The height of part A in Fig. 7.1 is affected by different studies such as kinetics, solid particles dynamics, and hydrodynamic and heat transfer studies. It is suggested to combine these studies to specify the height of part A.
c) In the Cu-Cl cycle, in order to integrate the oxygen SBCR with the electrolysis step, it is recommended to study the overflow of the CuCl molten salt in Part B of Fig. 7.1. The flow rate of the molten salt depends mainly on the results of Part A in Fig. 7.1, which include the results of the reaction kinetics, heat transfer and solid particles dynamics. Therefore, it is recommended to examine Part B in Fig. 7.1 after completing all the studies of Part A.

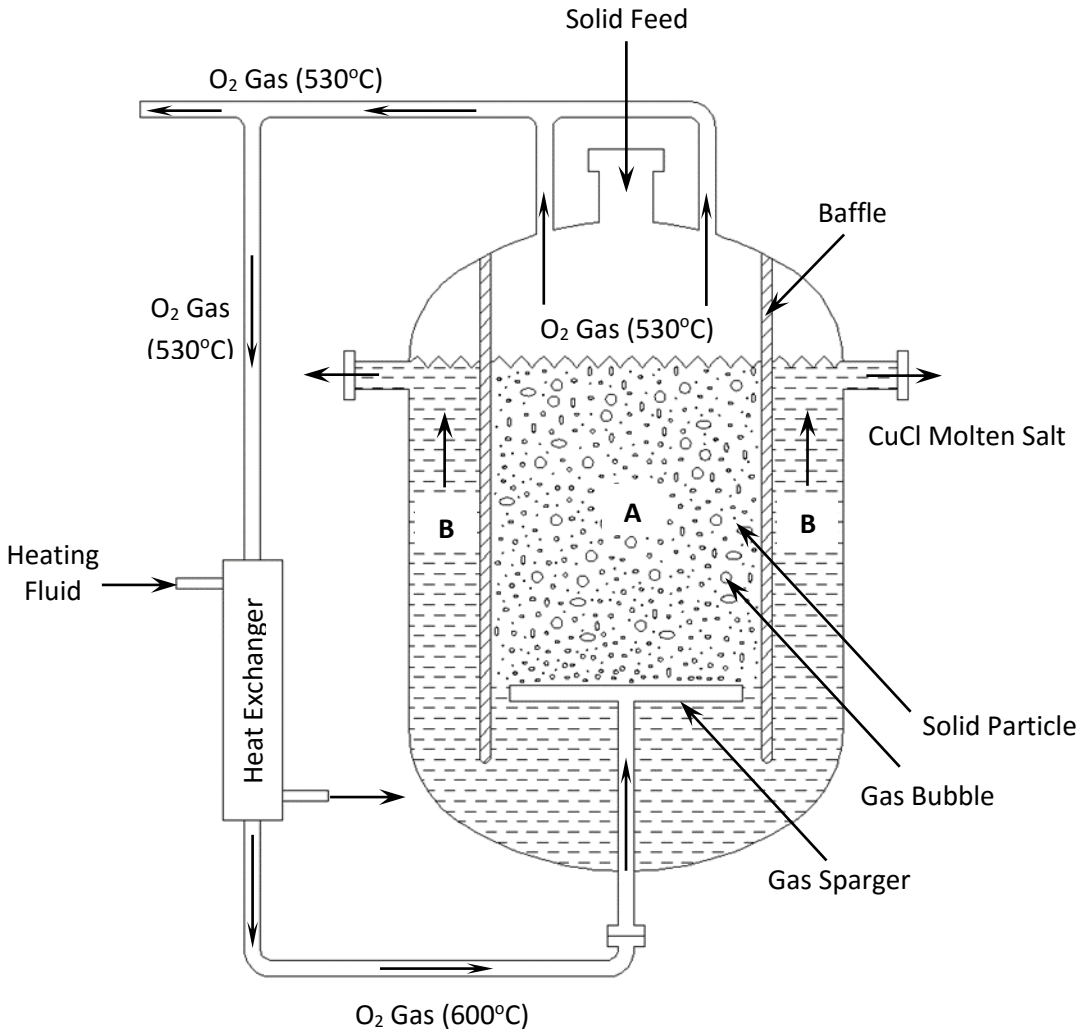

Fig. 7.1 Schematic diagram of the conceptual design of the oxygen SBCR.

REFERENCES

Abdulrahman, M. W. (2015). Experimental studies of direct contact heat transfer in a slurry bubble column at high gas temperature of a helium-water-alumina system. *Applied Thermal Engineering, 91*, 515-524.

Abdulrahman, M. W. (2016a). Similitude for thermal scale-up of a multiphase thermolysis reactor in the cu-cl cycle of a hydrogen production. *World Academy of Science, Engineering and Technology, International Journal of Electrical, Computer, Energetic, Electronic and Communication Engineering, 10* (5), 567-573.

Abdulrahman, M. W. (2016b). Heat transfer analysis of a multiphase oxygen reactor heated by a helical tube in the cu-cl cycle of a hydrogen production. *World Academy of Science, Engineering and Technology, International Journal of Mechanical, Aerospace, Industrial, Mechatronic and Manufacturing Engineering, 10* (6), 1018-1023.

Abdulrahman, M. W. (2016c). Experimental studies of gas holdup in a slurry bubble column at high gas temperature of a helium−water−alumina system. *Chemical Engineering Research and Design, 109*, 486-494.

Abdulrahman, M. W. (2016d). Experimental studies of the transition velocity in a slurry bubble column at high gas temperature of a helium–water–alumina system. *Experimental Thermal and Fluid Science, 74*, 404-410.

Abdulrahman, M. W., Wang, Z., & Naterer, G. F. (2013). Scale-up analysis of three-phase oxygen reactor in the Cu-Cl thermochemical cycle of hydrogen production. *EIC Climate Change Technology Conference 2013 (CCTC2013)*. Montreal, Canada.

Akhtar, M. A., Tadé, M. O. & Pareek, V. K. (2006). Two-fluid Eulerian simulation of bubble column reactors with distributers. *Journal of Chemical Engineering of Japan, 39* (8), 831-841.

Anderson, J. L., & Quinn, J. A. (1970). The transition to slug flow in bubble columns. *Chemical Engineering Science, 25*, 338-340.

ANSYS, Inc. (2012). *ANSYS FLUENT Theory Guide*, Release 14.5. ANSYS, Inc.

Auerkari, P. (1996). Mechanical and physical properties of engineering alumina ceramics. *VTT Manufacturing Technology, Technical Research Centre of Finland ESPOO*.

Bach, H. F., & Pilhofer, T. (1978). Variations of gas hold-up in bubble columns with physical properties of liquids and operating parameters of column. *German Chemical Engineering, 1,* 270-275.

Baldi, G., Conti, R., & Alaria, E. (1978). Complete suspension of particles in mechanically agitated vessels. *Chemical Engineering Science, 33,* 21-25.

Barnea, E., & Mizrahi, J. A. (1973). Generalized approach to the fluid dynamics of particulate system. Part 1 general correlation for fluidization and

sedimentation in solid multi particle systems. *The Chemical Engineering Journal, 5,* 171-189.

Batchelor, G. K. (1967). An introduction to fluid dynamics. *Cambridge University Press*, Cambridge, England.

Beaty, H. W., & Fink, D. (2013). *Standard handbook for electrical engineers* (16th ed.). McGraw Hill Professional.

Behkish, A. (2004). *Hydrodynamic and mass transfer parameters in large-scale slurry bubble column reactors*. (Doctoral Dissertation). University of Pittsburgh, Pennsylvania, USA.

Bejan, A. & Kraus, A. D. (2003). *Heat transfer handbook*. Hoboken, New Jersey: John Wiley & Sons, Inc.

Bejan, A. (1997). *Advanced engineering thermodynamics* (2nd ed.). New York: Wiley.

Bejan, A. (2004). *Convection heat transfer* (3rd ed.). John Wiley & sons, Inc.

Bevington, P. R., & Keith, R. (2003). *Data Reduction and Error Analysis for the Physical Sciences* (3rd ed.). McGraw-Hill, New York.

Borgnakke, C., & Sonntag, R. E. (2009). *Fundamentals of Thermodynamics* (7th ed.). USA: John Wiley & Sons, Inc.

Bukur, D. B., Patel S. A., & Daly, J. G. (1990). Gas holdup and solids dispersion in a three-phase slurry bubble column. *American Institute of Chemical Engineers Journal, 36*, 1731-1735.

Bukur, D. B., Petrovic, D., & Daly, J. G. (1987). Flow regime transitions in a bubble column with a paraffin wax as the liquid medium. *Industrial & Engineering Chemistry Research, 26* (6), 1087-1092.

Buscaglia, G. C., Bombardelli, F. A., & Garcı´a, M. H. (2002). Numerical modeling of large-scale bubble plumes accounting for mass transfer effects. *International Journal Multiphase Flow, 28*, 1763-1785.

Buwa, V. V., & Ranade, V. V. (2002). Dynamics of gas–liquid flow in a rectangular bubble column: Experiments and single/multi-group CFD simulations. *Chemical Engineering Science, 57*, 4715-4736.

Chen, C., & Fan, L. S. (2004). Discrete simulation of gas–liquid bubble columns and gas–liquid–solid fluidized beds. *American Institute of Chemical Engineers Journal, 50*, 288-301.

Chen, P., Sanyal, J., & Dudukovik, M. P. (2005). Numerical simulation of bubble columns flows: effect of different breakup and coalescence closures. *Chemical Engineering Science, 60*, 1085-1101.

Chen, R. C., Reese, J., & Fan, L. S. (1994). Flow structure in a 3-D bubble column and three-phase fluidized bed. *American Institute of Chemical Engineers Journal, 40*, 1093-1104.

Chen, W., Hasegawa, T., Tsutsumi, A., Otawara, K., & Shigaki, Y. (2003). Generalized dynamic modeling of local heat transfer in bubble columns. *Chemical Engineering Journal, 96*, 37-44.

Chilekar, V. P., van der S. J., van Ommen, J. R., Tinge, J. T., Kuster, B. F. M., Schouten, J. C. (2005). *Effect of elevated pressures on hydrodynamics of slurry bubble columns*. Paper presented at the annual meeting of American Institute of Chemical Engineers, Cincinati, Ohio.

Cho, Y. J., Woo, K. J., Kang, Y., & Kim, S. D. (2002). Dynamic characteristics of heat transfer coefficient in pressurized bubble columns with viscous medium. *Chemical Engineering and Processing, 41*, 699-706.

Chow, C. K., & Khartabil, H. F. (2007). Conceptual fuel channel designs for CANDU-SCWR. *Nuclear Engineering and Technology, Special issue on the 3rd international symposium on SCWR, 40* (2), 139-146.

Clark, K. N. (1990). The effect of high pressure and temperature on phase distributions in a bubble column. *Chemical Engineering Science, 45*, 2301-2307.

Clift, R., Grace, J. R., & Weber, M. E. (1978). *Bubbles, drops, and particles.* New York: Academic Press.

Core, K. L., & Mulligan, J. C. (1990). Heat transfer and population characteristics of disperse evaporating droplets. *American Institute of Chemical Engineers Journal, 36*, 1137-1144.

Crabtree, J. R., & Bridgwater, J. (1971). Bubble coalescence in viscous liquids. *Chemical Engineering Science, 26*, 839-851.

Daly, J. G., Patel, S. A., & Bukur, D. B. (1992). Measurement of gas holdups and Sauter mean bubble diameters in bubble column reactors by dynamic gas disengagement method. *Chemical Engineering Science, 47,* 3647-3654.

de Swart, J. W. A., Van Vliet, R. E., & Krishna, R. (1996). Size, structure and dynamics of “large” bubbles in a two-dimensional slurry bubble column. *Chemical Engineering Science, 51,* 4619-4629.

Deckwer, W. D. (1980). On the mechanism of heat transfer in bubble column reactors. *Chemical Engineering Science, 35,* 1341-1346.

Deckwer, W. D. (1992). *Bubble column reactor*. Chichester: John Wiley and Sons.

Deckwer, W. D., & Schumpe, A. (1993). Improved tools for bubble column reactor design and scale-up. *Chemical Engineering Science, 48,* 889-911.

Deckwer, W. D., Louisi, Y., Zaidi, A., & Ralek, M. (1980). Hydrodynamic properties of the Fisher–Tropsch slurry process. *Industrial & Engineering Chemistry Process Design and Development, 19,* 699-708.

Deen, N. G., Solberg, T., & Hjertager, B. H. (2001). Large eddy simulation of gas–liquid flow in a square cross-sectioned bubble column. *Chemical Engineering Science, 56*, 6341-6349.

Delnoij, E., Kuipers, J. A. M., & van Swaaij, W. P. M. (1997a). Computational fluid dynamics applied to gas–liquid contactors. *Chemical Engineering Science, 52*, 3623-3638.

Delnoij, E., Kuipers, J. A. M., & van Swaaij, W. P. M. (1997b). Dynamic simulation of gas–liquid two-phase flow: Effect of column aspect ratio on the flow structure. *Chemical Engineering Science, 52*, 3759-3772.

Delnoij, E., Kuipers, J. A. M., & van Swaaij, W. P. M. (1999). A three-dimensional CFD model for gas–liquid bubble columns. *Chemical Engineering Science, 54*, 2217-2226.

Delnoij, E., Lammers, F. A., Kuipers, J. A. M., & van Swaaij, W. P. M. (1997c). Dynamic simulation of dispersed gas–liquid two-phase flow using a discrete bubble model. *Chemical Engineering Science, 52*, 1429-1458.

Duffey, R. B., & Leung, L. (2010, September). *Advanced cycle efficiency: generating 40% more power from the nuclear fuel*. World Energy Congress (WEC), Montreal, Canada.

Eickenbusch, H., Brunn, P. O., & Schumpe, A. (1995). Mass transfer into viscous pseudo plastic liquid in large-diameter bubble columns. *Chemical Engineering and Proceedings, 34*, 479-485.

Einstein, A. (1906). Eine neue Bestimmung der Moleküldimensionen / A new determination of molecular dimensions. *Annalen der Physik, 19*, 289-306.

Fan, L. S., Yang, G. Q., Lee, D. J., Tsuchiya, K., & Luo, X. (1999). Some aspects of high-pressure phenomena of bubbles in liquid and liquid-solid suspensions. *Chemical Engineering Science, 54*, 4681-4709.

Felice, R., & Kehlenbeck, R. (2000). Sedimentation velocity of solids in finite size vessels. *Chemical Engineering & Technology, 23* (12), 1123-1126.

Forret, A., Schweitzer, J. M., Gauthier, T., Krishna, R., & Schweich, D. (2003). Influence of scale on the hydrodynamics of bubble column reactors: An experimental study in columns of 0.1, 0.4 and 1 m diameters. *Chemical Engineering Science, 58* (3), 719-724.

Forsberg C., (2003). Lowering peak temperatures for nuclear thermochemical production of hydrogen. In Proc. second int. symp. on safety and economy of hydrogen transport, Sarov, Nizhniy Novgorod Region, Russia, August 18–21.

Forsberg, C. W. (2007). Future hydrogen markets for large-scale hydrogen production systems. *International Journal of Hydrogen Energy, 32* (4), 431-439.

Godbole, S. P., Schumpe, A., Shah, Y. T., & Carr, N. L. (1984). Hydrodynamics and mass transfer in non-Newtonian solutions in a bubble column. *American Institute of Chemical Engineers Journal, 30*, 213-220.

Grover, G. S., Rode, C. V., & Chaudrai, R. V. (1986). Effect of temperature on flow regimes and gas holdup in a bubble column. *The Canadian Journal of Chemical Engineering, 64*, 501-504.

Guth, E., & Simba, H. (1936). Viscosity of suspensions and solutions: III Viscosity of sphere suspensions. *Kolloid-Z, 74*, 266-275.

Guy, C., Carreau, J. P., & Paris, J. (1986). Mixing characteristics and gas holdup of a bubble column. *The Canadian Journal of Chemical Engineering, 64* (1), 23-35.

Heijnen, J. J., & Van't Riet, K. (1984). Mass transfer and heat transfer phenomena in low viscosity bubble columns reactors. *Chemical Engineering Journal, 28*, B21-B42.

Hibiki, T., Ishii, M. (2000). Two-group interfacial area transport equations at bubbly-to-slug flow transition. *Nuclear Engineering and Design, 202*, 39-76.

Hills, J. H. (1976). The operation of a bubble column at high throughputs and gas holdup measurement. *Chemical Engineering Journal, 12*, 89-99.

Hyndman, C. L., Larachi, F., & Guy, C. (1997). Understanding gas-phase hydrodynamics in bubble columns: a convective model based on kinetic theory. *Chemical Engineering Science, 52*, 63-77.

Ikeda, B. M., & Kaye, M. H. (2008, August). Thermodynamic properties in the Cu-Cl- O-H system. *7th International Conference on Nuclear and Radiochemistry*. Budapest, Hungary.

Inga, J. R., & Morsi, B. I. (1999). Effect of operating variables on the gas holdup in a large-scale slurry bubble column reactor operating with organic liquid mixture. *Industrial and Engineering Chemistry Research, 38*, 928-937.

Jaber, J. (2009). *Heat and fluid flow analysis in a molten CuCl heat exchanger* (Master's thesis). University of Ontario Institute of Technology, Ontario, Canada.

Jakobsen, H. A., Sannaes, B. H., Grevskott, S., & Svendsen, H. F. (1997). Modelling of vertical bubble-driven flows. *Industrial & Engineering Chemistry Research, 36*, 4052-4074.

Jamialahmadi, M., & Mueller-Steinhagen, H. (1991). Effect of solid particles on gas hold-up in bubble columns. The *Canadian Journal of Chemical Engineering, 69* (1), 390-393.

Jamialahmadi, M., Muller-Steinhagen, H., Sarrafi, A., & Smith, J. M. (2000). Studies of gas holdup in bubble column reactors. *Chemical Engineering & Technology, 23* (10), 919-921.

Janz, G. J. (1988). Thermodynamic and transport properties for molten salts: Correlation equations for critically evaluated density, surface tension, electrical conductance, and viscosity data. *Journal of Physical and Chemical Reference Data, 17, Supplement No.* 2.

Jordan, U., & Schumpe, A. (2001). The gas density effect on mass transfer in bubble columns with organic liquids. *Chemical Engineering Science, 56*, 6267-6272.

Joshi, J. B. (2001). Computational flow modelling and design of bubble column reactors. *Chemical Engineering Science, 56*, 5893-5933.

Joshi, J. B., & Sharma, M. M. (1979). A circulation cell model for bubble columns. *Transactions of the Institution of Chemical Engineers, 57*, 244-251.

Joshi, J. B., Deshpande, N. S., Dinkar, M., & Phanikumar, D. V. (2001). Hydrodynamic stability of multiphase reactors. *Advances in Chemical Engineering, 26*, 1-130.

Joshi, J. B., Vitankar, V. S., Kulkarni, A. A., Dhotre, M. T., & Ekambara, K. (2002). Coherent flow structures in bubble column reactors. *Chemical Engineering Science, 57*, 3157-3183.

Kara, S., Kelkar, B. G., Shah, Y. T., & Carr, N. L. (1982). Hydrodynamics and axial mixing in a three-phase bubble column. *Industrial & Engineering Chemistry Process Design and Development, 21*, 584-594.

Kastanek, F., Zahradnik, J., Kratochvil, J., & Cermak, J. (1984). Modeling of large-scale bubble column reactors for non-ideal gas-liquid systems. In E. L. K. Doraiswamy, & R. A. Mashelkar (Eds.), *Frontiers in Chemical Reaction Engineering* (pp. 330-344). New Delhi, India: Wiley Eastern Ltd.

Kato, Y., Nishiwaki, A., Kago, T., Fukuda, T., & Tanaka, S. (1973). Gas holdup and overall volumetric absorption coefficient in bubble columns with suspended solid particles. *Transactions of the Institution of Chemical Engineers, 13*, 562-567.

Kawagoe, K., Inoue, T., Nakao, K., & Otake, T. (1976). Flow-pattern and gas holdup conditions in gas-sparged contactors. *International Journal of Chemical Engineering, 16*, 176-183.

Kawase, Y., & Moo-Young, M. (1987). Heat transfer in bubble column reactors with Newtonian and non-Newtonian fluids. *Chemical Engineering Research and Design, 65*, 121-126.

Kelkar, B. G., Godbole, S. P., Honath, M. F., Shah, Y. T., Carr, N. L., Deckwer, W. D. (1983). Effect of addition of alcohols on gas holdup and back mixing in bubble columns. *American Institute of Chemical Engineers Journal, 29*, 361-369.

Kemoun, A., Ong, B. C., Gupta, P., & Al-Dahhan, M. H. (2001). Gas holdup in bubble columns at elevated pressure via computed tomography. *International Journal of Multiphase Flow, 27*, 929-946.

Kim, H. S., Kim, J. H., Lee, C. G., Kang, S. H., Woo, K. J., Jung, H. J., Kim, D. W. (2014). Bubble and heat transfer phenomena in viscous slurry bubble column. *Advances in Chemical Engineering and Science*, *4*, 417-429.

Kim, S. D., Kang, Y., & Kwon, H. K. (1986). Heat transfer characteristics in two- and three-phase slurry fluidized-beds. *American Institute of Chemical Engineers Journal. 32*, 1397-1400.

Kline, S. J., & McClintock, F. A. (1953). Describing uncertainties in single-sample experiments. Journal of *Mechanical Engineering, 75*, 3-8.

Koide, K., Morooka, S., Ueyama, K., Matsuura, A., Yamashita, F., Iwamoto, S., Kato, Y., Inoue, H., Shigeta, M., Suzuki, S., & Akehata, T. (1979). Behavior of bubbles in large scale bubble column. *Journal of Chemical Engineering of Japan, 12*, 98-104.

Koide, K., Takazawa, A., Komura, M., & Matsunga, H. (1984). Gas holdup and volumetric liquid phase mass transfer coefficient in solid-suspended bubble column. *Journal of Chemical Engineering of Japan, 17*, 459-466.

Kolbel, H., Borchers, E., & Martins, J. (1960). Warmeubergang in Blasensaulen. III. Messungen an Gasdurchstromten Suspensionen / Warm transition in bubble columns. III. Flocked measurements on gas. *Chemical Engineering & Technology, 32*, 84-88.

Krishna, R., & Sie, S. T. (2000). Design and scale-up of the Fischer-Tropsch bubble column slurry reactor. *Fuel Processing Technology, 64*, 73-105.

Krishna, R., & van Baten, J. M. (2001). Eulerian simulations of bubble columns operating at elevated pressures in the churn turbulent flow regime. *Chemical Engineering Science, 56*, 6249-6258.

Krishna, R., De Stewart, J. W. A., Ellenberger, J., Martina, G. B., & Maretto, C. (1997). Gas holdup in slurry bubble columns: effect of column diameter and slurry concentrations. *American Institute of Chemical Engineers Journal, 43*, 311-316.

Krishna, R., Ellenberger, J., & Maretto, C. (1999). Flow regime transition in bubble columns. *International Communications in Heat and Mass Transfer, 26* (4), 467-475.

Krishna, R., van Baten, J. M., Urseanu, M. I., & Ellenberger, J., (2001). Design and scale-up of the bubble column slurry reactor for Fischer-Tropsch synthesis, *Chemical Engineering Science, 56* (2), 537-545.

Krishna, R., Wilkinson, P. M., & Van Dierendonck, L. L. (1991). A model for gas holdup in bubble columns incorporating the influence of gas density on flow regime transitions. *Chemical Engineering Science, 46* (10), 2491-2496.

Kumar, S., Kusakabe, K., Raghuathan, K., & Fan, L.S. (1992). Mechanism of heat transfer in bubbly liquid and liquid–solid systems: Single bubble injection. *American Institute of Chemical Engineers Journal, 38*, 733-741.

Laı´n, S., Bröder, D., Sommerfeld, M., & Göz, M. F. (2002). Modelling hydrodynamics and turbulence in a bubble column using the Euler–Lagrange procedure. *International Journal of Multiphase Flow, 28*, 1381-1407.

Lapin, A., & Lu¨bbert, A. (1994). Numerical simulation of the dynamics of two phase gas–liquid flows in bubble columns. *Chemical Engineering Science, 49*, 3661-3674.

Lau, R., Peng, W., Velazquez-Vargas, G., Yang, G. Q., & Fan, L. S. (2004). Gas-liquid mass transfer in high-pressure bubble columns. *Industrial and Engineering Chemistry Research, 43*, 1302-1311.

Launder, B. E., & Spalding, D. B. (1972). *Lectures in mathematical models of turbulence*. Academic Press, London, England.

Law, D., Battaglia, F., & Heindel, T. (2006, November). Numerical simulations of gas-liquid flow dynamics in bubble columns. In: *Proceedings of 2006 ASME International Mechanical Engineering Congress and Exposition* (pp. 593–600). Chicago, Illinois, USA.

Lee, D. J., Luo, X., & Fan, L. S. (1999). Gas disengagement technique in a slurry bubble column operated in coalesced bubble regime. *Chemical Engineering Science, 54*, 2227-2236.

Lee, D. J., McLain, B. K., Cui, Z., & Fan, L. S. (2001). Pressure effect on the flow fields and the Reynolds stresses in a bubble column. *Industrial and Engineering Chemistry Research, 40*, 1442-1447.

Lemenand, T., Durandal, C., Valle, D. D., & Peerhossaini, H. (2010). Turbulent direct-contact heat transfer between two immiscible fluids. *International Journal of Thermal Sciences*, 49 (10), 1886-1898.

Lemmon, E. W., & Jacobsen, R. T. (2004). Viscosity and thermal conductivity equations for nitrogen, oxygen, argon, and air, *International Journal of Thermophysics, 25*, (1), 21-69.

Letan, R. (1988). Liquid-liquid processes. In F. Kreith, & R. H. Boehm (Eds.), *Direct contact heat transfer* (pp. 3-118). New York: Hemisphere.

Letzel, H. M., Schouten, J. C., Krishna, R., & Van Den Bleek, C. M. (1997). Characterization of regimes and regime transitions in bubble columns by chaos analysis of pressure signals. *Chemical Engineering Science, 52* (24), 4447-4459.

Lewis, M. A., Masin, J. G., & Vilim, R. B. (2005, May). Development of the low temperature Cu-Cl thermochemical cycle. *Argonne National Laboratory, International Congress on Advances in Nuclear Power Plants*, Seoul, Korea.

Lewis, M. A., Serban, M., & Basco, J. K. (2003). Generating hydrogen using a low temperature thermochemical cycle. *Proceedings of the ANS/ENS Global International Conference on Nuclear Technology*. New Orleans.

Li, H., & Prakash, A. (1997). Heat transfer and hydrodynamics in a three-phase slurry bubble column. *Industrial & Engineering Chemistry Research, 36*, 4688-4694.

Li, H., & Prakash, A. (1999). Analysis of bubble dynamics and local hydrodynamics based on instantaneous heat transfer measurements in a slurry bubble column. *Chemical Engineering Science, 54*, 5265-5271.

Li, H., & Prakash, A. (2000). Influence of slurry concentrations on bubble population and their rise velocities in three-phase slurry bubble column. *Powder Technology, 113*, 158-167.

Li, H., & Prakash, A. (2002). Analysis of flow patterns in bubble and slurry bubble columns based on local heat transfer measurements. *Chemical Engineering Journal, 86*, 269-276.

Lin, T. J., Juang, R. C., Chen, Y. C., & Chen, C. C. (2001). Predictions of flow transitions in a bubble column by chaotic time series analysis of pressure fluctuation signals. *Chemical Engineering Science, 56* (3), 1057-1065.

Lin, T. J., Tsuchiya, K., & Fan, L. (1999). On the measurements of regime transition in high-pressure bubble columns. The *Canadian Journal of Chemical Engineering, 77* (2), 370-374.

Lockett, M. J., & Kirkpatrick, R. D. (1975). Ideal bubbly flow and actual flow in bubble columns. *Transactions of the Institution of Chemical Engineers, 53*, 267-273.

Lopes, R. J. G., & Quinta-Ferreira, R. M. (2007). Multiphase CFD modeling of trickle-bed reactor hydrodynamics. *Proceedings of the World Congress on Engineering and Computer Science (WCECS)*. San Francisco, USA.

Luo, X., Lee, D. J., Lau, R., Yang, G., & Fan, L. (1999). Maximum stable bubble size and gas holdup in high-pressure slurry bubble columns. *American Institute of Chemical Engineers Journal, 45*, 665-85.

Mahajan, V. (2010). *CFD analysis of hydrodynamics and mass transfer of a gas-liquid bubble column* (Bachelor's project). Rourkela, Orissa, India.

Marin, G. D. (2012). Kinetics and transport phenomena in the chemical decomposition of copper oxychloride in the thermochemical Cu-Cl cycle (Doctoral dissertation). University of Ontario Institute of Technology, Ontario, Canada.

Marin, G. D., Wang, Z., Naterer, G. F., & Gabriel, K. (2011). By products and reaction pathways for integration of the Cu-Cl cycle of hydrogen production. *International Journal of Hydrogen Energy, 36*, 13414-13424.

McCutcheon, S. C., Martin, J. L., & Barnwell, T. O. (1993). Water quality. In D. R. Maidment (Editor), *Handbook of Hydrology* (p. 11.3). New York: McGraw-Hill.

Mena, P. C., Ruzicka, M. C., Rocha, F. A., Teixeira, J. A., & Drahos, J. (2005). Effect of solids on homogeneous heterogeneous flow regime transition in bubble columns. *Chemical Engineering Science, 60* (22), 6013-6026.

Mersmann, A., North, H., & Wunder, R. (1982). Maximum heat transfer in equipment with dispersed two-phase systems. *International Journal of Chemical Engineering, 22*, 16-29.

Michele, V., & Hempel, D. C. (2002). Liquid flow and phase holdup—Measurement and CFD modeling for two- and three-phase bubble columns. *Chemical Engineering Science, 57*, 1899-1908.

Millies, M., & Mewes, D. (1999). Interfacial area density in bubbly flow. *Chemical Engineering and Processing, 38*, 307-319.

Monahan, S., & Fox, R. O. (2002, September). Effect of grid resolution and force models. *Proceeding of 8th International Conference on Multiphase Flow in Industrial Plants*. Alba, Italy.

Morrison, T. J., & Johnstone, N. B. (1954). Solubilities of the inert gases in water. *Journal of Chemical Society*, 3441-3446.

Moustiri, S., Hebrard, H., Thakre, S. S., & Roustan, M. (2001). A unified correlation for predicting liquid axial dispersion coefficient in bubble columns. *Chemical Engineering Science, 56*, 1041-1047.

Mudde, R. F., & Simonin, O. (1999). Two- and three-dimensional simulations of a bubble plume using a two-fluid model. *Chemical Engineering Science, 54*, 5061-5069.

Munson B. R., Young, D. F., & Okiishi, T. H. (2006). *Fundamentals of fluid mechanics (5th ed.)*. John Wiley & Sons, Inc.

Naterer, G. F., Fowler, M., Cotton, J., & Gabriel, K. (2008a). Synergistic roles of off-peak electrolysis and thermochemical production of hydrogen from nuclear energy in Canada. *International Journal of Hydrogen Energy, 33*, 6849-6857.

Naterer, G. F., Gabriel, K., Wang, Z. L., Daggupati, V. N., & Gravelsins, R. (2008b). Thermochemical hydrogen production with a copper–chlorine cycle. I: Oxygen release from copper oxychloride decomposition. *International Journal of Hydrogen Energy, 33*, 5439-5450.

Naterer, G. F., Suppiah, S., Stolberg, L., Lewis, M., Ferrandon, M., Wang, Z., …. Avsec, J. (2011a). Clean hydrogen production with the Cu–Cl cycle - Progress of international consortium, I: Experimental unit operations. *International Journal of Hydrogen Energy, 36* (24), 15472-15485.

Naterer, G. F., Suppiah, S., Stolberg, L., Lewis, M., Ferrandon, M., Wang, Z., …. Avsec, J. (2011b). Clean hydrogen production with the Cu–Cl cycle - Progress of international consortium, II: Simulations, thermochemical data and materials. *International Journal of Hydrogen Energy*, 36 (24), 15486-15501.

Natesan, K., Moisseytsev, A., Majumdar, S., & Shankar, P. S. (2006). Preliminary issues associated with the next generation nuclear plant intermediate heat exchanger design. *ANL/EXT-06/46*. Argonne National Laboratory.

Neme, F., Coppola, L., & Böhm, U. (1997). Gas holdup and mass transfer in solid suspended bubble columns in presence of structured packings. *Chemical Engineering Technology, 20*, 297-303.

Nguyen, A., & Schulze, H. J. (2003). *Colloidal science of flotation*. New York: CRC Press.

Nguyen, T., Ward, J., & Johnson, K. (2013). *Well-to-wheels greenhouse gas emissions and petroleum use for mid-size light-duty vehicles,* U.S. Department of Energy, Hydrogen Program Record #13005 (rev. 1).

Nigam, K. D. P., & Schumpe, A. (1996). Three-phase sparged reactors. Amsterdam, the Netherlands: Gordon and Breach Publishers.

Nigar, K., Fahir, B., & Kutlu, O. U. (2005). Review: Bubble column reactors. *Process Biochemistry, 40*, 2263-2283.

Oels, U., Lucke, J., Buchholz, R., & Schugerl, K. (1978). Influence of gas distributor type and composition of liquid on the behavior of a bubble column bioreactor. *German Chemical Engineering, 1*, 115-129.

Ohki, Y., & Inoue, H. (1970). Longitudinal mixing of the liquid phase in bubble columns. *Chemical Engineering Science, 25* (1), 1-16.

Oldshue, J. Y. (1983). *Fluid mixing technology*. McGraw-Hill.

Olmos, E., Gentric, C., Vial, C. Wild, G., & Midoux N. (2001). Numerical simulation of multiphase flow in bubble column reactors. Influence of bubble coalescence and break-up. *Chemical Engineering Science, 56*, 6359-6365.

Omega.com (2009). *Flow, level and environmental handbook and encyclopedia* (8th ed.). Volume MMXI. USA.

Omega.com (2010). *Omega pressure and strain measurement handbook* (9th ed.). Volume MMXI. USA.

Orhan, M. F. (2011). *Analysis, design and optimization of nuclear-based hydrogen production with copper-chlorine thermochemical cycles* (Doctoral dissertation). University of Ontario Institute of Technology, Oshawa, Ontario, Canada.

Osborne, Stimson, & Ginnings, B. (1939). *Handbook of Chemistry and Physics* of S. Jour. Res., 23, 238. In, 53rd ed., Cleveland, Ohio, D128 (1972-1973).

Petersen, H. (1970, September). The properties of helium: Density, specific heats, viscosity, and thermal conductivity at pressures from 1 to 100 bar and from room temperature to about 1800 K. *Risö Report No. 224*. Danish atomic energy commission research establishment Risö.

Pfleger, D., Gomos, S., Gilbert, N., & Wagner, H. G. (1999). Hydrodynamic simulation of laboratory scale bubble columns: fundamental studies of Eulerian–Eulerian modeling approach. *Chemical Engineering Science, 54*, 5091-5099.

Pino, L. Z., Solari, R. B., Siuier, S., Estevez, L. A., Yepez, M. M., Saez, A. E. (1992). Effect of operating conditions on gas holdup in slurry bubble columns with a foaming liquid. *Chemical Engineering Communications, 117*, 367-82.

Pohorecki, R., Moniuk, W., & Zdrojkowski, A. (1999). Hydrodynamics of a bubble column under elevated pressure. *Chemical Engineering Science, 54*, 5187-5193.

Prakash, A., Margaritis, A., & Li, H. (2001). Hydrodynamics and local heat transfer measurements in a bubble column with suspension of yeast. *Biochemical Engineering Journal, 9*, 155-163.

Rafique, M., Chen, P., & Duduković, M. P. (2004). Computational modeling of gas-liquid flow in bubble columns. *Reviews in Chemical Engineering*, *20* (3-4), 225–375.

Ramires, M. L. V., Nieto de Castro, A., Nagasaka, Y., Nagashima, A., Assael, M. J., Wakeham, W. A. (1994). Standard reference data for the thermal conductivity of water. *American Institute of Physics and the American Chemical society.*

Rampure, M., Buwa, V., & Ranade, V. (2003). Modelling of gas-liquid/gas-liquid-solid flows in bubble columns: Experiments and CFD simulations. *The Canadian Journal of Chemical Engineering, 81* (3-4), 692-706.

Reid, R.C., Prausnitz, J.M., & Poling, B.E. (1987). *Properties of gases and liquids*, New York: McGraw-Hill.

Reilly, I. G., Scott, D. S., De Bruijn, T. J. W., & MacIntyre, D. (1994). The role of gas phase momentum in determining gas holdup and hydrodynamic flow regimes in bubble column operations. The *Canadian Journal of Chemical Engineering, 72* (1), 3-12.

Reilly, I. G., Scott, D. S., de Bruijn, T. J. W., Jain, A., & Piskorz, J. (1986). A correlation for gas holdup in turbulent coalescing bubble columns. *The Canadian Journal of Chemical Engineering, 64*, 705-717.

Reilly, I. G., Scott, D. S., de Bruijn, T. J. W., MacIntyre, D., & Piskorz, J. (1990). Axial solid concentrations in three-phase bubble columns. *Chemical Engineering Science, 45*, 2293-2299.

Richardson, J. F., & Zaki, W. M. (1954). Sedimentation and fluidisation: Part I. *Transactions of the Institution of Chemical Engineers, 32*, 35-53.

Riquarts, H. P. (1978). *Disperse two-phase flows: Calculation principles and their application*. Habilitationsschrift, TU Muenchen.

Robert, F. B., (2003). Direct contact heat transfer. In A. Bejan, & A. D. Kraus (Eds.), *Heat transfer handbook* (p. 1374). John Wiley & Sons, Inc.

Roscoe, R. (1952). The viscosity of suspension of rigid spheres. *British Journal of Applied Physics, 3* (8), 267-269.

Rowley, R. L., Wilding, W. V., Oscarson, J. L., Yang, Y., Zundeland, N. A., …Daubert, T. P. (2004). *DIPPR data compilation of pure chemical properties*. New York: Taylor & Francis.

Ruthiya, K. (2005). *Mass transfer and hydrodynamics in catalytic slurry reactors* (Doctoral dissertation). Eindhoven University, the Netherlands.

Ruzicka, M. C., Drahoš, J., Fialová, M., & Thomas, N. H. (2001a). Effect of bubble column dimensions on flow regime transition. *Chemical Engineering Science, 56*, 6117–6124

Ruzicka, M. C., Zahradnik, J., Drahos, J., & Thomas, N. H. (2001b). Homogeneous-heterogeneous regime transition in bubble columns. *Chemical Engineering Science, 56* (15), 4609-4626.

Sada, E., Katoh, S., & Yoshil, H. (1984). Performance of the gas–liquid bubble column in molten salt systems. *Industrial & Engineering Chemistry Process Design and Development, 23*, 151-154.

Sanyal, J., Va´squez, S., Roy, S., & Dudukovic, M. P. (1999). Numerical simulation of gas–liquid dynamics in cylindrical bubble column reactors. *Chemical Engineering Science, 54*, 5071-5083.

Sarah, M. M., Vivek, S. V., & Rodney, O. F. (2005). CFD predictions for flow-regime transitions in bubble columns. *American Institute of Chemical Engineers Journal, 51* (7), 1897-1923.

Sarrafi, A., Jamialahmadi, M., Muller-Steinhagen, H., & Smith, J. M. (1999). Gas holdup in homogeneous and heterogeneous gas-liquid bubble column reactors. The *Canadian Journal of Chemical Engineering, 77* (1), 11-21.

Sauer, T., & Hempel, D. C. (1987). Fluid dynamics and mass transfer in a bubble column with suspended particles. *Chemical Engineering and Technology, 10*, 180-189.

Saxena, S. C., & Chen, Z. D. (1994). Hydrodynamics and heat transfer of baffled and unbaffled slurry bubble column. *Reviews in Chemical Engineering, 10* (3-4), 193-400.

Saxena, S. C., Rao, N. S., & Saxena, A. C. (1990). Heat-transfer and gas-holdup studies in a bubble column: Air–water–glass bead system. *Chemical Engineering Communications, 96*, 31-55.

Saxena, S. C., Rao, N. S., & Thimmapuram, P. R. (1992). Gas phase holdup in slurry bubble column for two and three-phase systems. *The Chemical Engineering Journal, 49*, 151-159.

Schiller, L., & Naumann, A. (1933). Uber die grundlegenden berechnungen bei der schwerkraftaufbereitung / About the basic calculations in the gravity-treatment. *Zeitung des vereins deutscher ingenieure / Newspaper of the Association of German Engineers*, pp. 77–318.

Schügerl, K., Lücke, J., & Oels, U. (1977). Bubble column bioreactors. *Advances in Biochemical Engineering, 7*, 1-84.

Schumpe, A. (1981). Chemical determination of the phase boundaries in bubble columns by inconsistent bubble sizes (Doctoral dissertation), Universität Hannover, Hannover, Germany.

Schumpe, A., & Deckwer, W. D. (1987). Viscous media in tower bioreactors: hydrodynamic characteristics and mass transfer properties. *Bioprocess and Biosystems Engineering, 2* (2), 79-94.

Schumpe, A., & Grund, G. (1986). The gas disengagement technique for studying gas holdup structure in bubble columns. *The Canadian Journal of Chemical Engineering, 64*, 891-896.

Serban, M., Lewis, M. A., & Basco, J. K. (2004, April). Kinetic study of the hydrogen and oxygen production reactions in the copper-chloride thermochemical cycle. *American Institute of Chemical Engineers Journal*, Spring National Meeting, New Orleans, LA, pp. 2690-2698.

Shah, Y. T., Kelkar, B. G., Godbole, S. P., & Deckwer, W. D. (1982). Design parameters estimations for bubble column reactors. *American Institute of Chemical Engineers Journal, 28*, 353-379.

Shaikh, A. (2007). Bubble and slurry bubble column reactors: mixing, flow regime transition and scale-up (Doctoral dissertation). Sever Institute of Washington University, Saint Louis, Missouri, USA.

Shaikh, A., & Al-Dahhan, M. (2005). Characterization of the hydrodynamic flow regime in bubble columns via computed tomography. *Flow Measurement and Instrumentation, 16* (2-3), 91-98.

Shaikh, A., & Al-Dahhan, M. (2006). Hydrodynamics of slurry bubble column reactors. *CREL Internal Report.*

Shaikh, A., & Al-Dahhan, M. H. (2007). A review on flow regime transition in bubble columns. *International Journal of Chemical Reactor Engineering, 5*, *Review* R1

Sheoran, S., Belusko, M., Bruno, F., & Saman, W. Y. (2010, December). Modelling of a direct contact two immiscible phase molten salt system for high temperature solar thermal storage. *Proc. Solar 2010, the 48th AuSES Annual Conference*. Canberra, Australia.

Shimizu, K., Takada, S., Minekawa, K., & Kawase, Y. (2000). Phenomenological model for bubble column reactors: Prediction of gas holdups and volumetric mass transfer coefficients. *Chemical Engineering Journal, 78*, 21-28.

Shimizu, Y., & Mori, Y. H. (1988). Evaporation of single liquid drops in an immiscible liquid at elevated pressures: Experimental study with n-pentane and R113 drops in water. *International Journal of Heat and Mass Transfer, 31*, 1843-1851.

Sideman, S., & Gat, Y. (1966). Direct contact heat transfer with change of phase: Spray column studies of a three-phase heat exchanger. *American Institute of Chemical Engineers Journal, 12*, 296-303.

Smith, R. C., Rohsenow, W. M., & Kazimi, M. S. (1982). Volumetric heat-transfer coefficients for direct-contact evaporation. *ASME, Journal of Heat Transfer, 104*, 264-270.

Sokolichin, A. & Eigenberger, G. (1994). Gas–liquid flow in bubble columns and loop reactors: Part I. Detailed modelling and numerical simulation. *Chemical Engineering Science, 49* (24, Part 2), 5735-5746.

Sokolichin, A., & Eigenberger, G. (1999). Applicability of the standard $k-\varepsilon$ turbulence model to the dynamic simulation of bubble columns: Part I. Detailed numerical simulations. *Chemical Engineering Science, 54*, 2273-2284.

Sokolichin, A., Eigenberger, G., & Lapin, A. (2004). Simulation of buoyancy driven bubbly flow: Established simplifications and open questions. *American Institute of Chemical Engineers Journal, 50*, 24-45.

Sokolichin, A., Eigenberger, G., Lapin, A., & Lübbert, A. (1997). Dynamic numerical simulation of gas–liquid two-phase flows: Euler–Euler versus Euler–Lagrange. *Chemical Engineering Science, 52*, 611-626.

Sonin, A. A. (2001). *The physical basis of dimensional analysis* (2nd ed.), Department of Mechanical Engineering, Cambridge.

Soong, Y., Harke, F. W., Gamwo, I. K., Schehl, R. R., & Zarochak, M. F. (1997). Hydrodynamic study in a slurry bubble-column reactor. *Catalysis Today, 35*, 427-434.

Studely, A. F. (2010). *Numerical Modeling of Air-Water Flows in Bubble Columns and Airlift Reactors* (Master's Thesis). Virginia Polytechnic Institute and State University, Blacksburg, Virginia.

Suh, I. S., & Deckwer, W. D. (1989). Unified correlation of heat transfer coefficients in three-phase fluidized beds. *Chemical Engineering Science, 44*, 1455-1458.

Thomas, D. G. (1965). Transport characteristics of suspension: VIII. A note on viscosity of Newtonian suspensions of uniform spherical particles. *Journal of Colloid Science, 20*, 267-277.

Thorat, B. N., & Joshi, J. B. (2004). Regime transition in bubble columns: Experimental and predictions*. Experimental Thermal and Fluid Science, 28* (5), 423-430.

Trevani, L. (2011, May). The copper-chloride cycle: synthesis and characterization of copper oxychloride. *Hydrogen and Fuel Cells International Conference and Exhibition*. Vancouver, BC, Canada.

Tropea C., Yarin A. L., & Foss J. F. 2007. *Springer Handbook of Experimental Fluid Mechanics*. Springer.

Tsoulfanidis, N. (2012). *Nuclear energy: selected entries from the encyclopedia of sustainability science and technology,* New York: Springer.

Urseanu, M. (2000). *Scaling up bubble column reactors* (Doctoral dissertation). University of Amsterdam, Amsterdam, the Netherlands.

Vand, V. (1948). Viscosity of solutions and suspensions. I. Theory. *Journal of Physical Chemistry, 52*, 277-299.

Vandu, C. (2005). *Hydrodynamics and mass transfer in multiphase reactors* (Doctoral dissertation). University of Amsterdam, Amsterdam, the Netherlands.

Vandu, C. O., & Krishna, R. (2004). Volumetric mass transfer coefficients in slurry bubble columns operating in churn-turbulent flow regime. *Chemical Engineering and Processing, 43*, 987-995.

Vargaftik, N. B., Volkov, B. N., & Voljak, L. D. (1983). International tables of the surface tension of water. Moscow Aviation Institute, Moscow, U.S.S.R. *Journal of Physical and Chemical Reference Data, 12* (3), 817-820.

Vial, C., Laine, R., Poncin, S., Midoux, N., & Wild, G. (2001). Influence of gas distribution and regime transition on liquid velocity and turbulence in a 3-d bubble column. *Chemical Engineering Science, 56*, 1085-1093.

Wallis, G. B. (1969). *One dimensional two phase flow*. New York: McGraw Hill.

Wijeysundera, N. E., Hawlader, M. N. A., Chan A., & Kamal Hossain, M. (2004). Ice-slurry production using direct contact heat transfer. *International Journal of Refrigeration, 27*, 511-519.

Wikle, C. R., Cheng, C. T., Ledesma, V. S., & Porter, J. W. (1963). Direct contact heat transfer for sea water evaporation. *Chemical Engineering Progress, 59*, 69-75.

Wilkinson, P. M. (1991). *Physical aspects and scale-up of high pressure bubble columns* (Doctoral dissertation). University of Groningen, Groningen, the Netherlands.

Wilkinson, P. M., & Van Dierendonck, L. L. (1990). Pressure and gas density effects on bubble break-up and gas hold-up in bubble columns. *Chemical Engineering Science, 45*, 2309-2315.

Wilkinson, P. M., Spek, A. P., & Van Dierendonck, L. L. (1992). Design parameters estimation for scale up of high-pressure bubble columns. *American Institute of Chemical Engineers Journal, 38* (4), 544-554.

Wright, J. D. (1988). *Design of direct-contact preheater/boilers for solar pond power plants. In F. D. Kreith, R. H. Boehm (Eds.). Direct contact heat transfer* (pp. 299-334). New York: Hemisphere.

Wu, Y., Ong, B. J., & Al-Dahhan, M. H. (2001). Predictions of gas hold-up profiles in bubble column reactors. *Chemical Engineering Science, 56*, 1207-1210.

Yamashita, F., & Inoue, H. (1975). Gas holdup in bubble columns. *Journal of Chemical Engineering of Japan, 8*, 444-449.

Yang, G. Q., Luo, X., Lau, R., & Fan, L. S. (2000). Heat-transfer characteristics in slurry bubble columns at elevated pressures and temperatures. *Industrial and Engineering Chemistry Research, 39*, 2568-2577.

Yasunishi, A., Fukuma, M., & Muroyama, K. (1986). Measurement of behavior of gas bubbles and gas holdup in a slurry bubble column by a dual electro-resistivity probe method. *Journal of Chemical Engineering of Japan, 19*, 444-449.

Yetisir, M. (2012, July). Generation IV supercritical water-cooled reactor. *Deep River Science Academy Summer Lecture*. AECL, Ontario, Canada.

Yoshida, F., & Akita, K. (1965). Performance of gas bubble columns: volumetric liquid-phase mass transfer coefficient and gas holdup. *American Institute of Chemical Engineers Journal*, 11, 9-13.

Zahradnik, J., Fialova, M., Ruzicka, M., Drahos, J., Kastanek, F., Thomas, N. H. (1997). Duality of the gas-liquid flow regimes in bubble column reactors. *Chemical Engineering Science, 52* (21/22), 3811-3826.

Zamfirescu, C., Dincer, I., & Naterer, G. F. (2010). Thermophysical properties of copper compounds in copper–chlorine thermochemical water splitting cycles. *International Journal of Hydrogen Energy, 35*, 4839-4852.

Zehner, P. (1986). Momentum, mass and heat transfer in bubble columns. *Transactions of the Institution of Chemical Engineers, 26*, 29-35.

Zou, R., Jiang, X., Li, B., Zu, Y., & Zhang, L. (1988). Studies on gas holdup in a bubble column operated at elevated temperature. *Industrial and Engineering Chemistry Research, 27*, 1910-1916.

APPENDIX I
DETAILS OF DIMENSIONAL ANALYSIS

In this section, the dimensional analysis is performed by using Buckingham pi theorem as follows (Sonin, 2001);

1- Identifying independent parameters of the studied system: The number of independent parameters (n) of the heat transfer study is 14 parameters as specified in Eq. (3.1).

2- Specifying the basic dimensions according to $FLT\theta$ unit system: The number of basic dimensions (k) is 4. The basic dimensions involved in the studies of U_V and α_g are summarized in the Table I.1.

Table I.1 Basic dimensions of the parameters involved in hydrodynamic study of oxygen SBCR.

Parameter	Basic Dimensions
ρ_l, ρ_g	$F\ L^{-4}\ T^2$
μ_l, μ_g	$F\ L^{-2}\ T$
σ	$F\ L^{-1}$
U_{gs}	$L\ T^{-1}$
C_{pl}, C_{pg}	$L^2\ T^{-2}\ \theta^{-1}$
k_l, k_g	$F\ T^{-1}\ \theta^{-1}$
D_R, H_R, d_o	L
U_V	$F\ L^{-2}\ T^{-1}\ \theta^{-1}$
α_g	1

3- Calculating the number of dimensionless parameters (Π groups) in the oxygen SBCR system:

$$n - k = 14 - 4 = 10 \qquad (I.1)$$

4- Selecting the repeating parameters: In the study of U_V, the four selected repeating parameters are ρ_l, μ_l, k_l and D_R.

5- Calculating the dimensionless groups (Π groups): The results of π groups are shown in Table I.2.

Table I.2 Dimensionless groups involved in heat transfer and hydrodynamic studies.

Dimensionless group	
$\Pi_1 = \frac{U_V\, D_R^2}{k_l}$	$\Pi_6 = \frac{H_R}{D_R}$
$\Pi_2 = \frac{\rho_g}{\rho_l}$	$\Pi_7 = \frac{d_o}{D_R}$
$\Pi_3 = \frac{\mu_g}{\mu_l}$	$\Pi_8 = \frac{k_g}{k_l}$
$\Pi_4 = \frac{\sigma\, \rho_l\, D_R}{{\mu_l}^2} = \frac{Re_l^2}{We_l}$	$\Pi_9 = \frac{C_{pl}\, \mu_l}{k_l} = Pr_l$
$\Pi_5 = \frac{U_{gs}\, \rho_l\, D_R}{\mu_l} = Re_l$	$\Pi_{10} = \frac{C_{pg}\, \mu_l}{k_l}$ $\frac{\Pi_{10}}{\Pi_9} = \frac{C_{pg}}{C_{pl}}$

After determining the π groups and doing some mathematical operations on $\Pi's$, Eq. (3.1) can be written as;

$$Nu_V = f\left(\frac{\rho_g}{\rho_l}, \frac{\mu_g}{\mu_l}, \frac{k_g}{k_l}, \frac{C_{pg}}{C_{pl}}, Re_l, \frac{Re_l^2}{We_l}, Pr_l, \frac{H_R}{D_R}, \frac{d_o}{D_R}\right), \qquad (I.2)$$

where $Nu_V = \frac{U_V\, D_R^2}{k_l}$, $Re_l = \frac{\rho_l\, U_{gs}\, D_R}{\mu_l}$, $We_l = \frac{\rho_l\, {U_{gs}}^2\, D_R}{\sigma}$ and $Pr_l = \frac{C_{pl}\, \mu_l}{k_l}$

APPENDIX II
INSTRUMENTS

II.1. Pressure Transducers

Four pressure transducers provided by OMEGA (PX209-030GI) were used in the experiments. Quasi-instantaneous pressures at four locations were measured at the same time. These high accuracy pressure transducers provide the signal output of electrical current (4-20 mA). The four transducers could measure pressures up to 207 kPa. Table II.1 shows the specifications of the pressure transducers (omega.com, 2010).

Table II.1 Specifications of the pressure transducers.

Specification	Description
Accuracy	0.25% full scale
Response time	2ms typical
Output	4 to 20 mA (2-wire) ±1% FSO
Operating temperature	-54 to 121°C

II.2. Pressure Gages

Two pressure gages of type OMEGA (PGH-45L-100) were installed at the inlet and outlet of the column. Table II.2 shows the specifications of these pressure gages (omega.com, 2010).

Table II.2 Specifications of the pressure gauges.

Specification	Description
Accuracy	0.5% FS
Operating Temperature	121°C maximum

II.3. Pressure Regulator

A pressure regulator of type OMEGA (PRG501-120), with hand-wheel adjustment, was placed before the flow meter to adjust accurately the quantity of

the gas flow rate. Table II.3 shows the specification of this pressure regulator (omega.com, 2010).

Table II.3 Specifications of the pressure regulator.

Specification	Description
Minimum Regulated Pressure	2 psi
Response Time to 50% Load Change	0.2 seconds
Adjustable Regulation Range	2 to 120 psig

II.4. Thermocouple Probes

Quick Disconnect Thermocouples with Removable Standard Size Connectors were used for measuring temperatures at various locations inside, and at the inlet and outlet of the slurry column. The probe consists of four copper-constantan thermocouples, which were placed inside an Inconel Sheath with a diameter of 3 mm and a length of 300 mm. Table II.4 shows the specifications of the thermocouple type K.

Table II.4 Specifications of the thermocouple of type K.

Specification	Description
Maximum Temperature Range (Thermocouple Grade)	-200-1250 ^{o}C
Special Limits of Error (whichever is greater)	1.1 ^{o}C or 0.4%

II.5. Flow Meter

A volumetric flow meter of type (FMA-1612A-I) was installed after the gas supply vessel to measure and control the volumetric flow rate of the gas. Table II.5 shows the specifications of the flow meter (omega.com, 2009).

Table II.5 Specifications of the flow meter.

Specification	Description
Accuracy	± (0.8% of Reading + 0.2% of Full Scale)
Maximum Flow	500 SLM
Operating Temperature	−10 to +50 ºC

APPENDIX III
EXAMPLES OF UNCERTAINTY CALCULATIONS

III.1. Example of Systematic Uncertainty Calculations of α_g

From Eqs. (5.7) and (5.48), the systematic uncertainty of the gas holdup can be written as;

$$\sigma_{\alpha_g}^2 = \sigma_{P_1}^2 \left(\frac{\partial \alpha_g}{\partial P_1}\right)^2 + \sigma_{P_2}^2 \left(\frac{\partial \alpha_g}{\partial P_2}\right)^2 \qquad (III.1)$$

where σ_{P_1} and σ_{P_2} are the uncertainties of the pressure transducers that measure P_1 and P_2 respectively. By substituting the derivatives of $\left(\frac{\partial \alpha_g}{\partial P_1}\right)$ and $\left(\frac{\partial \alpha_g}{\partial P_2}\right)$ from Eq. (5.7), Eq. (III.1) can be written as;

$$\sigma_{\alpha_g}^2 = \sigma_{P_1}^2 \left(\frac{-1}{\rho_{sl}\, g\, \Delta H}\right)^2 + \sigma_{P_2}^2 \left(\frac{1}{\rho_{sl}\, g\, \Delta H}\right)^2 \qquad (III.2)$$

Since the pressure transducers of the same type have same uncertainties, then $\sigma_{P_1} = \sigma_{P_2} = \sigma_P$, and Eq. (III.2) is written as;

$$\sigma_{\alpha_g}^2 = 2\sigma_P^2 \frac{1}{(\rho_{sl}\, g\, \Delta H)^2} \qquad (III.3)$$

The uncertainty of the pressure transducer (σ_P) can be calculated from;

$$\sigma_P = Accuracy \times Full\ Scale \qquad (III.4)$$

where the accuracy is 0.25% as shown in Table II.1, and the full scale is 207 kPa as indicated in section (II.1). From Eq. (III.4), σ_P is calculated to be 517.5 Pa. For $C_s = 0\%$ ($\rho_{sl} = \rho_l = 997.8\ kg/m^3$) and $\Delta H = 60\ cm$, the systematic uncertainty of the gas holdup (σ_{α_g}) is calculated from Eq. (III.3) to be 0.125%.

III.2 Example of Systematic Uncertainty Calculations of U_V

In Eq. (5.34), the mass flow rate of the gas can be expressed as;

$$\dot{m}_g = \rho_g\, \dot{V}_g \qquad (III.5)$$

and the average slurry temperature for a height of 45 cm, where there are four thermocouples, can be expressed as;

$$\bar{T}_{sl} = \left(\frac{T_1 + T_2 + T_3 + T_4}{4}\right) \qquad (III.6)$$

In Eqs. (III.5) and (III.6), $\dot{V}_g$ is the volumetric gas flow rate, and T_1, T_2, T_3, and T_4 are the thermocouples readings. By substituting Eqs. (III.5) and (III.6) into Eq. (5.34), it can be written as;

$$U_V = \frac{\rho_g \, \dot{V}_g \, C_{p,g}}{V_R} \, ln\left(\frac{T_{g,in} - \left(\frac{T_1 + T_2 + T_3 + T_4}{4}\right)}{T_{g,out} - \left(\frac{T_1 + T_2 + T_3 + T_4}{4}\right)}\right) \qquad (III.7)$$

From Eqs. (III.7) and (5.48), the systematic uncertainty of the volumetric heat transfer coefficient can be written as;

$$\sigma_{U_V}^2 = \sigma_{\dot{V}_g}^2 \left(\frac{\partial U_V}{\partial \dot{V}_g}\right)^2 + \sigma_{T_{g,in}}^2 \left(\frac{\partial U_V}{\partial T_{g,in}}\right)^2 + \sigma_{T_{g,out}}^2 \left(\frac{\partial U_V}{\partial T_{g,out}}\right)^2 + \sigma_{T_1}^2 \left(\frac{\partial U_V}{\partial T_1}\right)^2 + \sigma_{T_2}^2 \left(\frac{\partial U_V}{\partial T_2}\right)^2 + \sigma_{T_3}^2 \left(\frac{\partial U_V}{\partial T_3}\right)^2 + \sigma_{T_4}^2 \left(\frac{\partial U_V}{\partial T_4}\right)^2 \qquad (III.8)$$

The uncertainty of the flow meter ($\sigma_{\dot{V}_g}$) can be calculated from the accuracy and the maximum flow of the flow meter (see Table II.5) as;

$$\sigma_{\dot{V}_g} = (0.8\% \times Reading\ of\ Flow\ Meter) + (0.2\% \times Full\ Scale) \qquad (III.9)$$

where the full scale is 500 SLM as shown in Table II.5. For a flow meter reading of 22 SLM, $\sigma_{\dot{V}_g}$ is calculated from Eq. (III.9) to be $1.95 \times 10^{-5}\ m^3/s$.

The uncertaity of the thermocouple probe, which is the same for all thermocouples, is taken to be 1.1°C (see Table II.4). The derivatives in Eq. (III.8) can be obtained from Eq. (III.7) as follows;

$$\frac{\partial U_V}{\partial \dot{V}_g} = \frac{\rho_g \, C_{p,g}}{V_R} \, ln\left(\frac{T_{g,in} - \bar{T}_{sl}}{T_{g,out} - \bar{T}_{sl}}\right) \qquad (III.10)$$

$$\frac{\partial U_V}{\partial T_{g,in}} = \frac{\rho_g \dot{V}_g C_{p,g}}{V_R} \frac{1}{T_{g,in} - \bar{T}_{sl}} \qquad (III.11)$$

$$\frac{\partial U_V}{\partial T_{g,out}} = -\frac{\rho_g \dot{V}_g C_{p,g}}{V_R} \frac{1}{T_{g,out} - \bar{T}_{sl}} \qquad (III.12)$$

$$\frac{\partial U_V}{\partial T_1} = \frac{\partial U_V}{\partial T_2} = \frac{\partial U_V}{\partial T_3} = \frac{\partial U_V}{\partial T_4} = \frac{\rho_g \dot{V}_g C_{p,g}}{4V_R} \frac{T_{g,in} - T_{g,out}}{\left(T_{g,out} - \bar{T}_{sl}\right)\left(T_{g,in} - \bar{T}_{sl}\right)} \qquad (III.13)$$

The parameters used in Eqs. (III.10) to (III.13) are shown in Table (III.1).

Table III.1 Parameters used in Eqs. (III.9) to (III.12)

$T_{g,in} = 90\ ^oC$
$T_{g,out} = 25\ ^oC$
$\bar{T}_{sl} = 24\ ^oC$
$V_R = 0.0165\ m^3 \quad (H = 45\ cm)$
$C_{p,g} = 5193\ \frac{J}{kg.K}$
$\dot{V}_g = 3.66 \times 10^{-4}\ m^3/s \quad (U_{gs} = 0.01\ m/s)$
$\rho_g = 0.1344\ kg/m^3$

By substituting the above equations and the values of the parameters in Table III.1 into Eq. (III.8), the systematic uncertainty of the volumetric heat transfer coefficient (σ_{U_V}) is calculated to be 19.28 W/m^3.K.

III.3. Examples of Random Uncertainty Calculations of α_g and U_V

The formula of the sample standard deviation (σ) is;

$$\sigma = \sqrt{\frac{1}{N-1}\sum_{i=1}^{N}(x_i - \bar{x})^2} \qquad (III.14)$$

where x_i is the i'th measured value of the sample (α_g or U_V), $\bar{x}$ is the mean of the measured values, and N is the number of measured values in the sample. The relative standard deviation (*RSD*) is calculated from;

$$RSD = \frac{\sigma}{\bar{x}} \times 100 \qquad (III.15)$$

As indicated in the experimental procedure (section 3.3), each experimental run with a fixed static liquid level and solid concentration was repeated three times and the mean values of α_g and U_V were calculated. For each gas flow rate, the readings of the pressure and temperature were also repeated three times and the average values of α_g and U_V for each gas flow rate were calculated. In this way, there are nine repeated measurements for each value of α_g and U_V. Table III.2 shows the repeated measured values of α_g and U_V with their mean values and relative standard deviations for $C_s = 0\%$, $H = 45\ cm$ and $U_{gs} = 0.1\ m/s$.

Table III.2 Relative standard deviations of α_g and U_V.

	Measured α_g (%)	Measured U_V $(W/m^3.K)$
Run 1	23.25	1139.5
$C_s = 0\%$	22.65	1132.6
$H = 45\ cm$	22.6	1127.7
Run 2	23.24	1137.5
$C_s = 0\%$	24.46	1225.9
$H = 45\ cm$	23.52	1152.7
Run 3	25.42	1314.7
$C_s = 0\%$	25.97	1337.1
$H = 45\ cm$	24.35	1219
Mean value	24	1198.5
RSD (%)	5.07	9.38